Title
A Songbird Model of Genetically Based Speech Disorders

Author
Condro, Michael Christopher

Publication Date
2013

Peer reviewed|Thesis/dissertation

UNIVERSITY OF CALIFORNIA

Los Angeles

A Songbird Model of Genetically Based Speech Disorders

A dissertation submitted in partial satisfaction of the requirements for the degree Doctor of Philosophy in Molecular, Cellular & Integrative Physiology

By

Michael Christopher Condro

2013

ABSTRACT OF THE DISSERTATION

A Songbird Model of Genetically-Based Speech Disorders

By

Michael Christopher Condro

Doctor of Philosophy in Molecular, Cellular & Integrative Physiology

University of California, Los Angeles, 2013

Professor Stephanie White, Chair

Language is a complex communicative behavior unique to humans, though its genetic basis is still poorly understood. Genes associated with human speech and language disorders have provided a basis for study, originating with the *FOXP2* transcription factor, a mutation in which is the source of an inherited form of developmental verbal dyspraxia. Subsequently, targets of *FOXP2* regulation have been investigated for their associations with language-related disorders. One such target, contactin associated protein-like 2 (CNTNAP2), is associated with autism and specific language impairment. Due to the exclusivity of language to humans, no single animal model is sufficient to study the complete behavioral effects of these genes. However, some animals do possess components of language. One such component is vocal learning, which though rare in the animal kingdom, is shared with songbirds. Here, I use the zebra finch songbird as an animal model to investigate the role of Cntnap2 in birdsong. Cntnap2

is enriched in several song production nuclei in the zebra finch brain, including the striatopallidal nucleus area X, and the cortical lateral magnocellular nucleus of the anterior nidopallium and the robust nucleus of the arcopallium (RA). In adult RA, the distribution of Cntnap2 protein corresponds to the sexually dimorphic singing behavior of this species: males sing, and have enrichment of Cntnap2-expressing neurons, whereas females display neither the behavior nor the enrichment. In juveniles, however, there is comparable enrichment in RA in both sexes until the onset of sensorimotor learning in males, at which time the percentage of Cntnap2-expressing neurons in female RA declines. The neurons in RA that express Cntnap2 are projection neurons that directly innervate the motor neurons that control the vocal organ, analogous to human layer 5 pyramidal neurons of the primary motor cortex that innervate the motor neurons of the larynx. To test the function of Cntnap2 in zebra finch song, I designed and tested RNA interference constructs, which can be used to knock down Cntnap2 in RA. The songbird model can be used to understand the impact of Cntnap2 and other vocal learning genes as they relate to human speech and language.

The dissertation of Michael Christopher Condro is approved.

David L. Glanzman

Bennett G. Novitch

Felix E. Schweizer

Stephanie A. White, Committee Chair

University of California, Los Angeles

2013

To my grandmother, Barbara Good, who would have been proud.

Table of Contents

List of Tables

List of Figures

Acknowledgements

Sincerest thanks to Dr. Stephanie White, for all the support and guidance she provided throughout my predoctoral studies. Thanks to my doctoral committee members, Drs. Schweizer, Glanzman, and Novitch, for their contributions toward the success of this dissertation.

Chapter 1 is a version of an invited review article in preparation for Comparative Cognition & Behavior Reviews: Condro, M.C., White, S.A.

Chapter 2 is a version of a manuscript in press in the Journal of Comparative Neurology: Condro, M.C., White, S.A. Distribution of language-related Cntnap2 protein in neural circuitry dedicated to vocal learning. The authors thank Melissa Coleman and Felix Schweizer for assistance in the use of their equipment for retrograde labeling, and confocal fluorescence imaging, respectively. Brett Abrahams and Hongmei Dong provided the zebra finch Cntnap2 cDNA construct used in tests of antibody specificity. Yuichiro Itoh and Arthur Arnold provided the ZFTMA cell line. Vijayendran Chandran identified potential FoxP2 binding sites in zebra finch Cntnap2. Thanks to Alice Fleming for advice on immunohistochemistry and to Julie Miller for revising drafts of this manuscript and guidance on the methodology used within. Thanks also to Dorsa Beroukhim, Guillermo Milian, and Diana Sanchez for their assistance with collecting tissue samples. The authors wish to acknowledge two anonymous reviewers for their constructive comments.

Chapter 3: Thanks to Dr. Brett Abrahams for the first round of shRNA constructs. Dr. Julie Miller contributed to testing these shRNA constructs in zebra finch primary telencephalic cell culture. Qianqian Chen assisted with cloning and vetting the second round of shRNA constructs. Thanks to Drs. Bennett Novitch and Zachary Gaber for providing the pCIGRNAi plasmid and their advice regarding the cloning of shRNA constructs.

Appendix 1 is a version of Duistermars, B.J., Chow, D.M., Condro, M., Frye, M.A. (2007). The spatial, temporal and contrast properties of expansion and rotation flight optomotor responses in Drosophila. Journal of experimental biology, 210(18), 3218–3227. Thanks to Dr. Martin Egelhaaf and Dr. Andrew Straw for constructive feedback on an earlier version of the manuscript. We also thank Dr. Michael Reiser for engineering the LED display panels.

Appendix 2 is a version of Miller, J.E., Spiteri, E., Condro, M.C., Dosumu-Johnson, R.T., Geschwind, D.H., & White, S.A. (2008). Birdsong decreases protein levels of FoxP2, a molecule required for human speech. Journal of Neurophysiology, 100(4), 2015–2025. We thank Drs. R. H. Crosbie, K. Martin, T. O'Dell, A. Peter, B. Schlinger, and F. E. Schweizer for generosity in sharing resources and technical expertise. Three anonymous reviewers provided helpful comments.

Appendix 3 is a version of Fulton, D., Condro, M.C., Pearce, K., & Glanzman, D.L. (2008). The potential role of postsynaptic phospholipase C activity in synaptic facilitation and behavioral sensitization in Aplysia. Journal of Neurophysiology, 100(1), 108–116. We thank Drs. Greg Villareal and Adam Roberts for helpful comments on the manuscript.

The work presented in this dissertation was supported by the Molecular, Cellular & Integrative Physiology Interdepartmental Program, the Neural Microcircuits Training Grant T32 NS058280-04S1 (MCC), the UCLA Eureka Scholarship (MCC), the UCLA Edith Hyde Fellowship (MCC), NIH 5 R21 HD065271 (SAW), US Army AR093327 (SAW).

VITA

2005	B.S., Biology Cornell University, Ithaca, NY
2006	Substitute Teacher Utica, Whitesboro, and Westmoreland School Districts, NY
2007-2008	Teaching Assistant Department of Physiological Science University of California, Los Angeles
2007-2009	Neural Microcircuit Training Grant University of California, Los Angeles
2011-2012	Eureka Scholarship Department of Integrative Biology & Physiology University of California, Los Angeles
2012-2013	Edith Hyde Graduate Fellowship Department of Integrative Biology & Physiology University of California, Los Angeles

Publications and Presentations

Duistermars BJ, Chow DM, Condro M, Frye MA. 2007. The spatial, temporal and contrast properties of expansion and rotation flight optomotor responses in Drosophila. J Exp Biol 210:3218–3227.

Miller JE, Spiteri E, Condro MC, Dosumu-Johnson RT, Geschwind DH, White SA. 2008. Birdsong decreases protein levels of FoxP2, a molecule required for human speech. J Neurophysiol 100:2015–2025.

Fulton D, Condro MC, Pearce K, Glanzman DL. 2008. The potential role of postsynaptic phospholipase C activity in synaptic facilitation and behavioral sensitization in Aplysia. J Neurophysiol 100:108–116.

Condro MC, Miller JE, White SA. Autism susceptibility gene contactin associated protein-like 2 expression in a songbird model for vocal learning. Program No. 150.19. 2011 Neuroscience Meeting Planner. Washington, DC: Society for Neuroscience, 2011. Online.

Condro MC, White SA. Distribution of language-related Cntnap2 protein in neural circuitry dedicated to vocal learning. Manuscript submitted for publication to J Comp Neurol.

Condro MC, White SA. Recent advances in the genetics of vocal learning. Manuscript in prep for Comp Cog Behav Rev.

Chapter 1: Recent Advances in the Genetics of Vocal Learning

Michael C. Condro and Stephanie A. White

Introduction

Vocal learning, which includes the ability to imitate sounds with one's voice, is a rare trait in the animal kingdom. To date, only a few groups of mammals have demonstrated a capacity for vocal learning. These include certain species of echolocating bats, cetaceans, pinnipeds, elephants, and of course, humans. Outside of mammals, three groups of birds are capable of learning a portion of their vocalizations, namely hummingbirds, parrots, and songbirds, the last of which make up ~half of all bird species. The disparate pattern of vocal learning across taxa is characteristic of convergent evolution. A parsimonious explanation is thus that preadaptations for vocal learning emerged from non-learning ancestors of each taxon. These preadaptations are likely genetically encoded, which suggests that despite the distant relationships between vocal learners, there are some common genetic factors. One such example is the transcription factor *FOXP2*, a gene that is important for both human and songbird learned vocalizations, the evidence for which is discussed in this review. In addition to *FOXP2*, we examine current evidence for other molecules implicated in the neurogenetics of vocal learning.

FOXP2

Human disease studies of FOXP2

Transcription factor Forkhead Box P2 (FOXP2) became the first gene associated with language ability through the study of a human pedigree, referred to as the KE family (Lai et al., 2001), with inherited developmental verbal dyspraxia (DVD; also known as childhood apraxia of speech). DVD is characterized by an impaired ability to correctly execute orofacial movements

required for speech (Lai et al., 2001; MacDermot et al., 2005). In the KE family, the disorder is inherited in a Mendelian dominant manner, the locus of which was mapped to chromosome 7q31 (Fisher et al., 1998). An unrelated boy who exhibited the DVD phenotype harbored a genetic disruption in the same region, leading to the identification of *FOXP2* as the cause of the disorder. *FOXP2* codes for a transcription factor found primarily in the brain, lung, and spleen (Shu et al., 2001). The KE mutation results in an amino acid substitution, R553H, in the conserved DNA-binding forkhead box (FOX) region of the protein, which, in *in vitro* studies, causes abnormal levels of extra-nuclear localization of FOXP2 and impedes its ability to bind to DNA (Mizutani et al., 2007; Vernes et al., 2006). Since the discovery of the relationship between the KE mutation and DVD, other FOXP2 variants have emerged that are associated with speech and language disorders (MacDermot et al., 2005; Feuk et al., 2006; Shriberg et al., 2006; Zeesman et al., 2006; Rice et al., 2012; Palka et al., 2012; Raca et al., 2013), strengthening the link between FOXP2 and language. Notably a non-sense mutation, R328X, was discovered in three related individuals with verbal deficiencies (MacDermot et al., 2005). This mutation results in the loss of the FOX, zinc finger, and leucine zipper domains (Figure 1), the last of which is hypothesized to be crucial for dimerization (Li et al., 2004). Yet, *FOXP2* coding variants have not been associated with autism spectrum disorder (ASD) or specific language impairment (SLI; Scott-Van Zeeland et al., 2010; Newbury et al., 2002; Marui et al., 2005; Toma et al., 2012), despite the fact that these disorders are also characterized by language deficits. In a sample of children with dyslexia and unaffected relatives, a single nucleotide polymorphism in an intron of *FOXP2* identified as rs7782412 correlated with nonword repetition (NWR) score (Peter et al., 2011). Since dyslexia is associated with impairments of written, but not spoken, language (Lyon et al., 2003), these data suggest that *FOXP2* aberrations affect language processing as well as motor

ability. Notably, language processing deficits and low verbal IQ are symptomatic in the KE family as well (Vargha-Khadem et al., 1995), though it is unclear whether these traits are directly related to the *FOXP2* mutation, or are sequelae of DVD.

FOXP2 function in the developing brain

In all animals, the forkhead box family of transcription factors are involved in biological processes that affect embryogenesis and tissue development, as well as processes underlying underlying adult cancer and aging (Carlsson and Mahlapuu, 2002; Benayoun et al., 2011). FoxP1, 2, and 4 are expressed in embryonic neural tissues (Shu et al., 2001; Lu et al., 2002), and may therefore mediate neurogenesis and/or differentiation. Experimental reduction of FoxP2 in the cortex of embryonic mice through either shRNA or overexpression of the dominant negative KE form of FoxP2 repressed the transition from radial precursor to immediate neuronal progenitor, resulting in decreased cortical neurogenesis (Tsui et al., 2013). Interestingly, overexpression of human FOXP2 increases neurogenesis, whereas overexpression of murine Foxp2 does not. These data indicate that human FOXP2 exerts a greater neurogenic effect, which is perhaps significant for the construction of neural circuits involved in language processing. Foxp2 in conjunction with Foxp4, appears to promote neurogenesis by regulation of N-cadherin (Rousso et al., 2012). In embryonic chick and mouse spinal cord, overexpression of either Foxp increases the release of neural progenitors from the neuroepithelium, whereas knockdown of both prevents this release. These effects have yet to be tested in the cortex.

Another mechanism whereby FoxP2 may promote the development of vocal learning circuitry is through neurite development, at least in embryonic tissue when Foxp2 gene targets are enriched for this function. *In vitro*, overexpression of *Foxp2* accelerates neurite growth, whereas overexpression of the KE mutant form has the opposite effect (Vernes et al., 2011). Ectopic expression of Foxp2, achieved by removing the 3'UTR which includes its regulatory elements, delays neurite outgrowth *in vitro*, though by 7 days neurites form properly (Clovis et al., 2012).

FOXP2 regulates gene activity by binding to DNA either as a homodimer, or by heterodimerizing with FOXP1 or FOXP4. There are six known isoforms of FOXP2 (Figure 1-1), two of which are truncated and lack FOX domains (Bruce and Margolis, 2002). The truncated forms, referred to as FOXP2.10+ due to their alternate splicing at exon 10, do not localize to the nucleus, but may still dimerize with other FOXP2 isoforms (Vernes et al., 2006). Therefore it is hypothesized that FOXP2.10+ act as post-translational regulators of FOXP2 activity. FOXP2 can also interact with C-terminal binding protein (CtBP) to repress transcription (Li et al., 2004). A new association has been identified between FOXP2 and protection of telomeres 1 (POT1; Tanabe et al., 2011). In cell culture, when POT1 is expressed alone or coexpressed with the KE dominant negative mutation (R553H) of FOXP2, it is not localized in the nucleus. Only when POT1 is coexpressed with wild type FOXP2 is nuclear localization observed. Loss of POT1 can elicit a DNA damage response and cause cell arrest (Hockemeyer et al., 2005). FOXP2, in conjunction with POT1, could therefore affect cell cycling during development. The human phenotype exhibited by the KE mutation may be partly mediated by the inability of the mutant FOXP2 to associate with POT1, thereby disrupting cell cycling during the development of neural tissues subsequently necessary for vocal learning (Tanabe et al., 2011).

Molecular phylogeny of FoxP2

FoxP2 is highly conserved across species, particularly in the zinc finger and DNA-binding FOX domains. Two amino acid differences between humans and chimpanzees (303N and 325S in the human isoform) are unique to humans among living primates (Enard et al., 2002). Interestingly, these substitutions are shared with extinct hominids such as Neanderthals (Krause et al., 2007; Green et al., 2010; Reich et al., 2010), for whom the capability for language is still uncertain (Benítez-Burraco and Longa, 2012). Between the zebra finch songbird and human isoforms, there are only 5 additional substitutions, including one in the zinc finger domain that is conserved in primates and rodents, but differs in the zebra finch isoform (Teramitsu et al., 2004). Importantly, the DNA binding region is conserved between zebra finches and humans, including the arginine residue corresponding to position 553 in humans that is the site of the KE mutation. There is a considerable amount of homology (>80%) in the zinc finger, leucine zipper, and DNA-binding domains between human FOXP2 and the single FoxP isoform of fruitflies and honeybees (Kiya et al., 2008; Scharff and Petri, 2011). As in vertebrates, the invertebrate FoxP is predicted to be involved in procedural learning and communication (Colomb et al., 2012; Scharff and Petri, 2011). Interestingly, FoxP2 is not well-conserved among echolocating bats nor between bats and other mammals, which has been postulated to be the result of a selection pressure on FoxP2 in bats for the evolution of echolocation (Li et al., 2007).

Songbird Studies of FoxP2

Humans are the only living animals that communicate with language (Berwick et al., 2013), leaving no single animal model that sufficiently encapsulates every component of the behavior. However, facets of language are shared with other species. Vocal learning is one such facet that is shared with select groups of mammals, but as yet common laboratory models (e.g. rats, mice, non-human primates) fail to demonstrate this ability (Fitch, 2000; Arriaga et al., 2012; Mahrt et al., 2013). Rather, songbirds have been the principal animal models for vocal imitation in a laboratory setting (Panaitof, 2012). Vocal learning in both humans and songbirds relies on connections between the cortex, basal ganglia, and thalamus (Doupe and Kuhl, 1999). An advantage of the songbird model is that the neural structures responsible for vocal production and learning, called song production nuclei, are interconnected and anatomically distinct from the larger neurological subdivisions in which they reside, but are comprised of similar cell types. The song production nuclei are therefore assumed to function similarly to the circuits underlying other forms of procedural learning, but are dedicated to vocal learning. This feature of the songbird neuroanatomy has been an incredibly useful for studies of vocal learning genes, many of which are discussed in this review. Among songbirds, zebra finches have been widely used due to their ease of breeding in captivity, as well as the sexual dimorphism of vocal learning (only males sing; (Immelmann, 1969)) and the song production system, which is incomplete in females (Nottebohm et al., 1976; Konishi and Akutagawa, 1985).

FoxP2 mRNA expression is robust in the basal ganglia of humans and zebra finches (Teramitsu et al., 2004). In the zebra finch striatopallidal song nucleus, area X, FoxP2 transcript and protein levels correlate negatively with early morning singing. FoxP2 protein decreases in area X over the course of two hours when a male directs his songs at a female or when he practices them alone (Miller et al., 2008; Thompson et al., 2013); the latter is referred to as

undirected singing. The transcript decreases during the course of two hours of undirected, but not directed, singing (Teramitsu and White, 2006; Hilliard et al., 2012b; Teramitsu et al., 2010). The distinct behavioral regulation of the two molecular types suggests that there is post-transcriptional regulation of FoxP2, at least in the case of directed singing. MicroRNA, discussed below, may provide a mechanism for the social regulation of the transcript (Li et al., 2012). FoxP2 down regulation during singing appears largely due to motor activity, rather than auditory input, as levels continue to decrease in birds that have been deafened. However, there may be an additional auditory component to this phenomenon, as the degree of down regulation is only correlated with the amount of singing (Hilliard et al., 2012a) in birds that maintained their hearing (Teramitsu et al., 2010).

Recently, (Thompson et al., 2013) further investigated FoxP2 protein expression in zebra finch area X. Here, using immunohistochemistry, the authors identified two categories of FoxP2-labeled neurons: those with large nuclei intensely labeled by the FoxP2 antibody, and those with smaller nuclei and weaker labeling. One possibility is that these subtypes represent different stages of maturation within a single population of medium spiny neurons (MSNs). Intensely labeled neurons may be younger neurons either in the process of migrating or already having migrated to area X, whereas weakly labeled neurons may be mature and integrated into the basal ganglia microcircuitry. The intensely labeled neurons peak in density within area X around 35 days, and decline with age. The density of weakly labeled 'mature' neurons, does not change with age. However, the density of these neurons in area X is behavioral context-dependent. Adult males that sing for 2 hours in the morning exhibit a reduced density of weakly labeled neurons, a finding that replicates the behaviorally modulated levels of FoxP2 described in (Miller et al., 2008). It is possible that pallidal-like projection neurons in area X also express FoxP2. Given the

intensity of *FOXP2* radiolabeling in the internal globus pallidus of embryonic human brain (Teramitsu et al., 2004), the singing-related activity of the corresponding cell type in zebra finch area X (Goldberg et al., 2010), and that only ~78% of FoxP2 immunoreactive cells in area X expressed a marker for MSNs (Rochefort et al., 2007), it is possible that some of the weakly labeled neurons in area X are pallidal-like projection neurons.

In the zebra finch, experimentally induced reduction of FoxP2 at a developmental stage prior to the onset of vocal motor learning via injection of lentivirus containing an shRNA construct impedes the ability to learn the tutor's song (Haesler et al., 2007). Though shRNA-injected young zebra finches are capable of producing sounds similar to those of their tutors, they consistently fail to accurately imitate the tutor's song, often omitting or repeating individual syllables. Additionally, they are unable to accurately imitate the spectral characteristics and timing of the tutor's song. During this period of song learning, new neurons expressing FoxP2 migrate into area X, which are hypothesized to affect behavioral plasticity (Rochefort et al., 2007). Surprisingly, though, knockdown of FoxP2 does not prevent the proliferation of new neurons from the ventricular zone. It does, however, reduce the number of dendritic spines on MSNs, suggesting that FoxP2 affects neuronal plasticity without affecting proliferation and migration of new neurons (Schulz et al., 2010). These data provide support for a functional role of FoxP2 in vocal learning subserved by basal ganglia circuits, in addition to mediating the development of the brain regions involved.

Mouse models of Foxp2

Several mutant mice strains have been generated to study the effects of *Foxp2* on brain morphology as well as vocal and non-vocal behaviors. In one such model, the two amino acids characteristic to humans (Enard et al., 2002) were changed to conform to the human sequence (Enard et al., 2009). The resulting mice have altered cortico-basal ganglia circuitry in the form of increased dendrite length in Foxp2-expressing layer 6 bipolar spiny neurons in the primary motor cortex, MSNs in the striatum, and neurons in the parafascicular nucleus of the thalamus. Long-term depression (LTD) is increased in MSNs of the striatum, and dopamine concentrations are reduced in several brain regions, including the striatum (Reimers-Kipping et al., 2011). Despite also expressing the human-like Foxp2 protein, dendrite lengths of amygdalar and cerebellar Purkinje neurons are unchanged. Purkinje cell LTD is also similar to control levels, which suggests that the human-like Foxp2 impacts mainly basal ganglia microcircuits (Enard et al., 2009; Reimers-Kipping et al., 2011). In terms of behavior, the mutant mice exhibit decreased exploration, spend more time in groups, and, as neonates emit ultrasonic vocalizations with reduced pitch and increased frequency modulation compared to control mice. Interestingly, *FOXP2* knockout heterozygotes with a functional wild type allele have the opposite effects on dopamine levels and behavior (Enard et al., 2009).

Several mouse models have been generated to mimic FOXP2 mutations associated with human disease. These knock-in mice include murine versions of the KE mutation (R552H; Groszer et al., 2008; Fujita et al., 2008), a similar mutation that results in an amino acid substitution at a different site within the DNA binding domain (N549K; Groszer et al., 2008), and a truncation (S321X) that fails to produce a protein, similar to a human mutation associated with speech impairment (Groszer et al., 2008). These loss of function knock in mutations are lethal in homozygotes, with mice usually dying within the first month of life, though N549K

homozygotes can survive for several months. All knock-in mutants have decreased cerebellar volume and Purkinje cell dendritic arbor (Fujita et al., 2008; Groszer et al., 2008), but otherwise no gross anatomical disturbances were observed in the rest of the brain. Homozygous knockout, R552H, and S321X mutant pups make fewer ultrasonic distress calls, though there are mixed reports about the quality of these vocalizations (Shu et al., 2005; Fujita et al., 2008; Groszer et al., 2008; Gaub et al., 2010). Recently, Bowers et al. (2013) investigated these calls from wild type rats and found qualitative and quantitative sex differences. Separation calls are emitted from pups separated from their dam and trigger the dam to retrieve the pup back to the nest. Bowers et al. found that male pups call more frequently, at a lower pitch, and more quietly than females. In turn, the dam responds differently to calls made by each sex, preferentially retrieving male before female pups. Male pups have more Foxp2 protein than females in several brain areas. Interestingly, in humans more FOXP2 is found in the cortices of 4-year-old girls than age-matched boys, which coincides with gender-based language differences in children at this age. Reduction of Foxp2 in mouse pups by injection of siRNA into the ventricles during the first two days of life reverses the sex effect in calling behavior. Affected male pups call less frequently and at a higher pitch than control males. Notably, treatment of female pups with siRNA causes their vocalizations to become male-like, with higher frequency of calling, lower pitch, and lower amplitude. The authors posit that the reversal caused by Foxp2 siRNA is the result of a decrease in Foxp2 in males and a rebound-effect increase in females. The dam retrieves siRNA-injected females before siRNA-treated males, providing evidence that the retrieval response of the dam depends on the vocal behavior rather than other sexually dimorphic characteristics. Foxp2 does not appear to be necessary for these innate separation calls (Gaub et al., 2010) though it is possible that FoxP2 can effect learned vocalizations through common pathways.

Since separation calls are unlearned (Arriaga et al., 2012) and therefore bear little, if any, resemblance to human speech, studies in *Foxp2* mutants examined other learned behavioral skills. Heterozygote knockout mice perform the Morris water maze as well as wild types (Shu et al., 2005), indicating that this hippocampal-based learning task is not affected by loss of *Foxp2*. However, R552H mutants are impaired on the accelerating rotarod, a procedural learning task that relies on basal ganglia activity (Groszer et al., 2008; French et al., 2012). Interestingly, these mutant mice can perform other striatal-based learning tasks, such as pressing a lever for a reward, equally well as controls. R522H heterozygous mutant mice have corresponding neurophysiological abnormalities, including reduced striatal LTD and increased cerebellar paired pulse facilitation (Groszer et al., 2008). *In vivo* recordings of these mice during the accelerating rotarod learning task show that striatal firing rate activity decreases in R552H mutants, whereas it increases in wild types, and temporal coordination is altered (French et al., 2012). These data suggest that Foxp2 activity in the basal ganglia is involved in procedural learning tasks in non-vocal learning species, perhaps in a similar manner to vocal learning in humans and songbirds.

FOXP1

FoxP1 is the most similar molecule to FoxP2 and, perhaps not surprisingly, is also linked to human speech. As previously mentioned, *FoxP1* and *FoxP2* may form heterodimers that regulate transcription in areas where their expression overlaps (Li et al., 2004; Wang et al., 2003; Shu et al., 2001). Initial support for a role of FOXP1 in vocal learning stems from a study of comparative gene expression in two vocal learners: humans and zebra finches. Unlike *FoxP2*, for which differential expression in song nuclei depends on behavior, *FoxP1* signals constitutively

'mark' the song system, with mRNA enrichment in area X (in males), HVC, and RA relative to their surrounding tissues (Teramitsu et al., 2004). In humans, *FOXP1* and *FOXP2* are found in separate cortical layers: the former is found primarily in layers 2/3 with less expression in deeper layers, whereas the latter is primarily in layer 6 (Teramitsu et al., 2004; Ferland et al., 2003). Both transcripts are expressed in the human striatum, similar to the expression pattern in the basal ganglia nucleus area X of songbirds. The possible co-regulation of transcription by FoxP members in the songbird song production system, and the comparative gene expression in humans suggested that FOXP1 also plays a role in human language (Teramitsu et al., 2004). Subsequently, Pariani et al., 2009 reported the first human case of *FOXP1* alteration and speech impairment, in which the patient had a large deletion in chromosome 3 including the *FOXP1* gene. Speech delay was one of several deficits, which also included anatomical and neurological abnormalities. Shortly after this report, several similar cases were published in which patients with *FOXP1* deletions presented cognitive deficits, motor control deficits, speech delay and autism (Carr et al., 2010; Horn et al., 2010; Hamdan et al., 2010; Palumbo et al., 2012; O'Roak et al., 2011; Talkowski et al., 2012; Horn, 2012). In all the reported cases, however, the language impairment described was more consistent with speech delay than DVD. A screen of patients with DVD failed to identify FOXP1 as a risk factor, even in a pedigree in which only *FOXP1* was affected (Vernes et al., 2009). Though many of the phenotypes associated with mutations in FOXP1 and FOXP2 are non-overlapping, language impairment is common to both (Bacon and Rappold, 2012).

CNTNAP2

Cntnap2 in human disease

Similar to the discovery of the relationship between FOXP2 and language through the KE family, a rare mutation in the contactin associated protein-like 2 (*CNTNAP2*) gene was discovered in a genetically related population of Old Order Amish children. Some members of this group are afflicted with cortical dysplasia-focal epilepsy (CDFE). The disorder is characterized by the onset of seizures at ~2 years of age, mental retardation, hyperactivity, pervasive developmental delay or autism in the majority of cases, and language regression by the age of three in all cases. Patients with CDFE have a homozygous for a deletion in *CNTNAP2* exon 22, 3709delG. The deletion causes a frameshift that results in the loss of the single transmembrane and intracellular domains of the protein (Figure 2). This causes the normally membrane-bound protein to instead be secreted (Falivelli et al., 2012), presumably eliminating its functionality. Subsequent to the initial association between *CNTNAP2* mutation and CDFE, it was revealed that it is regulated by FOXP2. In chromatin immunoprecipitation (ChIP) assays, fragments of intron 1 of *CNTNAP2* were bound by FOXP2 at the canonical binding sequence CAAATT (Vernes et al., 2011; 2008). Mutation of these sites to CGGGTT prevented FOXP2 binding. Overexpression of FOXP2 in the human-derived neuroblastoma cell line SY5Y decreased CNTNAP2 transcription. To further investigate the relationship between CNTNAP2 and language ability, variants of the gene were screened in a cohort of families with SLI-afflicted members. Nine intronic SNPs between exons 13 and 15 of CNTNAP2 correlated with NWR scores. The one SNP most correlated, rs17236239, was also associated with expressive language score. Quantitative transmission disequilibrium testing (QTDT) confirmed a relationship between measures of language ability four of these SNPs, but failed to confirm a relationship for rs7794745 in a new sample of families containing members with SLI (Newbury et al., 2011).

None of the SNPs associated with language-related QTDT measures in a sample of families with dyslexia, indicating that there are other factors in addition to variation in CNTNAP2 that affect language ability.

Other common CNTNAP2 polymorphisms have been identified that associate with diagnoses of autism (Bakkaloglu et al., 2008; Arking et al., 2008), for which language impairment is a core deficit, and a language-related measure, age at first word (Alarcón et al., 2008). Interestingly, inherited CNTNAP2 polymorphisms that are associated with disease occur mainly in introns (Alarcón et al., 2008; Arking et al., 2008), suggesting either these SNPs are in linkage disequilibrium with yet unidentified markers in exons, or the SNPs themselves affect transcriptional regulation of the gene. Quantitative transmission disequilibrium testing revealed a association between the SNP rs2710102 and NWR (Peter et al., 2011). 13 *de novo* mutations in CNTNAP2 have been described that result in an amino acid change in the protein, 8 of which were predicted to hinder function (Bakkaloglu et al., 2008). The *de novo* mutations, along with the CDFE mutation identified by Strauss et al. (2006), were investigated further to determine whether they did in fact affect protein function. HEK cells and rat hippocampal neurons transfected with either wild type human Cntnap2 or the mutant forms (Falivelli et al., 2012). The CDFE mutation results in a premature stop codon that prevents the transcription of the transmembrane and intracellular domains of the protein. As expected, this causes the formation of a secreted protein, which is detected in the culture medium, but not on cell surfaces. Another mutant, D1129H (Figure 1-2), also prevents surface expression of Cntnap2, and instead the protein remains restricted to the endoplasmic reticulum, unable to transport to the plasma membrane. This mutation interferes with LNS4 domain of CNTNAP2, and is presumed to cause misfolding of the protein. Most other mutations investigated did not show restricted localization

to the ER, though the highly conserved mutation I869T (Figure 1-2) had less surface staining than the wild type form of the protein. Theoretically, mutations that interfere with intracellular trafficking of Cntnap2 would also interfere with protein function. However, with the exception of 3709delG, these mutations do not always result in an autistic phenotype, indicating that other genetic, environmental, and developmental factors are involved in the presentation of the disorder.

Cntnap2 function in the brain

Investigation of genes related to the formation of language-related brain areas revealed *CNTNAP2* enrichment in the cortical superior temporal gyrus, associated with language processing and production (Abrahams and Geschwind, 2008). Moreover, CNTNAP2 is enriched in embryonic human frontal cortex, but not in rat or mouse at comparable stages of development. Not only do these data suggest a role for Cntnap2 in the development of neural circuitry underlying language, they suggest that this enrichment is relevant to vocal learning in humans, a behavior not shared with rodents.

The brains of healthy and autistic individuals homozygous for risk alleles rs7794745 and rs2710102 exhibit functional differences. Subjects with one or both risk variants exhibit increased activation of the frontal operculum and medial frontal gyrus relative to subjects homozygous for the non-risk allele (Whalley et al., 2011). Event-related brain potentials are altered during a language perception task in individuals carrying the rs7794745 risk allele (Kos et al., 2012). Scott-Van Zeeland et al. (2010) investigated the correlation of risk allele rs2710102

with connectivity both within the mPFC and between other areas. Decreased lateralization of activity in language areas of the brain is associated with autism-like behaviors. Subjects with the Cntnap2 risk allele rs2710102, when given a reward-based learning task that is known to activate frontostriatal circuits, exhibit increased local connectivity in the mPFC relative to subjects without the risk variant. This occurs in a genetically dominant fashion regardless of the autism phenotype of the risk allele carriers. In addition, risk allele carriers have less focused long-range connectivity between the mPFC and several other brain areas, as well as decreased lateralization. These data suggest that Cntnap2 variants increase the risk of autism through alteration of frontal lobar connectivity.

As yet, the most well-characterized function of Cntnap2 is to cluster voltage-gated potassium channels at juxtaparanodes of axons in the peripheral nervous system (Poliak et al., 2003). Recently, another potential function of was discovered through an RNA interference (RNAi) survey of autism susceptibility genes (Anderson et al., 2012). Of the 13 genes included in the RNAi screen, Cntnap2 knockdown had the most pronounced effects on network activity in mouse hippocampal cultures. In cultures transfected with short hairpin RNA (shRNA) targeting Cntnap2, picrotoxin-induced action potentials were reduced in amplitude to ~70% of controls, though action potential frequency was not affected. Conversely, knockdown of the binding partner of Cntnap2, contactin 2, had the opposite effect, increasing the amplitude of the action potential. Cntnap2 expression level has no effect on neuronal excitability. Instead, the underlying cause of the action potential attenuation is a global decrease in synaptic transmission. Both excitatory and inhibitory evoked currents are reduced by the shRNA, as well as the frequency of miniature postsynaptic potentials, suggesting that the number of synaptic sites on affected neurons is reduced. This is further confirmed by changes to cellular morphology of transfected

neurons. Cntnap2 knockdown results in shorter neurites with fewer branches, and dendritic spines with smaller spine heads. These data are evidence that Cntnap2 may affect the development of neurons by increasing the number of active synaptic sites and facilitating network activity.

Animal models for Cntnap2

Given the evidence for a role of *CNTNAP2* in human speech, it may also function in birdsong (Panaitof et al., 2010). In adult male zebra finches *Cntnap2* transcript is enriched in the robust nucleus of the arcopallium (RA) and the lateral magnocellular nucleus of the anterior nidopallium (LMAN), cortical nuclei in the song production system. Projection neurons from RA are similar to layer 5 pyramidal neurons in mammalian cortex whose axons descend below the telencephalon to synapse onto motor neurons (Jarvis, 2004), and LMAN shares similarities with the mammalian prefrontal cortex (Kojima et al., 2013). No such enrichment of *Cntnap2* is observed in HVC (acronym used as proper name), another song nucleus analogous to mammalian cortical layer 2/3 (Jarvis, 2004), and there is reduced expression in area X relative to the striatopallidum. Each song nucleus is comprised of similar cell types as those in the surrounding tissues, which suggests that the differential expression of genes within the song nucleus indicates a specific role for those genes in vocal learning and/or production. In contrast to males, adult females have moderate transcript levels in RA and LMAN. Female zebra finches have an underdeveloped area X that is not visible by common staining procedures (Balmer et al., 2009), but still *Cntnap2* is uniform across the entire striatopallidum. Interestingly, in young females (<50d) *Cntnap2* is enriched in RA to the same degree as for males, and declines to the

level of the surrounding arcopallium with age. The reduction in gene expression coincides with the sensorimotor period of song learning in males, a time at which the male begins to practice singing. The percentage of cells expressing the protein in female RA decreases at this time point (Condro and White, *in press*). This sexually dimorphic expression supports the hypothesis that *Cntnap2* expression in RA is important for proper production of learned vocalizations in songbirds. According to this hypothesis, interference of Cntnap2 translation in male RA should disrupt song learning and/or production, similar to FoxP2 knockdown in area X (Haesler et al., 2007).

As with Foxp2, mouse models of Cntnap2 risk variants may not capture language deficits associated with their respective disorders. However, they can be used to study other aspects of behavior and physiology that may impact future studies focused on vocal learning. Initially, outbred Cntnap2(-/-) mice were reported to have no gross anatomical or neurological abnormalities (Poliak et al., 2003). However, when these mice were crossbred with the C57BL/6J strain, subsequent generations exhibited neurological abnormalities similar to human patients with CDFE (Strauss et al., 2006), including epileptic seizures induced by mild handling starting before 6 months of age (Penagarikano et al., 2011). These knockout mice present neuronal migration abnormalities, with an increase in the incidence of ectopic neurons, a reduced number of inhibitory interneurons in the cortex and the striatum, along with impaired network synchrony in the cortex. Additionally, there is increased spontaneous inhibitory activity in cortical layers 2/3, disrupting the balance between inhibition and excitation (Lazaro et al., 2012). These mice exhibit behavior similar to the human autistic phenotype, including repetitive motions, such as self-grooming and digging, behavioral inflexibility on learned tasks, such as the Morris water maze or T maze, decreased social activity with other mice, reduced nest building,

and a decrease in the number of ultrasonic separation calls. Less frequent vocalizations could be symptomatic of impaired communication similar to language regression in autism, or alternatively due to a decreased motivation to for the maternal interaction, similar to social impairment in autistic children. The two hypotheses are not mutually exclusive, though the former is less likely, since this particular call type in mice is innate (Arriaga et al., 2012) and therefore not subject to regression. Interestingly, many of the behavioral deficits in the knockout mice can be partially rescued by treatment with risperidone, a medication used to treat the symptoms of autism (Penagarikano et al., 2011). However, the drug does not improve social interactions for the knockout mice. The effects of risperidone on communicative behavior have not yet been reported. Rescue by the drug of some of the effects of knocking out *Cntnap2* further validates the relationship between *Cntnap2* and autism. These knockout mice can be used to test other drugs to treat some of the symptoms of autism, though perhaps not language impairment. This model is especially pertinent to CDFE, for which the mutation renders CNTNAP2 non-functional. The more common polymorphisms associated with ASD and SLI risk lie in introns, creating a challenge to develop mouse models. A songbird model may offer an advantage in understanding the role of CNTNAP2 in language in that knockdown of Cntnap2 can be targeted to song nuclei, isolating its effects on vocal behavior.

Hepatocyte Growth Factor Signaling Pathway Genes

In keeping with the theme of FoxP2 as a molecular entry point into gene networks involved in speech and language, another class of FoxP2 target genes is implicated in language deficits. Three genes in the hepatocyte growth factor (HGF) signaling pathway are each targets

of FOXP2 regulation and associated with disorders of human speech and language. The first is the HGF receptor tyrosine kinase MET (Bottaro et al., 1991), which has been linked to ASD (Mukamel et al., 2011). The second, also linked to ASD, is the urokinase plasminogen activator receptor (uPAR, or *PLAUR* when referring to the human gene; Campbell et al., 2007), which was long thought to indirectly activate HGF through its binding partner urokinase (Mars et al., 1993), though more recently this function has been challenged (Owen et al., 2010; Eagleson et al., 2011). The third is sushi-repeat protein, X-linked 2 (SRPX2), a uPAR ligand (Royer-Zemmour et al., 2008) that also binds HGF (Tanaka et al., 2012), and may account for the HGF-mediated effects of uPAR signaling. FOXP2 binds the promoter regions of all three genes (Roll et al., 2010; Mukamel et al., 2011). SRPX2 is linked to language through association with childhood seizures of the Rolandic fissure, which can cause language disabilities (Roll et al., 2006). FOXP2 binds the promoter regions of all three genes and represses transcription (Mukamel et al., 2011; Roll et al., 2010; Konopka et al., 2012). Similar to *CNTNAP2,* the distribution of *MET* in human fetal brain is complimentary to that of *FOXP2*. In cultures of normal human neural progenitors and established cell lines, endogenous *FOXP2* expression increases with maturity as *MET* decreases (Konopka et al., 2012). Notably, the KE mutant (R553H) fails to repress *uPAR or SRPX2* (Roll et al., 2010). These data suggest that HGF signaling is altered in cases of language disorders associated with *FOXP2*. Interestingly, to date HGF itself has not been directly associated with a disorder relating to speech.

MET was initially investigated as an autism susceptibility gene due to the similarity of neuroanatomical abnormalities attributed to loss of MET signaling in the cortex and those found in cases of autism (Campbell et al., 2006). A SNP in the promoter region of MET, rs1858830, was identified as a site associated with elevated risk of diagnosis of autism. The “C” variant at

this site causes a reduction in transcription of the gene, and alters transcription factor binding relative to the non-risk "G" variant. The "C" variant is overrepresented in cases of ASD, associated with reduced Met protein in the cortex (Campbell et al., 2007; 2008) and social and communication impairments in cases of ASD (Campbell et al., 2010). In healthy human embryonic, brains *MET* is enriched in the temporal cortex, an area involved in language processing, and to a lesser degree in the hippocampus and occipital cortex (Mukamel et al., 2011). HGF signaling through MET promotes development of cortical projection neurons (Eagleson et al., 2011). In microarray analysis, *MET* has been identified as a member of a gene module correlated with differentiation, particularly with axon guidance (Konopka et al., 2012). Though protein levels are dynamic during development, a peak of expression coincides with increased development of neurites and synapse formation, suggesting a role for MET in neuronal connectivity (Judson et al., 2009). MET is expressed in axon tracts of projection neurons of the neocortex, including those that descend into the striatum, consistent with the hypothesis that MET is a factor in development of neural circuits, which when perturbed, leads to symptoms of ASD and language impairment.

In a screen for other ASD-related genes in the MET signaling pathway, a SNP in the promoter region of *PLAUR*, rs344781, was identified as a risk factor for autism diagnosis with an interaction effect with *MET* rs1858830. uPAR knockout mice have been generated, but thus far studies have focused on the effects of knockout on neural migration and seizure activity. Whereas MET seems to promote cortical projection neuron migration and growth, uPAR seems to affect inhibitory neurons in much the same manner, though the mechanism remains unclear (Eagleson et al., 2011). Homozygous knockouts exhibit spontaneous seizures as well as a reduction of parvalbumin-positive interneurons in the anterior cingulate and parietal cortices

(Powell et al., 2003; Eagleson et al., 2005). The loss of inhibitory interneurons may affect the balance of excitation and inhibition associated with autism (Eagleson et al., 2011). Interestingly, uPAR may be absent in birds (NCBI search, BLAST), suggesting that it is not common to all vocal learning species. There may be a different molecule in songbirds that replaces uPAR function. Though uPAR was originally thought to be involved in the activation of HGF required for binding to MET (Mars et al., 1993), recent evidence suggests that uPAR and its binding partner urokinase contribute very little to the process, and rather other serine proteases are responsible for HGF activation (Owen et al., 2010). Phenotypic differences in *uPAR* and *MET* knockout mice support this hypothesis (Eagleson et al., 2011). However, uPAR is involved in several signaling cascades independent of MET (Blasi and Carmeliet, 2002), any of which may be related to autism or language impairment.

SRPX2 is a chondroitin sulfate proteoglycan that binds to both HGF and uPAR (Tanaka et al., 2012; Royer-Zemmour et al., 2008). Mutations in SRPX2 can result in seizures originating in the Rolandic fissure, which can lead to abnormal brain morphology in the form of polymicrogyria, and are associated with oral and speech dyspraxia and cognitive impairment (Roll et al., 2006). One such mutation, resulting in a tyrosine-to-serine substitution at position 72, is related to both Rolandic seizures and orofacial and fine motor impairment. The substitution occurs in a region thought to affect protein-protein interactions. In this same region is a site at position 75 that is highly conserved among primates, but has changed in humans since the split from chimpanzees, suggesting an evolutionary mechanism (Royer et al., 2007), reminiscent of the amino acid substitutions in FOXP2 between the two species (Enard et al., 2002). Very little is known about the mechanism by which SRPX2 affects physiology. As yet, no mouse model for speech-related SRPX2 mutations has been generated. Other chondroitin sulfate proteoglycans are

involved in formation of perineuronal nets, which can affect plasticity of sensory systems (McRae et al., 2007). In songbirds, development of perineuronal nets around song nuclei correlate with the development of song, and it is hypothesized that destruction of these nets permits the re-opening of critical period for song learning after crystallization (Balmer et al., 2009). It is possible, therefore, that SRPX2 is involved in similar processes, which could affect learned vocalizations in humans and songbirds alike.

Stuttering Genes

Stuttering, or stammering, is a condition in which speech is interrupted by involuntary repetitions of syllables or words, prolongation of syllables, or pauses during speech. Inheritance patterns strongly suggest a multifactorial genetic basis for the disorder, with relatively little environmental influence (Kraft and Yairi, 2012; Kang and Drayna, 2011). However, it was not until recently that any specific gene was identified as a factor in stuttering. Genomewide linkage revealed a locus of disequilibrium on chromosome 12 for stuttering (Riaz et al., 2005), which was investigated more closely in a large pedigree, identified only as Family PKST72, in which roughly half of the living members stutter (Kang et al., 2010). Genotyping in this pedigree revealed a relationship with a SNP, (G3598A), which causes a glutamine-to-lysine amino acid substitution in a gene encoding a subunit of *N*-acetylglucosamine-1-phosphate transferase (*GNPTAB*) gene. The ‘A’ variant was more common in stuttering family members, and family members homozygous for the ‘G’ variant were much less likely to stutter. Unlike *FOXP2* in the KE family, though, G3598A exhibits some phenotypic plasticity, in that not every family member with an ‘A’ variant stutters, and some family members homozygous for the ‘G’ variant

do stutter. Sex has been previously shown to be a factor in recovery of stuttering, with females being four times more likely to recover from stuttering than males (Ambrose et al., 1997). Such may be the case for the two female non-stuttering family members homozygous for the 'A' variant (Kang et al., 2010). Three more amino acid changes in GNPTAB were associated with stuttering in a broader population sample, as well as three others found in each of GNPTG, another subunit of the phosphotransferase, as well as *N*-acetylglucosamine-1-phosphodiester alpha-*N*-acetylglucosaminidase (NAGPA). These mutations account for a small percentage (<10%) of stuttering cases used in this study, indicating that still unidentified factors contribute to the disorder. GNPTAB/G and NAGPA act as enzymes in the lysosomal targeting pathway. Mutations in GNPTAB/G are associated with mucolipidoses, disorders associated with deficits in development, mental ability, and speech, though this study is the first to link mutations in these genes to stuttering (Kang et al., 2010; Kang and Drayna, 2012). The mechanisms by which these mutations affect speech are unknown. Other loci have been identified as potential sites for mutations associated with stuttering (Kraft and Yairi, 2012; Raza et al., 2012), but as yet no other genes have been discovered. One study did find an association between a SNP in the *DRD2* gene in a Chinese Han population (Lan et al., 2009), but this result was not replicated in a larger sample (Kang et al., 2011). Additionally, a case was reported in which a partial deletion of CNTNAP2 was found in a stuttering patient, (Petrin et al., 2010) suggesting that there may be some overlap of genetic factors in stuttering and other language disorders.

Other Genes of Interest

Additional genes likely contribute to vocal learning. In a screen of genes within a region on chromosome 16 associated with SLI, two candidates correlated with measures of language ability: c-maf-inducing protein (CMIP) and calcium-importing ATPase, type 2C, member 2 (ATP2C2; Newbury et al., 2009). Subsequent study found an association of CMIP with reading-related measures, but did not with ATP2C2 (Newbury et al., 2011; Scerri et al., 2011). Though both molecules are expressed in the brain, their functions therein are still poorly understood. In other tissues, CMIP is involved in a cell signaling cascade (Grimbert et al., 2003), and ATP2C2 is part of a pathway responsible for shuttling divalent ions to the Golgi apparatus (Faddy et al., 2008; Missiaen et al., 2007). Other genes potentially involved in language comprehension include doublecortin domain containing protein 2 (*DCDC2*) and *KIAA0319*, which have both been associated with dyslexia (Scerri et al., 2011; Rice et al., 2009; Newbury et al., 2011; Czamara et al., 2011). The only known effect of DCDC2 is to increase the length of cilia in ciliated neurons and thereby affect cell signaling (Massinen et al., 2011; Ivliev et al., 2012). Given that the other genes implicated in language acquisition and production seem to be involved in either neurogenesis or neurite growth, perhaps CMIP, ATP2C2, and DCDC2 affect either or both of these processes. However, the function of KIAA0319 in language processing is beginning to be better understood. KIAA0319 is involved in the clatherin endocytosis pathway (Levecque et al., 2009). Knock down of Kiaa0319 expression in rat auditory cortex results in increased neuronal input resistance accompanied by increased excitability in response to auditory stimuli (Centanni et al., 2013). The authors hypothesize that this change in neuronal excitability, relevant to variants of KIAA0319 in cases of dyslexia, impedes differentiation of speech and non-speech sounds. Another gene of interest in relation to its role in language is *FMR1*, which encodes the fragile X mental retardation protein (FMRP). Language delay and impairments in

both receptive and expressive language are characteristic of children with fragile X syndrome (FXS; Finestack et al., 2009). In the zebra finch song system, FMRP is expressed in song nuclei HVC, LMAN, RA, and area X (Winograd et al., 2008). Interestingly, FMRP is enriched in male RA around the onset of the sensorimotor learning phase. These data suggest that FMRP may be a common factor in learned vocalizations in both humans and songbirds.

MicroRNA

MicroRNAs (miRs) are short (~22 nucleotide), non-coding RNAs that post-transcriptionally regulate synthesis of specific proteins through either degradation of the mRNA or inhibition of translation (He and Hannon, 2004; Pasquinelli, 2012). These small molecules are thought to "fine-tune" gene expression involved in many biological processes. Research on miR functions in the brain has focused primarily on roles in development and neurogenesis (Sun et al., 2013; Liu and Zhao, 2009), though studies are starting to emerge on activational effects in the mature brain (Bredy et al., 2011; Fiore et al., 2011). MicroRNAs can affect learning and memory-based tasks, such as fear conditioning, context conditioning, place preference, and Morris water maze performance (Konopka et al., 2010; Olde Loohuis et al., 2011; Wang et al., 2012; Griggs et al., 2013). Another class of small noncoding RNAs are those that interact with Piwi (piRNAs), whose mechanisms and functions are still poorly understood, though evidence suggests they are involved in epigenetic control of transcription (Kuramochi-Miyagawa et al., 2008). Recently, piRNAs have been identified as factors contributing to associative learning in *Aplysia* through regulation of CREB2 (Rajasethupathy et al., 2012). However, investigation into the role of small RNAs in vocal learning has only just begun.

As with many of the genes described in this review, FOXP2 may be used as a starting point by identifying miRs that regulate expression of FOXP2, or are targets of FOXP2 regulation (or in some cases, both). In microarray analysis used to identify gene networks influenced by Foxp2 expression, 22 miRs were identified as transcriptional targets of murine Foxp2 (Vernes et al., 2011). Of these, several have documented functions in the brain: miR-9, -29a, -30a, -30d, -34b, 124a, -125b, and -137. Additional sources of potential vocal learning-associated miRs come from studies in songbirds. In zebra finches, miR-137 was included in a microarray study investigating genes regulated by singing in basal ganglia nucleus area X, and was found to belong to the same gene network module as FoxP2, and negatively associated with the number of motifs sung (Hilliard et al., 2012a). miR-9 and -140-5p are expressed in zebra finch area X, and are regulated by singing in juveniles and adults (Shi et al., 2013). Expression of five miRs in cortical auditory regions are affected by exposure to conspecific song: mir-92, -124, and -129-5p decreased, and mir-25 and -192 increased (Gunaratne et al., 2011). Though the birds in this latter study were adults, and therefore past the critical phase of song learning, the miRs involved in auditory processing may very well impact song learning earlier in life. mir-2954, a putatively avian-specific miR, is expressed at greater levels in males than females in all tissues tested, including brain (Luo et al., 2012). miR-2954 may therefore play a role in the sex-based differences in neuroanatomy and song learning in this species. miRs like miR-2954, which appear to be unique to birds or specifically zebra finch (Gunaratne et al., 2011; Luo et al., 2012), are not likely a common factor underlying behavior in all vocal learning species, although they may regulate genes in a manner common to all vocal learners. A better understanding of the mRNA targets of these miRs will be required to parse out this hypothesis.

How might miRs in the brain affect vocal learning? As with other genes implicated in vocal learning, many miRs act early in development to regulate neurogenesis (Sun et al., 2013), which may contribute to the organization of brain structures underlying speech and vocal learning. In chick spinal cord, miR-9 acts through regulation of FoxP1 to direct motor neuron specification (Otaegi et al., 2011). In the ventricular zone of developing mouse and zebra fish brain, miR-9 promotes neural differentiation by suppression of proteins involved in the proliferation of neural stem cells (Tan et al., 2012; Coolen et al., 2012; Saunders et al., 2010; Shibata et al., 2011; Zhao et al., 2009). Similarly, miR-124 expression in the developing CNS is thought to direct cell differentiation to a neuronal fate by suppressing non-neuronal transcripts (Lim et al., 2005; Makeyev et al., 2007; Visvanathan et al., 2007; Cheng et al., 2009; Sanuki et al., 2011). miR-137 also regulates maturation of neurons (Smrt et al., 2010).

Additionally, miRs may have activational effects that support vocal learning. Several miRNAs impact neurite outgrowth and synaptogenesis. miR-9, for example, is expressed in axons of post-mitotic cortical neurons and limits or fine-tunes axon growth (Dajas-Bailador et al., 2012). Brain-derived neurotrophic factor (BDNF) indirectly affects axon growth through regulation of miR-9. Short BDNF application reduces miR-9 levels and subsequent growth of the axon, but prolonged exposure leads to an increase in miR-9 and a cessation of axon growth. In the songbird, BDNF is thought to be an important factor for neural connectivity between motor song nuclei in development and in adulthood in seasonal learners (Brenowitz, 2013). Additionally, predicted binding sites for miR-9 are found in the 3'-untranslated region of matrix metallopeptidase-9 (*MMP9*), an enzyme that affects synaptic morphology (Konopka et al., 2010). miR-9 represses both *Foxp1* (Otaegi et al., 2011) and *Foxp2* (Clovis et al., 2012; Shi et al., 2013), whereas Foxp2 promotes miR-9 expression in neuron-like cells in culture (Vernes et al., 2011).

This argues for the existence of a Foxp2/miR-9 feedback loop, in which miR-9 indirectly affects gene expression downstream of FoxP2. miR-29a/b changes dendritic spine morphology in hippocampus (Lippi et al., 2011). In *Aplysia*, miR-124 restricts serotonin-induced synaptic plasticity through regulation of CREB (Rajasethupathy et al., 2009). In mouse differentiating and adult primary cortical neurons, overexpression of miR-124 increases neurite outgrowth, whereas functional blockade causes a delay (Yu et al., 2008). miRs may affect synaptic plasticity by regulating synaptic molecules. miR-137 has potential binding sites in the 3'UTR of GluR1 mRNA, and miR-124 in *GluR2* (Konopka et al., 2010). Regulation of these proteins could impact the synaptic plasticity required for vocal learning.

Conclusions

Recent advances have augmented our understanding of the genetic basis for vocal learning by 1) uncovering new genetic factors through studies of human pathology, 2) discovering new vocal learning-related genes through network analysis of neural tissues pertaining to human speech and birdsong, and 3) gaining a better understanding of the physiological effects of known speech-related genes, such as *FOXP1*, *FOXP2*, and *CNTNAP2* using animal models. *FOXP2* was the first gene directly correlated with a language disorder, and through its molecular connections other language-related genes are being discovered, including those in the HGF signaling pathway. As small RNA regulatory factors become better cataloged, we are likely to learn even more about the genetic basis of vocal learning. Since convergent evolution has produced vocal learning in humans, other mammals, and songbirds, we might expect that there are overlapping genes between the clades, but equally we expect some

differences. This is likely the case with uPAR, which has no direct avian correlate, but is associated in human speech pathology. Continuing investigation into genes that affect language and vocal learning in other species will provide a better understanding of the mechanisms that govern this complex communicative behavior.

Figures

Figure 1-1: Schematic of human FOXP2 isoforms I-VI.

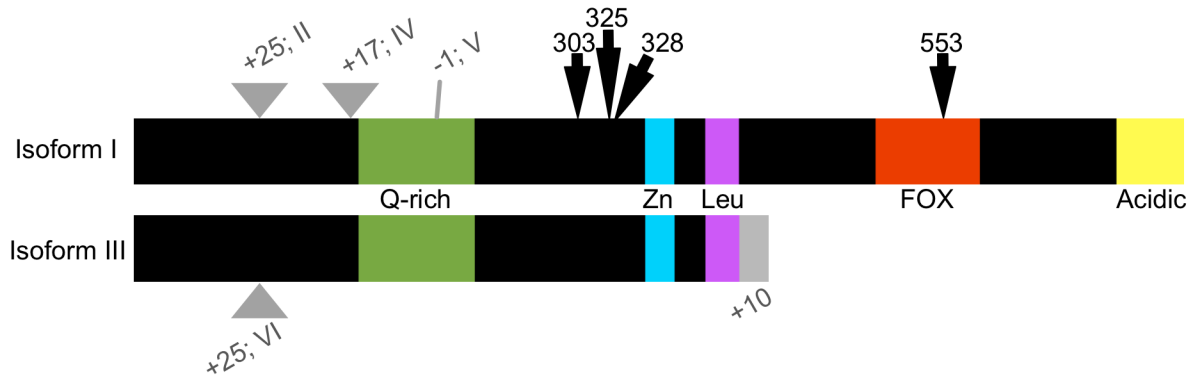

FOXP2 is alternatively spliced as two major isoforms: the full-length isoform I and a truncated isoform III. Variations of either major isoform contain inserted or omitted amino acids (II, IV-VI), indicated here as the difference in number of amino acids (gray triangles). Both major isoforms possess a glutamine rich (Q-rich) area, zinc finger (Zn) and leucine zipper (Leu) domains. Full-length isoforms of FOXP2 also possess a DNA-binding domain and an acid region on the C-terminus. Isoforms III and VI also have an additional 20 amino acids on the C-terminus that are not shared with the full-length isoforms. Arrows indicate amino acid substitutions between human and chimpanzee (303 and 325) or related to human speech disorders (328 and 553).

Figure 1-2: Schematic of human CNTNAP2.

Schematic of human CNTNAP2. CNTNAP2 consists of a single discoidin domain (DISC), four laminin-G domains (LamG), EGF repeats, a single transmembrane region (TM), and a putative protein 4.1 binding region (4.1m). CDFE indicates the subregion of the protein that is deleted in cases of cortical dysplasia-focal epilepsy in an Old Order Amish population (Strauss et al., 2006). Arrows indicate two other amino acid changes associated with language impairment (869 and 1129).

Chapter 2: Distribution of Language-Related Cntnap2 Protein in Neural Circuits Critical for Vocal Learning

Michael C. Condro and Stephanie A. White

Abstract

Variants of the contactin associated protein-like 2 (Cntnap2) gene are risk factors for language-related disorders including autism spectrum disorder, specific language impairment, and stuttering. Songbirds are useful models for study of human speech disorders due to their shared capacity for vocal learning, which relies on similar cortico-basal ganglia circuitry and genetic factors. Here, we investigate Cntnap2 protein expression in the brain of the zebra finch, a songbird species in which males, but not females, learn their courtship songs. We hypothesize that Cntnap2 has overlapping functions in vocal learning species, and expect to find protein expression in song-related areas of the zebra finch brain. We further expect that the distribution of this membrane-bound protein may not completely mirror its mRNA distribution due to the distinct subcellular localization of the two molecular species. We find that Cntnap2 protein is enriched in several song control regions relative to surrounding tissues, particularly within the adult male, but not female, robust nucleus of the arcopallium (RA), a cortical song control region analogous to human layer 5 primary motor cortex. The onset of this sexually dimorphic expression coincides with the onset of sensorimotor learning in developing males. Enrichment in male RA appears due to expression in projection neurons within the nucleus, as well as to additional expression in nerve terminals of cortical projections to RA from the lateral magnocellular nucleus of the nidopallium. Cntnap2 protein expression in zebra finch brain supports the hypothesis that this molecule affects neural connectivity critical for vocal learning across taxonomic classes.

Introduction

Language is a complex phenotype unique to humans, though facets of the behavior are shared with other species. Vocal learning, the ability to imitate or to produce novel sounds, is rare in the animal kingdom; so far found only in bats, cetaceans, elephants, pinnipeds, and songbirds. Humans are the only living primate species with this ability (Knornschild et al., 2010; Stoeger et al., 2012; Fitch, 2012). Genes underlying vocal learning and language are beginning to emerge with a major breakthrough being the identification of Forkhead Box P2 (FOXP2) as the monogenetic locus for a human speech disorder. (Abbreviations in all capitals denote the human form of the molecule, lowercase is used for animal homologs, and italics denote nucleic acids). FOXP2 is a transcription factor, and a mutation in its DNA binding domain leads to orofacial dyspraxia in a multigenerational pedigree known as the KE family (Lai et al., 2001). Additional FOXP2 mutations are associated with specific language impairment (SLI) and developmental verbal dyspraxia, further strengthening the link between the gene and language ability (Graham and Fisher, 2013). As a transcription factor, FOXP2's effects on language must be mediated through its gene targets. Chromatin immunoprecipitation has revealed that contactin associated protein-like 2 (*CNTNAP2*) is a direct transcriptional target of FOXP2 (Vernes et al., 2008). *CNTNAP2* is a particularly interesting target because it has independently been associated with a language-related disorder. Specifically, Old Order Amish children afflicted with cortical dysplasia-focal epilepsy (CDFE) harbor a deletion in *CNTNAP2*. CDFE is characterized by epilepsy, mental retardation, hyperactivity, impaired social behaviors, and language regression. A majority of affected children meet criteria for autism spectrum disorder (ASD), of which language impairment is a core deficit (Strauss et al., 2006). Within the general population, *CNTNAP2* polymorphisms are associated with language-related disorders, including increased

risk for ASD (Arking et al., 2008; Li et al., 2010), delayed age of first word (Alarcón et al., 2008), SLI (Whitehouse et al., 2011; Newbury et al., 2011), and decreased long-range connectivity of the medial prefrontal cortex (Scott-Van Zeeland et al., 2010).

The mechanistic basis of these disorders is still unclear. The best characterized function of Cntnap2 is to cluster voltage-gated potassium channels (VGKCs) to the juxtaparanodes of nerves (Poliak et al., 2003; Horresh et al., 2008). In the central nervous system, Cntnap2 may also affect synaptic development (Anderson et al., 2012). Transgenic mice lacking *Cntnap2* exhibit behavioral abnormalities reminiscent of patients with CDFE, namely epilepsy, hyperactivity, diminished social activity, repetitive behaviors, and reduced frequency of ultrasonic vocalizations when pups are separated from their dams (Penagarikano et al., 2011). This diminished vocal behavior could be due to vocal impairment or lack of motivation as a form of reduced social activity. In either case, this aspect of the model is limited because pup isolation calls are innate. Songbirds, including zebra finches, offer an advantageous model for studying the impact of Cntnap2 given that they are vocal learners with a well-characterized neural circuitry that underlies this ability.

Like other songbirds, zebra finches possess a distinct set of interconnected brain nuclei dedicated to vocal learning and production termed the 'song circuit' (Figure 2-1). The circuit consists of two pathways: the posterior vocal pathway, required for vocal production, includes a projection from the cortical nucleus HVC (proper name; Reiner et al., 2004a) to the robust nucleus of the arcopallium (RA), which in turn projects to the hypoglossal nucleus (nXIIts) that controls the avian vocal organ, the syrinx (Nottebohm et al., 1976). The anterior forebrain pathway (AFP), required for song modification (Brainard and Doupe, 2000a), begins with a

separate subset of HVC projections to the striatopallidal nucleus area X, which projects to the medial portion of the dorsolateral nucleus of the anterior thalamus (DLM), which then projects to the lateral magnocellular nucleus of the nidopallium (LMAN), which sends nerves terminals to RA as well as back to area X. This latter pathway is a cortical-basal ganglia-thalamo-cortical loop similar to the circuitry thought to underlie vocal learning in humans (Simonyan et al., 2012). An advantage of the zebra finch model is that vocal learning behavior and anatomy is sexually dimorphic. Females have an incomplete song circuit in which area X is not fully developed (Nottebohm et al., 1976), and RA is not innervated by HVC, causing the nucleus to shrink through apoptosis (Konishi and Akutagawa, 1985; Nixdorf-Bergweiler, 1996). Consequently, males begin to sing around 35d (Immelmann, 1969; Price, 1979), whereas females have never been observed to sing in nature. The sexually dimorphic singing behavior and the underlying song circuit anatomy make zebra finches an advantageous model for studying genes related to vocal learning including human speech.

As an initial step toward using songbirds as a model for vocal deficits associated with Cntnap2, Panaitof et al., (2010) described endogenous mRNA expression in the zebra finch. Remarkably, *Cntnap2* punctuates the song circuit with differential expression in song nuclei relative to their surrounding tissues. In juvenile and adult males, *Cntnap2* is enriched in two cortical song nuclei, RA and LMAN, but diminished in area X. In females, *Cntnap2* levels in RA and LMAN are equivalent to or lower than those of the surrounding arco- and nidopallium, respectively (Panaitof et al., 2010). Differential *Cntnap2* expression in the song circuit suggests that it serves a purpose in vocal learning (White, 2010; Hilliard et al., 2012a). If so, translation is required for any effects on anatomy or physiology. Protein expression does not always follow that of the encoding mRNA, with a precedent in songbirds for socially regulated translation

(Whitney and Johnson, 2005). We hypothesized that protein expression patterns would be largely similar to those for the mRNA, but with some differences due to post-transcriptional changes and to localization of the protein not only to cell bodies, but also along axons.

Here we validate an antibody against Cntnap2 for use in zebra finch tissue and describe the Cntnap2 protein distribution in the zebra finch brain at time points during male song development. We find that expression in song circuit neuronal cell bodies largely follows the mRNA but also highlights axonal connections critical for the vocal learning capacity. In line with this idea, within the sexually dimorphic nucleus RA, we identify projection neurons as the cell type that expresses Cntnap2 protein.

Materials and Methods

Animals and tissue preparation

All animal use and experimental procedures were in accordance with NIH guidelines for experiments involving vertebrate animals and approved by the UCLA Chancellor's Animal Care and Use Committee. Zebra finches (n=32 male and 21 female) between 25 and 500 days of age (d) used in this study were obtained from our breeding colony. Sex was determined based on sexually dimorphic plumage, or by postmortem identification of gonads at ages prior to the emergence of dimorphic plumage.

Antibody characterization

Cntnap2

In order to assess endogenous zebra finch Cntnap2 protein levels and distribution, a commercially available anti-Cntnap2 primary polyclonal antibody (Table 2-2) was selected for testing based on the perfect homology of the antigenic site (amino acids 1315-1331 in the C terminus of NCBI accession number NP_054860) between humans, rats, mice, and zebra finches. A translated nucleotide BLAST (National Center for Biotechnology Information, U.S. National Library of Medicine, Bethesda, MD) search revealed no other plausible targets in the zebra finch genome. The ability of this antibody to detect zebra finch Cntnap2 was vetted as described below (Figure 2-2).

Gapdh

Used here to measure relative levels of glyceraldehyde 3-phosphate dehydrogenase (Gapdh) as a loading control in Western analysis, the antibody (Table 2-2) detects a 38kDa band in mammalian lysates, according to the manufacturer. It has been previously used in Western analysis in mice (Jones et al., 2008; Fortune and Lurie 2009) and in zebra finch (Miller et al., 2008; Hilliard et al., 2012b), detecting a protein band ~36kDa in the latter animal.

Kvβ2

The Kvβ2 antibody (Table 2-2) was selected for use in zebra finch due to perfect homology of the antigenic site, amino acids 17-22 (TGSPG) of rat (accession number NP_034728) and zebra finch (NCBI RefSeq NC_011485.1). A translated nucleotide BLAST search revealed no other plausible targets of the antibody in zebra finch. Specificity of this antibody is described by the manufacturer. In Western analysis, the antibody detects a major protein band at 38kDa and a minor band at 41kDa in brain lysates from wild type mice, but no bands in lysates from knockout mice (http://neuromab.ucdavis.edu/datasheet/K17_70.pdf). Though the specificity of this antibody has not been confirmed for use in zebra finch, a recent study using this antibody found significant overlap of Kv1.1, Kv1.2, and Kvβ2 (Ovsepian et al., 2013) suggesting that even if the antibody is not specific to Kvβ2, it will at least have a similar immunostaining pattern. We use this antibody only to show that Cntnap2 colocalizes with potassium channel subunits and do not make any claims as to its specificity.

NeuN

The anti-NeuN antibody (Table 2-2) is used in this study to identify morphology in the zebra finch brain, as it was in Scott and Lois (2007). According to the manufacturer, the antibody detects protein bands at 46 and 48kDa in Western analysis.

Parvalbumin

The anti-parvalbumin antibody (Table 2-2) was characterized in Celio et al. (1988). It has since been used to detect the zebra finch isoform in immunohistochemistry to identify parvalbumin-positive neurons in song control nuclei (Wild et al., 2001; 2005; 2009; Roberts et al., 2007), as it is used in this study.

Cell Culture

Whole brain homogenate was obtained from an adult male zebra finch. Following overdose with inhalation anesthetic (isoflurane, Phoenix Pharmaceutical Inc., St. Joseph, MO), the brain was dissected without fixation and homogenized with a hand-held homogenizer (Kontes, Thermo Fisher Scientific, Pittsburgh, PA) in ice-cold modified RIPA lysis buffer with protein inhibitors (No. P8340, Sigma-Aldrich) and an RC DC Protein Assay (Bio-Rad, Hercules, CA) was performed to determine protein concentration as in (Miller et al., 2008). Zebra finch ZFTMA cells (Itoh and Arnold, 2011) which do not endogenously express Cntnap2 (Figure 2-2B) were transfected with either a pCR-TOPO vector (Life Technologies, Grand Island, NY)

containing the complete coding sequence for zebra finch Cntnap2 (Panaitof et al., 2010) or a pGIPz vector (Thermo Scientific, Lafayette, CO) containing the GFP coding sequence only, as a negative control. Cells were transfected using a Nucleofector II and chicken nucleofector solution (Lonza, Basel, CH) and distributed on BD Falcon tissue culture dishes (100x20 mm style, Fisher Scientific). At 24 hours post-transfection, GFP expression was observed in ~70% of cells in the plate transfected with the pGIPz vector (not shown). 48 hours after transfection, cells were dissolved in ice-cold modified RIPA lysis buffer with protease inhibitors and a protein assay was performed as above.

Western analysis

Samples of both brain homogenates and cell culture lysates were prepared for immunoblotting by diluting with 2X 5% betamercaptoethanol in Laemmli buffer (Bio-Rad) and storing at -80°C until use. Samples of 25 μg of brain and 100 μg of cell culture lysates were boiled for 2 minutes and then resolved on a 10% isocratic SDS-polyacrylamide gel in tris-glycine-SDS buffer (Bio-Rad) at 100 V. A Precision Plus Protein™ Dual Color Standard (Bio-Rad) was included on the gel as a molecular mass marker. Protein was then transferred onto a PVDF membrane with a pore size of 0.45 μm in Tris-glycine (Bio-Rad) with 20% methanol and 1% SDS. The membrane was blocked with 5% milk in Tris-buffered saline with 0.1% tween-20 (TBST) for 2 hours and then incubated with the anti-Cntnap2 antibody at 1:250 and anti-Gapdh (Table 2-2) at 1:100,000 in 2.5% milk-TBST overnight at 4°C. A replicate set of samples was incubated with the anti-Cntnap2 antibody that had been pre-adsorbed with antigenic peptide (Millipore, Temecula, CA) at a ratio of 1:30 by mass. Blots were then incubated with horseradish

peroxidase (HRP)-conjugated anti-rabbit and anti-mouse secondary antibodies (Table 2-3) at 1:2,000 and 1:10,000, respectively, in 2.5% milk-TBST for 2 hours. Blots were developed with ECL Plus, imaged on a Typhoon scanner (GE Healthcare), and signal specificity assessed.

Tissue staining and immunohistochemistry

Dissection and preparation of tissues

Birds of known age and sex were overdosed with isoflurane, then transcardially perfused with warmed saline followed by 4% paraformaldehyde in phosphate buffered saline (PBS). Brains were dissected out and cryoprotected in a 20% sucrose solution. 40 μm thick sections were cut in either the coronal or sagittal orientation on a cryostat (Leica Microsystems, Bannockburn, IL) and thaw mounted onto microscope slides (Colorfrost® Plus; Fisher Scientific, Pittsburgh, PA) in a manner that produced replicate sets of adjacent or near-adjacent sections, then stored at -80°C until use. Sciatic and optic nerves were dissected from 2 adult males following brain removal and fixed in 4% paraformaldhyde for 20 minutes, then transferred to PBS. Optic nerves were cryoprotected in a 20% sucrose solution overnight, then cryosectioned at a 10 μm thickness and mounted on microscope slides. Sciatic nerves were mechanically desheathed in PBS, teased, and dried on microscope slides.

Nerve tissue

Prior to immunostaining, sciatic nerve slides were frozen on dry ice for 5 minutes, then allowed to come back to room temperature. Slides containing nerve samples were post-fixed and permeabilized in methanol at -20°C for 20 minutes. A liquid repellent border (Liquid Blocker; Ted Pella Inc., Redding, CA) was drawn along the edges of the slide, and then the samples were rehydrated with phosphate buffer (PB). Samples were blocked with 10% goat serum diluted in PB with 0.1% Triton-X and 1% glycine for 1 hour, then incubated with the anti-Cntnap2 antibody diluted to 1:500 in blocking solution overnight at 4°C. After washing with PB, samples were incubated with anti-rabbit Alexa Fluor 488 (Table 2-3) at 1:1,000 in blocking solution for 4 hours. The procedure was then repeated with anti-Kvβ2 (Table 2-2) at 1:250 and anti-mouse Alexa Fluor 568 (Table 2-3) at 1:1,000. Glass coverslips were mounted on slides using ProLong Gold antifade reagent (Life Technologies).

Brain sections

One of the replicate sets of brain sections from each bird was used to identify those that contained song control nuclei, using 1% thionin staining to reveal cytoarchitecture. In some cases, sections were alternatively incubated with NeuroTrace™ fluorescent Nissl stain (Life Technologies) diluted at 1:200 in 0.1M PB for 20 minutes. For quantification of Cntnap2 positive neurons in RA, slides were chosen with those sections that contained the largest cross sectional area of RA, in order to control for position within the nucleus, and thawed to room temperature. A liquid repellent border was drawn along the edges of the slide, and then the sections were rehydrated with PB. Endogenous peroxidases were quenched with 0.05% hydrogen peroxide diluted in PB for 30 minutes. Sections were incubated with 5% goat serum in

PB containing 0.1% Triton-X for 1 hour. Anti-Cntnap2 antibody was diluted to 1:1,000 in PB and applied to the sections overnight at 4°C. Sections were then incubated at room temperature with a biotinylated goat anti-rabbit secondary antibody (Table 2-3) at 1:200 in PB for 1 hour, washed, then incubated with avidin-biotin complex (VECTASTAIN Elite ABC Kit (Standard*), Vector Laboratories) at 1:200 in PB with 0.1% Triton-X for 90 minutes. Sections were stained with fluorescein- or rhodamine-tyramide (Hopman et al., 1998) at 1:1,000 in PB with 0.1% Triton-X and 0.003% hydrogen peroxide. For double labeling, following Cntnap2 immunostaining, sections were incubated overnight at 4°C with either anti-NeuN or anti-parvalbumin antibodies (Table 2-2) at 1:1,000 in PB. Sections were then incubated at room temperature for 4 hours with anti-mouse Alexa Fluor 488, 555, or 568 (Table 2-3) diluted at 1:1,000 in PB. In the hippocampus, tyramide signal amplification was used for both labels. As above, peroxidase activity was quenched and sections were incubated with anti-NeuN at 1:500, then with anti-mouse HRP at 1:1,000 for 2 hours. These sections were then stained with rhodamine-tyramide as previously described. Peroxidases were quenched again with 0.3% hydrogen peroxide and Cntnap2 immunostaining followed as described above. Slides were mounted with glass coverslips using ProLong Gold antifade reagent (Life Technologies).

Surgical procedures

General methods

Adult male zebra finches were anesthetized with 2-4% isoflurane carried by oxygen using a Universal Vaporizer (Summit Anesthesia Support, Menlo Park, CA) for the duration of the

surgery. The bird was placed on a homeothermic blanket mounted in a stereotaxic apparatus at a 45° head angle from the center of the ear bars to the tip of the beak. The cranial feathers were removed to expose the scalp, which was then cleansed using povidone-iodine. In order to preserve vascular flow to the region, a semi-circular incision was made originating and terminating at the caudal edge of the exposed scalp. The scalp was then folded back over a Gelitaspon (Gelita Medical, Amsterdam, Netherlands) moistened with sterile saline, to expose the skull. Injections and recordings, described below, were made through ~1 mm^2 windows cut in the skull. After each procedure, the scalp was closed and sealed with Vetbond (Fisher Scientific).

Retrograde targeting of RA projection neurons

A ~1 mm^2 window was cut into the skull over the cerebellum ~0.4 mm from the midline, bilaterally. A carbon fiber electrode (Kation Scientific, Minneapolis, MN) was lowered into the brain 4.0 mm below the surface. Multiunit activity was amplified (A-M Systems, Sequim, WA), filtered (300 Hz highpass, 5 kHz lowpass), digitized at 20 kHz (Micro1401, CED, Cambridge, England) and recorded with Spike 2 software (CED). The location of nXIIts was determined by moving the electrode until multiunit activity corresponded to respiratory expiration. The carbon fiber electrode was then replaced with a glass electrode filled with Green Retrobeads™ IX (Lumafluor Inc., Naples, FL). Retrobeads were injected into nXIIts with a picospritzer (Toohey Co, Fairfield, NJ) 3 times on each side for 30 ms at 20 psi. Six days after the procedure each bird was euthanized and perfused with paraformaldehyde as described above.

LMAN lesions

A window was cut in the skull 5.15 mm rostral and 1.7 mm lateral of the midsagittal bifurcation for a unilateral injection. A glass electrode was filled with 10 mg/mL ibotenic acid (Fisher Scientific) in PB, pH 7.0, and lowered into the brain 2.0 mm from the surface to target LMAN and 96.6 nL were injected using a Nanoject II (Drummond Scientific, Broomall, PA). Four days after injection, birds were euthanized and brains collected and sectioned as described above. Sections containing LMAN were stained with thionin as described above to verify the extent of the lesion.

Cntnap2 protein quantification and analysis

Images were acquired using an Axio Imager.A1, with an AxioCam HRm digital camera or LSM 410 laser scanning confocal imager attached to an Axiovert 100 (Carl Zeiss Inc., Oberkochen, GE). Axiovision software (Carl Zeiss Inc.) was used to optimize photomicrographs to remove background, improve brightness and contrast, and to pseudocolor the images. For consistency, Cntnap2 is always represented here in green despite the true color of the fluorophore. In most cases, adjustments were made to the entire image and not to selective subregions, with the exception of the photomicrographs in Figure 2-2, in which artifacts of the immunostaining were removed. Anatomical regions were identified according to the published stereotaxic zebra finch brain atlas (http://www.ncbi.nlm.nih.gov/books/NBK2348/, courtesy of Dr. Barbara Nixdorf-Bergweiler and Hans-Joachim Bischof). ImageJ (Rasband 1997-2012) was

used to quantify Cntnap2 positive cells, as follows. First, a border was drawn around RA based on the density of NeuN immunoreactivity. For areas outside of RA, a 600 pixel diameter circle was drawn laterally from RA in either the dorsal (AD) or ventral (AIV) part of the arcopallium. Within the border, all NeuN and Cntnap2 positive cells were counted. The total counts for each signal were adjusted using the Abercrombie method (Guillery 2002) to reduce errors due to the two-dimensional counting method. Each count was multiplied by the tissue thickness (T) and divided by the thickness plus the average diameter of the objects counted (T+d). This adjustment (T/(T+d)) was calculated separately for each section analyzed, and reduced the raw counts by 11-33%, with an average of 24%. To control for the different sizes of RA across sections and animals, statistical significance was determined by non-parametric resampling (bootstrapping) of the ratios of Cntnap2 to NeuN counts. This was done in two stages. First, a modified two-way analysis of variance (ANOVA) compared sex, age, and the interaction effect. A Fisher's F statistic was calculated for each of the groups, then the groups were pooled and data was sampled with replacement 10,000 times, generating a range of pseudo-F statistics. Statistical significance was achieved when the F statistic from the real data was greater than 95% ($p<0.05$) or 99% ($p<0.01$) of the pseudo-statistics. Then, for groups with an ANOVA p-value below 0.05, modified Student's T-tests were performed for individual groups with the same resampling protocol as described for ANOVA, instead using a Student's T statistic.

Results

Antibody validation

Bioinformatic analysis revealed that the C-terminus of Cntnap2 is highly conserved between humans and zebra finches (Panaitof et al., 2010), and that the last 76 amino acids are identical (amino acids 1255-1331 in human, 1252-1328 in zebra finch: GVNRNSAIIGGVIAVVIFTILCTLVFLIRYMFRHKGTYHTNEAKGAESAESADAAIMNND PNFTETIDESKKEWLI). A commercial antibody available from Millipore and raised against C-terminus amino acids 1315-1331 of human CNTNAP2 (1312-1328 of zebra finch Cntnap2) was thus selected to test its ability to specifically detect the zebra finch isoform. In Western analyses of zebra finch whole brain homogenate, this antibody detects a single prominent band at the predicted molecular weight of ~180 kDa. Preadsorption of the antibody with the antigenic peptide considerably decreases the intensity of this band (Figure 2-2A). The specificity of the antibody was further validated by over-expressing zebra finch Cntnap2 (accession number NM_001193337.1) in ZFTMA cells (Itoh and Arnold, 2011), a zebra finch immortalized cell line which does not endogenously express the protein. Cultures transfected with zebra finch Cntnap2 produce the same protein band, whereas those from untransfected cultures (not shown) or transfected with a control construct containing sequences coding only for GFP do not (Figure 2-2B). Specificity of the antibody was again confirmed by preadsorption (see Materials and Methods).

The Millipore antibody was subsequently tested for use in immunohistochemistry. In mammals, Cntnap2 is expressed in axons of myelinated nerves, colocalized with VGKC subunits (Poliak et al., 1999; 2001). To verify that the Millipore antibody detects zebra finch Cntnap2 *in*

situ, we immunostained optic (Figure 2-2C-E) and sciatic (Figure 2-2D-F) nerves dissected from zebra finches for both Cntnap2 and Kvβ2. In both nerve preparations, the signals from the two antibodies overlap, as evidenced by the colocalization tools in ImageJ, further confirming that the antibody specifically detects zebra finch Cntnap2.

Cntnap2 protein distribution in the zebra finch brain

Similar to reported mammalian data (Poliak et al., 1999), Cntnap2 distribution is extensive in zebra finch brains, though not expressed to the same level in all regions. Particular enrichment is observed in myelinated areas consistent with axonal expression, such as the fronto-arcopallial tract, optic tract, optic chiasm (not shown), the lateral forebrain bundle (Figure 2-3A-C), and layer 5 of the optic tectum (Figure 2-3D-F). In the cerebellum, the Purkinje cell layer is marked by intense Cntnap2 immunostaining of cell bodies, and fibers containing Cntnap2 can be observed in the cerebellar white matter. Much less Cntnap2 is found in the granular and molecular layers (Figure 2-3G-I). In the midbrain, Cntnap2 is found in the parvocellular portion of the isthmus nucleus (not shown). Thalamic regions containing high levels of Cntnap2 include the anterior dorsomedial nucleus, dorsal portion of the lateral mesencephalic nucleus, rotund nucleus, lateral spiriform nucleus, and pretectal nucleus. In the telencephalon, enrichment of Cntnap2 is found in the entopallium, the anterior hyperpallium, striatopallidum, globus pallidus, field L (not shown), and cell bodies resembling pyramidal neurons (Montagnese et al., 1996) in the medial hippocampus (Figure 2-3J-L).

Within the song circuit of an adult male zebra finch, Cntnap2 protein distribution generally follows the mRNA distribution reported in Panaitof et al. (2010), with some exceptions. Though cortical nucleus HVC does contain Cntnap2 positive cells, expression is not enriched relative to the surrounding nidopallium (Figure 2-4A-C). As with the mRNA, cortical nuclei RA (Figure 2-4D-F) and LMAN (Figure 2-4G-I) have elevated Cntnap2 levels relative to the surrounding nido- and arcopallium, respectively. In contrast with the reported mRNA levels, the basal ganglia song control region, area X, exhibits greater Cntnap2 protein expression than the surrounding striatopallidum (Figure 2-4J-L). The Cntnap2 protein in the aforementioned areas is present not only on cell bodies, but also in the neuropil. The thalamic song nucleus DLM, however, has Cntnap2 positive cell bodies, but relatively less protein in the neuropil than the surrounding thalamic regions (Figure 2-4M-O).

Sexually dimorphic expression of Cntnap2 in RA

Cntnap2 mRNA expression is sexually dimorphic in LMAN and RA in developing zebra finches. Males have slightly more *Cntnap2* in LMAN than females throughout development, though the level of expression increases in both sexes with age. There is a more striking difference in expression in RA at 50d. Similar *Cntnap2* levels are detected in both sexes prior to 35d. Between the two time points, expression in females begins to decrease, while males maintain a high level through adulthood (Panaitof et al., 2010). We therefore compared levels of Cntnap2 immunostaining in RA in both sexes at developmental time points within sensory acquisition and sensorimotor learning periods, and after song crystallization (males, Figure 2-5A-E; females, Figure 2-5F-J). At 25 and 35d leading up to the onset of sensorimotor learning,

the fraction of RA neurons that are positive for Cntnap2 are comparably enriched in both sexes relative to the surrounding dorsal and ventral intermediate arcopallium (AD and AIV, respectively). However, by 50d, the fraction of Cntnap2 positive neurons in female RA significantly decreases (Figure 2-5L), and falls to levels comparable to those in AD and AIV (Fig 2-5M,N). This time point falls within the sensorimotor phase of vocal learning, during which males practice their memorized song (Eales, 1985). Male Cntnap2 enrichment in RA is maintained throughout development and into adulthood and crystallization of song, whereas in females it is significantly reduced. The difference in Cntnap2 protein expression within the arcopallium between males and females and at different developmental stages appears unique to RA. A comparison of the number of Cntnap2 enriched cells in AD and AIV reveals no significant effect of age or sex (Figure 2-5M,N).

LMAN projections contribute to Cntnap2 expression in RA

To test the possible contribution of LMAN terminals to Cntnap2 in RA, LMAN was unilaterally lesioned using ibotenic acid in three adult males (Figure 2-6A-C; Figure 2-6D-F; Figure 2-6G-I). The resulting Cntnap2 protein expression was observed in the ipsilateral RA and compared to that in the non-lesioned contralateral side. Somatic expression of Cntnap2 remained unaffected in the ipsilateral RA, but there was a decrement in immunostaining intensity in the neuropil compared with the contralateral RA, suggesting that some of the Cntnap2 is indeed from LMAN projections. In summary, within the vocal production circuit, Cntnap2 enrichment appears to be most prominent in RA and due to expression in both neuronal somata and neuropil, including that arising from within LMAN nerve terminals.

Cntnap2 is expressed in RA projection neurons

Within RA, Cntnap2 somal expression is restricted to a subset of the neuronal phenotypes. At least two distinct neuronal populations in RA have been defined based on their electrophysiological signatures and morphology: GABAergic interneurons, and glutamatergic projection neurons (Spiro et al., 1999). The latter directly synapse onto neurons within nXIIts, which directly innervates the syrinx. Parvalbumin staining has been used to differentiate these two types. Whereas some interneurons stain intensely for parvalbumin, projection neurons stain relatively weakly (Wild et al., 2001). To determine whether Cntnap2 is expressed in projection neurons, fluorescent retrobeads were injected into nXIIts (Figure 2-7A-C). Following retrograde transport, fluorescent signals colocalized with Cntnap2 signals in RA (Figure 2-7D-F), but not in cells that expressed a high level of parvalbumin (Figure 2-7G-I). Rather, we found that Cntnap2 signals overlapped only with weakly parvalbumin positive neurons, consistent with the interpretation that RA projection neurons express Cntnap2 (Figure 2-7J-L). The overlap of retrobeads with Cntnap2 signals further supports the hypothesis that Cntnap2 is expressed in RA neurons which project to nXIIts.

Discussion

Here we have characterized the protein distribution of Cntnap2, a molecule linked to human language disorders, in the brain of a non-human vocal learner, the zebra finch species of songbird. Because the neurons that are dedicated to vocal learning are clustered together in the songbird brain (Figure 2-1), this analysis enables direct comparison of Cntnap2 levels within song-dedicated neurons relative to their levels in surrounding tissues, which, though made up of similar cell types, contribute to non-vocal related functions. Moreover, the sexual dimorphism of vocal learning and the underlying song control circuitry allow us to compare protein expression between vocal and non-vocal learners within the same species. We can further draw parallels between humans and songbirds by investigating the cell types within a song nucleus in which we detect Cntnap2 expression.

Outside the song circuit, immunoreactivity is widespread throughout the telencephalon with areas of particularly high expression, such as in myelinated regions, and in the Purkinje cell layer of the cerebellum, and in pyramidal-like cells (Montagnese et al., 1996) in layers 2 and 3 of the hippocampus (Figure 2-3), similar to that described for mammals (Poliak et al., 1999). Notably, however, expression within several nuclei of the song circuit in the adult brain is strikingly different than in their respective surrounding regions, which are not part of the song control circuitry (Figure 2-4). In the AFP, Cntnap2 protein is enriched in cortical LMAN relative to the anterior nidopallium, in area X relative to the striatopallidum, and in the somata of DLM relative to the anterior thalamus. Though enrichment in LMAN and DLM is expected based on the mRNA data, the enrichment in area X is surprising given the lower transcript levels in this region relative to the surrounding striatopallidum (Panaitof et al., 2010). Cntnap2 protein is

found in the neuropil of area X leaving open the possibility that some of the protein arises from HVC and/or LMAN terminals, similar to the contribution of LMAN to Cntnap2 expression in RA (Figure 2-6). There is also somal Cntnap2 expression suggesting at least some protein originates in area X. The difference between the observed mRNA and protein data may reflect state-dependent regulation of the protein, perhaps by transcription factors such as FoxP2 (Teramitsu and White, 2006; Miller et al., 2008). Whether Cntnap2 is a direct target of FoxP2 in zebra finches, as it is in humans (Vernes et al., 2008), remains to be tested. The zebra finch genomic Cntnap2 sequence (RefSeq assembly ID GCF_000151805.1) contains many potential FoxP2 binding sites (Stroud et al., 2006), mostly in the first intron. The FOXP2 binding site in humans was confirmed to be in the first intron by chromatin immunoprecipitation (Vernes et al., 2008). The lower mRNA levels and higher protein in area X thus likely reflect a combination of cellular trafficking, transcriptional and post-transcriptional regulation. Whatever the mechanism, Cntnap2 mRNA and protein expression within the nucleus differs from levels in the surrounding tissue, despite the similar cell type composition of these subregions.

Cntnap2 protein distribution in the posterior pathway is similar to that for the mRNA. The amount within HVC is comparable to the surrounding nidopallium, whereas it is enriched in RA of males and juvenile females (Panaitof et al., 2010). The connectivity of the posterior vocal pathway in males suggests that RA-projecting neurons in HVC are analogous to mammalian neurons in cortical layer 2/3, which do not show prominent Cntnap2 staining, whereas RA projection neurons are analogous to mammalian cortical layer 5 pyramidal neurons (Jarvis, 2004), which exhibit prominent Cntnap2 levels (Poliak et al., 1999). The projection from RA to nXIIts is a corticospinal connection shared with mammalian motor cortex and is hypothesized to allow direct activation of individual muscles necessary for fine motor control (Vicario, 1991).

Notably, these direct connections onto motor neurons controlling the muscles involved in phonation are posited to enable the vocal learning capacity of select species such as humans and songbirds (Jürgens, 2009; Arriaga et al., 2012). Overlap of retrobeads injected into nXIIts in RA and Cntnap2 positive neurons (Figure 2-7) indicates that Cntnap2 is present in this connection, raising the possibility that Cntnap2 is required for its establishment and/or proper function. Additionally, the reduction of Cntnap2 in the neuropil of RA following an ipsilateral LMAN lesion (Figure 2-6) suggests that some of the enrichment in RA is provided from LMAN projections. This long-range connection is reminiscent of the connectivity that is altered in humans bearing the *CNTNAP2* risk alleles for ASD and SLI who exhibit increased local and decreased long-range connectivity of the medial prefrontal cortex (mPFC), and less lateralization than their non-risk allele counterparts (Scott-Van Zeeland et al., 2010). In fact, LMAN is postulated to be homologous to human PFC based on shared physiologic and anatomic features including connectivity (Kojima et al., 2013). Taken together, these parallel observations in humans and songbirds support the idea that Cntnap2 affects neural connectivity critical for vocal learning across taxonomic classes.

This hypothesis is further supported by the sexually dimorphic expression in zebra finch brain. Similar to that reported for *Cntnap2* mRNA, males and females share protein enrichment in RA early in development. However, by 50d the enrichment in female RA wanes, whereas it persists in males throughout adulthood. Since Cntnap2 is similarly enriched in RA in males and females prior to 50 days, the sexual dimorphism may reflect a change in cell composition in RA or a sex-based difference in gene expression within each cell. These data demonstrate a loss of Cntnap2 labeled cells in female RA with age. This may be due to preferential apoptosis (Konishi and Akutagawa, 1990) of neurons that express Cntnap2 or down regulation of both Cntnap2

mRNA and protein in female zebra finches, who do not use this nucleus for producing learned vocalizations. In mammals, some sex typical behaviors have been associated with sexually dimorphic expression of individual genes, supporting the hypothesis that sex-related behaviors driven by hormones are mediated in part by genes (Xu et al., 2012) or in fact by genes independent of hormones (Arnold et al., 2013). In the case of the zebra finch, genes that exhibit sexually dimorphic expression in song circuitry are likely to be involved, perhaps even crucial, for singing. These same genes may also be involved in human speech and language. This hypothesis was the basis for the prediction that FOXP1 mutations would impair human speech. FOXP1 is a transcription factor closely related to FOXP2, and the two form heterodimers to control gene expression. Sexually dimorphic expression of *FoxP1*, but not *FoxP2*, was found in the song circuit of quiescent zebra finches, leading to the aforementioned prediction (Teramitsu et al., 2004). Subsequently, several cases were described of FOXP1 mutations in people with language disorders (Carr et al., 2010; Hamdan et al., 2010; Palumbo et al., 2012; Pariani et al., 2009). The sexually dimorphic expression of Cntnap2 in RA also fits this pattern, and may in fact be regulated by FoxP1 in tandem or independent from FoxP2.

What might be the mechanistic function of Cntnap2 in the song circuit, or RA specifically? Cntnap2 is closely related to the neurexins, which have also been implicated in ASD (Südhof, 2008). Though neurexins function at the synapse, Cntnap2 is found at the juxtaparanodes of myelinated axons. There, it is responsible for the clustering of *Shaker*-type VGKCs (Poliak et al., 1999; 2003; Horresh et al., 2008). Selective blockade of these channels on axons from rat central nervous system during myelination early in development leads to aberrant action potential waveforms. However, when the animal becomes mature, application of the blocker no longer affects the waveform (Devaux et al., 2002). In songbirds, all song circuit

nuclei send and receive long-range connections, which may require Cntnap2 at a macrocircuit level to cluster VGKCs at juxtaparanodes in order to establish and/or maintain synaptic connections required for learning and producing vocalizations. Loss of Cntnap2 in the neuropil of RA following LMAN lesion is evidence for a macrocircuit role for Cntnap2 in this cortical-cortical connection. This suggests that if the role of Cntnap2 in clustering VGKCs is important for vocal learning, it will have the greatest impact early in development, while the process of myelination is still ongoing. Cntnap2 may have additional, yet unknown functions, suggested by *CNTNAP2* enrichment in human embryonic cortex well before myelination (Abrahams et al., 2007). Recent evidence suggests that Cntnap2 may influence synaptic connectivity, increasing cell-autonomous dendritic arborization and the number of synaptic sites in cultured neurons. Contactin 2, the binding partner of Cntnap2, appears to have the opposite effect on synaptic connectivity (Anderson et al., 2012). Contactin 2 and Cntnap2 together may affect the development of brain areas related to vocal learning and language. Cntnap2 may be important for microcircuit connectivity in song nuclei of the adult zebra finch brain as well, by establishing and maintaining local connections within each nucleus through increasing dendritic arborization and the number of active postsynaptic connections. According to this hypothesis, we expect that loss of Cntnap2 in male RA before the onset of sensorimotor learning would lead to fewer connections with HVC and an impaired ability to mimic the tutor's song.

Further investigation into the role of Cntnap2 in vocal learning in songbirds will certainly benefit our understanding of human speech disorders associated with risk variants of the gene, as well as the neurobiology of language as a whole. Taking advantage of the well-characterized song circuitry, an individual song nucleus could be targeted for Cntnap2 RNA interference. If Cntnap2 is involved in song learning, as it seems to be in human speech, we expect knockdown

to impair vocal learning in juvenile males, whose songs have not yet crystallized. This system may also be used to parse activational versus organizational effects of Cntnap2 in vocal learning by manipulating Cntnap2 levels at different times during development. Besides behavior, we additionally expect to find neurophysiological changes. Knocking down Cntnap2 in RA may result in a mislocalization of potassium channels, which could slow the repolarization phase of an action potential similar to the effects of blocking those channels, particularly prior to the completion of myelination (Devaux et al., 2002). There may also be changes to synaptic connectivity between RA and HVC or LMAN concurrent with decreased dendritic arborization of projection neurons originating in RA, similar to the effects reported *in vitro* reported by Anderson et al. (2012). Reducing Cntnap2 levels in LMAN may augment its local connectivity and decrease its long-range connectivity to RA, similar to the altered connectivity in forebrains of humans with risk variants of Cntnap2 (Scott-Van Zeeland et al., 2010). The balance between inhibition and excitation is also likely to be affected, as it is in cases of autism (Cline, 2005) and *Cntnap2* knockout mouse models (Penagarikano et al., 2011). The present and future investigation into the role of Cntnap2 in vocal learning using songbirds complements studies in mammals moving toward a better understanding of its associated disorders in humans.

Acknowledgements

The authors thank Melissa Coleman and Felix Schweizer for assistance in the use of their equipment for retrograde labeling, and confocal fluorescence imaging, respectively. Brett Abrahams and Hongmei Dong provided the zebra finch Cntnap2 cDNA construct used in tests of antibody specificity. Yuichiro Itoh and Arthur Arnold provided the ZFTMA cell line. Vijayendran Chandran identified potential FoxP2 binding sites in zebra finch Cntnap2. Thanks to Alice Fleming for advice on immunohistochemistry and to Julie Miller for revising drafts of this manuscript and guidance on the methodology used within. Thanks also to Dorsa Beroukhim, Guillermo Milian, and Diana Sanchez for their assistance with collecting tissue samples. The authors wish to acknowledge two anonymous reviewers for their constructive comments.

Tables

Table 2-1: List of Abbreviations Used in Figures in Chapter 2.

AD	dorsal arcopallium
AFP	anterior forebrain pathway
AIV	ventral intermediate arcopallium
Arco	arcopallium
Cntnap2	contactin associated protein-like 2
d	days of age
DLM	medial portion of the dorsolateral nucleus of the anterior thalamus
DMP	dorsomedial nucleus of the posterior thalamus
Gapdh	glyceraldehyde 3-phosphate dehydrogenase
GFP	green fluorescent protein
GP	globus pallidus
Gran	granule cell layer of the cerebellum
Hyper	hyperpallium
Kvβ2	potassium channel beta subunit
LFB	lateral forebrain bundle
LMAN	lateral magnocellular nucleus of the anterior nidopallium
Meso	mesopallium
Mol	molecular cell layer of the cerebellum
NeuN	neuronal nuclei
Nido	nidopallium
nXIIts	hypoglossal nucleus
Ov	ovoid nucleus
Pur	purkinje cell layer of the cerebellum
PV	parvalbumin
RA	robust nucleus of the arcopallium
St-P	striatopallidum
VGKC	voltage-gated potassium channel
X	area X
ZFTMA	zebra finch immortalized cell line

Table 2-2: Primary Antibodies.

Primary Antibody	Immunogen	Manufacturer	Catalog Number	Species
Cntnap2 (Caspr2)	Synthetic peptide corresponding to amino acids 1315-1331 of rat Caspr2, accession number NP_054860)	Millipore (Temecula, CA)	AB5886	Rabbit polyclonal
Gapdh	Purified GAPDH from rabbit muscle	Millipore	MAB374	Mouse monoclonal
Kvβ2	Amino acids 17-22 of rat Kvβ2 (accession number NP_034728), conserved in zebra finch	Neuromab (Davis, CA)	K17/70	Mouse monoclonal
NeuN	Purified cell culture nuclei from mouse brain	Millipore	MAB377	Mouse monoclonal
Parvalbumin	Parvalbumin purified from carp muscles	Swant (CH)	235	Mouse monoclonal

Table 2-3: Secondary Antibodies.

Catalog Number	Manufacturer	Reactivity	Conjugate
NA931	GE Healthcare, Piscataway, NJ	Mouse IgG	Horseradish peroxidase (HRP)
NA934	GE Healthcare	Rabbit IgG	HRP
A-11008	Life Technologies, Grand Island, NY	Rabbit IgG	Alexa-Fluor 488
A-11001	Life Technologies	Mouse IgG	Alexa-Fluor 488
A-21422	Life Technologies	Mouse IgG	Alexa-Fluor 555
A-11004	Life Technologies	Mouse IgG	Alexa-Fluor 568
B-1000	Vector Laboratories, Burlingame, CA	Rabbit IgG	Biotin

Figures

Figure 2-1: Diagram of the songbird brain.

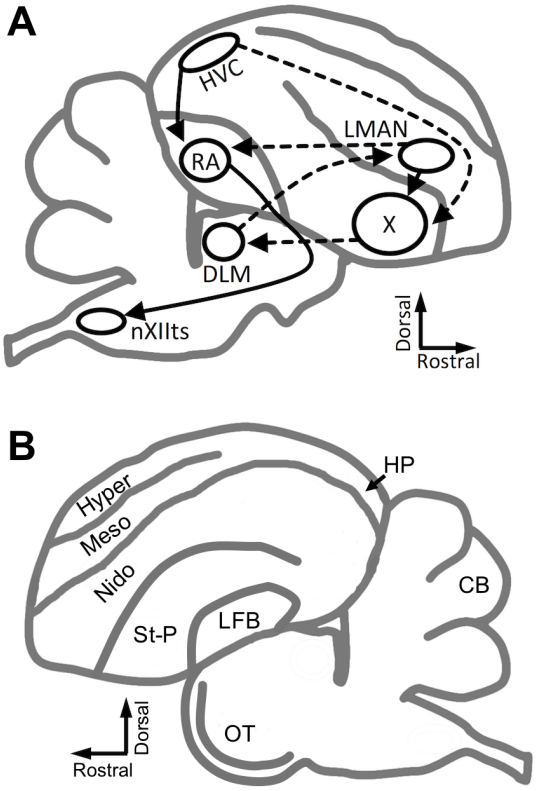

A) Schematic sagittal drawing depicts simplified song control circuitry. Solid lines indicate the posterior motor pathway, beginning with HVC, which projects to RA. RA directly projects to nXIIts, which controls the motor neurons of the syrinx. Dashed lines indicate connections of the AFP, in which HVC, X, DLM, and LMAN comprise a cortical-basal ganglia-thalamo-cortical loop like those underlying procedural learning in mammalian brains. LMAN completes the song circuit by projecting to RA, as well as back to X. **B)** Schematic sagittal drawing depicts non-song brain regions in which Cntnap2 immunostaining was analyzed in this study.

Figure 2-2: Antibody detection of zebra finch Cntnap2.

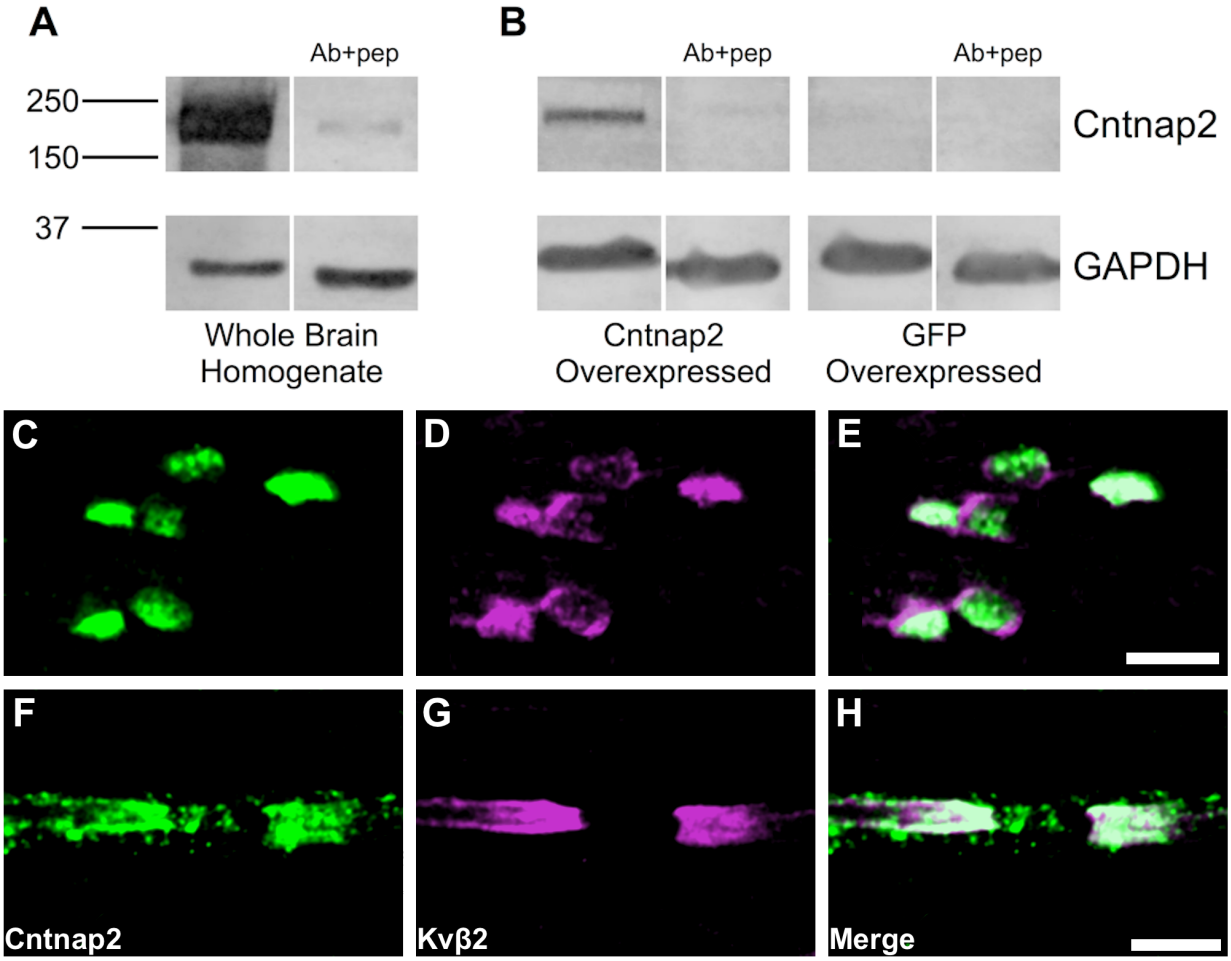

A) Western blot of zebra finch whole brain homogenate. Anti-Cntnap2 primary antibody detects a single prominent protein band at the predicted molecular weight (~180 kDa) for endogenous zebra finch Cntnap2. **B)** Western blots of the ZFTMA zebra finch established cell line with a plasmid expressing zebra finch Cntnap2 or GFP. Transfection of the Cntnap2 construct results in a detectable signal at the predicted molecular weight for Cntnap2 (left). In contrast, transfection of GFP results in no detectable signal at the same molecular weight, confirming no endogenous Cntnap2 expression in this skin-derived cell line (right). For each condition, preadsorption of the primary antibody with its antigenic peptide (Ab+pep) dramatically reduces or removes the

signal. Molecular weight markers are given in kDa. **C-E)** Zebra finch optic and **F-H)** sciatic nerves double labeled with Cntnap2 and potassium channel subunit Kvβ2 antibodies. Cntnap2 signal colocalizes with putative signals for potassium channel subunit Kvβ2 in both nerves, consistent with its expression in rodents (Poliak et al., 1999; 2003). Overlap of these signals in zebra finch nerves further validates the Cntnap2 antibody for use in this model. (Dotted green signals outside the putative nodal area in panels F and H are likely non-specific staining due to the thick tissue preparation). Scale bars = 10 μm C-E; 5 μm F-H.

Figure 2-3: Cntnap2 distribution in non-song circuit brain regions.

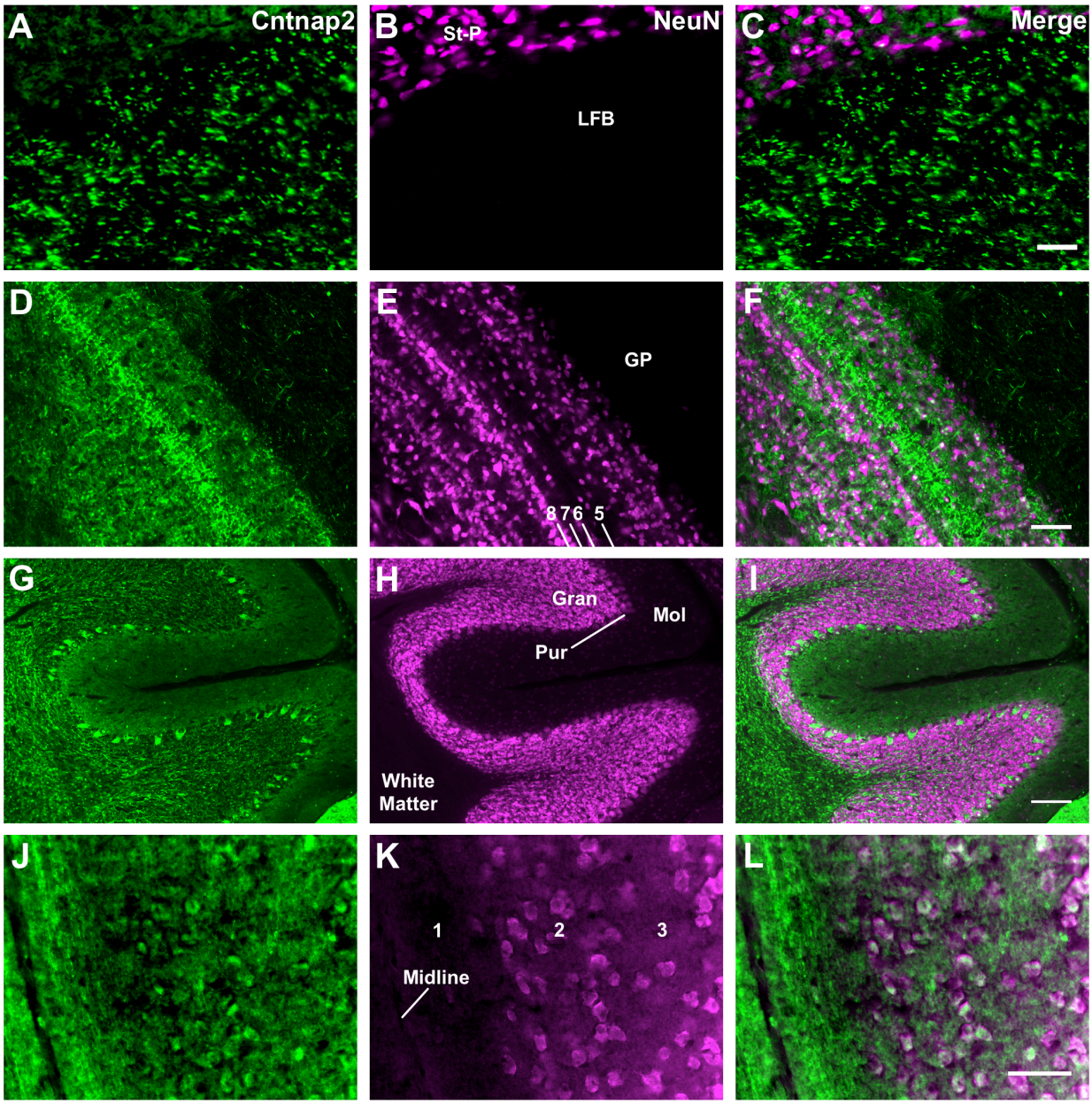

Cntnap2 is detected in several areas outside the song circuit of the zebra finch brain, including in structures reported to express Cntnap2 in rodents (Poliak et al., 1999). Non-song circuit tissue in this figure are taken from regions depicted in Figure 2-1B. Neuron specific marker NeuN (magenta) is used for reference. **A-C)** Axonal patterning of Cntnap2 label in the lateral forebrain

bundle within the telencephalon. **D-F)** intense Cntnap2 (green) labeling along axons in layer 5 of the optic tectum. Numbers in 3B indicate the layers of the optic tectum according to Ramón y Cajal (1911). **G-I)** Purkinje cell bodies and the cerebellar white matter strongly express Cntnap2, with less in the molecular layer, and fibrous signal in the granular layer and white matter. **J-L)** Coronal section of the medial hippocampus; numbers indicate layers (Montagnese et al., 1996). Cntnap2 marks neuronal somata in the pyramidal cell region (white arrows). Scale bars = 50 μm A-C; 200 μm D-L.

Figure 2-4: Cntnap2 protein in song circuit nuclei.

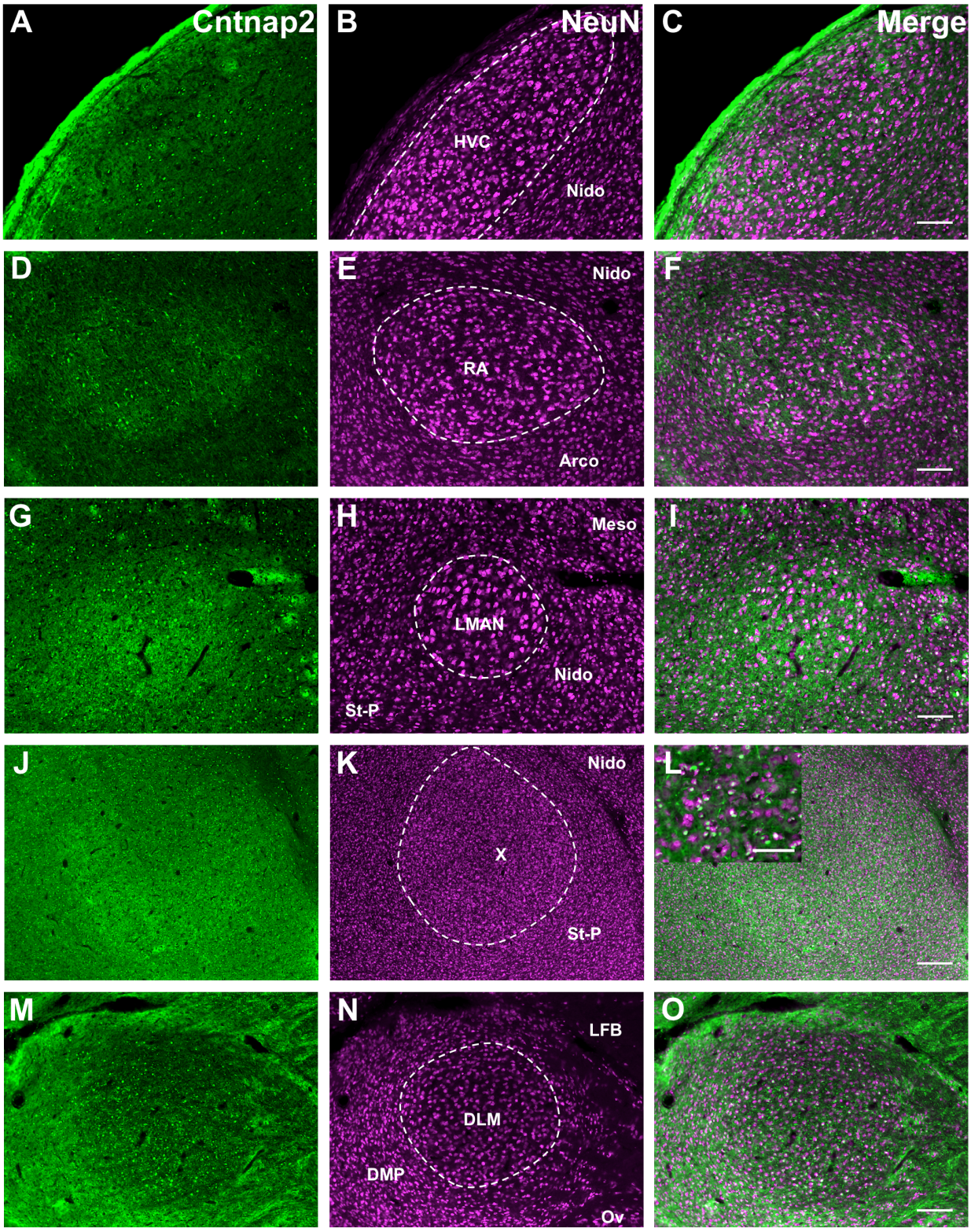

Fluorescent photomicrographic images of song control nuclei. Cntnap2 signals are in green, and NeuN signals in magenta. **A-C)** HVC in the nidopallium; **D-F)** RA in the arcopallium; **G-I)** LMAN in the nidopallium; **J-L)** Area X in the striatopallidum, inset: higher magnification inside X; **M-O)** DLM in the thalamus, along with the ovoid nucleus, the dorsomedial nucleus of the posterior thalamus, and the lateral forebrain bundle. Each nucleus is indicated by dashed line traces on the NeuN (middle column) panels. Greater Cntnap2 labeling is found within RA, LMAN, and area X relative to surrounding brain regions on both cell bodies and in the neuropil. HVC and DLM contain Cntnap2-expressing cells, but with expression levels comparable to their surrounding tissues. Scale bars = 200 μm A-I; 100 μm J-L (50 μm inset); 200 μm M-O.

Figure 2-5: Cntnap2 within RA in both sexes at developmental time points during male song learning.

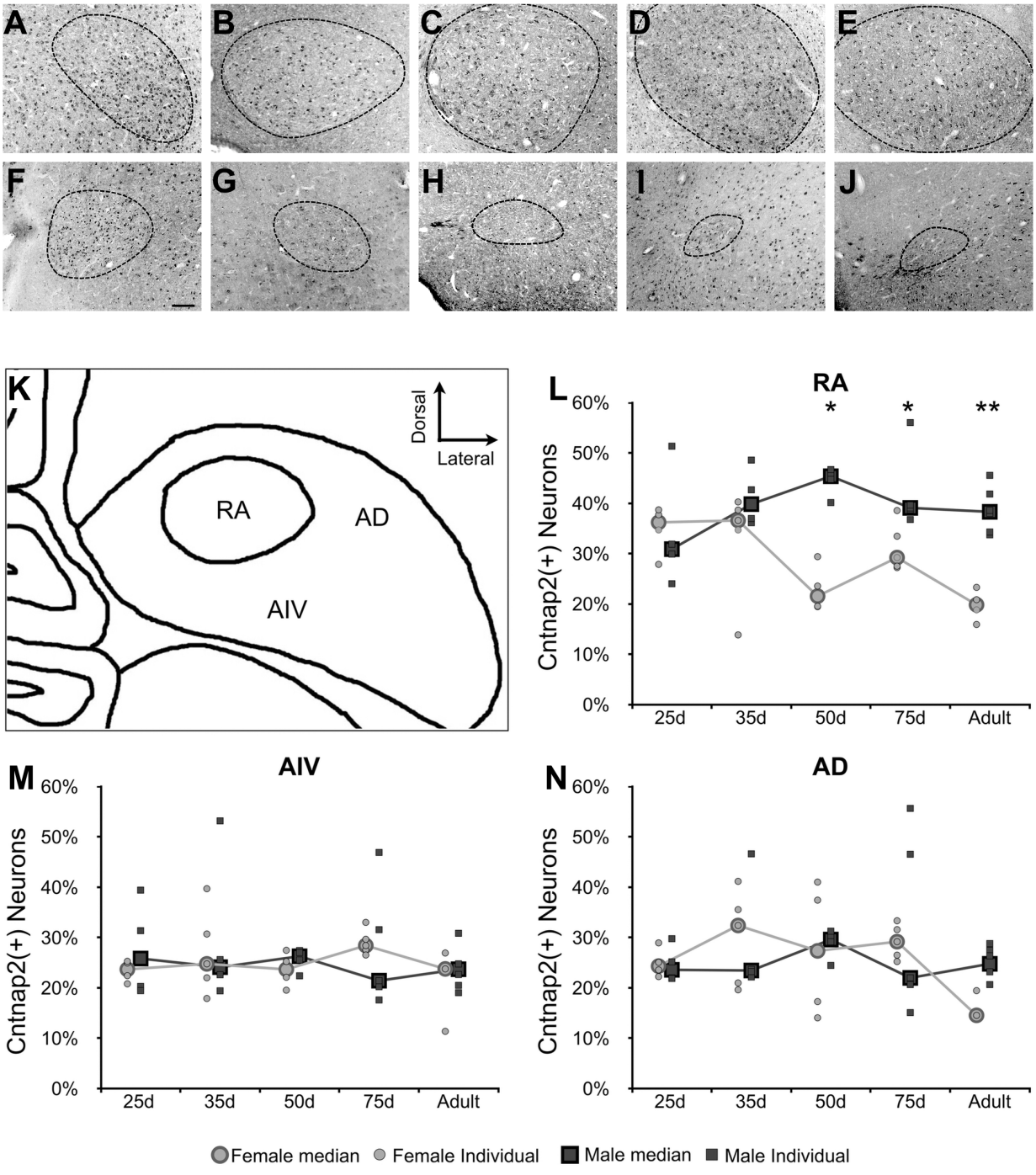

A-J) Representative images of Cntnap2 immunolabeling of cells in male (A-E) and female (F-J) RA at time points during development encompassing the onset of sensory acquisition,

sensorimotor learning, and crystallization of song. Anti-NeuN signals (not shown) were used to trace the border of RA in each image. As previously reported (Konishi and Akutagawa, 1985), the size of RA begins to decrease in females and increase in males starting around 35d and continues through development until maturity. **K)** A diagram of RA and the two arcopallial regions in which labeled cells were counted: the ventral intermediate arcopallium (AIV) and the dorsal arcopallium (AD)**. L-N)** Graphs representing the percentage of Cntnap2 positive neurons out of the total number of NeuN positive cells found in RA, AIV, and AD, respectively, for 3-6 birds of each sex at each time point. Statistical significance was determined by resampling ANOVA, followed by individual Student's T-tests *$p<0.05$, **$p<0.01$. Scale bar = 100 μm.

Figure 2-6: Unilateral LMAN lesions result in an ipsilateral decrease of Cntnap2 in RA.

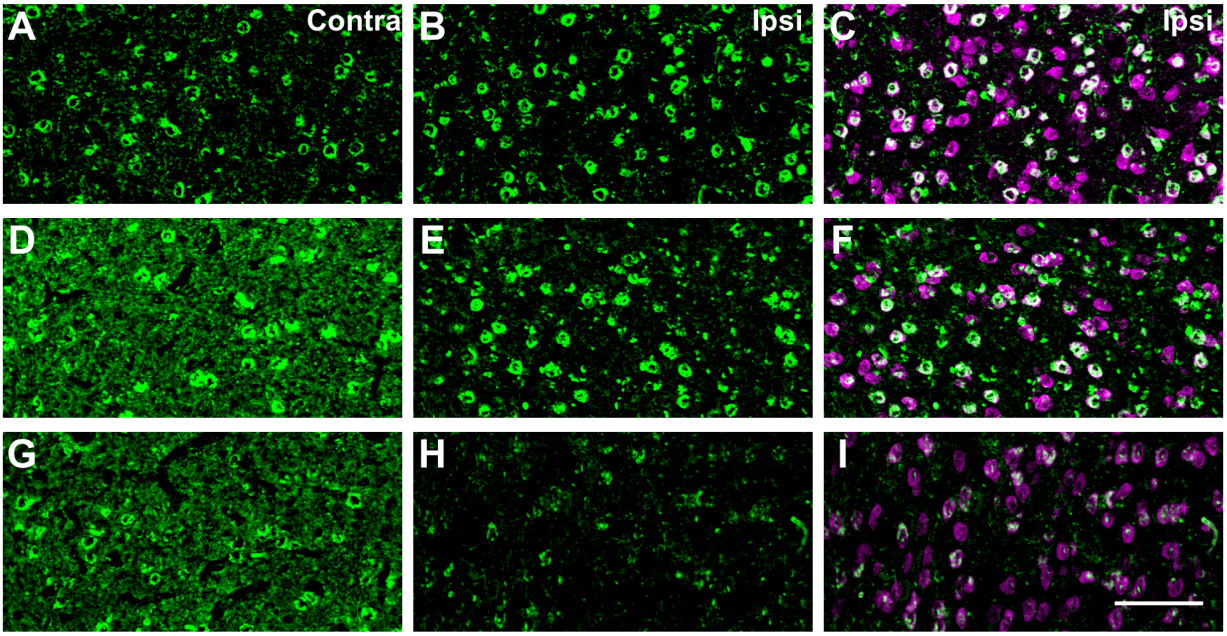

Representative photomicrographic images of Cntnap2 labeling (green) in RA from three adult male zebra finches (**A-C, D-F, G-I**) in which LMAN was lesioned unilaterally by injection of ibotenic acid. Double labeling with NeuN (magenta; C,F,I) indicates neuronal cell bodies. In all cases, the lesion reduces the amount of Cntnap2 in the neuropil, but not cell bodies, in ipsilateral RA relative to the contralateral nucleus, indicating that some of the Cntnap2 in the neuropil originates from LMAN projections. Scale bar = 25 μm.

Figure 2-7: Cntnap2 is expressed in RA projection neurons, not parvalbumin positive interneurons.

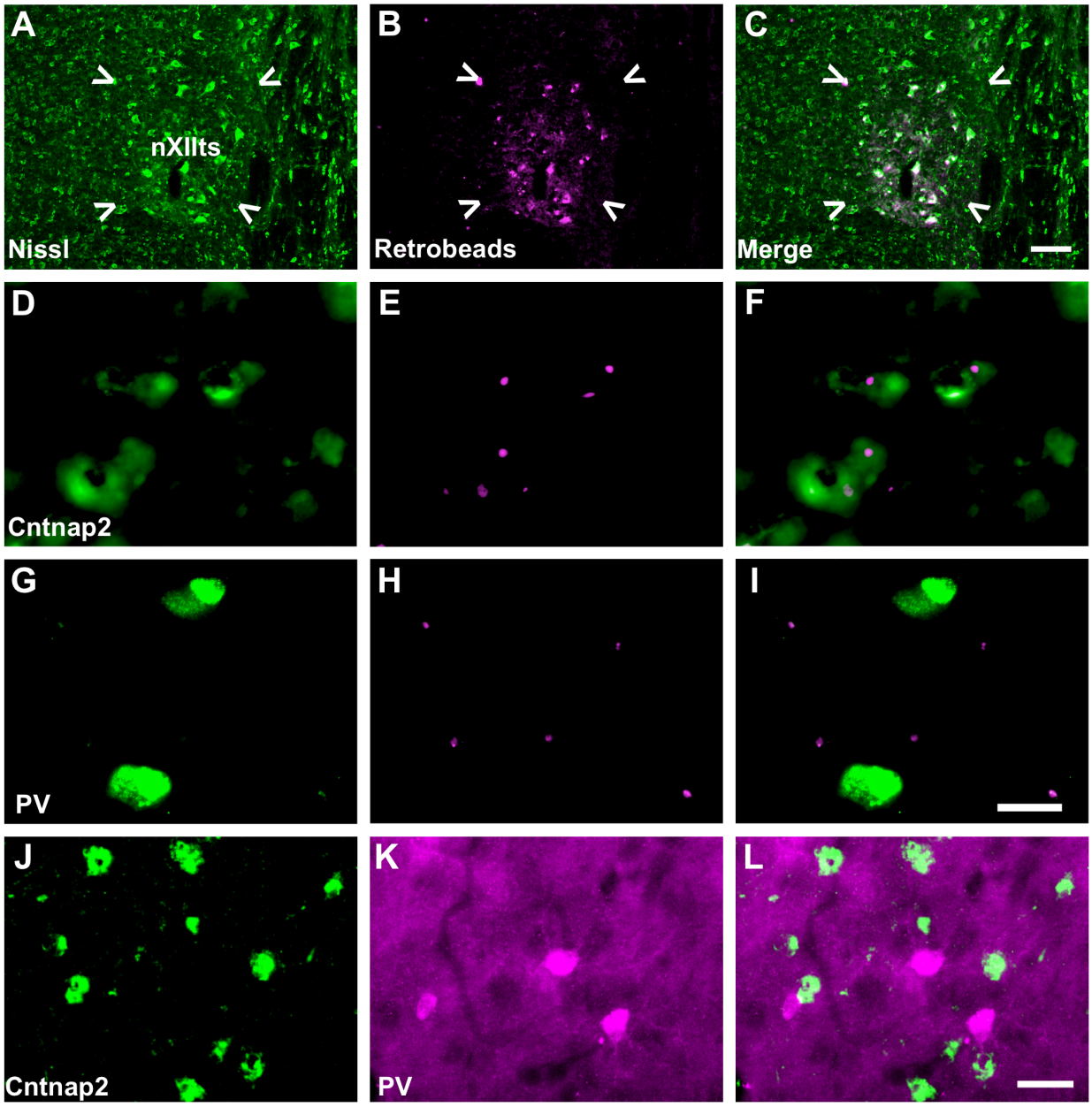

A-C) Injection site of retrobeads (magenta) in nXIIts (indicated by white arrows), identified by Nissl stain (green). **D-F)** Retrobeads overlap with Cntnap2 (green) expressing cells in RA. **G-I)**. Retrobeads do not overlap with strongly parvalbumin positive interneurons. **J-L)** Cntnap2 immunolabeling (green) does not overlap with RA inhibitory interneurons intensely labeled with

parvalbumin (magenta). Retrograde labeling reveals that RA projection neurons express Cntnap2 and confirms its absence in parvalbumin positive interneurons. Scale bar = 50 μm A-C; 20 μm D-I; 25 μm J-L.

Chapter 3: Toward Attenuation of Cntnap2 Expression in the Zebra Finch Song System

Michael C. Condro

Abstract

Variations of *CNTNAP2* are associated with disorders that are characterized by human language impairments. Cntnap2 protein distribution in the zebra finch song system suggests that it functions in the learned vocalizations of this species as well. Specifically, neural expression within the song motor control cortical area known as RA is enriched in males, who learn their songs, yet wanes in females, who do not, over the course of development. To test the impact of Cntnap2 in RA of male zebra finches, I vetted 10 shRNA constructs in cell culture for the ability to knock down the target protein, in two rounds. The first round of constructs yielded no shRNAs that effectively reduced Cntnap2 protein. The second round of constructs were designed and tested first as siRNAs, all of which reduced Cntnap2 protein >70%. These siRNAs were then converted into shRNAs, and their ability to knockdown Cntnap2 was reconfirmed in culture. An adeno-associated virus was assessed as a vehicle for *in vivo* transgene expression in RA. The virus transduces RA neurons, including those that project to the brainstem motor neurons that control the song organ. No somal expression of the transgene was detected in other song circuit nuclei. These molecular and viral tools will prove useful for investigating the function of Cntnap2 in the zebra finch song system.

Introduction

The endogenous distribution of Cntnap2 in the zebra finch brain suggests a role in song learning (Chapter 2). There is enrichment in two cortical song nuclei, the robust nucleus of the arcopallium (RA) and the lateral magnocellular nucleus of the nidopallium (LMAN), relative to their surrounding cortical regions. The enrichment in RA is age-dependent and sexually dimorphic. Before the onset of sensorimotor learning, Cntnap2 is enriched in RA in both males and females. However, during the sensorimotor learning period, the fraction of Cntnap2-positive neurons declines in female RA to levels comparable to neighboring arcopallial regions. The neurons that express Cntnap2 are projection neurons that synapse onto the motor neurons of the hypoglossal nucleus, which controls the muscles of the vocal organ. These neurons are analogous to pyramidal neurons in mammalian layer 5 primary motor cortex that innervate the motor neurons of the larynx (Jarvis, 2004). The correlation between the reduction of these Cntnap2-expressing cells and the onset of vocal learning in male finches suggests that Cntnap2 is necessary for the male behavior and may play a similar in human speech.

To test this hypothesis, Cntnap2 expression will be experimentally manipulated in male zebra finches and the resulting behavioral and physiological effects will be analyzed. Though a recent report describes methodology for generating transgenic zebra finches (Agate et al., 2009), there are several reasons to instead to knock down Cntnap2 through virally-mediated gene expression. First, production of transgenic zebra finches is laborious and inefficient. The process involves removing a small piece of eggshell to gain access to the embryo, then injecting a lentivirus containing a plasmid with transgene, and subsequently sealing the hole in the egg and returning it to the nest after a brief period in an incubator. The reported survival rate of the

injected eggs is quite low (13%), but most of those that do survive exhibit mosaic expression of the transgene. These mosaic animals may then be bred with uninjected partners to produce transgenic offspring. Agate et al. were able to produce three such offspring from 265 eggs injected, resulting in a 1.1% success rate. Despite this effort, the benefits are relatively few. Though transgene expression can be restricted to neuronal cell types by driving expression through a human synapsin I promoter (Teramitsu, 2007), as yet there are no proven methods for restricting expression to specific neuronal subtypes in this species. It is therefore possible that the transgene could have off-target effects, beyond song learning, such as general physiology or other behaviors.

Such a global influence can be ideal when used to model the general pathology of genetically based human disorders. For example, human variation in *CNTNAP2* is associated with autism (chapter 1), Tourette syndrome (Verkerk et al., 2003), schizophrenia, and epilepsy (Friedman et al., 2008; Poot et al., 2011). *Cntnap2* knockout mice exhibit behavioral abnormalities similar to humans afflicted with cortical dysplasia-focal epilepsy (CDFE), a disorder caused by a *CNTNAP2* loss of function mutation (Penagarikano et al., 2011; Strauss et al., 2006). These transgenic mice are hyperactive, less inclined to interact with conspecifics, and exhibit behavioral inflexibility in non-social behaviors. While these mice are valuable models for studying the overall effects of loss of *Cntnap2*, it can be difficult to isolate the specific effects on individual behaviors. For example, homozygous *Cntnap2* knockout mouse pups make fewer ultrasonic distress calls when separated from the dam, than do their wild type littermates. One interpretation is that Cntnap2 loss effects processes specific to vocalization, but an alternate explanation is that the pups are less motivated to call due to social impairments associated with the mutation. Similarly, developing a zebra finch that transgenically represses Cntnap2 may

result in non-vocal behavioral effects that could potentially confound any effects on song learning. Compromised sociability in affected young male zebra finches may obstruct song learning by resulting in fewer interactions with the tutor. Affected adult males may be less likely to sing to pursue mates. Though the full impact of Cntnap2 loss on zebra finch social interactions would be an interesting subject of study *per se*, it is not the immediate goal of the current study.

Instead we seek to isolate the vocal learning deficits associated with loss of Cntnap2. The advantage of the songbird vocal production system is the distinct nuclei dedicated to song learning and production (Doupe and Kuhl, 1999). These include cortical nuclei HVC (proper name), LMAN and RA, striatopallidal nucleus area X, and the medial part of the dorsolateral nucleus of the anterior thalamus (DLM; Figure 3-1). These nuclei can be targeted stereotaxically or through their signature electrophysiological activity. Lentiviral vectors have been used to constitutively overexpress singing-regulated genes in area X and LMAN (Wada et al., 2006) and to express short hairpin RNAs (shRNAs) to knock down FoxP2 exclusively in area X, without affecting the rest of the brain (Haesler et al., 2007). FoxP2 knockdown in juvenile males results in an impaired ability to replicate the song of the tutor compared to controls. Targeting of the song nucleus reveals the effects of gene manipulation with specific reference to the vocal learning behavior. In the case of Cntnap2, a targeted virus-mediated transgene delivery strategy will isolate the effects of the knockdown to vocal behavior, presumably without the other symptoms of Cntnap2 mutation in humans or knockout mice, such as impaired social interactions, repetitive behaviors, hyperactivity, or epilepsy (Strauss et al., 2006; Penagarikano et al., 2011).

Here, we test RNA interference constructs targeting zebra finch Cntnap2 for use *in vivo*. Several constructs were tested against zebra finch *Cntnap2* in cell culture. Two shRNA

constructs were found to reduce Cntnap2 protein expression by >70% individually, and three combinations of two were similarly effective. Additionally, an adeno-associated virus (AAV) serotype 5 was vetted as a vector to transduce RNAi constructs in RA neurons. These tools will be used to test the hypothesis that reduction of Cntnap2 expression in RA of juvenile males will impair song learning.

Materials and Methods

Cell Culture

Zebra finch primary telencephalic culture

2-4 hatchling zebra finches 1-4 days old were rapidly decapitated, telencephali quickly extracted and stored temporarily in Leibovitz's L-15 medium (Fisher Scientific, Cat. No. 21083-027) on ice. The hemispheres were separated with a scalpel blade, then the meninges carefully removed with forceps. Each hemisphere was bisected, then transferred to a 15mL conical tube and excess media was aspirated. Cells were digested with 0.5% papain (Sigma Aldrich, St. Louis, MO, Cat. No. P-4762), 0.03% bovine serum albumin (BSA; Sigma Aldrich, Cat. No. A7030), in L-15 medium heated to 37°C for 15 minutes. Cells were dissociated by triturating with glass pipettes with increasingly smaller diameters for 15 minutes. Solution containing the dissociated cells was strained with a 70μm strainer. The density of dissociated cells in medium was estimated by adding 10μL trypan blue (Sigma Aldrich, Cat. No. T8154) to an equal volume of cell suspension and counting on a hemacytometer.

HEK 293 cell culture

Human embryonic kidney (HEK) 293 cells were received as a gift from Professor Kelsey Martin at UCLA in the form of a 1mL culture frozen in liquid nitrogen. The culture was rapidly heated to 37°C in a water bath, then added to 9mL of 37°C HEK cell culture medium, comprised of Dulbecco's modified eagle medium (DMEM; Life Technologies, Cat. No. 11995-065) with

10% fetal bovine serum (FBS; Life Technologies, Cat. No. 10082-139) and 1% Antibiotic-Antimycotic solution (Life Technologies, Cat. No. 15240-062). Cell suspension was centrifuged at 500rcf for 5 minutes, then the supernatant was discarded, leaving a cell pellet. Cells were resuspended in fresh culture medium, then plated in 10cm petri dishes (Fisher Scientific, Waltham, MA; Cat. No. 353003) and incubated at 37°C with 5% CO_2. Cells were passaged as needed to keep the density on the plate below confluence by sucking up culture medium in a Pasteur pipette and releasing it to apply pressure to dissociate cells from the plate. Cells were then re-plated at a higher dilution, sometimes onto multiple plates. Aliquots of HEK cultures were frozen by dissociating cells from a nearly confluent plate, centrifuging at 500rcf for 5 min, reconstituting cells in 750μL culture medium, then adding and equal volume of culture medium with 20% dimethyl sulfoxide (DMSO; Fisher Scientific, Cat. No. BP231-100) dropwise while vigorously mixing. The cell suspension in 10% DMSO was immediately frozen to -20°C for 2-4 hours before freezing to -80°C for 16-24 hr. Frozen cultures were permanently stored in liquid nitrogen.

RNAi Design and Construction

siRNA

Three short interfering RNA (siRNA) constructs were designed using the BLOCK-iT™ RNAi designer. In order to ensure that both splice variants of Cntnap2 would be targeted by the same construct, only the part of the zebra finch Cntnap2 cDNA (NM_001193337) corresponding to the last 140 amino acids of the resulting protein (nucleotides 4104-4524), comprised of the C-

terminus, the transmembrane region, and part of the extracellular domain between the transmembrane region and the first laminin-G domain (Figure 3-1). These regions were included for targeting based on the alternative splicing of closely-related neurexin-1, which includes the homologous regions and a single laminin-G domain (Kleiderlein et al., 1998; Ushkaryov et al., 1994). The four 19mer siRNA designs rated highest by the BLOCK-iT™ design tool were chosen for further processing, named each named for its corresponding start position on the zebra finch Cntnap2 cDNA: siRNA-4282, -4288, -4372, -4502. Criteria for each siRNA maintaining candidacy were 1) no more than 1 mismatch with the zebra finch *Cntnap2* genomic sequence, 2) no less than 2 mismatches with any transcript in either the zebra finch genome or EST libraries, 3) no less than 2 mismatches with any transcript in the human genome or EST libraries. The last criterion was included so that the siRNAs can be tested against zebra finch Cntnap2 overexpressed in a human embryonic kidney (HEK 293) established cell line. Since the HEK 293 cell line demonstrated no endogenous CNTNAP2 expression (personal observations), homology between the candidates and human *CNTNAP2* was not included as a criterion, though a BLAST search failed to match the candidates to the human sequence. All four candidates met the first two criteria. All sequences matched the genomic zebra finch *Cntnap2* sequence, except siRNA-4372, for which only the 19th base was T in the siRNA and C in the corresponding genomic position. Only siRNA-4502 failed the third criterion, having only a single mismatch with a human transcript for AGT protein. Therefore, only siRNA-4282, -4288, and -4372 were considered for knockdown of zebra finch Cntnap2. siRNA duplexes with fluorescein tags on the 5' end of the guide strand were purchased from Life Technologies (Carlsbad, CA).

shRNA

19mer siRNA sequences were modified to 21mer shRNA through the BLOCK-iT RNAi designer by restricting the input target sequence from the zebra finch Cntnap2 cDNA to 100bp surrounding the 4282, 4288, and 4372 target sites. In this way the algorithm chose which nucleotides to each sequence. An additional shRNA, 4328, was generated using the same algorithm, but using nucleotides 4104-4524 of the zebra finch Cntnap2 cDNA as an input. Each 21mer was again modified to a 22mer by adding the nucleotide to the 5' end that corresponds to the target site, as in Dow et al. (2012).

pCIGRNAi plasmid empty vector (Megason and McMahon, 2002) and a pCIGRNAi plasmid containing a non-targeting shRNA (shGEN; Skaggs et al., 2011) was obtained as a gift from Bennett Novitch. The procedure for cloning shRNAs into the vector were adapted from Van Hateren et al. (2009) and briefly described here. All primers described in the following section were obtained from Life Technologies. Specific forward primers consisted of each shRNA target sequence with a mismatched nucleotide on the 5' end (A switched to C, T switched to G, and vice versa) flanked on the 5' end by AGGTGCTGCCAGTGAGCG and on the 3' end by TAGTGAAGCCACAGATGTA. Specific reverse primers consisted of each shRNA target sequence (without the mismatch) flanked on the 5' end by CACCACCACCAGTAGGCA and on the 3' end by TACATCTGTGGCTTCACT.

Oligonucleotides for insertion into the pCIGRNAi vector were constructed by polymerase chain reaction. For each shRNA, 200ng each specific forward and reverse primer was combined with 2μL each of 10μM universal forward and reverse primers, 25μL GoTaq® Green Mastermix (Promega, Madison, WI, Cat. No. M712B), and nuclease-free water added for

a final volume of 50μL. Each reaction was initially heated to 95°C for 2 minutes, then subjected to 40 cycles of melting at 95°C for 30s, annealing at 55°C for 30s, and elongating at 72°C for 60s. After the last cycle, the reaction was finished with a final elongation step for 4 min. The entire PCR reaction was resolved on a 2% agarose gel, and the ~180bp band was extracted using a gel extraction kit (PureLink™, Life Technologies, Cat. No. K2100-12). The entire elution was digested in a 50μL reaction with one unit each FastDigest NheI and MluI (Thermo Scientific, Waltham, MA, Cat. No. FD0974 and FD0564, respectively). PCR digests were again resolved on a 2% agarose gel and the ~180bp band extracted. pCIGRNAi vector was linearized by digestion with one unit each of NheI and MluI, then treated with calf intestinal alkaline phosphatase (Life Technologies, Cat. No. 18009-027), and purified with a PCR purification kit (PureLink™, Life Technologies, Cat. No. K3100-01). 4ng of PCR digest was combined with 50ng linearized pCIGRNAi plasmid, and ligated with 1μL T4 DNA ligase (Life Technologies, Cat. No. 15224-017) for 2h. Chemically competent *E. coli* (One Shot® Mach1™T1, Life Technologies, Cat. No. C8620-03) were transformed with 5μL of the ligation reaction and grown on agar plates with 50mg/mL ampicillin overnight. Individual bacterial colonies were grown in liquid culture, then plasmid DNA was extracted by maxiprep (Plasmid *Plus* Maxi kit, Qiagen, Cat. No. 12963) and sequenced by the UCLA Genotyping and Sequencing Core using a chicken U6 primer (ACAGTCACTGTGTTCTAAAAGAACTTG) to verify insertion of the shRNA construct.

Transfection Procedures

Nucleofection

Following dissociation, cell suspension was centrifuged at 100rcf for 5 minutes to pellet the cells, and all media was removed. Cells were resuspended in 100µL chicken nucleofector solution (Amaxa, Walkersville, MD, Cat. No. VGP-1002) per ~4 million cells. 100µL aliquots of cell suspension were prepared for each transfection and 8µg of plasmid DNA were added and mixed into each. Cells were nucleofected with a Nucleofector™ 2b (Lonza), then immediately resuspended in DMEM with glutamax (Life Technologies, Cat. No. 41090-036) with of 2.5% fetal bovine serum (Life Technologies, Cat. No. 10082-147), 2.5% horse serum (Life Technologies, Cat. No. 26050-070), 0.3% glucose, 1X penicillin-streptomycin (Life Technologies, Cat. No. 15140-122), and 2% B27 (Life Technologies, Cat. No. 17504-044). Cells were subsequently plated onto glass coverslips coated with poly-L-lysine (Fisher Scientific, Cat. No. 08-774-383) and incubated in 5% carbon dioxide at 37°C.

Lipofection

siRNA constructs were co-transfected with a pCDNA3.1 vector expressing the coding sequence of zebra finch Cntnap2 (Accession number NM_001193337.1), or with a control pGIPz vector expression GFP, via lipofection. The day before transfection HEK cells were transferred to fresh plates in media with serum, but without Antibiotic-Antimycotic at a density such that they would reach ~70% confluence by the following day. The morning of transfection the media was changed again without Antibiotic-Antimycotic. Transfection solution was prepared in aliquots of 250µL Opti-MEM (Life Technologies, Cat. No. 31985-062) without serum or antibiotics added. 100ng plasmid DNA was added to each aliquot, followed by 6µL Lipofectamine® 2000 (Life Technologies, Cat. No. 11668030). The solution was mixed, then

incubated at room temperature for 5 min. 50-100 pmol of siRNA duplexes were added to the solution, mixed, then incubated an additional 20 min. Transfection solution was added to an appropriate plate of HEK cells, and incubated at 37°C overnight. The following day the cells were replated at a lower density and allowed to grow an additional 24h before protein was harvested as described below.

Calcium Phosphate

The day before transfection, HEK cells were plated to ~10% confluence. The morning of transfection the culture media was removed and replaced with 8mL fresh media. Aliquots of 500mL HEPES buffered saline were made for each transfection. 20μg of total DNA was added to each aliquot and mixed well before adding 37.5μL of 2M calcium chloride. The transfection solution was incubated at room temperature for 20 min, and then added dropwise to the appropriate plate. 16h after transfection the media was changed and cells were cultured for another 24h before protein was harvested as described below.

Surgical Procedures

All animal use and experimental procedures were in accordance with NIH guidelines for experiments involving vertebrate animals and approved by the UCLA Chancellor's Animal Care and Use Committee. Coordinates for targeting RA were provided by Todd Roberts. Adult male zebra finches used in this study were obtained from our breeding colony. Adult male zebra finches were anesthetized with 2-4% isoflurane carried by oxygen using a Universal Vaporizer

(Summit Anesthesia Support, Menlo Park, CA) for the duration of the surgery. Prior to surgery, a stereotaxic apparatus was prepared by setting a guide pipette to 0.3mm caudal to interaural zero, i.e. between the ear bars that are used to hold the head in place. The bird was then placed on a homeothermic blanket mounted onto the stereotaxic apparatus. The cranial feathers were removed to expose the scalp, which was then cleaned using povidone-iodine. In order to preserve vascular flow to the region, a semi-circular incision was made originating and terminating at the caudal edge of the exposed scalp. The scalp was then folded back over a Gelitaspon (Gelita Medical, Amsterdam, Netherlands) moistened with sterile saline, to expose the skull. The head angle was adjusted so that the guide pipette was positioned directly above the exposed midsagittal bifurcation (~18-22°). ~1mm^2 windows were cut in the skull 1mm caudal and 2.4mm lateral from the midsagittal bifurcation. A glass electrode mounted on a Nanoject II (Drummond Scientific, Broomall, PA) was filled with high titer (10^{13} vector genomes) AAV2/1-CAG-GFP (Virovek, Hayward, CA), and lowered into the brain 2.0 mm from the surface of the brain. After a resting period, 40 injections of 27.6 nL each were made 15s apart for ~1μL total volume. 5 minutes after the last injection the electrode was withdrawn and the procedure was repeated on the contralateral hemisphere. After each procedure, the scalp was closed and sealed with Vetbond (Fisher Scientific). Each bird was given 2-5 drops of oral anesthetic Metacam® (Boehringer Ingelheim Vetmedia, Inc. St. Joseph, MO) after recovery from anesthesia, and was subject to quarantine for 72h. 14-21 days after injection, the birds were sacrificed at lights-on (0h singing) via overdose of isoflurane and perfused through the heart with 4% paraformaldehyde in phosphate buffered saline (PBS). Brains were dissected out and cryoprotected with 20% sucrose solution and stored in darkness at 4°C until use.

Immunocytochemistry

Coverslips of nucleofected telencephalic cultures were incubated for 4 days, and then fixed with 4% paraformaldehyde in phosphate buffered saline (PBS) for 10 min. Since cultures contained GFP, all subsequent steps were performed in low light conditions. Cells were blocked with 10% goat serum in tris buffered saline with 2% triton-X (TBS-Tx) for 1hr, then incubated overnight at 4°C with anti-Cntnap2 antibody (anti-Caspr2; Millipore, Temecula, CA, Cat. No. AB5886) diluted at 1:2,000 in TBS-Tx with 1% goat serum. Primary antibody was washed away with TBS-Tx, then cells were incubated in anti-rabbit Alexa Fluor® 546 secondary antibody (Life Technologies, Cat. No. A11010) diluted at 1:1,000 in TBS-Tx with 1% goat serum for 2hr. Coverslips were mounted onto slides using Prolong Antifade Gold Reagent (Life Technologies, Cat. No. P36934) and stored at 4°C until use.

Tissue Staining

40μm thick sections were cut in the sagittal orientation on a cryostat (Leica Microsystems, Bannockburn, IL) and thaw mounted onto microscope slides (Colorfrost® Plus, Fisher Scientific) in a manner that produced replicate sets of adjacent or near-adjacent sections, then stored at -80°C until use. A liquid repellent border (Super PAP Pen, Life Technologies, Cat. No. 008899) was drawn along the edges of one of the replicate sets of slides. Sections were rehydrated with 0.1M phosphate buffer, and then stained with red NeuroTrace Fluorescent Nissl stain (Life Technologies, Cat. No. N21481) at 1:200 in phosphate buffer for 20 minutes. Slides were mounted with glass coverslips using ProLong® Gold Antifade Reagent (Life Technologies).

Western Blot

Cell culture medium was removed from the dish, cells were washed once in phosphate buffered saline, then incubated on ice in radioimmunoprecipitation assay (RIPA) lysis buffer with 10% protease inhibitor cocktail (Sigma Aldrich, Cat. No. P8340) for 20 minutes. Lysates were collected and stored at -80°C. To determine the concentration of total protein a Lowry assay was performed using an RC-DC Protein Assay (Bio-Rad Laboratories, Hercules, CA, Cat. No. 500-0120). 25µg protein was diluted into 25µL RIPA lysis buffer, then added to an equal volume of 5% betamercaptoethanol (Sigma Aldrich, Cat. No. M6250) in Laemmli buffer (Bio-Rad, Cat. No. 161-0737). Samples were boiled for 2 minutes, then resolved on a 10% isocratic SDS-polyacrylamide gel in tris-glycine-SDS buffer (Bio-Rad) at 200V. A Precision Plus Protein™ Dual Color Standard (Bio-Rad) was included on the gel as a molecular mass marker. Protein was then transferred onto a PVDF membrane with a pore size of 0.45µm in tris-glycine (Bio-Rad) with 20% methanol and 1% SDS. The membrane was stained with Ponceau S solution (Sigma Aldrich) and cut along the 50 kD molecular mass marker. Both halves of the membrane were blocked with 5% milk in tris-buffered saline with 0.1% tween-20 (TBST) for 1 hour. Subsequently the half containing proteins >50kD were incubated in anti-Cntnap2 antibody (Millipore) solution diluted 1:2000 in 2.5% milk-TBST overnight at 4°C. The half containing proteins <50kD were incubated in anti-GAPDH (Millipore, Cat. No. MAB374) diluted at either 1:100,000, 1:50,000, or 1:20,000 in 2.5% milk-TBST overnight at 4°C. The blot was washed in TBST, then incubated in HRP-labeled secondary antibodies (GE Healthcare, Piscataway, NJ) diluted in 2.5% milk-TBST for 2 hours: >50kD in anti-rabbit diluted to 1:2000, <50kD in anti-

mouse diluted to 1:10,000. The blot was washed in TBST, then developed with ECL Plus and imaged on a Typhoon scanner (GE Healthcare) and signal specificity assessed.

Image Acquisition and Analysis

Images were acquired using an Axio Imager.A1, with an Axiocam HRm digital camera (Carl Zeiss Inc., Oberkochen, GE). Axiovision software (Carl Zeiss Inc.) was used to optimize photomicrographs to remove background, improve brightness and contrast, and to pseudocolor the images. Adjustments were made to the entire image and not to selective subregions. For tissue sections, anatomical regions were identified according to the published stereotaxic zebra finch brain atlas (http://www.ncbi.nlm.nih.gov/books/NBK2348/, courtesy of Dr. Barbara Nixdorf-Bergweiler and Hans-Joachim Bischof). Transduction rate was estimated using ImageJ (Schneider et al., 2012). Decreasing density and increasing size of Nissl stained bodies were used to determine the border of RA. The transduction rate was estimated by dividing the number of GFP-expressing cells by the number of Nissl stained cells within the RA border.

Results

Zebra Finch Cntnap2 RNA Interference

In order to experimentally reduce Cntnap2 protein in zebra finch, we first tested six shRNA constructs designed and provided by Dr. Brett S. Abrahams. Two, designated 148 and 154, target the 5' end of the coding sequence of the zebra finch *Cntnap2* cDNA (Accession number NM_001193337.1), corresponding to the N-terminus of the protein. The other four, 155, 156, 157, and 158, target the 3' untranslated region (UTR; Figure 3-1). In primary telencephalic cultures transfected with each shRNA construct, there was no apparent reduction in Cntnap2 protein in cells that expressed the GFP reporter relative to those without GFP (Figure 3-2A). To further investigate the potency of the shRNA constructs in decreasing Cntnap, HEK 293 cell cultures were co-transfected with zfCntnap2 cDNA and the coding sequence-targeting shRNA constructs (the zfCntnap2 plasmid did not contain the 3'UTR) or a control plasmid that expressed only GFP. No attenuation of Cntnap2 protein for either shRNA was detected by Western analysis (Figure 3-2B, C).

These shRNA constructs may fail to silence *Cntnap2* due to the sequence of the shRNAs themselves ineffectively incorporating into the RNA-induced silencing complex and binding to *Cntnap2* transcript. Alternatively the failure may be due to a defect in the pGIPz vector system to produce the shRNAs. To avoid any confounding factors due to the vector, three siRNA sequences (4282, 4288, and 4372) were designed to target the 3' end of the coding sequence (Figure 3-1). The primary reason for designing constructs to target the 3' end of the coding sequence was a concern over potential Cntnap2 splice variants. Two splice variants have been identified in mouse (Poliak et al., 1999), though little has been reported on the shorter β isoform.

The murine *Cntnap2β* (NM_025771.3) retains the 3,279 nucleotides on the 3' end of the coding sequence of the full-length α isoform (NM_001004357.2) at the 3' end of the coding sequence, including the sequence that codes for the transmembrane region and the first laminin G domain (Figure 3-1). Therefore, siRNAs were designed to target only this region of the zebra finch isoform of *Cntnap2*.

siRNA duplexes allow direct interference with the mRNA in transfected cells without the intermediate step of transcription from a plasmid vector. The tradeoff is that the effect is transient, often lasting no longer than 1-2 days (Strapps et al., 2010). In an attempt to identify the cells in culture that take up the siRNA duplexes, the 5' end of the guide strand was tagged with fluorescein. However, the tag proved to be useless for the identification of transfected cells, as it weakly labeled all cells in the culture (data not shown). Each siRNA or a non-targeting control was cotransfected in HEK 293 cells with either zebra finch *Cntnap2* or GFP, the latter as a control. At 2 doses tested, 50 and 100pmol, all 3 siRNAs reduced Cntnap2 protein expression relative to the scrambled control (Figure 3-3). 70% reduction in protein is considered effective knockdown (Ui-Tei et al., 2004). The 50pmol doses of 4282 and 4372 reduced Cntnap2 protein >70%, but 4288 did not meet criteria for effective knockdown. Doubling the dose to 100pmol caused >70% reduction in protein for all siRNA constructs. Therefore, all three siRNA constructs were considered for insertion into a viral vector for *in vivo* Cntnap2 knockdown.

Stereotaxic Targeting of RA with AAV

AAV2/5-CAG-GFP was injected into the brain of an adult male zebra finch targeting RA bilaterally (Figure 3-4). Transduction rates in RA are estimated at 35% of cells on the left hemisphere, 43% on the right. Many of the cells labeled by GFP have long processes that appear to be neurites, though it is possible that GFP labels non-neuronal cell types as well. GFP expression in axon tracts extending from RA to the hindbrain suggests that at least some of the transduced cells are projection neurons. Some cell bodies in the taenia nucleus of the arcopallium (TnA), which lies adjacent to the axon tracts descending from RA, are labeled with GFP. There is no known connection between RA and TnA, nor any association of this nucleus with learned vocalizations. Some GFP is found in the dorsomedial nucleus of the intercollicular complex (DM), a midbrain target of RA projections related to respiratory activity (Nottebohm et al., 1976). No GFP was detected in afferent connections from HVC (proper name) nor LMAN, nor the cell bodies within the two song nuclei, suggesting that terminals or axons originating outside the target nucleus do not take up the virus. DLM was recently identified as a target of a subset of RA projection neurons (Goldberg and Fee, 2012). No GFP was detected in this nucleus on either side, suggesting that the projections from RA that project to this nucleus were not transduced.

Discussion

I have designed RNAi constructs to determine whether Cntnap2 expression in the zebra finch song system is necessary for vocal production and/or learning. Though several of the constructs failed to reduce Cntnap2 protein in cell culture, two promising candidates have emerged in our screen. Individually, 4282 and 4288 seemed to have strong knockdown effects as 19mer siRNAs, their conversion to 22mer shRNAs seems to have reduced their effectiveness. However, 4372 was able to significantly reduce Cntnap2 in both forms. Additionally, 4328, which was initially designed as a 22mer, is also able to reduce protein by >70% in cell culture. Combinations of 4282+4288, 4288+4328, and 4372+4382 also effectively knock down Cntnap2 protein. These preliminary results suggest that insertion of these constructs into a viral vector may be used separately or together to knock down Cntnap2 expression *in vivo*.

Though RNAi has been delivered using lentiviruses in the past (Wada et al., 2006; Haesler et al., 2007), we have chosen instead to use AAV. This latter virus was used previously to overexpress a potassium channel in zebra finch neurons (Teramitsu, 2007). While lentivirus can be used to stably express a transgene in non-dividing cells, it has potentially oncogenic effects (Baum and Fehse, 2003; Baum et al., 2006; Li et al., 2002). AAV can also express a transgene for more than 6 months, with less risk of random insertion into the genome, which potentially causes oncogenesis (Papale et al., 2009; Doherty et al., 2011). Though less genetic material can be inserted into the backbone of an AAV than lentivirus, the relatively small amount required for shRNA expression is not a challenge. There are several AAV serotypes, each of which has different tropisms for specific cell types. A serotype with a high tropism for neurons can be used for optimal transduction efficiency in the brain. Furthermore, injections of high titer

AAV seem to transfect a greater proportion of cells than lentivirus (Doherty et al., 2011; Hutson et al., 2012; Mason et al., 2010). The sparser transduction rate of lentivirus can be profitable in some applications, such as expression of GFP in cells for two-photon imaging of dendritic spines (Roberts et al., 2010). However, a higher transduction rate is preferable for affecting changes in behavior. Preliminary findings in the current study suggest that AAV2/1 can transduce 30-40% of the neurons in RA. Haesler et al. (2007) reported a behavioral change with only an estimated 20% of the volume of area X transduced by a lentivirus, suggesting that higher transduction rate of AAV2/5 will be sufficient to affect behavior if our hypothesis about the role of Cntnap2 in the song system is correct.

Considerations for Continuation

We have evaluated the use of shRNAs targeting *Cntnap2* cDNA in HEK cell culture, but this may not be an accurate reflection of the ability of these constructs to reduce endogenously expressed Cntnap2 in zebra finch cells. Possible reasons include mismatches between the cDNA and genomic versions of the gene or potentially toxic off-target effects of the shRNA in zebra finch tissues. It will be important, therefore, to further test the shRNA constructs in zebra finch primary cell cultures. The nuclear GFP reporter in the pCIGRNAi vector will identify transfected cells, which may then be analyzed for Cntnap2 expression either through immunocytochemistry (ICC) or Western analysis, as in Figure 3-2A. The latter technique requires either a high rate of transfection to ensure that the reduction in Cntnap2 can be detected against a high background of untransfected cells, or fluorescence-activated cell sorting prior to retrieval of the protein. ICC may therefore be the preferable approach, since Cntnap2 expression can be evaluated on a cell-

by-cell basis. Following successful knock down of endogenous Cntnap2, the silencing operon can be cloned into an AAV backbone and inserted into a virus. Transduction of neuronal cultures with this virus can be used to verify the correct expression of the shRNA constructs and reporter gene.

Cntnap2 knockdown: expected physiological effects

Primary telencephalic cultures will provide the basis for studying aspects of the physiological effects of knocking down Cntnap2. Knocking down Cntnap2 in mouse cortical cultures reduces the dendritic arbor and spine density of affected neurons (Anderson et al., 2012). The result is that affected neurons make fewer synaptic contacts, and therefore have weaker responses to synaptic stimulation without any changes to intrinsic electrophysiological properties. These effects have not yet been reported *in vivo*. These results can be replicated in zebra finch telencephalic cultures, which presumably contain a more diverse array of cell types than mouse cortical cultures. Patch clamp electrophysiology can be used to measure synaptic events and fill cells with a dye, such as neurobiotin, which may be used to analyze morphology of dendritic spines. It is unlikely there are major species differences in the effects of knocking down Cntnap2 in culture; therefore zebra finch telencephalic cultures are expected to have the same physiological responses to knockdown of Cntnap2 as are described for mouse cortical cultures. Potential differences may be due to the variety of cell types when culturing cells from the entire telencephalon rather than from the cortex alone.

Morphological and physiological effects of Cntnap2 reduction may also be studied *in vivo*. Injections of AAV carrying Cntnap2 shRNA and a typical GFP reporter (i.e. one that does not restrict GFP to the nucleus) in small volumes or lower concentrations will sparsely label cells, which can then be used to determine the *in vivo* morphological effects of Cntnap2 knockdown when compared with a control virus expressing only the GFP reporter or in conjunction with non-targeting shRNA. We predict that neurons transduced with the knock down constructs will have decreased dendritic arbor, similar to those in culture. Affected neurons may also be recorded in slice, cut in such a way as to preserve the inputs from HVC or LMAN (Spiro et al., 1999). In culture, both excitatory and inhibitory synaptic transmission were reduced by knockdown of Cntnap2 (Anderson et al., 2012). We predict, therefore, that monosynaptic excitatory input from HVC and LMAN projections would also be reduced in shRNA-transduced RA neurons. In order to isolate these synaptic events from polysynaptic inhibition through RA interneurons, these experiments must be done in the presence of $GABA_A$ receptor antagonists (Mooney, 1992). Monosynaptic inhibitory activity can also be evaluated by bathing the slice in AMPA and NMDA receptor blockers and stimulating various sites within RA (Spiro et al., 1999). Inhibitory neurons in this song nucleus make long-range connections that can coordinate firing of multiple projection neurons. We predict that these inhibitory events will also be reduced in neurons with Cntnap2 knocked down.

In the peripheral nervous system (PNS), a well-described function of Cntnap2 is to localize *Shaker*-type voltage-gated potassium channels (VGKCs) to the juxtaparanodes along axons (Poliak et al., 2003). In *Cntnap2* knockout mice, these channels are distributed throughout the interneurons. Though this doesn't affect axon conduction velocity or refractory period, action potential waveform properties and synaptic transmission have not been assessed in these animals.

Selective blockade of these channels can increase action potential amplitudes and broaden waveforms, particularly in unmyelinated axons or during development of the myelin sheath (Devaux et al., 2002). These changes to the action potential can have downstream effects on synaptic release. Broadening of the waveform may prolong activation of voltage-gated calcium channels at synaptic terminals, leading to augmented synaptic release (Kole et al., 2007). It is not clear whether Cntnap2 significantly contributes to the clustering of VGKCs in the central nervous system (CNS). Immunostaining reveals fairly uniform Cntnap2 staining along the length of cortical neuron axons, rather than the punctate expression pattern found in the PNS (Poliak et al., 1999; Strauss et al., 2006), suggesting that it may have different effects in these neuronal types. However, the effects of Cntnap2 knockdown on synaptic release may be measured in zebra finch telencephalic cultures via paired recordings, or in brain slices in which the connections between RA and target nuclei (nXIIts, DM, or DLM; Goldberg and Fee, 2012; Reiner et al., 2004a) are intact. For the latter method, neurons may be recorded in target nuclei while RA is stimulated with a bipolar electrode. When stimulating RA that has been injected with virus carrying shRNA or a transduced neuron in culture, we expect to find increased amplitudes of excitatory events relative to controls.

Cntnap2 knockdown: expected behavioral effects

Of course, the goal of these studies is to determine whether Cntnap2 expression in RA is necessary for vocal learning and/or production. The onset of sexually dimorphic Cntnap2 expression coincides with that for sensorimotor learning in zebra finches (chapter 2), beginning ~30d (Immelmann, 1969; Price, 1979). AAV requires 1-2 weeks for initial expression, with a

peak at 3-4 weeks (Doherty et al., 2011; Papale et al., 2009). Therefore, injection of the virus at 15d would begin to knock down Cntnap2 around the onset of this critical phase of song learning. shRNA expressing juvenile males are expected to have impaired ability to learn song, similar to the language regression found in CDFE patients. Complete lesions of RA result in the inability of the male to sing, and partial lesion can affect the acoustic features of the song (Simpson and Vicario, 1990). We don't expect knock down of Cntnap2 in RA to have the same effects as a complete lesion since transduction rate will likely not reach 100%, and we do not anticipate neuronal death as a result of transduction. However, the extent to which viral transduction is toxic should be measured using terminal deoxynucleotidyl transferase dUTP nick end labeling or an alternative method in injected birds, as in Haesler et al. (2007). Instead, we hypothesize that loss of Cntnap2 in RA will reduce its afferent connectivity with HVC and LMAN. In juvenile birds, partial HVC lesions typically result in attenuation of song production (Gentner et al., 2000). Cntnap2 loss in RA may have an effect similar to the disconnection from HVC, and thereby reduce the amount of singing in the juvenile male. This effect is similar to the delayed age at first word observed in autistic children with *CNTNAP2* risk variants (Alarcón et al., 2008). LMAN lesions in juvenile birds result in premature crystallization of song (Scharff and Nottebohm, 1991). Temporary inactivation of LMAN inputs onto RA neurons in juvenile male zebra finches result in reduced acoustic and sequence variability (Olveczky et al., 2005). Since injections of AAV are not likely to affect all RA neurons with LMAN afferents, the effects are expected to be intermediate to LMAN lesion or inactivation. Instead, affected juvenile birds may develop song more slowly than controls, and having adult song that is less similar to the tutor, similar to language impairment associated with autism in humans.

Little is known about the function of Cntnap2 in mature neurons in established circuits. There are no animal models yet in which Cntnap2 was conditionally manipulated in adulthood. Therefore, it is difficult to predict the effects of knocking down of Cntnap2 in adult birds whose song has already crystallized. It is possible that knocking down Cntnap2 in RA in adult zebra finches will have no effect on vocal behavior. If Cntnap2 does localize VGKCs to juxtaparanodes in the CNS, disruption of this process could lead to abnormal action potential waveforms and stimulation of nXIIts neurons. This could disrupt song by mismatch of auditory feedback, similar to studies in which variations of spectral features of notes are "punished" by playing back white noise (Tumer and Brainard, 2007). Over time this could result in a change in spectral features of the crystallized song. It is also possible that Cntnap2 is required for the maintenance of dendritic arborization and spine density, in which case disruption of Cntnap2 in adulthood is expected to result in deterioration of song. This can be measured by comparing recorded song before and after injection of the virus, and using quantification methods, such as those included in Sound Analysis Pro (Tchernichovski et al., 2000), to detect changes as a result of shRNA expression.

RA is the cortical song nucleus with the most apparent sexual dimorphism in adulthood, so the effects of Cntnap2 loss on physiology and behavior may be most apparent there. However, Cntnap2 is also differentially expressed in LMAN compared to the surrounding nidopallium. The same viral construct may be used to knockdown Cntnap2 in LMAN to determine its physiological and behavioral effects there. LMAN receives long-range excitatory input DLM. Projection neurons within LMAN send axons to both RA and area X. LMAN projections to RA also recursively innervate LMAN. Knock down of Cntnap2 may affect these connections in a similar manner as described above. Since LMAN is involved in vocal learning, but not

production, we would not expect to observe a decrease in vocal production, but perhaps and arrest of song development in young males.

The preliminary work here provides the molecular tools with which to study the role of Cntnap2 in vocal learning and production. Based on cases of human pathology related to variation in the *CNTNAP2* and the distribution of Cntnap2 protein in the zebra finch song system, we hypothesize that reduction of the transcript in zebra finch song nuclei will adversely affect song learning.

Acknowledgements

Thanks to Dr. Brett Abrahams for the first round of shRNA constructs. Dr. Julie Miller contributed to testing these shRNA constructs in zebra finch primary telencephalic cell culture. Qianqian Chen assisted with cloning and vetting the second round of shRNA constructs. Thanks to Drs. Bennett Novitch and Zachary Gaber for providing the pCIGRNAi plasmid and their advice regarding the cloning of shRNA constructs.

Tables

Table 3-1: Zebra finch Cntnap2 siRNA sequences.

siRNA	Guide Strand	Passenger Strand
4282	UAACUCCAUCUCCUAUAGCTT	GCUAUAGGAGAUGGAGUUATT
4288	UUCUGUUAACUCCAUCUCCTT	GGAGAUGGAGUUAACAGAATT
4372	AAACAUGUAGCGGAUCAGGTT	CCUGAUCCGCUACAUGUUUTT
NT	CUUGGUAGUUCGCUGAUCUTT	AGAUCAGCGAACUACCAAGTT

Sequences of each strand of siRNA duplexes designed to target the 3' end of the zebra finch Cntnap2 coding sequence, and one non-targeting (NT) control. Passenger strands correspond to the target sequence.

Table 3-2: Zebra finch Cntnap2 shRNA sequences.

shRNA	Target Sequence
148	ATCGGATGCTCTATAGTGATAC
154	TGTCATCTCTCTGAAATTTAAG
155	ATGTGTTTGTATGCATAAATAT
156	CTGAAAGGGTGTCATTCTTGAA
157	ATGGTTTATCCCATGAATGATT
158	GGTGTATATGTACAAGTTTATT
4282	CAAGCTATAGGAGATGGAGTTA
4288	ATAGGAGATGGAGTTAACAGAA
4328	GTTCCTGATCCGCTACATGTTT
4372	GGTTCCTGATCCGCTACATGTT

shRNA construct designations and target sequences designed to knock down zebra finch *Cntnap2.*

Figures

Figure 3-1: Schematic of zebra finch *Cntnap2* cDNA.

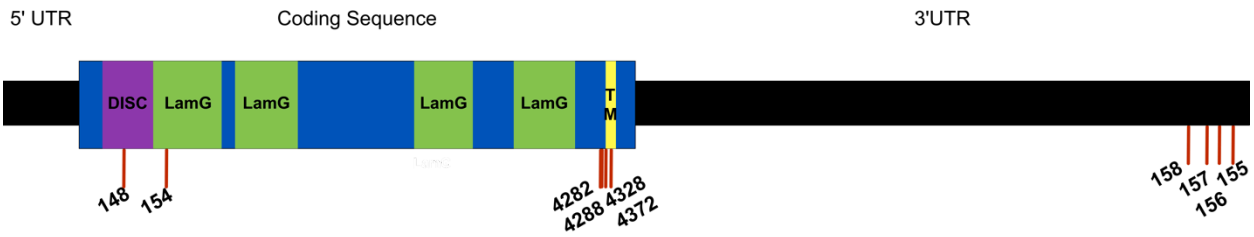

Discoidin (DISC) and laminin G (LamG) protein domains, and the transmembrane (TM) region are superimposed over their corresponding sequences on the cDNA. Target sequences of each shRNA construct in Table 3-2 are indicated by red lines.

Figure 3-2: Initial shRNA constructs are ineffective at knocking down Cntnap2 in culture.

A

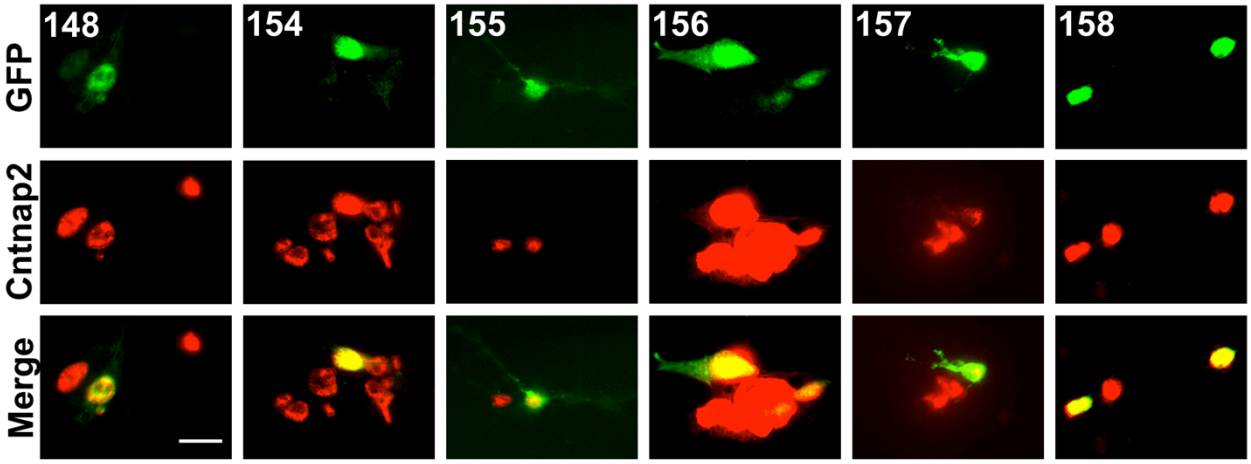

B

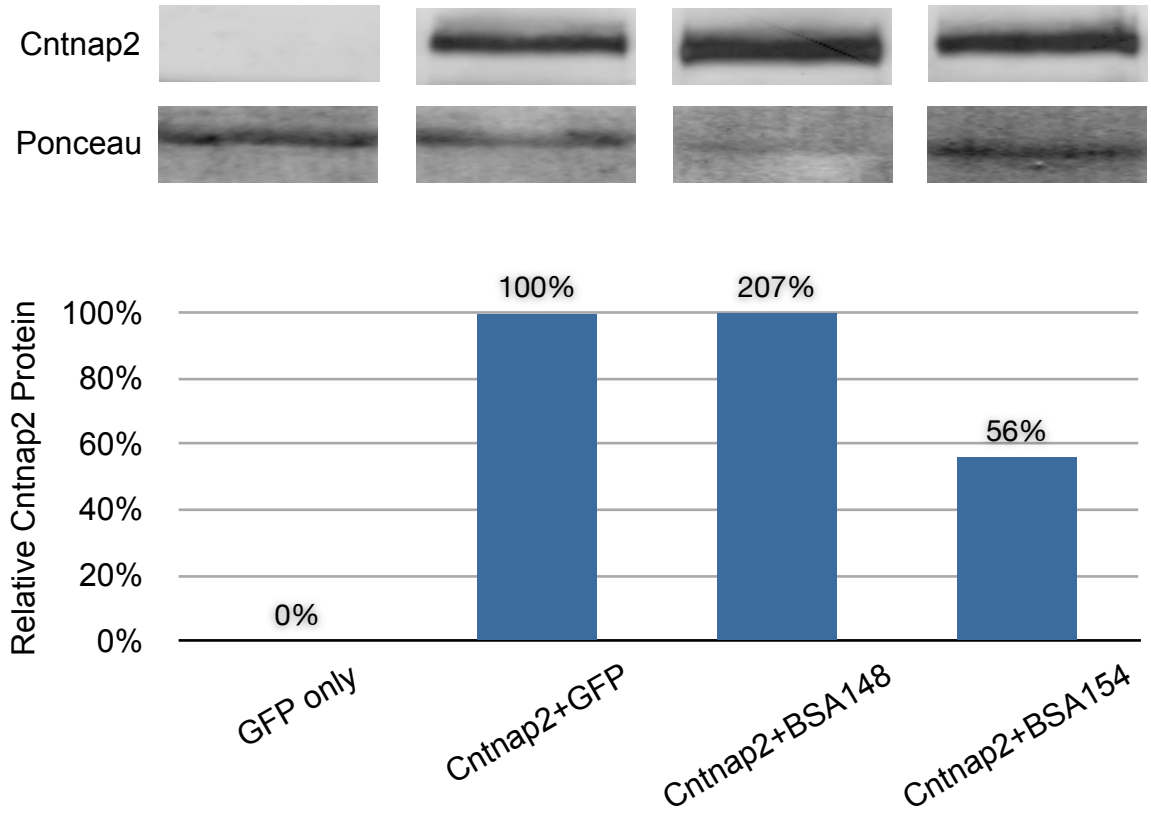

A) Zebra finch telencephalic cultures were nucleofected with a plasmid containing each shRNA construct and a GFP reporter (green). GFP-positive and -negative cells exhibit no qualitative difference in Cntnap2 immunoreactivity (red). Scale bar = 20μm. **B)** Western analysis reveals that coding sequence-targeting shRNA constructs cotransfected in HEK 293 cultures with zebra finch *Cntnap2* fail to adequately reduce protein levels. Cntnap2 protein band intensity was normalized to the intensity of a protein band stained by Ponceau S solution.

Figure 3-3: siRNA constructs reduce zebra finch Cntnap2 in culture.

A

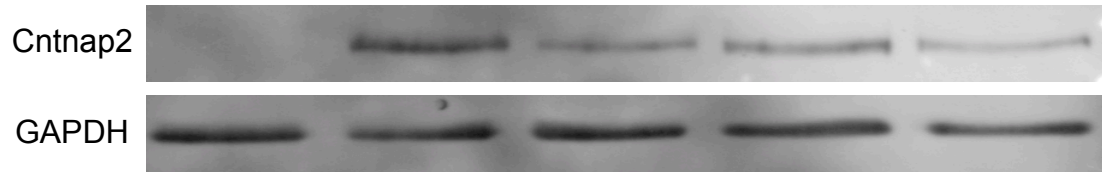

B

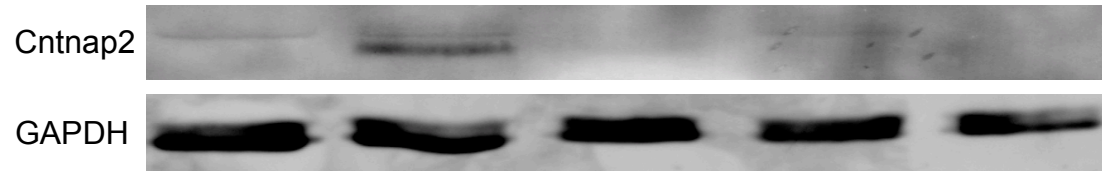

C

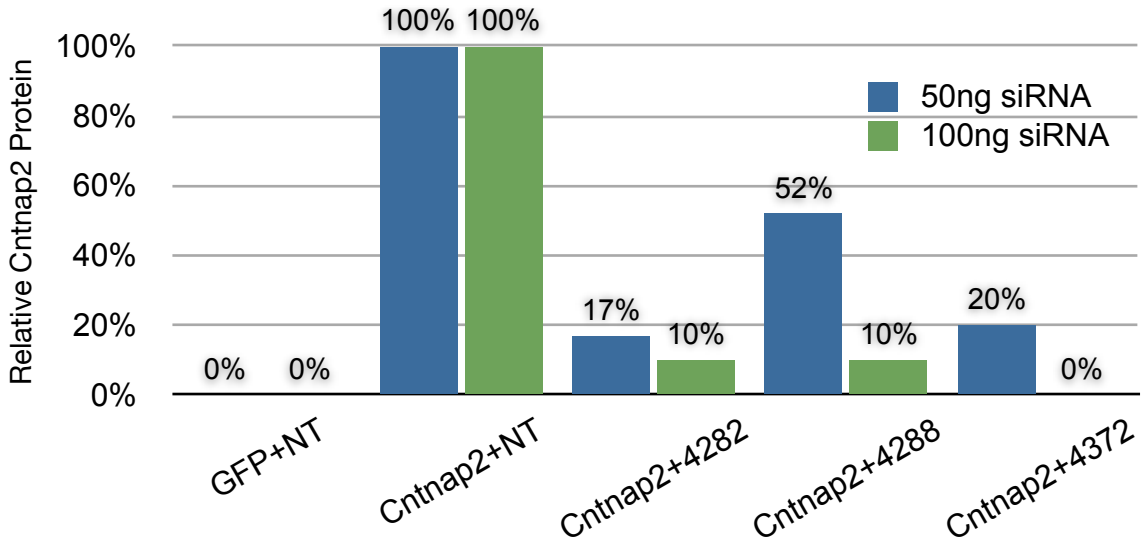

A) Western blots of HEK 293 cell lysates in which 50 and **B)** 100pmol of siRNA duplexes were cotransfected with zebra finch Cntnap2.

Figure 3-4: Newly-designed shRNA constructs effectively reduce zebra finch Cntnap2 in HEK 293 cell culture.

A

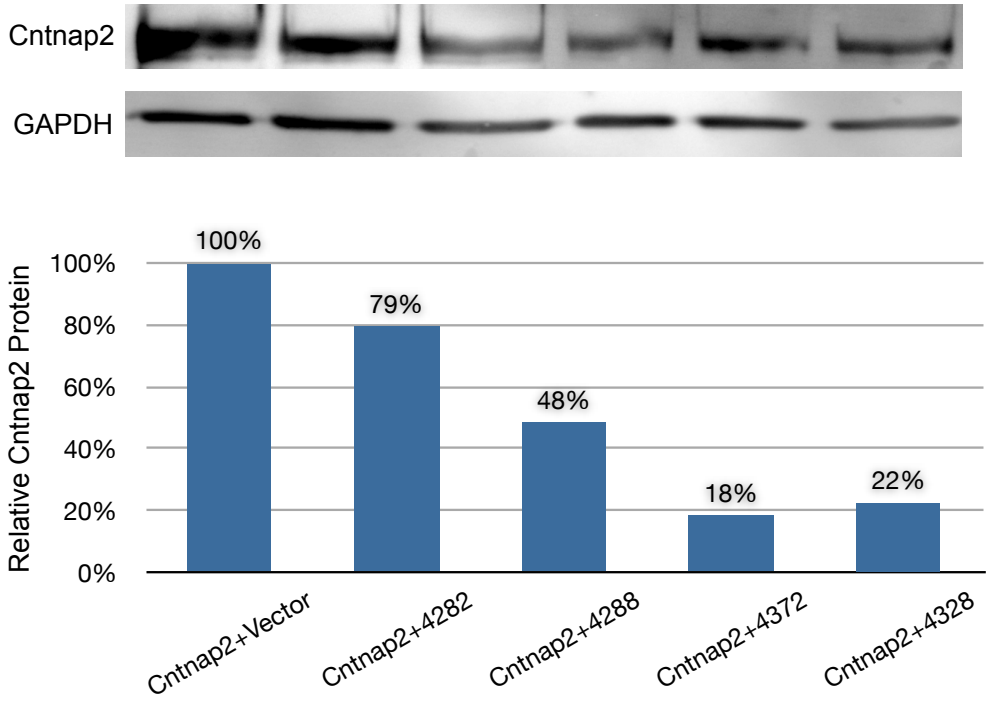

B

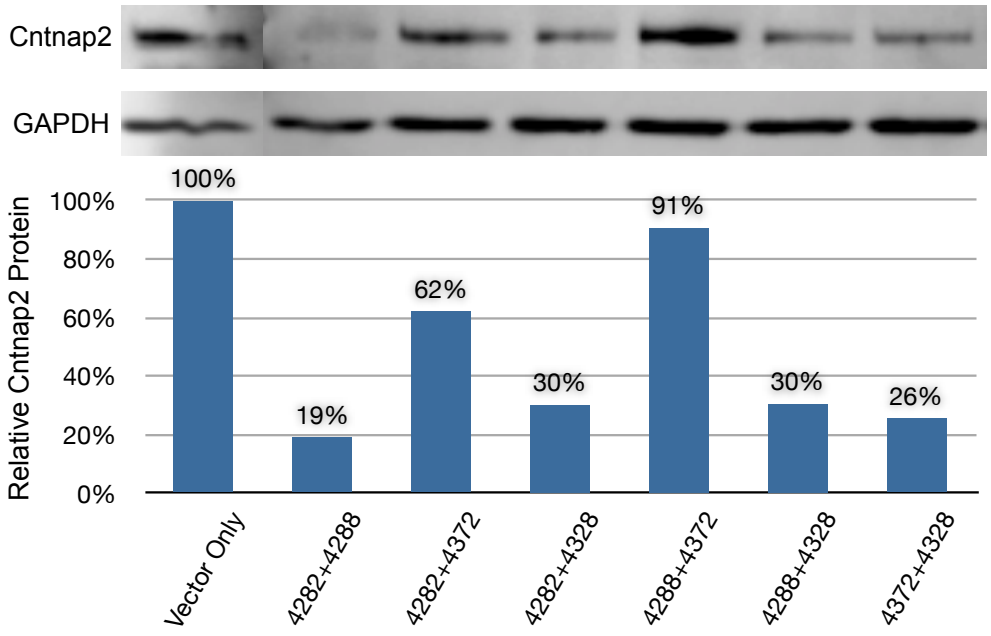

A) HEK 293 cells cotransfected with individual shRNA constructs at a 1:9 ratio show that 4328 and 4372 prevent >70% of Cntnap2 expression. **B)** shRNA constructs cotransfected with Cntnap2 in pairs at a 1:4.5:4.5 ratio. Several combinations of shRNA constructs reduce Cntnap2 expression by >70%.

Figure 3-5: GFP expression in RA as the result of AAV injection targeting the nucleus.

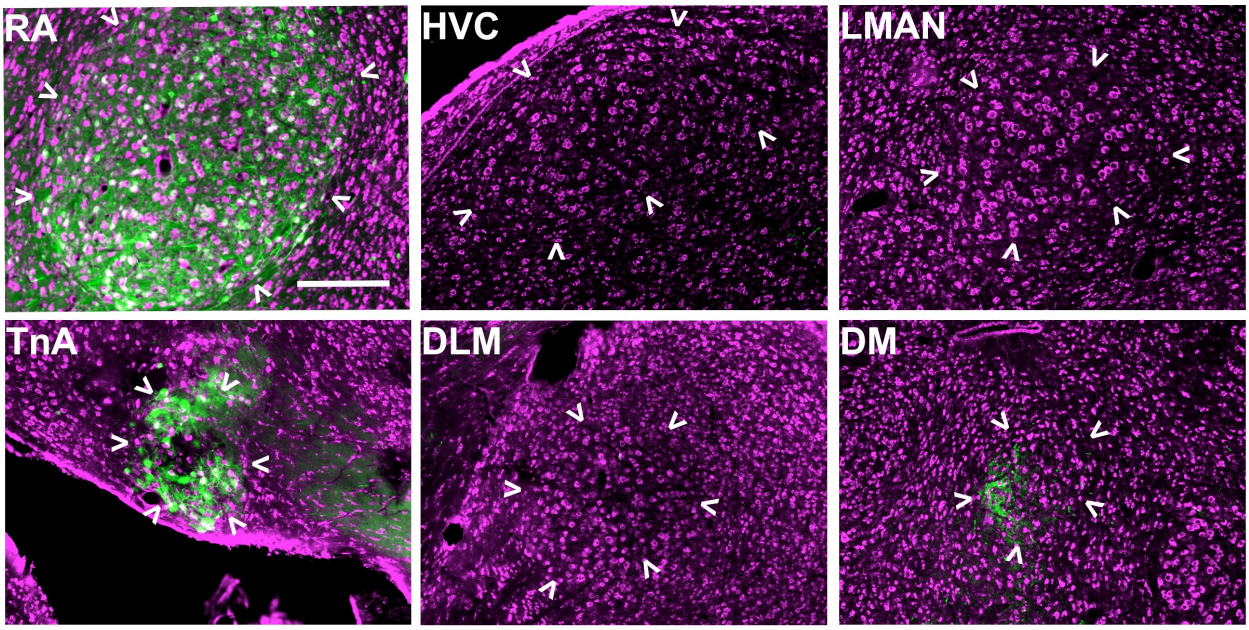

Some GFP is observed on cell bodies in the taenia nucleus of the arcopallium (TnA), adjacent to projections originating in RA. No GFP is observed in afferent cortical song nuclei HVC or LMAN. No GFP is observed in one target of RA projections, song nucleus DLM, but there is expression in the neuropil of another target, the midbrain nucleus DM, which are likely projection neuron axons originating in RA. Scale bar = 200µm.

Chapter 4: Conclusion

The broad scope of my research has been to identify the mechanisms by which genetic factors influence vocal learning. Mutations in the genes I review in Chapter 1 all give rise to speech and language disorders, exclusively in some cases. If a male zebra finch is deprived of a tutor's song and his progeny are never exposed to conspecific song outside the bloodline, within a few generations his descendants will develop complex song complete with all the spectral features of a non-isolated male (Fehér et al., 2009). This phenomenon is remarkably similar to language formation from pidgin languages or the sign language that spontaneously developed *de novo* in a Nicaraguan deaf community (Kegl, 2002). How can genes give rise to not only the ability, but the propensity for language or birdsong? Toward the questions, I have focused on the continued development the songbird as a model for the study of genes related to vocal learning, specifically Cntnap2. In Chapter 1, I describe investigations of genes in relation to their contributions to speech and language, spurred by the initial association of *FOXP2* with developmental verbal dyspraxia. The findings I describe in Chapter 2 augment the evidence described in Chapter 1 that support the hypothesis that *contactin associated protein-like 2* (*Cntnap2*), a target of FOXP2, is a key molecule in neurophysiological mechanisms underlying vocal learning in humans and songbirds alike. In Chapter 3 I explore a method for assessing the influence of Cntnap2 on song learning in the zebra finch through RNA interference. This chapter represents a concise synopsis of my work, which has made progress toward understanding the impact of Cntnap2 on learned vocalizations, and also provides a solid platform for the continued studies of this and other genes related to vocal learning.

One could argue that the KE family catalyzed the study of vocal learning genes. Their speech disorder, inherited in a Mendelian dominant fashion, promoted search for a single genetic cause. It was not until a chromosomal rearrangement involving *FOXP2* in an unrelated

individual with a similar disorder was discovered that the R553H mutation was identified as the cause of the KE family speech impairment. The story of *CNTNAP2* parallels this progression in that the first hints of association with a language came first in another closely-related population of Old Order Amish, but was not appreciated until the discovery of its regulation by FOXP2. Unlike FOXP2, common variants of *CNTNAP2* have been identified that are associated with speech-related disorders including autism and specific language impairment. In Old Order Amish children afflicted with cortical dysplasia-focal epilepsy, CNTNAP2 is truncated and language regression is one symptom out of many that characterize the disorder. Expressed only in the nervous system, the best characterized function of Cntnap2 is in clustering potassium channels along axons, though it also potentially functions in the development of dendrites and synapses in the brain. Cntnap2 is a member of the neurexins superfamily of neuronal adhesion molecules. Perhaps future studies will reveal that Cntnap2 is part of a cellular signaling system, closely associated with a receptor molecule or acting as a receptor itself, which may stimulate signaling cascades within the neuron that promote dendritic growth and/or synapse formation. As more functions for Cntnap2 are discovered, its role in vocal learning will be better understood.

Toward the goal of studying the relationship between Cntnap2 and vocal learning in an animal model, I describe the distribution of the protein in the zebra finch song system in Chapter 2. The protein is enriched in several song production system nuclei, including the robust nucleus of the arcopallium (RA), the lateral magnocellular nucleus of the anterior nidopallium (LMAN), and area X. This differential distribution of the protein in the song production system suggests that Cntnap2 expression in these regions is important for learned vocalizations. In adult zebra finches, a species in which song learning is sexually dimorphic, the distribution of Cntnap2-expressing neurons in RA is also sexually dimorphic, in that males have a greater percentage in

RA relative to neighboring arcopallial regions, whereas females do not. However, the onset of sexually dimorphic Cntnap2 expression does not occur in juvenile birds until after the onset of sensorimotor learning in males. Prior to that, females have a comparably Cntnap2-enriched RA to males. These data suggest that Cntnap2 enrichment in RA is involved in sensorimotor learning in males, but is not necessary in females, who do not sing. Furthermore, the neurons in RA that express Cntnap2 are projection neurons whose axons innervate the motor neurons that control the syrinx. The mammalian analogs of these neurons are pyramidal neurons in layer 5 of the primary motor cortex, whose axons innervate the motor neurons controlling the larynx. Cntnap2 may therefore be important for the development and/or maintenance of neuronal connections between song nuclei. This hypothesis is further supported by evidence of Cntnap2 expression in LMAN axons projecting into RA.

To begin to test these hypotheses, I describe methods in Chapter 3 that may be used to reduce Cntnap2 protein in the songbird brain, to probe its effects on physiology and behavior. Many of the genes described in Chapter 1 have roles in both the development of neural structures and in the formation of connections between mature neurons. *CNTNAP2* is enriched in the frontal cortex in the human fetus, suggesting that it contributes to the development of regions necessary for language in the mature brain. However, it also affects the development of dendrites and synaptic connections in mature neurons. Creating a transgenic zebra finch lacking *Cntnap2* would result in perturbation of both these processes. However, manipulating Cntnap2 expression in juvenile zebra finch song system through targeted viral injection will allow the study of the post-developmental effects of Cntnap2. There is precedent for the use of viruses to deliver RNA interference constructs to zebra finch song nuclei in order to study the resulting effects on song. Chapter 3 describes such an approach using adeno-associated virus, which has greater

transfection efficiency than lentivirus, and is able to transduce projection neurons in RA, as demonstrated here. I have designed four short hairpin RNA (shRNA) constructs and tested their efficacy at reducing zebra finch Cntnap2 in HEK 293 cell culture, both individually and in pairs. Combinations of hairpins may improve knockdown efficiency while reducing off-target effects. Additional testing of these constructs in zebra finch primary telencephalic neurons will be required to determine which combinations are suitable for *in vivo* knockdown. Three of the hairpins in Chapter 3 were adapted from short interfering RNA constructs that efficiently reduced Cntnap2 by adding bases and a loop sequence, though in retrospect this intermediate step seems unnecessary, and in future studies I recommend designing hairpins from the start.

The procedures described in Chapter 3 for cloning and testing RNAi constructs may be adapted to target other vocal learning genes, such as those described in Chapter 1, taking full advantage of the songbird as a genetic model for human speech. FoxP1 is a good example, since transcript distribution in the zebra finch has already been described, and like *Cntnap2* is enriched in several song nuclei. Though distributions of hepatocyte growth factor signaling pathway genes, such as Srpx2 and Met, have not yet been described in the songbird, such studies would be merited given the evidence the involvement of this pathway in human speech outlined in Chapter 1. An exciting new area of research is behavior-driven activation of microRNAs, which represent a new class of genetic factors that likely contribute to learned vocalizations across species, as well as other procedurally learned behaviors. The work that I describe in this volume is a single thread that can be used to further unravel the complex tapestry of genes involved in language through the use of the songbird model. A better comprehension of the relationship between genes and language will benefit the development of therapies used to treat speech and language disorders, as well as what makes this behavior unique to our species.

Appendix 1: The Spatial, Temporal and Contrast Properties of Expansion and Rotation Flight Optomotor Responses in *Drosophila*

Brian J Duistermars, Dawnis M Chow, Michael Condro, and Mark A Frye

Statement of Contribution

A concern of the testing paradigm described blow in which flies were presented with either an expanding or rotation contrast pattern is that until this study it was unclear whether the flies detected the movement as smooth motion or as a progression of still images. To test this I adjusted the program to produce a contrast gradient for the visual stimulus, to provide a better simulation of smooth motion. The results are depicted in Figure A1-7, in which we found the wing beat response varies as a function of stimulus type and contrast. Flies first presented with the stimulus exhibit a greater response to expansion than rotation at higher contrast ratios. Flies that had been adapted to the stimulus exhibited a greater response to expansion than rotation even at low contrast. These results confirm that flies are sensitive to stimulus contrast, and provide an additional line of evidence for separate processing pathways for rotational and expansion visual stimuli.

Summary

Fruit flies respond to panoramic retinal patterns of visual expansion with robust steering maneuvers directed away from the focus of expansion to avoid collisions and maintain an upwind flight posture. By contrast, panoramic rotation elicits relatively weak syndirectional steering maneuvers, which also maintain visual equilibrium. Full-field optic flow patterns like expansion and rotation are elicited by distinct flight maneuvers such as body translation during straight flight or body rotation during hovering, respectively. Recent analyses suggest that under some experimental conditions the rotation optomotor equilibrium response reflects the linear sum of different expansion response components. Are expansion and rotation-mediated optomotor behaviors manifestations of a single optomotor equilibrium response subserved by one neural circuit that is differentially stimulated by the two flow fields, or rather do the responses reflect distinct behaviors controlled by separate pre-motor visual processing pathways? Guided by the principle that the properties of neural circuits are revealed in the behaviors they mediate, we systematically varied the spatial, temporal, and contrast properties of expansion and rotation stimuli, and quantified the time course and amplitude of optomotor equilibrium responses during tethered flight. Our results support the conclusion that expansion and rotation optomotor responses likely draw from the same system of elementary motion detectors, but that after this early stage the two behaviors are mediated by separate pre-motor circuits that have different receptive field properties, low-pass characteristics, and contrast sensitivity.

Introduction

Insects (as well as virtually all seeing animals) respond to a rotating visual panorama by turning in the direction of motion. For flying insects, this robust behavioral attempt to minimize retinal slip comprises a classical 'optomotor' response thought to help maintain stability in the face of external perturbations such as a gust of wind, or internal perturbations such as bilaterally asymmetric motor output (Collett, 1980; Götz and Wandel, 1984; Götz, 1964; Heisenberg and Wolf, 1984). Behavioral optomotor responses, as well as their electrophysiological correlates within motion processing interneurons in the brain, show distinct tuning curves for the spatial, temporal, and contrast structure of moving images (Buchner, 1984; Götz, 1975; O'Carroll et al., 1996).

A recent study of optomotor responses in fruit flies explicitly compared optomotor responses to rotation and translation stimuli and reported that panoramic patterns of image expansion/contraction centered laterally (approximating a visual stimulus generated during a side-slip maneuver) triggered optomotor responses that were three times stronger than responses to a rotating panorama of identical spatial and temporal structure (Tammero et al., 2004). This increase in gain emerges because the directional optomotor response to motion restricted to the rear hemisphere is *reversed* compared to frontal hemisphere motion. Thus, counterclockwise motion across the front coupled with clockwise motion across the rear produces a strong counterclockwise steering response oriented away from the focus of expansion (centered at the animal's right side in this example). The time course and magnitude of full-field rotational optomotor responses are nearly identical to the arithmetic sum of half-field expansion responses. Are rotation and expansion optomotor responses controlled by a single expansion-sensitive

circuit that is sub-optimally stimulated by a rotating flow field? Or instead are panoramic equilibrium responses mediated by separate optomotor pathways tuned specifically for rotation and expansion cues, respectively?

Here, we tested the hypothesis that the spatial, temporal, and contrast sensitivity of panoramic (i.e. large-field) optomotor responses vary for rotational *versus* translational flow fields, which would support the idea that these motor responses are mediated by separate and parallel pre-motor visual processing circuits. Using a tethered flight simulator, we measured the time course and amplitude of yaw torque wing kinematics in response to systematic variation of spatial frequency, temporal frequency, vertical pattern size, and contrast for optic flow fields that differ only in gross spatial organization. Our results show that spatial and temporal frequency sensitivity is similar for rotation and expansion optomotor responses, suggesting common elementary motion detection. However, impulse-response dynamics, receptive field size, and contrast sensitivity vary markedly for the two stimulus types, suggesting that after the first stages of motion coding, the two patterns of optic flow are processed by separate circuits within the fly's brain.

Materials and Methods

Animals and preparation

A *Drosophila* colony is reared on standard media under a 12:12 L:D cycle. Female adult flies, 4-6 days post pupal eclosion, were selected for use in this study. Animals were cold-anesthesized and tethered to a 0.1 mm tungsten rod with UV- activated glue (Kemxert Corp., York, PA, USA). After at least one hour of recovery, individual animals were placed within a custom-built computer-controlled electronic flight simulator composed of a cylindrical 96x32 array of green light emitting diodes (LEDs) spanning 330 degrees in azimuth and ±60 degrees in zenith as seen by the animal (Figure A1-1A). Each pixel was independently addressable at eight grayscale levels at a maximum of 72 cd m^{-2}, and maximum periodic contrast of 93%. Each individual LED subtended 3.75 degrees on the retina, therefore pattern motion was approximated using apparent motion stimuli. Both the motion of the projected pattern and the spatial pattern itself could be instantaneously modified under computer control. The manufacture, control, and spectral details of the LED display used here are detailed elsewhere (Reiser and Dickinson, 2008).

The wing kinematics exhibited in response to optomotor stimuli were encoded by an optical wingbeat analyzer in which an infrared beam casts a shadow of each beating wing onto a photodiode pair (Figure A1-1A). The two optical signals are conditioned such that sensor output represents time varying wing position. Associated electronics then process the analog position signal to extract total wing beat amplitude for the left and right wings, as well as total wing stroke frequency for each individual stroke. The difference in amplitude between the left and right wings (ΔWBA) is directly proportional to yaw torque (Götz, 1987; Tammero et al., 2004).

These values are digitized by a standard PC data acquisition system, and also relayed to control the velocity of the LED display under closed-loop conditions.

Visual motion stimuli, acquisition, and data analysis

Apparent motion was generated by panoramic patterns of vertical stripes moving horizontally. We examined responses to two motion patterns. The first is a classical optomotor stimulus consisting of a rotating striped "drum". For this stimulus, the pattern simply rotated at constant velocity around the fly in a clockwise direction (viewed from above), therefore the velocity profile was constant along 360 degrees of azimuth. The second stimulus was identical to the rotating drum except that the direction of motion in the rear visual hemisphere was reversed, forming a pseudo-translation flow field. This pattern of image motion produced a focus of expansion centered 90 degrees to the left of the animal, and a focus of contraction 90 degrees to the right. In other words, the pattern expanded from the left and contracted to the right of the fly (Figure A1-1B). The azimuthal velocity profile follows a square-wave trajectory rather than following a smooth sinusoidal trajectory. This stimulus produces strong motion cues near the poles of expansion and contraction, and we therefore refer to this stimulus as an "expansion" cue. The large-field visual expansion elicits robust steering responses in *Drosophila* (Tammero et al., 2004). During flight, expansion generated on the animal's left as well as clockwise rotation resulted in increased left minus right wing beat amplitude (ΔWBA), which is tightly correlated with rightward yaw torque. In related experiments, we tested for any influence of side-bias by periodically inverting the direction of visual expansion and rotation. Consistent with many

studies of optomotor behavior, we found no significant difference between responses to leftward or rightward motion.

The pattern gratings used here vary as a square wave of intensity along the azimuth, not as a sine wave. As such, there is significant frequency content above the fundamental spatial frequency defined by the grating period. However, in fruit flies the square-wave does not significantly impair perception of motion responses to the fundamental wavelength. For a related series of experiments, controls were performed with high temporal-resolution sine wave patterns and revealed that neither the time course nor the magnitude of optomotor flight responses vary between a square-wave pattern and a smooth sinusoidal pattern of the same wavelength (Duistermars et al., 2007). The relative insensitivity to high frequency components of a square-wave pattern likely reflects the well-known spatial low-pass characteristics of *Drosophila's* photoreceptor optics as well as the temporal low-pass characteristics of motion processing pathway through the brain, pre-motor pathways, and musculoskeletal system.

We first mapped the spatial and temporal sensitivity of expansion and rotation responses by systematically varying the spatial period of the projected visual pattern and its velocity. The stimulus regime was composed of open-loop large-field expansion or rotation test stimuli interspersed with periods during which the fly had active closed-loop control of a 30 degree vertical stripe. This stimulus regime insured that flies were actively engaged in optomotor behavior when the test patterns were presented. For all experiments, closed-loop periods lasted five seconds and test periods lasted three seconds each. Test stimuli consisted of a sequence of four (4) increasing velocities repeated for five (5) consecutive spatial period patterns, both for expansion and rotation (2) stimuli. Thus for this experiment, each fly was stimulated with a set of

4 x 5 x 2 = 40 different stimulus conditions – expansion and rotation of five spatial period patterns at four velocities. The spatial patterns were composed of (1) $\lambda = 15°$ spatial period with a 75- 25%, light-dark duty cycle, (2) $\lambda = 15°$, 50-50 duty cycle, (3) $\lambda = 30°$, 50-50 duty cycle, (4) $\lambda = 60°$, 50-50 duty cycle, (5) $\lambda = 90°$, 50-50 duty cycle. Velocity test values were 10, 169, 232, and 431° sec^{-1}. These spatial period and velocity combinations correspond to temporal frequencies ranging from 0.11 Hz to 35.4 Hz.

To examine the receptive field size of expansion and rotation responses, we systematically varied the vertical dimension of the striped pattern. This was done by first horizontally "scanning" the visual field with a one-pixel row of moving stripes to identify the most sensitive vertical region (Figure A1-5A), at which location the pattern was extended vertically in random increments between one pixel (3.75 degrees) and 32 pixels (120 degrees). To be clear, the pattern subtended the full 360 degree azimuth, but simply varied in the angle subtended in zenith.

To map the sensitivity of image contrast for the expansion versus rotation stimuli we chose one combination of spatial period and velocity conditions that consistently produced strong optomotor steering responses ($\lambda = 30°$ at 232° sec^{-1}). We then constructed expansion and rotation patterns that varied systematically in the intensity of the "light" and "dark" parts of the pattern. Contrast, estimated by the Michelson definition as the difference between "on" and "off" LED intensity values divided by the sum of "on" and "off" values (I_{max} - I_{min} / I_{max} + I_{min}). We tested optomotor responses to 27 unique contrast values, which were shuffled, and presented in expansion and rotation.

We repeated these contrast response experiments under two conditions – contrast-unadapted and contrast-adapted. For the unadapted condition, flies were presented with the stripe under closed-loop control prior to the open-loop test stimulus. As such, there was no prior exposure to the test contrast. To examine the influence of contrast adaptation prior to the test, the usual vertical stripe was replaced with the wide-field test pattern at the selected contrast during the closed-loop period, followed by the open-loop test. Thus, for the adapted treatment, there was seven seconds of exposure to the test contrast level prior to the test itself.

For each experimental treatment (variation in spatial and temporal frequency, vertical extent, and contrast), each fly received the entire series of expansion and rotation stimulus conditions. This design enabled statistical analyses with two-way repeated measures ANOVA for two within-subjects variables (Table A1-1). Because the different conditions were tested with the same subjects (i.e. within-subject design), statistical significance between the expansion and rotation treatments are not represented by error bars (Masson, 2003), which are therefore omitted for clarity.

Time series data including the instantaneous azimuthal position of the visual pattern, stimulus waveform and TTL sync pulse, ΔWBA, raw left and right wing stroke amplitude, and wingbeat frequency were digitized at 500Hz (Axon Instruments DigiData 1320, Sunnyvale, CA, USA) and stored on a PC workstation. All analyses were performed with custom software routines written in Matlab (Natick, MA, USA). The raw wingbeat amplitude signals were low-pass filtered at 200Hz with a 5^{th} order zero-phase digital Butterworth filter. For each three-second test stimulus cycle, we measured the maximum ΔWBA value within the first 1.5 seconds

of the test (roughly 300 wing beats) to quantify response amplitude. Data were then normalized to the highest value of the entire data set (R/Rmax).

Results

We examined the spatial, temporal, and contrast sensitivity of visual motion detection during tethered flight in *Drosophila melanogaster*. During periods of closed- loop control of a single vertical stripe, flies actively balanced the amplitude of the right and left wing beats such that the difference was near zero (Figure A1-2A). By contrast, in response to either rotation of the visual panorama, or expansion from one side, stroke amplitude increased on the left side and decreased on the right side (Figure A1-2A). Thus, the difference in stroke amplitude increased during test periods corresponding to attempted turns to the right - away from the center of visual expansion (for the expansion stimulus) and following the direction of panoramic visual rotation (for the rotation stimulus). The magnitude and time course of the steering reactions varied according to (1) the temporal frequency of image motion, (2) the spatial period of the display pattern, (3) the spatial organization of the stimulus (rotation or expansion). During the test sequences, steering responses to open-loop visual stimuli were robust in that they persisted for the duration of the stimulus, and were also repeatable in that the variance about the mean response trajectory was low (Figure A1-2B). On average, low spatial period patterns comprising narrow stripes produced weaker responses by contrast to high spatial period patterns which produced the largest steering responses.

The product of spatial frequency (cycles degree^{-1}, reciprocal of spatial period) and velocity defines the frequency that moving stripes pass over the eye (temporal frequency in cycles sec^{-1}). Mean ΔWBA shows a characteristic tuning profile with respect to temporal frequency. For both expansion and rotation stimuli, responses were fairly consistent between 0.1 and 0.6 Hz, then rose steeply to a plateau between 3 and 10 Hz before rolling off at 30 Hz (two-

way repeated measures ANOVA $p<0.001$, Table A1-1). The rotation and expansion stimuli produced similar temporal frequency tuning curves, but rotation responses were attenuated by 20% across the entire range of temporal frequencies (Figure A1-3, $p<0.001$ Table A1-1). To highlight the similarity of temporal tuning between the two visual treatments, we fitted a Gaussian curve (Srinivasan et al., 1999) to the log-transformed expansion data using a least-squares optimization method. We then used the amplitude and position coefficients from the expansion fit and allowed only an offset parameter to be scaled for the rotation data set. R-square values were similar for both fits (0.82 and 0.89 respectively) with the rotation curve being offset downward on the y-axis by 20% compared to the expansion curve. These results suggest that whereas the gain of optomotor responses is higher for an expansion flow field, the temporal frequency optimum is the same for both expansion and rotation.

Likewise, the spatial frequency sensitivity for expansion and rotation are similar. Mean response values were plotted for each spatial pattern across each test velocity. The data were smoothed with shape-preserving interpolations (Figure A1-4). Whereas the plots for the rotation data are shifted downward approximately 20%, there are no conspicuous differences between the spatial tuning profiles for expansion and rotation stimuli – instead the functions peak at approximately 165 degrees per second for each spatial period tested (Figure A1-4).

We next explored how optomotor response magnitude is influenced by the vertical extent of pattern motion. On average, for a one-pixel row of horizontally (azimuthally) moving edges, optomotor steering responses were strongest near the visual equator (Figure A1-5B). As the vertical extent grows, so too does the amplitude of optomotor equilibrium responses. The stimulus-averaged response trajectories for each of 16 different vertical pattern sizes are color-

coded and overlaid in Figure A1-5C. These data indicate two things. First, as has been reported previously (Tammero et al., 2004), and indicated in Figure A1-2, the response trajectory varies in a categorical manner for expansion and rotation stimuli. At the onset of constant-velocity motion, expansion responses rise quickly, peak, then slowly decay. By contrast, rotation responses rise more slowly, but do not peak but rather continue to rise until the termination of the stimulus. Second, the response maxima for the expansion stimulus continue to increase with increasing vertical pattern size (color-coded waveforms in Figure A1-5C), but rotation responses are independent of pattern size after the pattern reaches roughly 30 degrees vertical extent (Figure A1-5D). Thus, the "receptive field" of expansion-mediated optomotor responses appears to occupy the entire visual field, whereas the rotation responses are mediated by a receptive field centered at the visual equator and subtending roughly ±30-degrees (Figure A1-5D, $p<0.001$ Table A1-1).

To further examine the low-speed range of optomotor dynamics, we stepped the panoramic visual stimulus in 3.75 degree increments at approximately two increments per second. The individual "jerky" image steps were clearly apparent to a human observer. For the fly, each 3.75-degree image expansion displacement resulted in a rapid turning response phase-locked to the motion cue (Figure A1-6). By contrast, the identical stepwise motion of the full-field rotating pattern did not elicit phase-locked torque responses, but rather elicited only a steadily increasing response that is more consistent with responses to smooth apparent pattern motion – motion that is not "jerky". These results indicate that rotation responses show low-pass characteristics that are largely absent in the expansion responses.

Finally, we explored how the periodic contrast of moving patterns differentially influenced optomotor equilibrium responses to rotation and expansion flow fields. Flies were presented a pattern composed of spatial wavelength $\lambda = 30°$ at a velocity of $232° \text{ sec}^{-1}$ for three seconds. Pattern contrast ratio varied between 0.008 and 0.93. As discussed above, we ran two experiments, the first was for flies that were tested without any prior exposure to the tested pattern contrast (unadapted) and the second for flies that were presented with the test contrast prior to the test (adapted). The results indicate that for both unadapted and adapted conditions, response magnitude varies according to both the contrast and the spatial organization of visual motion, (two-way repeated measures ANOVA $p<0.001$, Table A1-1). Expansion consistently elicited higher optomotor equilibrium responses. For the unadapted flies, low contrast rotation and expansion elicited similar response magnitude (Figure A1-7), and as contrast increased expansion responses saturated at 0.3, whereas rotation responses were lower in magnitude, increased monotonically with contrast, and saturated at near 0.93 contrast, 20% lower magnitude than for expansion (Figure A1-7, left). For the contrast adapted flies, the rotation responses were similar to the unadapted condition, but showed slightly elevated, but insignificant, responses across contrasts. Strikingly, after the adaptation regime the expansion responses were conspicuously elevated at low contrast (Figure A1-7, right).

To quantify contrast sensitivity we fit a sigmoidal function to the data that captures two critical elements of contrast sensitivity – a quadratic dependence at low contrast and response saturation at high contrast.

$$F(x) = \frac{\alpha}{1 + e^{(\beta(x-\gamma))}}$$

Parameters for the sigmoid function (indicated in Figure A1-7) were determined with a Nelder-Mead non-linear optimization algorithm. The parameters describe the saturation level (α), the steepness (β), and the rightward shift (γ) of the function, respectively. For the unadapted rotation function $\alpha = 0.83$, $\beta = -5.6$, and $\gamma = -0.1$, giving an R-square of 0.77.

For the unadapted expansion function $\alpha = 0.95$, $\beta = -26$, and $\gamma = 0.52$, for an R-square of 0.85. For adapted rotation $\alpha = 0.85$, $\beta = -5.7$, and $\gamma = -0.15$, giving an R-square of 0.6. For adapted expansion $\alpha = 0.94$, $\beta = -71$, and $\gamma = -0.04$, giving an R-square of 0.13 (note that the low R-square results from the wing steering responses being independent of contrast due to full saturation). Thus, the rotation response functions saturate at roughly 80% of the expansion response levels, rise roughly 4 times slower with increasing contrast, and are shifted to the right on the contrast axis. Contrast adaptation results in near-immediate saturation of the expansion response function, whereas there is very little change in the rotation function, indicating a strong separation of the two responses at low contrast levels.

Discussion

This central aim of this study was to map the spatial, temporal, and contrast sensitivity of optomotor equilibrium functions elicited by large-field patterns of visual rotation and side-centered visual expansion in order to examine the hypothesis that the two types of optic flow may be processed by parallel neural pathways. Our quantitative behavioral results provide evidence that large-field optomotor expansion and rotation equilibrium responses are mediated by a common array of elementary motion detectors, but then diverge into separate pre-motor motion processing pathways that have different spatial receptive fields, low-pass characteristics, and contrast sensitivity. These conclusions are based on several lines of evidence. The identical spatial and temporal frequency sensitivity optima (Figures A1-3,4) suggest that the two flow fields are processed by delay-and-correlate motion detectors containing similar time constants and spatial separation of the input channels. The evidence suggesting that the motion processing path diverges after the elementary motion stage into separate parallel pre-motor pathways comes from three subsequent results. First, expansion responses increase linearly with vertical stimulus extent whereas rotation responses saturate at ~30 degrees (Figure A1-5) suggesting distinct receptive field properties. Second, steering "spikes" in response to rapid low-amplitude image displacements are conspicuous for an expanding flow field, but not for a rotating one (Figure A1-6), suggesting distinct low-pass characteristics. Third, expansion responses persist and are near maximal even under very low contrast conditions, particularly after pre-exposure to the test contrast level (Figure A1-7) implying separate contrast sensitivity to expansion and rotation.

Insects (as well as virtually all seeing animals) respond to a rotating visual panorama by turning in the direction of motion. For flying animals such as fruit flies, this robust behavioral attempt to minimize large-field retinal slip comprises a classical syndirectional *optomotor* response thought to maintain a stable trajectory by correcting external perturbations such as gusty wind, or internal perturbations such as bilaterally asymmetric motor output (Collett, 1980; Götz and Wandel, 1984; Götz, 1964; Heisenberg and Wolf, 1984). Within the earliest stages of motion processing, the apparent direction and strength of image motion is thought to be determined by the spatial separation of visual sampling units such as neighboring ommatidia as well as the delay time constant imposed between two units prior to temporal correlation (Hassenstain and Reichardt, 1956). As such, the magnitude of electrophysiological responses in motion processing neurons as well as yaw torque reactions are bounded by separable spatial and temporal frequency-sensitivity functions reflecting the properties of the elementary motion detectors (EMDs; Borst and Egelhaaf, 1993; Egelhaaf and Borst, 1993; Srinivasan et al., 1999). As an abstract model, each EMD is characterized by a unique spatio-temporal frequency sensitivity surface. It follows that any two optomotor behaviors that are maximally sensitive to the same wavelength and temporal frequency likely draw from a common pool of EMDs. Our results show that the temporal frequency optima for both expansion and rotation optomotor responses lie between 3 and 12Hz (Figure A1-3), and the spatial wavelength sensitivity peaks at λ=30° (Figure A1-4). These values are consistent with findings for yaw torque flight optomotor responses in house flies (Borst and Bahde, 1987; Reichardt and Reichardt, 1966) and blow flies (Wehrhahn, 1985), as well as for walking fruit flies (Buchner, 1984), and lead us to the parsimonious conclusion that the same system of EMDs underlies optomotor responses to both flow fields during flight in fruit flies.

In larger flies, it is thought that input from the retinotopic local motion processing neurons comprising the EMDs is spatially pooled by neurons of the 3rd optic ganglion to construct neural responses to large-field patterns of optic flow (Higgins et al., 2004; Single and Borst, 1998). Tangential cells of the lobula plate (LPTCs) show receptive field properties tuned to the orientation and direction of wide-field movement across the retina and play a crucial role in the guidance of optomotor equilibrium responses (Hausen, 1982; Krapp et al., 1998). Thus, examining how optomotor behavioral responses vary with the extent of motion projected across the retina can be used to estimate the extent of EMD integration and by extension the underlying system of LPTCs (Borst and Bahde, 1987). We found that varying the vertical size of the moving pattern had different effects on the expansion and rotation optomotor equilibrium responses during flight. Whereas rotation responses saturated at roughly 30-degree pattern size, expansion response amplitude continually increased with increasing pattern size (Figure A1-5). These results support the hypothesis that the two flow fields are processed by separate ensembles of LPTCs with different, but perhaps overlapping, vertical receptive fields.

The temporal properties of optomotor steering responses to dynamic stimuli have been used to correlate behavior with specific LPTC circuits. House flies (genus Calliphora) show sluggish yaw torque and steering muscle spike modulations in response to panoramic image rotation by comparison to the rapid responses elicited by small object motion (Egelhaaf, 1987; 1989). These behavioral responses correlate tightly with the membrane responses of HS and FD cells, respectively, (Egelhaaf et al., 1988) implying that HS participates in relatively slow wide-field optomotor equilibrium reflexes, whereas FD participates in object tracking or body saccade maneuvers with a much shorter time constant. Here, we show that intermittent displacement steps of a laterally expanding image evoke rapid high-amplitude torque responses, whereas a

rotating image produces only gradual syndirectional shifts in the steering signal without phase-locked amplitude fluctuations (Figure A1-6). We take this as evidence that the expansion optomotor response is low-pass filtered with a shorter time constant than the rotation response owing to separate pre-motor motion processing pathways with different temporal dynamic properties. As an important caveat, currently little is known of motion processing in *Drosophila*, but the horizontal and vertical system cells show similar anatomical architecture, with apparently fewer large-field cells (Scott et al., 2002).

In addition to the spatial and temporal frequency characteristics, the detection of visual motion depends upon the periodic contrast of moving images. The sensitivity to image contrast of simulated EMDs, LPTC recordings, and behaving flies is non-linear such that at a given spatial wavelength, response amplitude shows a quadratic dependence at low contrast and saturates at higher contrast levels (Buchner, 1984; Dvorak et al., 1980; Harris et al., 2000). Flight optomotor equilibrium responses also show a saturated-quadratic functional dependence of image contrast, but the shape of the response functions differ in that expansion sensitivity shows a steeper rise, saturates at a higher value, and is shifted rightward on the contrast axis by comparison to rotation (Figure A1-7). Do these different parameters suggest separate underlying pathways? Individual LPTC neurons (e.g. HS) display motion adaptation that effectively shifts the sensitivity curve rightward on the contrast axis, but does not alter the shape of the response function (Harris et al., 2000). Our results show very different shaped sensitivity functions for the expansion and rotation data. Furthermore, these differences are amplified stronger after flies are exposed to the stimulus contrast pattern for some time prior to the actual open-loop test. We refer to this treatment as “contrast adaptation”, and it results in a strong increase in contrast sensitivity, particularly to low contrast, within expansion responses but no significant change in rotation

responses (Figure A1-7). Taken together, these results suggest that the sensitivity to image contrast is qualitatively different for responses to large-field patterns of rotation and expansion, which can be most parsimoniously explained by the presence of two parallel pre-motor large-field circuits with different intrinsic sensitivity to image contrast.

What are the possible parallel visual circuits for expansion and rotation selectivity? Whereas the reconstructed receptive fields of some LPTCs appear to be matched for spatially complex panoramic optic flow patterns generated by flight maneuvers such as pitch and roll (Krapp, 2000; Krapp and Hengstenberg, 1996), there are as yet no reports of LPTCs that specifically encode either patterns of image expansion centered laterally. HSE, once thought to encode panoramic rotation, fails to do sounder naturalistic optic flow conditions (Kern et al., 2001). There may simply not be a single LPTC responsible for the rotation optomotor or expansion optomotor equilibrium responses examined here. Since LPTCs show extensive heterolateral connections (Haag and Borst, 2002), it seems much more plausible that complex optic flow patterns are encoded by groups of LPTCs with distinct but overlapping receptive fields. Pre-motor descending visual interneurons postsynaptic to the LPTCs may assemble receptive fields for expansion and rotation, and convey this information to relevant steering and power muscle motor networks.

Whereas it is certainly the most studied visual neuropile in the fly, the lobula plate is by no means the only place where motion circuits reside. Expansion-sensitive interneurons have been reported within the optic lobes and midbrain in locusts (Gabbiani et al., 1999; Judge and Rind, 1997), mantids (Krai and Prete, 2004), and hawkmoths (Wicklein and Strausfeld, 2000).

Whatever the underlying visual circuit – it would appear that large-field rotation and expansion mediated optomotor behaviors are coordinated by separate parallel pathways.

Advantages of separate rotation and expansion pathways

Maintaining dynamic optomotor equilibrium, avoiding approaching obstacles, or tracking visual objects requires encoding these environmental features correctly. Separate neural circuits dedicated to expansion and rotation stimuli ensure response specificity under different sensory conditions. For example, the high-gain expansion circuit may mediate rapid collision avoidance and escape from approaching predators, whereas the rotation circuit may mediate stability during slow flight or hovering. As with larger flies, *Drosophila* show frequency-separated large-field and small-field optomotor steering responses, and large-field equilibrium dynamics are in part mediated by a segregation of rotation and expansion signals for the control of wing beat frequency, amplitude, and resultant mechanical power output (Duistermars et al., 2007).

There is some behavioral evidence for the operation of two distinct control systems. During free flight, fruit flies execute segments of straight flight interspersed with rapid ninety-degree turns called saccades (Tammero and Dickinson, 2002a). Saccadic motor patterns are used by animals as diverse as humans (Land, 1992) and houseflies (Schilstra and van Hateren, 1998) to minimize the corrupting influence of motion blur and maintain stable gaze. During free flight, *Drosophila* saccades are threshold-triggered by a monotonic increase in the magnitude of contralateral large-field retinal expansion, but not rotation (Tammero and Dickinson, 2002a). However, between ballistic expansion-elicited saccades, the flight path is not exactly straight but rather is slightly curved depending on the proximity of the nearest wall (although the direction of the curved turn is away from the closest wall, not toward it, so the turn can not be explained by a

purely syndirectional rotational optomotor reflex). Recent evidence from blow flies suggests that it is during these inter-saccade flight segments that the LPTCs encode the spatial layout of the visual environment (Kern et al., 2005).

Expansion responses themselves mediate several important behaviors during flight. Results obtained with tethered *Drosophila* show that visual processing is likely further segregated into parallel collision avoidance and landing behaviors. A laterally expanding object elicits rapid and robust steering responses oriented away from the focus of expansion. By contrast, the same stimulus presented within the frontal field of view elicits a leg kick, without a steering response, thought to comprise an attempt to land. Both the spatial and temporal properties of these two reflexes strongly implicate the operation of parallel underlying circuits (Tammero and Dickinson, 2002b). Aerodynamic and body dynamic simulations have suggested that visual expansion can itself provide an unambiguous cue to dynamically maintain an upwind flight posture (Reiser et al., 2004). Electrophysiological recordings from the cervical connective in blowflies have revealed a group of expansion-sensitive descending pre-motor interneurons that likely mediate landing responses (Borst, 1990). There are scant physiological analyses of identified descending neurons in flies (but see Gronenberg and Strausfeld, 1992) for small object selective cells). The evidence presented here motivates the hypothesis that descending pathways may draw from lobula plate cell systems with distinct but overlapping receptive fields in order to multiplex expansion and rotation sensitive signals passing to the flight motor circuits of the thorax. Disclosing these circuits will further illuminate the neural mechanisms of one Nature's most spectacular visual behaviors – fly flight.

Abbreviations

ΣWBA left plus right (sum) wing beat amplitude LPTC lobula plate tangential cell

Acknowledgments

The authors are indebted to Dr. Martin Egelhaaf and Dr. Andrew Straw for informally evaluating our results and providing feedback and suggestions. We also thank Dr. Michael Reiser for engineering the LED display panels. This work was supported by an Alfred P. Sloan Foundation Research Fellowship, Whitehall Foundation grant (2006-12- 10), and NIH training grant (T32 GM065823).

Tables

Table A1-1

ΔWBA source	df	F	p
vert extent	15	11	<0.001
exp vs rot	1	20	<0.001

ΔWBA source	df	F	p
temporal freq	19	9	<0.001
exp vs rot	1	37	<0.001

ΔWBA source	df	F	p
unadapted contrast	15	13	<0.001
exp vs rot	1	43	<0.001

ΔWBA source	df	F	p
adapted contrast	15	11	<0.01
exp vs rot	1	22	<0.001

Two-way repeated measures ANOVA for two within-subjects variables including: expansion versus rotation, vertical extent, temporal frequency, and two contrast treatments (unadapted and adapted, see Methods).

Figures

Figure A1-1: Experimental apparatus.

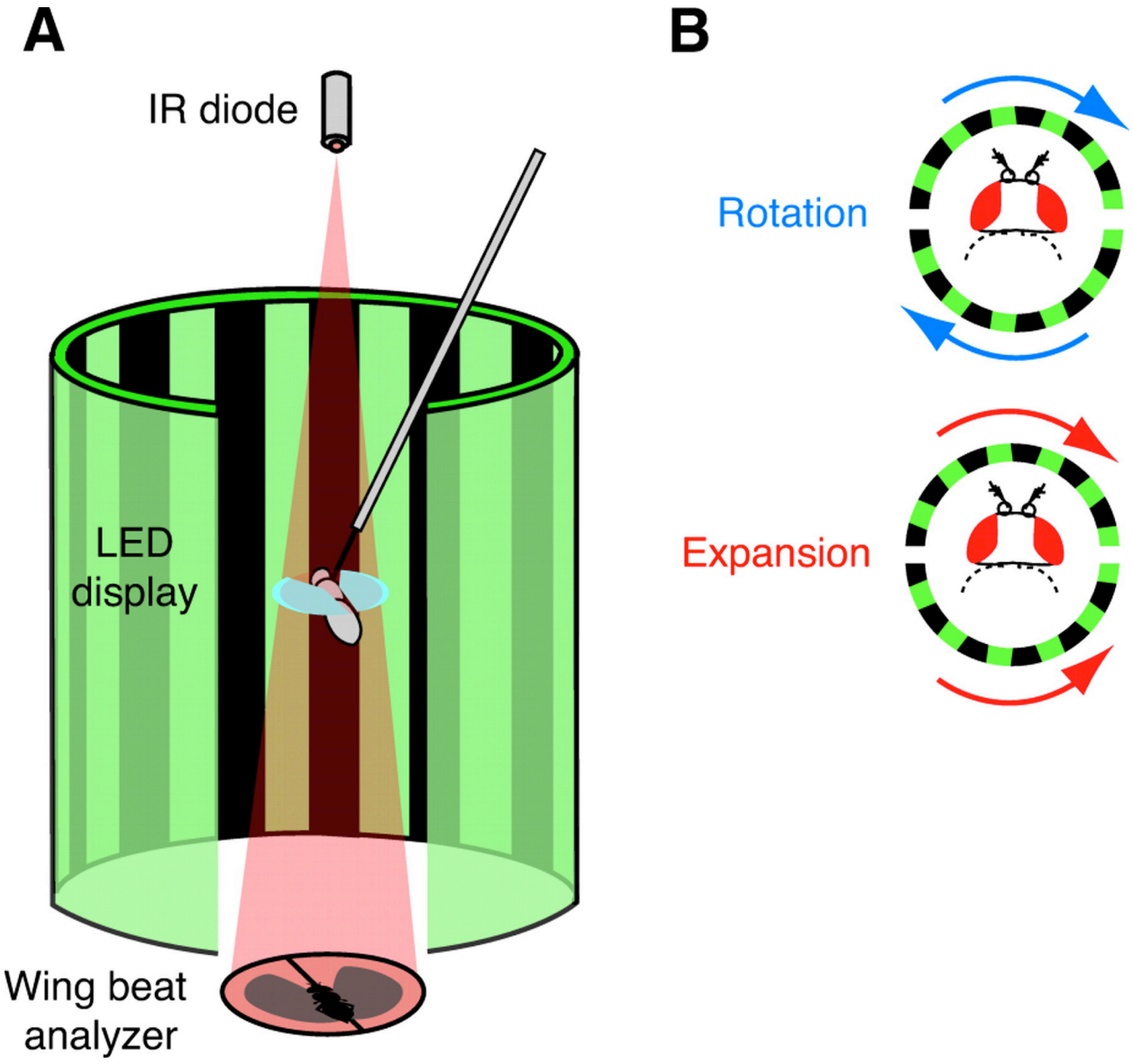

A) A digital flight simulator comprises a wrap-around cylinder of light emitting diodes (LED). An infrared (IR) beam casts a shadow of the two wings on an optoelectronic sensor that measures instantaneous changes in right and left wing beat amplitude and frequency in response to image motion. **B)** Panoramic patterns of vertical stripes move horizontally to elicit

compensatory optomotor steering responses. Visual expansion differs from visual rotation only in the direction of motion across the rear field of view.

Figure A1-2: Optomotor steering responses to panoramic image motion.

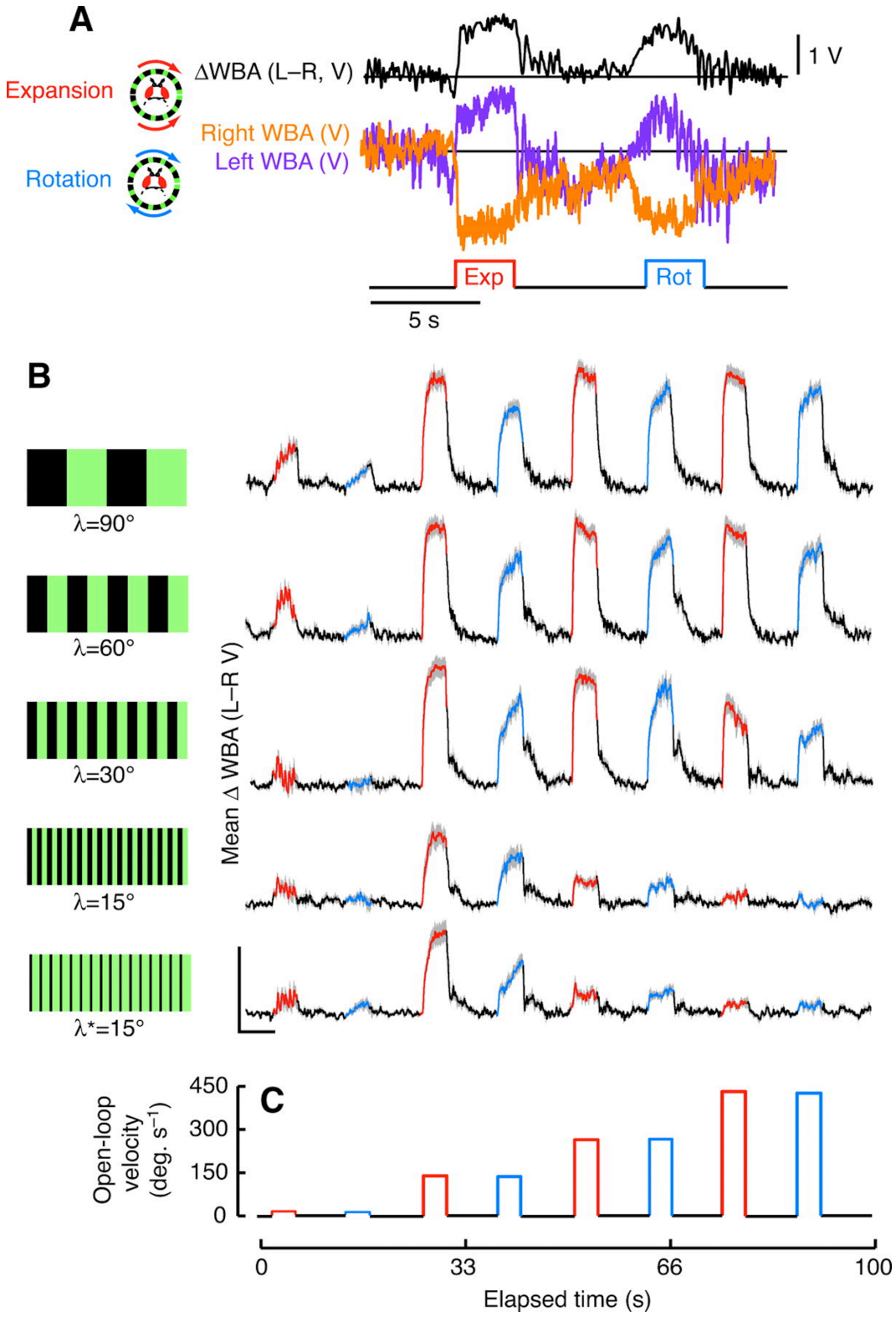

A) Example response to a test expansion and rotation stimulus. In response to expansion from the left, the amplitude of the right wing beat decreases while the amplitude of the left increases. As such left minus right amplitude (ΔWBA) increases in response to both stimuli, but with varying amplitude. Between test periods, the fly has active control of a single vertical stripe. **B)** Mean responses to systematic variation in the spatial period and velocity of pattern motion. Time-averaged responses indicated with solid line, with gray envelope indicating S.E.M. N=36 flies. 3-second open-loop expansion test periods are indicated with red line segments, rotation tests are indicated with blue segments, and intervening 5-second closed-loop control periods indicated with black segments. Each row shows mean responses to striped grating spatial period as indicated. Scale bar 3V, 5 seconds.

Figure A1-3: Temporal frequency tuning curves for expansion and rotation optomotor responses.

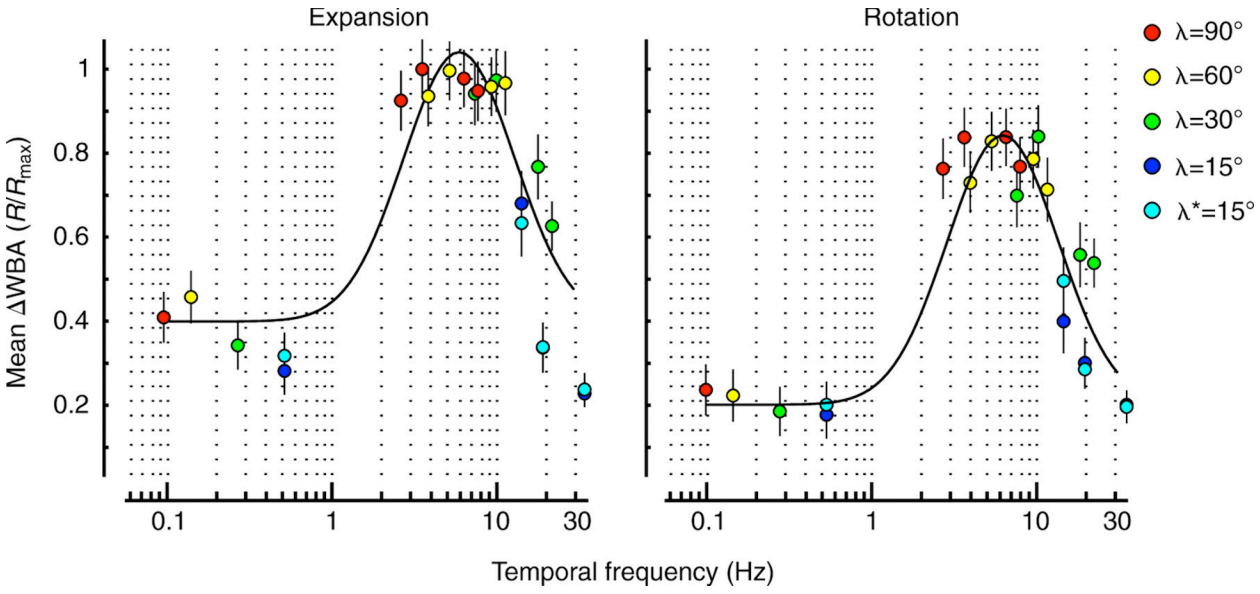

Responses to different spatial wavelengths are pooled. Points indicate means ±S.E.M. for N=36 flies. A Gaussian waveform is plotted in both panels, but is shifted downward ~20% for the rotation plot.

Figure A1-4: Tuning curves for spatial wavelength over velocity for expansion and rotation optomotor responses.

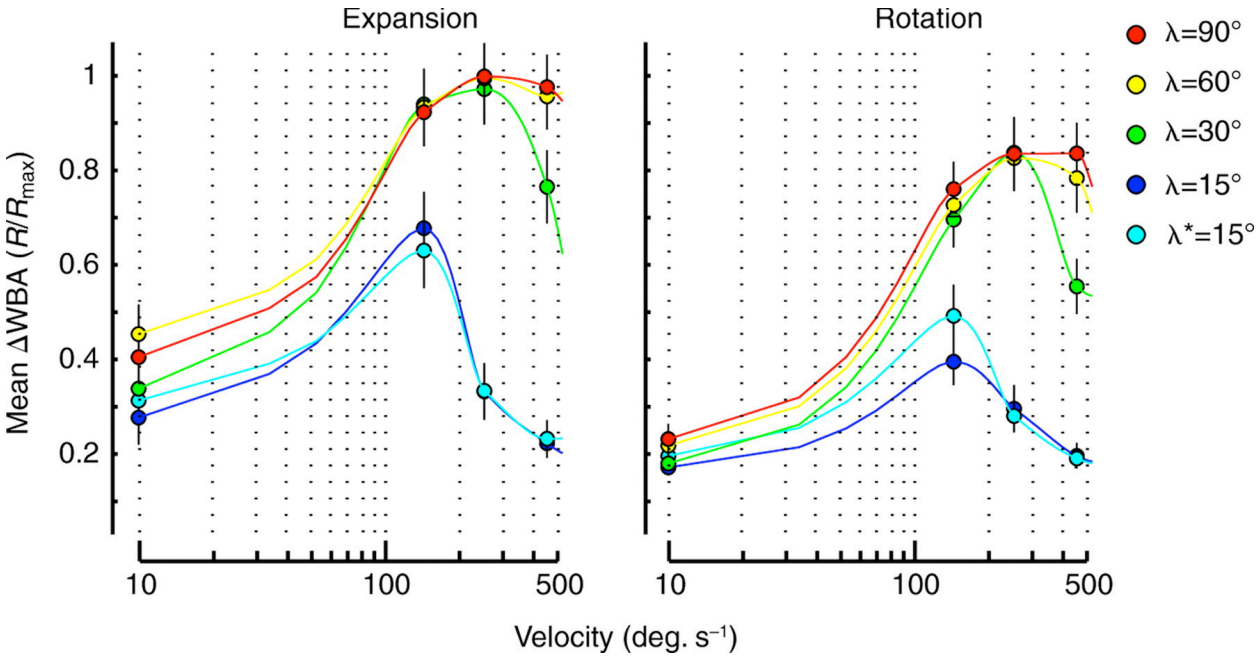

Data points from Figure A1-3 are re-plotted, fit with shape preserving interpolant functions, and color-coded for response amplitude to facilitate visual comparison.

Figure A1-5: Optomotor responses vary with the vertical extent of pattern motion.

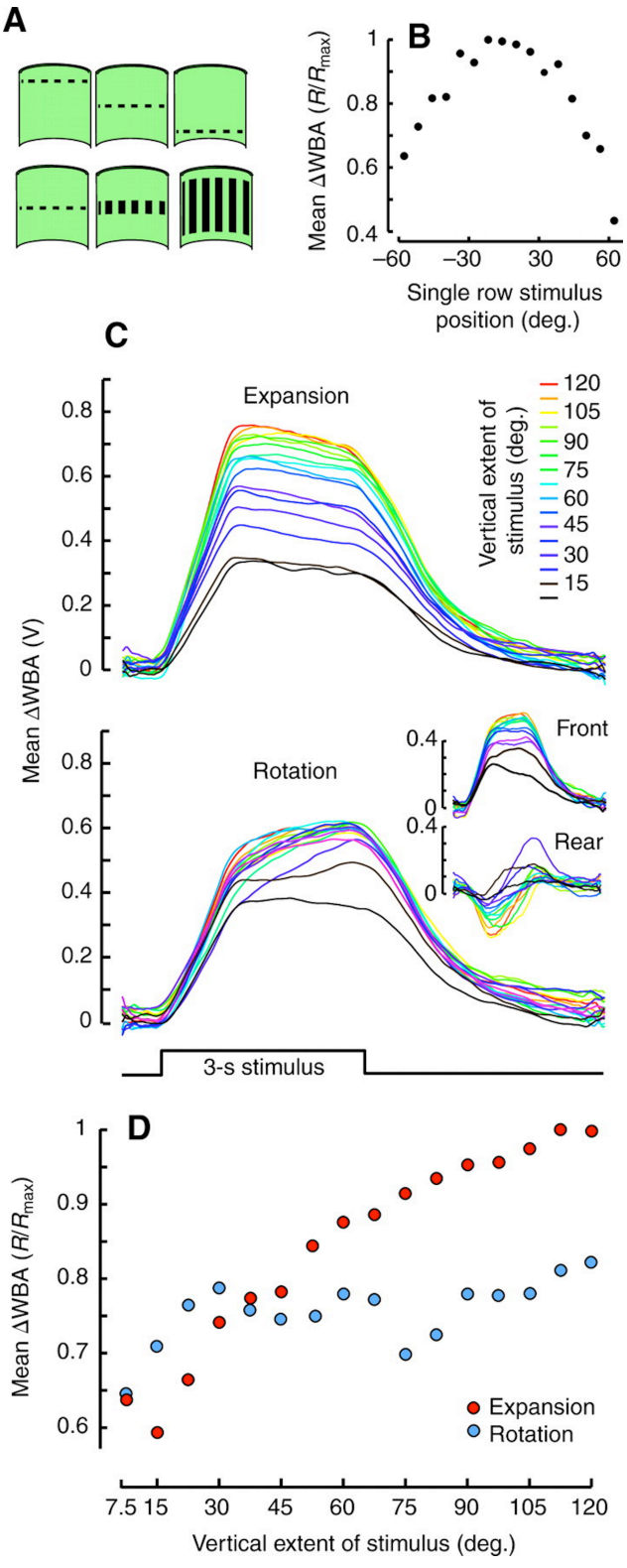

A) Diagram of visual stimuli. Top row: stimuli used to find the vertical location of the strongest sensitivity to horizontally moving stripe patterns. Bottom row: representations of stimuli that vary in vertical stimulus extent. **B)** Response magnitude for a single pixel row of expansion stimuli plotted against the vertical location of the row in the arena indicating maximum sensitivity in the middle of the arena, where the fly is positioned. **C)** Mean response waveforms to visual expansion (top) and visual rotation (bottom) that varies for the vertical extent of image motion (color coded). Insets indicate responses to motion restricted to only the front or rear 180 degrees of the cylindrical arena. **D)** Steady-state response amplitude of the waveforms indicated in (C) for N=50 flies.

Figure A1-6: Mean time course of responses to one pixel image displacements (3.75 degrees) at two steps per second.

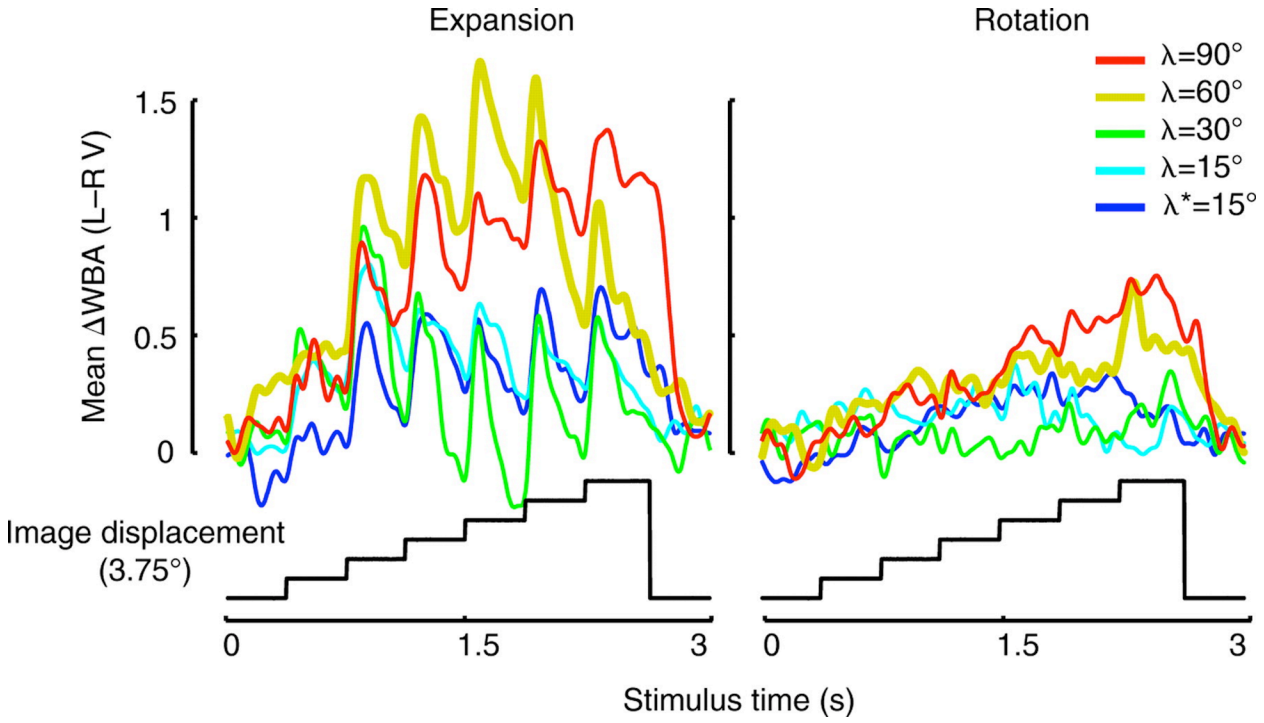

Each waveform represents the mean response for N=36 flies at the color-coded spatial wavelength.

Figure A1-7: Optomotor responses vary with image contrast.

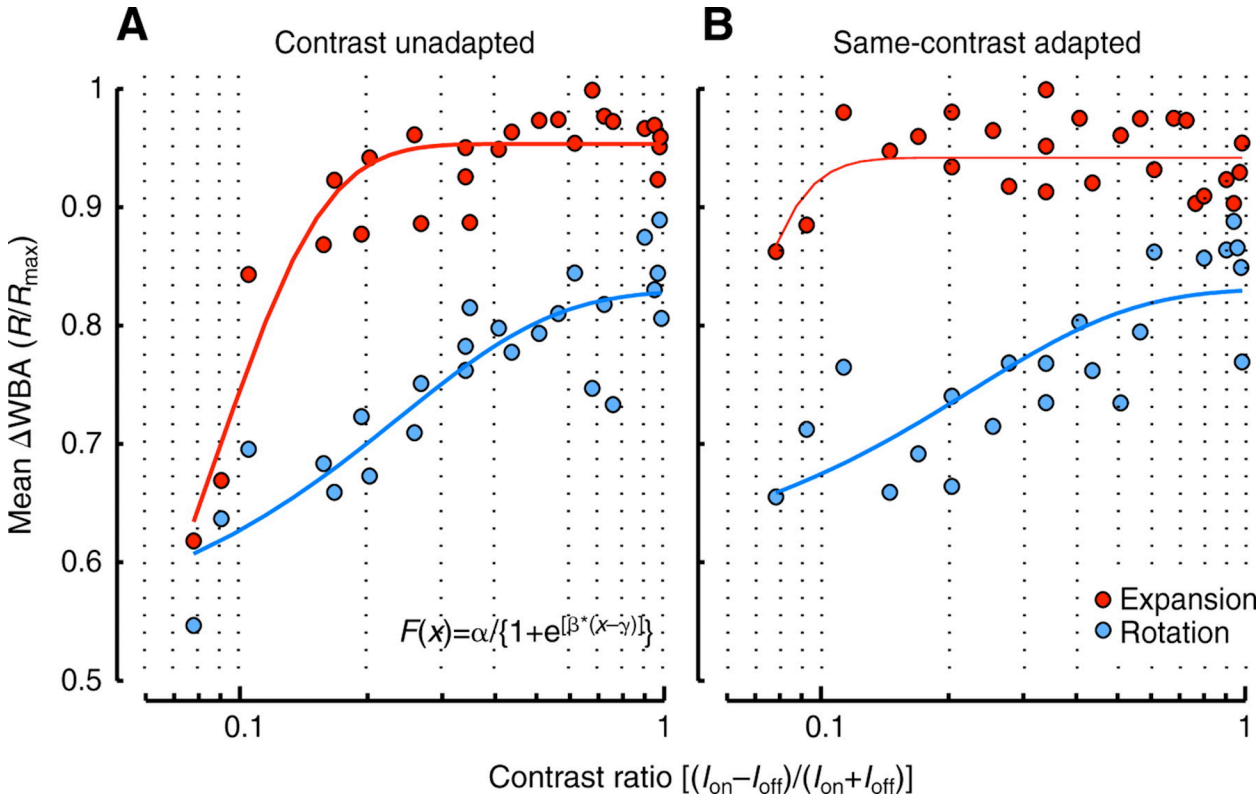

Left: mean responses for N=30 flies indicated for an unadapted treatment - flies had no prior exposure to the test stimulus. Right: mean responses for N=40 flies indicated for a "contrast adapted" treatment – flies were presented with the test pattern for 7 seconds prior to the open-loop test (see Methods). Data are fit with the sigmoid function indicated. The three function variables were identified with a non-linear least-squares optimization algorithm (see Methods).

Appendix 2: Birdsong Decreases Protein Levels of FoxP2, a Molecule Required for Human Speech

Julie E. Miller, Elizabeth Spiteri, Michael C. Condro, Ryan T. Dosumu-Johnson, Daniel H. Geschwind, and Stephanie A. White

Statement of Contribution

The experimental paradigm described in this publication involves comparing FoxP2 protein expression in zebra finches that were either isolated, presented with a series of females, or actively interrupted by an experimenter. This raised concerns about the differences in physiological states in each behavioral condition. Specifically it was unclear that the difference in gene expression between the conditions was not due in part to a stress response. To address this concern, I designed an experiment in which the stress hormone corticosterone was measured from blood in each condition. For this publication, I wrote the methods subsection titled "Assessment of Corticosteroid Levels" and provided Figure A2-6B. I found no statistical difference in corticosterone levels between experimental conditions, suggesting that stressors attributed to the behavioral condition did not affect the observed changes in protein expression.

Abstract

Cognitive and motor deficits associated with language and speech are seen in humans harboring FOXP2 mutations. The neural bases for FOXP2 mutation-related deficits are thought to reside in structural abnormalities distributed across systems important for language and motor learning including the cerebral cortex, basal ganglia and cerebellum. In these brain regions, our prior research showed that *FoxP2* mRNA expression patterns are strikingly similar between developing humans and songbirds. Within the songbird brain, this pattern persists throughout life and includes the striatal subregion, Area X, that is dedicated to song development and maintenance. The persistent mRNA expression suggests a role for FoxP2 that extends beyond the formation of vocal learning circuits to their ongoing use. Since FoxP2 is a transcription factor, a role in shaping circuits likely depends upon FoxP2 protein levels which might not always parallel mRNA levels. Indeed, our current study shows that FoxP2 protein, like its mRNA is acutely down-regulated in mature Area X when adult males sing, with some differences. Total corticosterone levels associated with the different behavioral contexts did not vary, indicating that differences in FoxP2 levels are not likely attributable to stress. Our data, together with recent reports on FoxP2's target genes, suggest that lowered FoxP2 levels may allow for expression of genes important for circuit modification and thus vocal variability.

Introduction

Language and speech deficits accompany a wide variety of cognitive impairments, most prominent examples of which are developmental dysphasia/dyslexia, Specific Language Impairment and autism spectrum disorders (Fisher, 2005; Muhle et al., 2004; Smith, 2007). Multi-genetic factors give rise to these disorders, thus presenting a challenge to researchers in understanding their neurological bases and in developing therapies. The gene encoding FOXP2, a member of the forkhead box (FOX) group of transcription factors, has provided a unique molecular entry point into the neural basis of speech since several forms of heterozygous mutations in FoxP2 cause developmental speech and language disorders with prominent features of apraxia (Lai et al., 2001; Watkins et al., 2002). (Of note, by convention, human 'FOXP2' is fully capitalized, mouse 'Foxp2' is not, and 'FoxP2' denotes the molecule in mixed groups of animals. Italics are used when referring to genetic material such as *FoxP2* mRNA; Carlsson and Mahlapuu, 2002). In the best-characterized case, members of the KE family have difficulty in the central control of sequential, complex orofacial movements, language skills, and impairments in verbal intelligence (Lai et al., 2001). In keeping with the evolving view that neural substrates for speech and language encompass more than just cortical regions (Lieberman, 2007), affected individuals show bilateral abnormalities in subcortical structures, namely the basal ganglia and cerebellum, in addition to cortical abnormalities that include classic language areas like Broca's in the inferior frontal gyrus, all of which are important for human linguistic ability, and motor and reward-based learning. Structural and functional magnetic resonance imaging reveal altered amounts of grey matter in these regions, and their underactivation during tasks of verbal fluency, respectively (Belton et al., 2003; Liegeois et al., 2003; Vargha-Khadem et al., 1998).

Natural constraints on the ability to explore cellular pathways for FOXP2 function in humans create the impetus for developing models in non-human species, particularly other vocal learners (White et al., 2006). Prominent among these are songbirds which are thought to share mechanisms and pathways for vocal learning with humans (Doupe and Kuhl, 1999). Songbirds, like humans but unlike traditional lab animals such as rodents, create new sounds by listening to others and to themselves in order to learn their vocalizations. Thus, while important advances in understanding Foxp2 function on motor learning, especially those involving the cerebellum, are being made using transgenic mice that lack Foxp2 (Shu et al., 2005) or possess mutant Foxp2 variants (Fujita et al., 2008; Groszer et al., 2008), the impact on learned vocal behaviors may not be observable in this species. A second key strength of the songbird model system is that the neural structures that subserve the learning and production of vocalizations are well-characterized, (Figure A2-1A), which is less the case for humans (Jarvis et al., 2005). In the zebra finch songbird, *Taeniopygia guttata,* vocal learning and the underlying neural circuitry is sexually dimorphic (Nottebohm et al., 1976). Males, but not females, acquire their song during critical developmental phases by listening to an adult male "tutor", then modify their own vocalizations to match the memorized model. Within the pallium, striatum and thalamus, the subregions dedicated to song are larger and interconnected in males, a feature that has facilitated their identification and characterization. The anterior forebrain pathway through these regions (Figure A2-1A) resembles mammalian cortico-basal ganglia loops (Bottjer and Johnson, 1997; Farries, 2001; Farries and Perkel, 2002; Jarvis et al., 2005; Reiner et al., 2004b).

In contrast to speech, zebra finch song stabilizes at sexual maturity, and each male thereafter sings one song. However, once learned, both speech and birdsong continue to rely on hearing in order to maintain the quality of the learned vocalizations in adulthood (Brainard and

Doupe, 2000b; Cynx and Rad, 2001; Nordeen and Nordeen, 1992; Williams and Mehta, 1999). Adult song can be characterized as either 'directed', when a male sings to a conspecific, often a female, or 'undirected', when the male practices alone (Dunn and Zann, 1996; Hall, 1962; Immelmann, 1969; Morris, 1954). While directed singing is likened to performance, undirected singing is thought to reflect a process of continuous action-based learning that contributes to song maintenance (Nelson and Marler, 1994; Jarvis et al., 1998). Although the behavioral output is similar in both contexts, underlying brain activation patterns are distinct (Hessler and Doupe, 1999a; Jarvis et al., 1998; Teramitsu and White, 2006).

Developing human and zebra finch brains exhibit strikingly similar patterns of *FOXP2* mRNA expression in the cortex/pallium, basal ganglia, thalamus, and cerebellum (Teramitsu et al., 2004). In zebra finches, these developmental patterns persist into adulthood (Haesler et al., 2004; Teramitsu and White, 2006) while human adult patterns are not yet known. The persistent expression of *FoxP2* mRNA in adult finches suggests that, in addition to *forming* brain regions during embryogenesis, FoxP2 could *regulate* circuits throughout the life of the songbird, during learning and ongoing communication phases. Our prior studies provided support for the latter hypothesis by showing that *FoxP2* mRNA is actively regulated during adult song maintenance within the basal ganglia subregion dedicated to song, known as Area X (Figure A2-1A), precisely when the bird sings and under certain social interactions (Teramitsu and White, 2006). However, the full significance of this observation rests on whether FoxP2 protein follows its mRNA levels, as this ultimately determines the effect on FoxP2's downstream transcriptional targets (Spiteri et al., 2007; Vernes et al., 2007). While such relationships may hold in cell culture, the *in vivo* situation in the brains of behaving animals is more complex.

We thus undertook the development of a new FoxP2 antibody and validated its ability to specifically detect FoxP2 expression *in vivo* and *in vitro* in the mature zebra finch brain. We then used it to characterize levels of protein expression within song nucleus Area X in response to different behavioral conditions and to compare these with previously obtained mRNA levels. Further, we investigated whether these conditions, experimentally implemented within the laboratory setting, impact total corticosterone (CORT) levels. We reasoned that CORT, as an indicator of stress in these animals, could present an uncontrolled influence on the relationship between levels of FoxP2, or other molecules, and singing. We find that FoxP2 protein is actively down-regulated within Area X in singing birds, compared to non-singers, and that CORT levels are similar across behavioral conditions. Thus, the down-regulation is likely due to singing rather than to stress. Recent experimental manipulations resulting in constitutively low levels of FoxP2 expression in Area X cause imprecise song development (Haesler et al., 2007). Our work extends these observations by showing that Area X FoxP2 protein levels are down-regulated naturally when birds sing. These findings, by analogy, provide insight into processes potentially important for human procedural learning and speech.

Methods

Subjects

All animal use was approved by the University of California at Los Angeles Institutional Animal Care & Use Committee. Tissue from 14 birds was used for the antibody validation (Figure A2-2C-E). Thirty birds were used for the experiments on FoxP2 protein levels as a function of behavioral condition (Figure A2-4A,B). Twenty-one birds were used to test levels of stress associated with the different behavioral conditions (Figure A2-6).

Behavioral manipulations

Adult male zebra finches (120-315 days of age) were moved from our breeding colony and housed individually in sound attenuation chambers (Acoustic Systems; Austin, TX) under a 14:10 hour light/dark cycle. Birds were left undisturbed for 2-3 days prior to the experiments to enable acclimation to the new environment. Experiments were conducted in the morning from the time of light onset ("lights-on") to the time of death by overdose with inhalation anesthetic (halothane or isoflurane; Halocarbon Laboratories, River Edge, NJ; Abbot Laboratories, Chicago, IL; Figure A2-1B). Sounds were recorded and digitized using National Instruments and PreSonus Firepod hardware, with custom LabView (Livingston et al., 2000) and Sound Analysis Pro 1.04 (Tchernichovski et al., 2000) software, respectively. Two groups of non-singing birds and two groups of singing birds that met our criteria (see below; Figure A2-1B) were generated. Non-singers were adult males that were sacrificed either at lights-on (0-NS), or two hours from lights-on (2-NS). The 0-NS group was used for baseline values in the Western immunoblotting

quantification because these animals were not subject to any experimental manipulation and were sacrificed following an undisturbed night of sleep. For the 2-NS group, if birds appeared to make any attempts to sing, they were distracted by the presence of the investigator. If distraction was ineffective and the bird sang ≥10 motifs across the two hours, the bird was excluded from that day's experiments. Singing birds were either males housed alone singing in a solo context (undirected, 2-UD) or males performing continuously to a succession of novel females presented every 4-7 minutes over a two hour period ensuring that the male was performing 100% directed behavior (directed, 2-D; Teramitsu and White, 2006).The acoustic structure of zebra finch song consists of a set of sound elements, known as syllables, which are repeated in what is referred to as a motif. Singing birds which sang >90 motifs of undirected or directed song within two hours from song onset (i.e. start of first motif) were considered to have met criteria established in prior studies of *FoxP2* mRNA (Teramitsu and White, 2006) and were sacrificed.

Tissue preparation for protein study

After undergoing the behavioral protocols, birds were overdosed, decapitated, and brains rapidly extracted and frozen in aluminum dishes on liquid nitrogen or dry ice and stored at –80°C until use. Brains were mounted in a coronal orientation on a cryostat (Leica Microsystems, Bannockburn, IL). Sections of 40μm thickness were cut prior to visualization of Area X, then bilateral tissue punches of Area X were obtained at a depth of 1mm using a 20 gauge Luer adaptor (Becton Dickinson, Sparks, MD) attached to a 1cc syringe. Our previous observations noted that Area X is located ~1250μm from the rostral-most point of the brain. In some cases, tissue punches of similar size were also taken from the outlying striatal and nidopallial regions,

for comparison (see Figure A2-2C schematic, plus signs) e.g. to determine any regional specificity of the double bands (see further Methods and Results, below). The anatomical precision of the punch technique was demonstrated by post-hoc thionin staining of coronal brain sections (Figure A2-2C). Tissue punches were homogenized in ice-cold modified RIPA lysis buffer: 1% octylphenoxy polyethoxyethanol (NP-40 substitute), 0.5% deoxycholate, 0.1% SDS, 1x Phosphate Buffered Saline; Gibco, Invitrogen, Carlsbad, CA; pH 7.6 with a cocktail of protease inhibitors (#P8340, Sigma-Aldrich, St. Louis, MO) using a hand-held homogenizer (Kontes, Fisher Scientific) followed by a 10 second homogenization by an ultrasonic cell disruptor (Misonix Inc, Farmingdale, NY) on ice to ensure complete disruption of the nuclear membranes. An aliquot of each sample was removed to determine protein concentration using the RC DC Protein Assay (Bio-Rad, Hercules, CA). Samples were aliquoted in 2x Laemmli loading buffer (Bio-Rad) with 0.1% beta-mercaptoethanol. Samples were stored at –80°C until use.

Immunoblotting

Samples were heated to 90-100°C for 3-5 minutes and lysates were resolved on 10% isocratic (avian tissue samples) or 4-20% gradient (in vitro transcription/translation protein products) SDS-polyacrylamide gels (Promega, Madison, WI). (Observed differences in the molecular mass of FoxP2 between the in vivo and in vitro conditions are likely due to the type of running buffer used and/or to unknown post-translational modifications of the protein *in vivo.* Pre-stained (Benchmark ladder) or chemilumescent (MagicMark) protein standards (Invitrogen, Carlsbad, CA) were included on gels as molecular mass markers. The Benchmark protein

standard gave signals that more closely bracketed the FoxP2 band and we proceeded to use this same standard in Figures A2-2B-E and A2-4A-C. However, the vendor changed the mass weight for the same standard protein from 79 to 82kDa over the course of several different lot numbers, and so our blots reflect this. Samples were subjected to electrophoresis in Tris-Glycine-SDS buffer (TGS, Bio-Rad, or TRIS-HEPES-SDS, Pierce, Rockford, IL) then transferred in TGS with 20% methanol for two hours at 400mA onto 0.45μm nitrocellulose membranes (Bio-Rad). Membranes were blocked with 5% non-fat dry milk in Tris-buffered saline containing 0.1% Tween-20 (TBST) for 1.5 hours at room temperature (RT). Blots were probed with FoxP2 antibodies (1:500-1:1000) in TBST containing 2.5% non-fat dry milk. Following primary antibody incubation (see below), blots were washed in TBST 3x10 minutes then probed with horseradish peroxidase-conjugated anti-rabbit IgG (1:2000 dilution) and anti-mouse IgG (1:5,000 dilution; Amersham Pharmacia Biotech, Piscataway, NJ). Enhanced chemiluminescence with ImmunoStar HRP detection kit (Bio-Rad) was used to develop immunoblots. In some blots we detected the presence of two bands (~69, ~66kDa: see Results) with the lighter band of lower molecular mass potentially representing another isoform of FoxP2. The resolution of this band appeared to depend upon the separation characteristics of the gel, including type of SDS-PAGE gel used (gradient gels enable better separation of bands), and the voltage (lower voltage also enhances band separation).

Antibodies

Two polyclonal antibodies directed against distinct polypeptide regions within the C-terminus of FoxP2 were employed for our studies. We originally tested a commercially available

primary antibody made in goat against a FoxP2 peptide (Abcam, Inc.). We found that it resulted in high background on Western blots and yielded multiple bands that were difficult to interpret. This motivated us to develop our own antibody. Of note, the vendor subsequently discontinued the goat primary antibody and replaced it with an antibody made in rabbit against FoxP2; see below. Throughout the text, we refer to the antibody that we generated as the FoxP2 antibody (Spiteri et al., 2007) which was used for all experiments described in this paper, unless otherwise noted. We distinguish it from the commercially available antibody by citing the vendor for the latter (i.e. Abcam). We selected a 14 amino acid sequence, corresponding to amino acids 643-656 of human FoxP2 (EDLNGSLDHIDSNG, Genbank AF337817) and predicted from the *FoxP2* coding sequences to be identical between humans and zebra finches (GenBank accession numbers AY395709 for zebra finch, and AF337817 for human). The selected peptide was conjugated with an extra cysteine on the amino terminus and coupled to MBS-KLH and injected into a female New Zealand white rabbit (Sigma-Aldrich, St. Louis, MO) then affinity purified. The second antibody (used only in the in vitro transcription and translation assays, see below) was a commercially available, polyclonal rabbit antibody against the peptide "REIEEEPLSEDLE", corresponding to amino acids 703-715 of human FOXP2 (#16046 Abcam, Cambridge, MA), a sequence also identical in zebra finches. For preadsorption experiments, the FoxP2 antibody was incubated with either immunizing or non-antigenic peptides in excess quantity relative to the antibody concentration. For the non-antigenic peptides, we used a synthetic peptide from Gas11-a (RNYFQLERDKI; gift from R.H. Crosbie, Ph.D, UCLA), a microtubule-associated protein (Bekker et al., 2007). The Gas11-a and FoxP2 peptide sequences are not similar as no two consecutive amino acids are shared. A monoclonal antibody raised

against Glyceraldehyde 3-phosphate dehydrogenase (#MAB374, 1:5000 GAPDH; Chemicon) was used to control for equal protein loading on immunoblots.

In vitro transcription and translation of zebra finch FoxP2

FoxP2 bacterial expression plasmids were constructed via directional cloning of PCR amplified zebra finch FoxP2 cDNA (GenBank AY395709) using primers designed with restriction sites for EcoRI and NotI into the vector pcDNA3 with the T7 and mammalian CMV promoters (Invitrogen). The correct FoxP2 cDNA sequence was confirmed by the UCLA Sequencing Core using an ABI 3700 DNA Analyzer (Applied Biosystems, Foster City, CA). In three separate experiments, FoxP2 protein was made from 1μg of plasmid DNA using T7 Quick-Coupled in vitro Transcription/Translation System (TnT; Promega). To confirm TnT protein product, Transcend® biotinylated lysyl tRNA reagent (Promega) was incorporated into the synthesis mixture, then samples were resolved by SDS-PAGE, transferred to nitrocellulose membranes, probed with streptavidin-conjugated alkaline phosphatase (Promega, 1:1000), and visualized with Western Blue® stabilized substrate (Promega). Identical blots containing TnT product were probed with anti-FoxP2 primary antibodies followed by detection with chemiluminescence reagents as previously described.

Quantification & Statistical Analyses

Parametric statistics with two-tailed probabilities were used unless otherwise indicated. We note that the use of parametric versus nonparametric measures did not alter any experimental

outcome. Immunoblots developed by enhanced chemiluminesence were imaged and analyzed using a cooled CCD camera-based image acquisition system (Chemi-Doc and Quantity One software package, Bio-Rad) and densitometric analysis using Quantity One. A total of 8 Western blots (exemplars are shown in Figure A2-4A,C) were probed with FoxP2 antibody. Each blot contained at least one bird from every behavioral condition. To determine whether FoxP2 levels varied as a function of behavioral condition, the FoxP2 value for each lane was normalized to its corresponding GAPDH value to obtain a ratio. The top band in each lane was quantified because of its robust signal strength although inclusion of the lighter, lower band did not alter the relative brain expression levels between groups. For example, in one blot, the normalized mean FoxP2 protein values per group (with 2-3 birds/group) obtained from quantifying the top bands only were: 0-NS: 1.00, 2-NS: 1.15, 2-D: 0.90, 2-UD: 0.90. Similar relationships between means were obtained when both top and bottom bands were included: 0-NS: 0.99, 2-NS: 1.24, 2-D: 0.96, 2-UD: 0.86 ($P>0.05$, paired Student's t-test). To aid in inter-blot comparisons, these values were normalized using the value obtained from the 0-NS birds within a given blot, since the 0-NS group did not undergo any experimental manipulation prior to sacrifice. The normalized values for individual birds are plotted in Figure A2-4B, along with the average values obtained per behavioral condition. Means were compared via one-way analysis of variance (ANOVA) with post-hoc Tukey-Kramer tests using JMP statistical software (Cary, NC).

To determine whether FoxP2 levels were correlated with the amount of song in the singing groups, two measures of singing were each compared to the normalized FoxP2 levels. We observed that the distribution of the number of motifs sung by birds in the UD group values did not conform to normal assumptions, using the goodness-of-fit test (Shapiro-Wilcox, $P<0.05$). Thus, we proceeded to conduct multivariate analyses using non-parametric tests for ranked order.

The Spearman's Rho correlation coefficient is reported for all comparisons between FoxP2 protein and motifs. The amount of time spent singing was calculated by selecting 10 random motifs within the 2 hour period for each bird and measuring the motif length. An average motif length was obtained and multiplied by the total number of motifs the bird sang to represent time spent singing (in seconds). The amount of song or time spent singing is reported as means ± standard error with comparisons between groups using Mann-Whitney U tests (Vassar Stats).

Immunohistochemistry

Within zebra finch striatum, immunohistochemical studies have shown that FoxP2 protein co-localizes with dopamine-and-cAMP-regulated phosphoprotein of molecular weight 32 kDa (DARPP-32; Reiner et al., 2004a) in a subset of medium spiny neurons (Haesler et al., 2004) including within Area X (Rochefort et al., 2007). To further validate our antibody by this additional methodology, we performed immunohistochemistry on adult brain sections containing Area X using our rabbit anti-FoxP2 antibody as the sole primary antibody, or together with the mouse anti-DARPP-32 monoclonal antibody used in the prior studies (Figure A2-3). Adult male zebra finches were overdosed with inhalant anesthesia and then perfused with prewarmed 0.9% saline followed by ice cold 4% paraformaldehyde in 0.1M phosphate buffer (PB) for brain fixation. Brains were extracted and then cryoprotected in 20% sucrose in PB at 4°C. Coronal sections that contained Area X were cut at 40μm and thaw-mounted onto slides (Superfrost, Fisher Scientific) and then stored at -80ºC until used for fluorescent immunohistochemistry. Brain sections were encircled by a hydrophobic barrier using a PAP pen (Ted Pella Inc, Reddington, CA) and washed in Tris Buffered Saline (TBS) with 0.3% Triton X-100 (Tx) for

3x5 minutes. Sections were incubated for 10 minutes in 50mM ammonium chloride in TBS to reduce autofluorescence followed by 3x5 minute washes in TBSTx. To block non-specific binding, tissue was incubated in TBSTx with 10% goat serum (Sigma) for one hour at room temperature followed by 3x5 minute TBSTx washes in 1% goat serum. Tissue was incubated overnight at 4°C in a TBSTx/1% goat serum solution of the polyclonal primary antibody to FoxP2 at 1:1000 and the monoclonal primary antibody (from mouse) to DARPP32 at 1:900 (gift of H. C. Hemmings, Jr., Ph.D, Weill Cornell Medical College, New York, NY). Following overnight incubation at 4ºC, sections were washed 5x5 minutes each with TBSTx then incubated for 4 hours at room temperature in a TBSTx/1% goat serum solution using two fluorescence-tagged secondary antibodies against rabbit or mouse IgG, each with distinct emission spectra (Alexafluor 488nm to detect FoxP2, Alexafluor 350nm to detect DARPP32; Molecular Probes, Eugene, OR). Sections were washed 5x5 minutes with TBS only. Sections were mounted with coverslips using ProLong Gold Antifade Reagent (Molecular Probes). Images were captured using an AxioImager microscope equipped with fluorescence and with the Axiovision 4.4 software program (Carl Zeiss MicroImaging Inc., Thornwood, NY). Coronal sections were imaged with a 40X objective, of 1.3 numerical aperature. For determination of cytoarchitectonic boundaries, adjacent sections were processed for Nissl substance using thionin staining.

Assessment of Corticosteroid Levels

Adult male zebra finches (*N*=21) >200d were used. Corticosterone (CORT) is the main avian stress steroid and, in zebra finches, its levels peak at 20 minutes following the onset of an acute stress and then return to baseline (Evans et al., 2006). To verify our ability to measure a

range of total CORT levels, “low stress” blood samples were obtained from 6 birds housed in the aviary or in the sound attenuation chambers, at 20 minutes after lights-on without prior experimental intervention. “High stress” samples were taken from these same birds but after they were actively restrained - kept captive by the investigator’s hand for ~15 minutes prior to blood sampling. Samples were taken from the brachial vein and treated with heparin (Sigma, St. Louis, MO). All samples were taken within 3 minutes of approach and handling, before the sampling procedure itself could contribute to CORT concentration in the blood (Romero and Reed, 2005; Wingfield et al., 1982).

To determine stress levels associated with different behavioral conditions, fifteen males were separated into three groups of five animals in a manner that minimized the difference in mean ages between groups. Similar to the conditions used for the protein study, birds were kept in an enclosed space near the investigator (non-singers), in a sound attenuation chamber (undirected singers), or subjected to directed singing conditions as described above (Figure A2-6A). Baseline CORT measurements were obtained at least one week prior, at 20 minutes following lights-on. Experimental samples were taken from these same birds at the 20 minute time point for each behavioral condition. In addition to reporting raw CORT values (Figure A2-6B), each bird’s experimental CORT levels were normalized using its baseline CORT levels, to control for individual variability in CORT levels. The normalized data are represented as fold-change from baseline. Two different investigators conducted these experiments, one to observe the birds during the directed or non-singing behavioral conditions and the other to collect the blood sample. Samples were kept on ice until they were centrifuged for 15 minutes at 2.3 rcf. CORT measurements were determined by use of an enzyme-linked immunosorbent assay kit (Assay Designs, Ann Arbor, MI) following the procedures outlined by the manufacturer with

these changes: plasma samples were diluted 40 times with assay buffer and treated with a steroid displacement agent, as it has been found that substances in avian plasma interfere with the measurement of CORT (Wada et al., 2007).

Results

Specific detection of FoxP2 protein in Area X

The predicted protein sequence for zebra finch FoxP2 is ~710 amino acids and 98% identical to mouse and human homologs, with 100% identity to the human Fox domain (Haesler et al., 2004; Teramitsu et al., 2004). Both our resultant polyclonal antibody and a commercially available one (Abcam Inc., Cambridge, MA), raised against two non-overlapping peptides, recognize FoxP2 protein generated by *in vitro* transcription and translation (TnT; Figure A2-2A). Preadsorption of our antibody with the immunizing peptide prevented antibody binding to immobilized FoxP2 TnT protein product, whereas pre-incubation with a non-antigenic peptide sequence from Gas11-a did not block antibody binding to FoxP2 (Figure A2-2B). This peptide competition experiment demonstrates that our FoxP2 polyclonal antibody recognizes zebra finch FoxP2 protein.

In zebra finch tissue, the FoxP2 antibody recognizes a protein of the expected molecular mass weight for FoxP2 similar to predicted zebra finch isoform III (69kDa; Haesler et al., 2004) in specific brain areas, as seen in bilateral punches taken from Area X of multiple male birds (Figure A2-2C), and from nidopallial and striatal regions outside of Area X (Figure A2-2D). These protein data suggest that the FoxP2 antibody is both specific and sensitive as it detects protein in Area X tissue punches taken from individual birds. Antibody specificity *in vivo* is confirmed by the preadsorption control which prevents antibody binding (Figure A2-2D, asterisk). As these experiments were not aimed at quantifying protein as a function of behavioral condition, the birds were in different behavioral contexts. For example, in Figure A2-2D, the Area X punch came from a 0NS bird, a condition in which we expect lower levels of FoxP2 than

at the 2NS time point. This may have contributed to the relatively low FoxP2 protein levels observed in the Area X lanes versus the striatal and nidopallial regions. In some immunoblots, we observed an additional fainter second band of slightly lower molecular mass by several kDa, similar to predicted zebra finch isoform 4 (see Methods, Figures A2-2E,4C). We wondered whether the second band was region-specific and thus ran additional blots that included tissue from the nidopallium as well as the striatum outlying Area X. We found that these bands are not restricted to Area X, but are found in the other tissue extracts, as shown in a representative Western blot (Figure A2-2E). Rather, as noted in the Methods, observation of the second band appeared to depend upon the resolution characteristics of the gel (e.g. the blot in Figure A2-2D which shows one band was run at twice the voltage as that in A2-2E showing 2 bands). Further, inclusion or exclusion of the second band in the quantification did not alter the relationships between behavioral condition and FoxP2 protein levels (see below).

FoxP2 protein signal colocalizes with that for DARPP-32 in striatal neurons

Conventional immunohistochemistry using our primary antibody against FoxP2 revealed stronger signals within the dorsal striatum compared with the nidopallium, (Figure A2-3A,B) consistent with mRNA expression data (Teramitsu et al., 2004; Haesler et al., 2004). No detectable signal was observed when the primary antibody was omitted (Figure A2-3C). The colocalization of FoxP2 signals (Figure A2-3D,F) with those for DARPP32 (Figure A2-3E,F) in a subset of neurons replicates previous findings (Rochefort et al., 2007) and provides further support for the specificity of our antibody.

Singing down-regulates FoxP2 protein in Area X

Representative immunoblots show FoxP2 signals obtained from birds under different behavioral conditions (Figure A2-4A,C). The summary graph (Figure A2-4B) shows values obtained from the blots of FoxP2 protein levels in Area X of individual birds plotted singly and as group means. A one-way ANOVA indicated overall differences between the groups and validated comparisons between them ($F = 4.70$, $P<0.01$; means±SEM: 0-NS = 1.00±0.10, 2-NS = 1.40±0.12, 2-D = 0.95±0.10, 2-UD = 0.86±0.09). These comparisons revealed that undirected singers and directed singers had lower amounts of FoxP2 protein than levels in birds that did not sing for two hours (*post-hoc* Tukey-Kramer, $P<0.05$, 2-NS: n=6; 2-UD: n=9; 2-D: n=8). In some cases, FoxP2 levels in Area X of undirected singers could appear as lower than those in directed singers. An example is provided in Figure A2-4C to enable a fuller representation of the range of results. However, across all samples, no significant difference was observed in protein levels between UD and D singers. Other post-hoc comparisons between groups did not attain statistical significance.

FoxP2 protein levels and amount of song

Previous studies have shown that mRNA and protein levels of the immediate early gene ZENK (acronym for zif-268, egr-1, NGF1-A, and Krox-24) correlate with the amount of singing (Jarvis and Nottebohm, 1997; Whitney and Johnson, 2005). Thus, we considered whether increased singing would increasingly down-regulate FoxP2, and examined levels of protein as a

function of the amount of song sung for UD and for D singers (Figure A2-5). We observed a trend within the undirected group in which higher numbers of motifs resulted in lower FoxP2 levels (Figure A2-5, Spearman's Rho, = -0.20, *P=0*.59, n=9), similar to what had been reported for *FoxP2* mRNA (Teramitsu and White, 2006). Like the mRNA data, this trend did not reach significance. One UD bird sang 1236 motifs (not represented in Figure A2-5), well beyond the range of song observed in all other UD birds (range = 98-215**;** mean±SEM = 143.9±16.5). Removal of this bird's data, however, did not alter the results (Spearman's Rho = -0.30, *P=0*.47, n=8).

In D singers, no trend is observed between protein and singing behavior (Figure A2-5, Spearman's Rho = 0, *P*=1.0, n=8). Of note, the amount of song sung by the two singing groups did not differ: the average number of motifs from the 2-D birds (range = 103-405; mean±SEM = 223±40.6), was similar to the 2-UD birds, regardless of whether the UD singer with the highest number of motifs is included (range = 98-1236; mean±SEM = 265±122.2; Mann-Whitney U = 45, n_1=9, n_2=8, *P*=0.41) or excluded (range = 98-215**;** mean±SEM = 143.9±16.5; Mann-Whitney U = 45, n_1=8, n_2=8, *P*=0.19). Similar, non-significant findings were observed when the estimated total amount of time spent singing (calculated per bird as the mean motif length of 10 motifs x total number of motifs sung in 2 hours; see Methods) was used (data not shown).

Corticosterone Levels Do Not Change Based on Behavioral Context

A potential confound for interpreting biological data obtained from behavioral manipulations such as those used here is that the housing conditions, including the presence or

absence of the investigator or conspecifics may induce stress differentially across groups. To test this, we first verified our ability to detect differences in CORT levels in control male zebra finches between conditions of high versus low stress (see Methods). As expected, when handled, birds had an average ~2 fold higher level of plasma total corticosterone (CORT) than when undisturbed (1-tailed t-test: t = -3.79, $P<0.01$, n=6), and these differences did not vary whether birds were housed individually in sound attenuation chambers or grouped in an aviary (2-way ANOVA without replication, F = 1.10, $P=0.46$).

Based on this validation of our measurement protocol, we proceeded to examine CORT levels in our experimental birds (see Methods). No differences in CORT levels were observed across NS, UD and D groups, neither when raw CORT values are compared (6B, two-way ANOVA without replication between groups F = 1.06, $P=0.44$; within group F = 1.71, $P=0.24$; means±SEM for NS, D, UD in ng/ml: 20.14±1.81, 25.80±4.59, 17.18±1.75), nor when each bird's 20 minute value was normalized by its baseline levels (one-way ANOVA F = 1.23, $P=0.33$). The average CORT levels for each of the three groups fell between values from the control low and high stress conditions. Additionally, blood samples were obtained at sacrifice for two of the non-singing birds used for the FoxP2 experiment, above. Despite having been distracted from singing by the investigator within the two hour period, we found that these birds had similarly low CORT levels (10.9 ng/ml, 7.8 ng/ml).

Discussion

Here, we present evidence for naturally-induced regulation of FoxP2 protein in Area X of adult zebra finches, similar to *FoxP2* mRNA. Singing down-regulates FoxP2 protein within Area X, the specific subregion of songbird striatum dedicated to song (Scharff and Nottebohm, 1991; Sohrabji et al., 1990). Both directed and undirected singers have lower FoxP2 levels at two hours after song onset compared with non-singing birds. These data suggest that FoxP2, previously implicated in the formation of vocal control circuitry and in human developmental-onset disorders also has an on-line function in the adult brain.

Our prior study showed that *FoxP2* mRNA is only down-regulated by undirected, but not by directed, singing (Teramitsu and White, 2006). The difference in social regulation between FoxP2 mRNA and protein, seen here, has been observed for other transcription factors, notably the immediate early gene *ZENK* in which mRNA is uncoupled from protein levels in sensory versus motor processes (Whitney and Johnson, 2005). One interpretation is that singing results in FoxP2 protein turnover, regardless of social context, but that mRNA levels persist in directed singers leading to faster replenishment of the protein molecule. A time-course study that investigates protein and RNA half-lives during singing in the different social contexts may address this and alternative explanations. We do not know whether the singing-driven down-regulation in FoxP2 protein in Area X occurs in other song control regions since we did not measure them. No obvious changes in FoxP2 mRNA levels as a function of behavioral state were previously noted in these regions. However, the difference in the social regulation between mRNA versus protein observed here raises the possibility that differential mRNA versus protein regulation could occur in other regions.

In line with our previous study on *FoxP2* mRNA (White et al., 2006), we observed a trend towards a negative correlation between the amount of undirected singing and Area X FoxP2 levels, while no such trend was observed in directed singers. We report this nonsignificant relationship due to a few considerations. First, in the mRNA study, we set a behavioral criterion of 90 motifs for inclusion of animals into singing groups in order to maximize the behavioral differences between groups. The 90 motif cut-off was preserved here to enable comparison between mRNA and protein studies. While this approach was successful in allowing us to discriminate differences in both mRNA and protein levels based on singing, it is not optimal for determining whether a wide range of singing levels is associated with a gradient in FoxP2 expression as it omits a substantial portion of the range (0-90 on the x-axis). Other studies have overcome this limitation by including birds that sang only a few motifs, and even non-singing birds, in correlations between amount of song and molecular expression (Jarvis et al., 1998; Jarvis and Nottebohm, 1997; Poopatanapong et al., 2006). Here, inclusion of data from non-singers with the UD data would indeed render a significant negative correlation between the number of UD motifs sung and the level of FoxP2 protein. However, non-singing birds were housed under conditions that were distinct from the UD singers (in a cage next to the investigator, versus undisturbed inside an acoustic attenuation chamber). It may not be valid to combine data from these groups. For example, it could be that birds that simply did not sing when housed alone in sound attenuation chambers would have different FoxP2 levels than the non-singing birds used here.

Perhaps more sensitive signal detection methods (e.g. the use of qRT-PCR for mRNA, or of a more sensitive antibody against FoxP2 protein) coupled with inclusion of a wider range of singing values would unveil a robust negative correlation between amount of UD song and

FoxP2 protein levels. It is less likely that such a relationship would emerge with the directed singers because the trend is lacking from the present data set on FoxP2 protein, and an opposite trend was observed when mRNA levels were analyzed (Teramitsu and White, 2006). Further, other groups have shown that directed and undirected singing are accompanied by distinct brain activation patterns; undirected singing corresponds to higher and more variable levels of neuronal activity and ZENK expression in Area X and LMAN, that is accompanied by slightly greater song variability (Hessler and Doupe, 1999b; Jarvis et al., 1998; Kao and Brainard, 2006; Kao et al., 2005; Sakata et al., 2008).

A working hypothesis is that FoxP2, like other forkhead family members (Carlsson and Mahlapuu, 2002), promotes the structural formation of anatomical regions, in this case including striatal areas that subserve vocal learning. This idea is consistent with FoxP2 protein localization to newly born neurons in zebra finch Area X (Rochefort et al., 2007), with the increase in *FoxP2* mRNA expression levels in canary Area X during seasonal periods of song circuit growth (Haesler et al., 2004) and with the structural abnormalities in the striatum of humans bearing FOXP2 mutations (Belton et al., 2003). In contrast to developmental and seasonal roles in promoting growth of specialized brain structures, the behavioral use of such regions may depend on FoxP2 down-regulation. Accordingly, a recent study showed that lentivirus-mediated RNA interference to reduce FoxP2 levels in Area X of young birds caused inaccurate imitation of the tutor song (Haesler et al., 2007). The abnormal songs were characterized by spectral and temporal differences in structure and resulted in more adult song variability compared with control birds. The constitutive knock-down of FoxP2, coupled with the naturally occurring dynamic variation in FoxP2 levels shown here, support the idea that low levels of FoxP2 may direct changes in transcriptional activity that promote vocal motor variability. The identification

of FOXP2 gene targets (Spiteri et al., 2007; Vernes et al., 2007; see below) further support this notion. Vocal motor variability has been hypothesized to allow reinforcement and stabilization of correct vocal motor patterns, occurring on both fast (Tumer and Brainard, 2007) and slower (Troyer and Doupe, 2000a; b) time scales. Future work that compares song stability when FoxP2 levels are high versus when they are low (e.g. in the 2-NS versus the 2-UD groups used in this study) might reveal corresponding differences in behavioral variability. Unfortunately, the 2-NS birds were sacrificed before any songs were sung – a criterion for group inclusion that precluded obtaining song records for such analysis.

One concern is that so-called behaviorally-driven changes in FoxP2, or other molecules, could actually be due to extraneous stress imposed by the experimental manipulations used to alter behavior, rather than the behavior itself. Previous reports have documented the effect of acute stress on memory tasks in zebra finches (Hodgson et al., 2007). Our findings do not appear to be confounded by the endogenous stress levels associated with the different behavioral conditions, as plasma CORT concentrations did not depend on the presence of a human or female bird nor on the surrounding environment. Male birds had low CORT at 20 minutes following experimental onset, despite the fact that 20 minutes corresponds to the peak in the acute stress response of zebra finches (Evans et al., 2006). In a separate exemplar experiment, CORT levels were also low in two birds sampled for FoxP2 protein at the two hour timepoint. We were able to document low and high CORT levels in another subset of birds kept in a low versus high stress condition, validating the effectiveness of our measurements. Together, these stress steroid measurements alleviate potential concerns that the changes observed here in FoxP2 protein, and previously in *FoxP2* mRNA (Teramitsu and White, 2006) are attributable to stress. To our knowledge, this is the first analysis of the effects of common laboratory environments

(e.g. sound attenuation chambers versus aviary) and social-context (alone versus in the presence of female birds or the investigator) on zebra finch stress. The surprising lack of stressful impact may be partly due to the acclimation period after birds are moved into the sound attenuation chamber and/or the familiarity of our birds with laboratory personnel as the investigators also provide daily care of our colony.

Identification of FoxP2 gene targets in songbird brain, including within Area X will help to elucidate molecular pathways important for motor learning. Already targets of FOXP2 have been identified in human neural tissue including in fetal basal ganglia and neuronal-like cell lines (Spiteri et al., 2007; Vernes et al., 2007). These targets are associated with neurite outgrowth, dendritic branching, intracellular signaling, and calcium mobilization, all processes important for remodeling of neuronal connections. Additional likely regulators of these target genes include transcription factors, such as CREB, known for their roles in neuronal plasticity (Bourtchuladze et al., 1994; Vernes et al., 2007). Some of these same targets may be shared with songbird brain, and analysis of how these targets vary in the songbird depending on developmental stage may be particularly informative with regard to formative versus on-line roles of FoxP2, as well as for roles shared with or unique to humans. Our current study, which links FoxP2 protein and learned vocal motor behavior are a step towards shedding insight on the function of FoxP2 in avian vocal learning, and by analogy to humans, in cognitive and motor processes important for speech and language.

Acknowdledgements

We thank Rachelle H. Crosbie, Ph.D, Kelsey Martin, MD, Ph.D, Tom O'Dell, Ph.D, Angela Peter, Ph.D, Barney Schlinger, Ph.D, and Felix Schweizer, Ph.D for their generosity in sharing resources and technical expertise. Three anonymous reviewers provided helpful comments. Supported by NIH training grants T32 HD07228, and T32 HD07032-28 (JEM) and T32 GM008243 (ES; currently in the Department of Pathology and Laboratory Medicine at UCLA), by R21 MH075028 (DHG) and by UCLA Tennenbaum and CART awards and R01 MHO70712 (SAW).

Figures

Figure A2-1: Schematic of avian song system and experimental design.

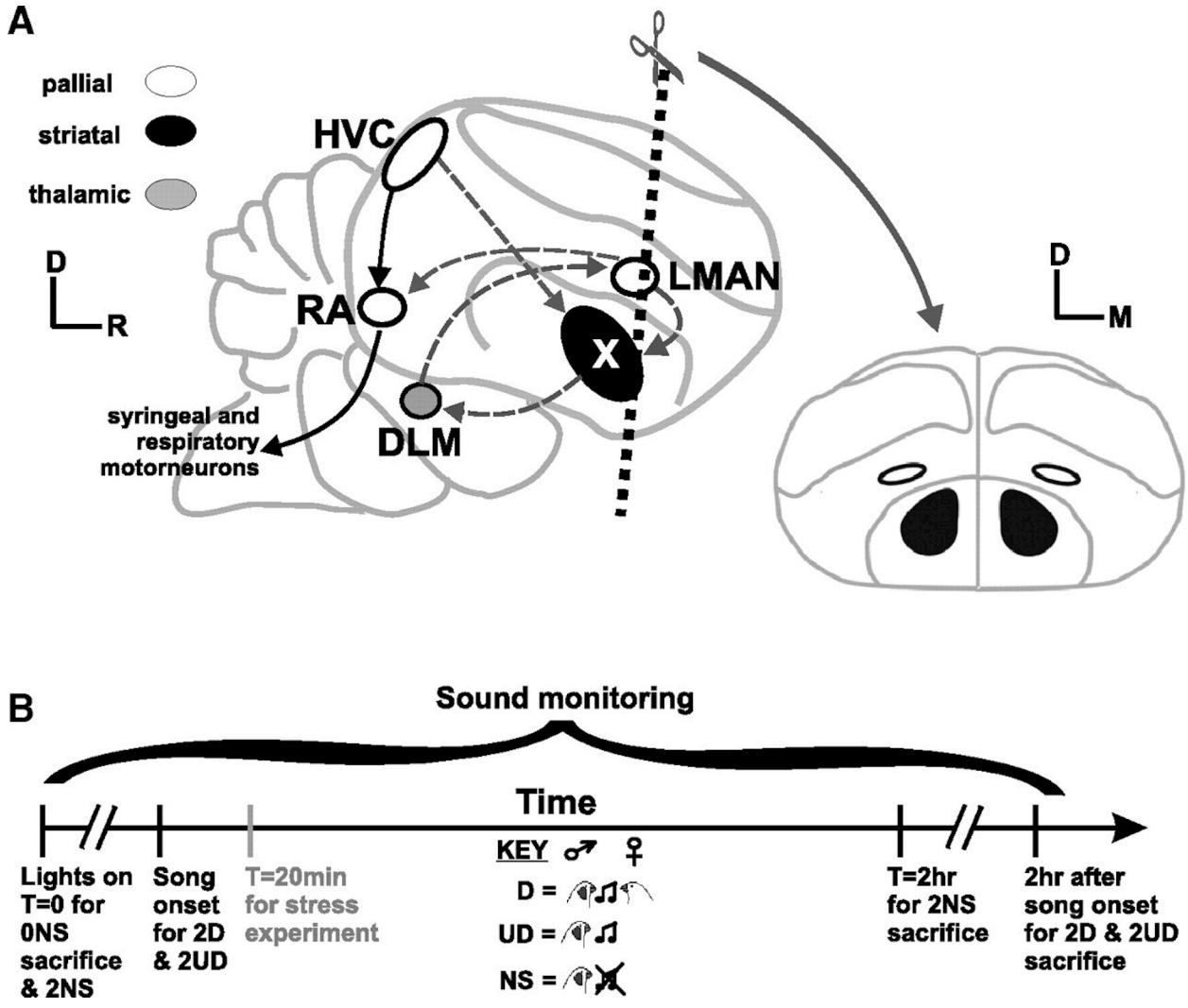

A) Left -- Primary components of two interconnected pathways for birdsong are shown (Jarvis et al., 2005; Reiner et al., 2004a; b). The posterior vocal motor pathway (solid dark arrows) controls song production (Nottebohm and Paton, 1982; Nottebohm et al., 1976; Wild, 1993). The anterior forebrain pathway (AFP, dashed gray arrows), containing Area X, subserves song modification both during juvenile song learning and adult song maintenance (Bottjer et al., 1984;

Brainard and Doupe, 2000b; Kittelberger and Mooney, 2005; Leonardo and Konishi, 1999; Scharff and Nottebohm, 1991; Sturdy et al., 2003; Williams and Mehta, 1999). Dark dashed line indicates approximate plan of section. Right -- Area X (black) tissue punches were acquired as described in the Methods. (Figure modified from Poopatanapong et al., 2006). Abbreviations: dorsal (D), rostral (R), medial (M). **B)** Timeline for the experimental procedure. Following lights-on (T=0), non-singing birds were immediately sacrificed (0-NS) or distracted from singing for two hours and then sacrificed (2-NS). Singing birds were sacrificed 2 hours after the first motif sung following lights-on. Songs were continuously recorded for both undirected (2-UD) and directed (2-D) behavioral conditions. In separate birds, blood samples were taken 20 minutes after lights-on and following 20 minutes under the non-singing (NS), undirected (UD) and directed (D) singing protocols.

Figure A2-2: Antibody specificity is confirmed for *in vitro* and *in vivo* FoxP2 proteins.

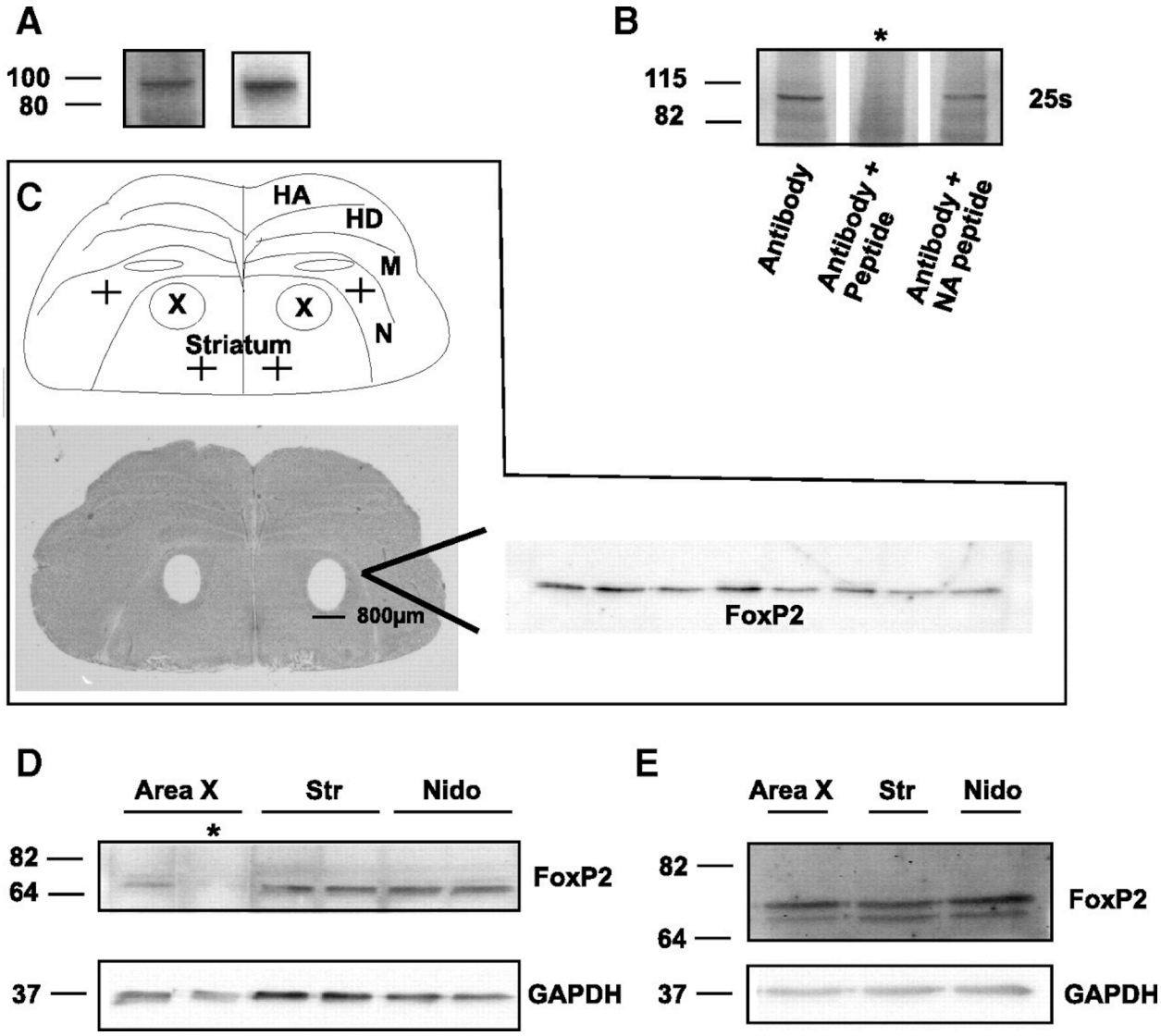

A) Immunoblot of FoxP2 protein produced from *in vitro* transcription and translation (TnT) of a bacterial plasmid containing the full coding sequence for zebra finch FoxP2. Polyclonal antibodies (In-house, left. Abcam, right.) raised against one of two non-overlapping peptides in the C-terminus of the FoxP2 recognize a band of similar molecular mass. **B)** The FoxP2 antibody detects the FoxP2 TnT product (first lane). Preadsorption of the antibody with 30x excess FoxP2 immunizing peptide (asterisk, middle lane) prevents antibody binding to FoxP2 protein whereas

preadsorption with a non-antigenic peptide from Gas11-a peptide (NR, last lane) does not. **C)** Top- Line drawing of anatomical regions highlights song region Area X, observable in the Nissl section below. Plus signs indicate the specific location of tissue punches in the ventral striatum and nidopallium. Right - FoxP2 protein signal is detectable in immunoblots of Area X bilateral tissue punches taken from each of 8 individual birds (50µg/lane). **D)** Immunoblot shows FoxP2 protein in punches from Area X, striatum (Str), and nidopallium (Nido) of two male birds (60µg/lane). Preadsorption of the antibody with 20x excess peptide (asterisk) prevents antibody binding to FoxP2 protein from Area X. Bottom-GAPDH is the loading control. **E)** Immunoblot shows the presence of double bands in Area X, striatum, and nidopallium (40µg/lane) from a single bird. Abbreviations: mesopallium (M), hyperpallium apicale (HA), hyperpallium densocellulare (HD).

Figure A2-3: Fluorescent immunohistochemistry shows FoxP2-specific signals.

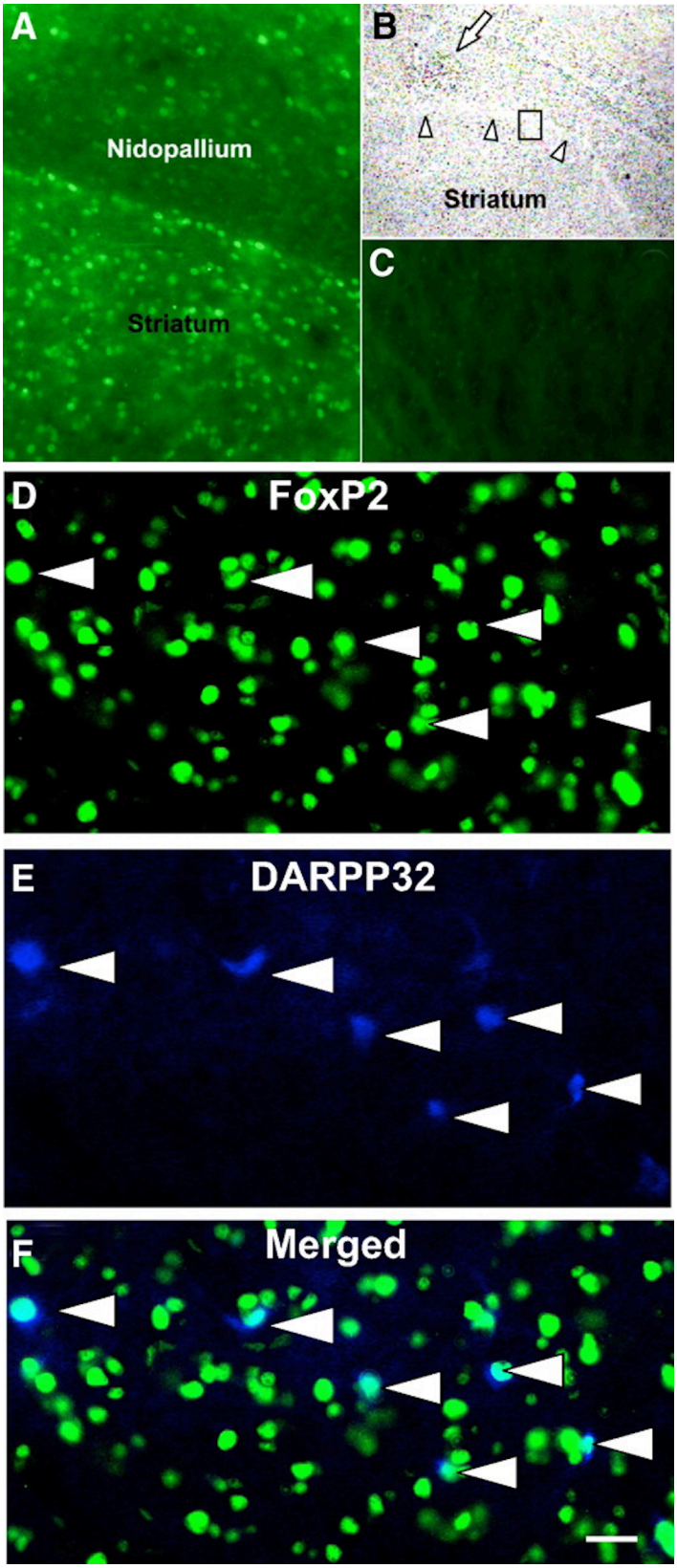

A) Exemplar section reveals signals obtained using our FoxP2 antibody against FoxP2 protein. **B)** Lower magnification view of a thionin-stained section, adjacent to that shown in (A). Arrow points to LMAN. Arrowheads demark the striatal-nidopallial border. Box shows region of enlargement shown in (A). **C)** Another section processed in the same experiment as that shown in (A) but without primary antibody lacks detectable signals. D-F) Immunohistochemical co-localization of FoxP2 and DARPP32 within striatal neurons of an adult male zebra finch. In each panel, arrowheads point to the location of the same six neurons, of many, that are immunoreactive for FoxP2. **D)** FoxP2 positive neurons appear in green. **E)** DARPP32 signal (blue) seen in the cell body and dendritic processes of neurons. **F)** FoxP2 and DARPP32 signals co-localize in a subset of striatal neurons (aqua, arrowheads). Scale bar = 40 (A), 160 (B,C) and 20 (D-F) μm

Figure A2-4: Behavioral regulation of Area X FoxP2 protein levels.

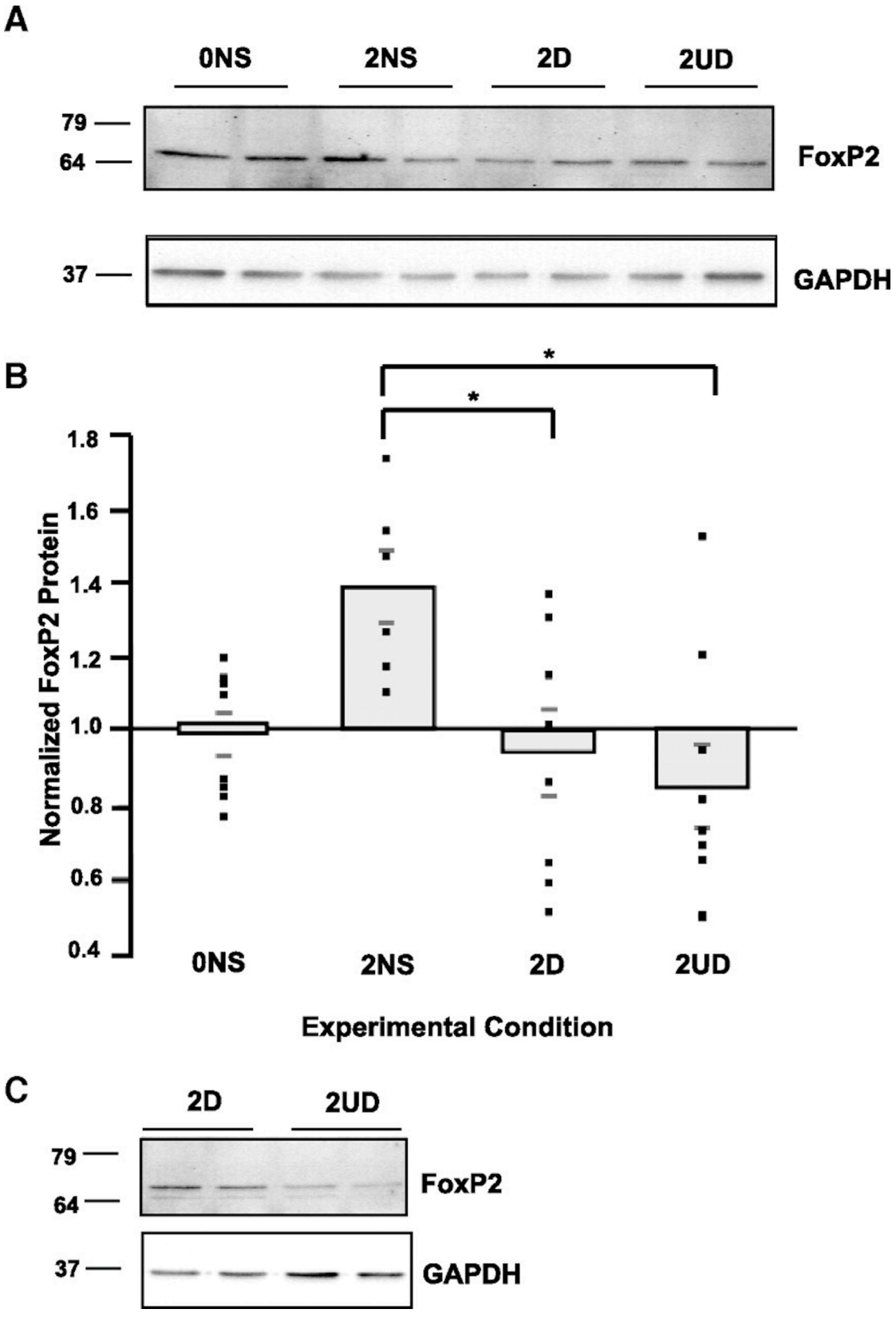

A) Exemplar Western blot shows FoxP2 (top) and GAPDH (bottom; used for normalization) signals obtained from Area X punches. Each lane is from a single bird in the indicated group. Of note, the 4th sample on this blot was not measured and not included in the study because at loading, it was noted that the sample volume was off by more than 25%. **B)** Graph of FoxP2 levels by experimental condition shows group means (bar) ± standard error (dark grey lines). Each point represents an individual bird. For the 2-UD group, two birds with protein values of 0.51 and 0.52 are represented by one point. With values from the 0-NS birds used as baseline, levels in 2-NS group are higher than those in the 2-D and 2-UD groups (asterisk, $P<0.05$). **C)** Another example blot shows signals obtained from two birds in the 2-D group and two in the 2-UD group. Abbreviations: NS=non-singers, UD=undirected singers, D=directed singers.

Figure A2-5: FoxP2 protein plotted as a function of the amount of singing in undirected (n=8, filled squares) or directed (n=8, solid squares) singers.

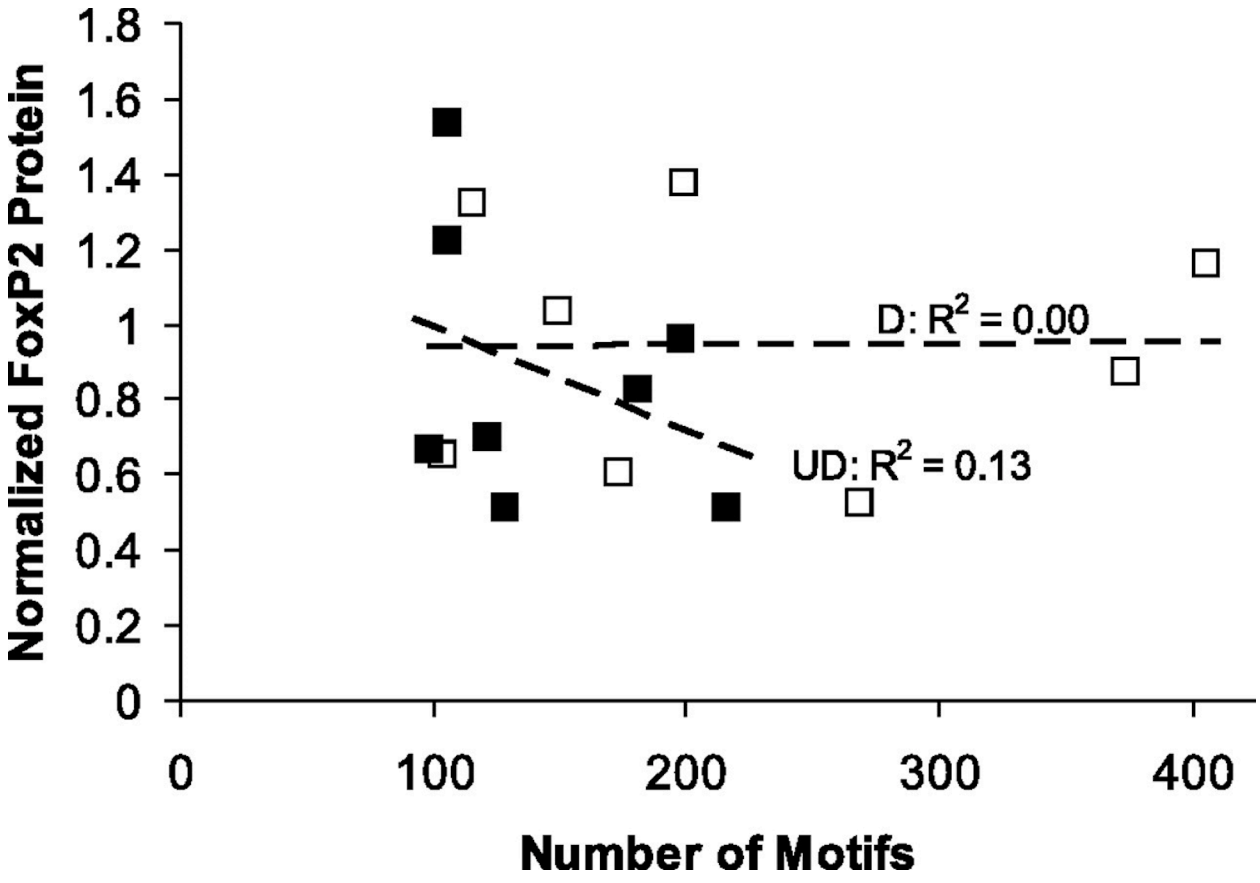

Dashed lines show simple linear regressions.

Figure A2-6: Total corticosterone (CORT) levels in experimental animals.

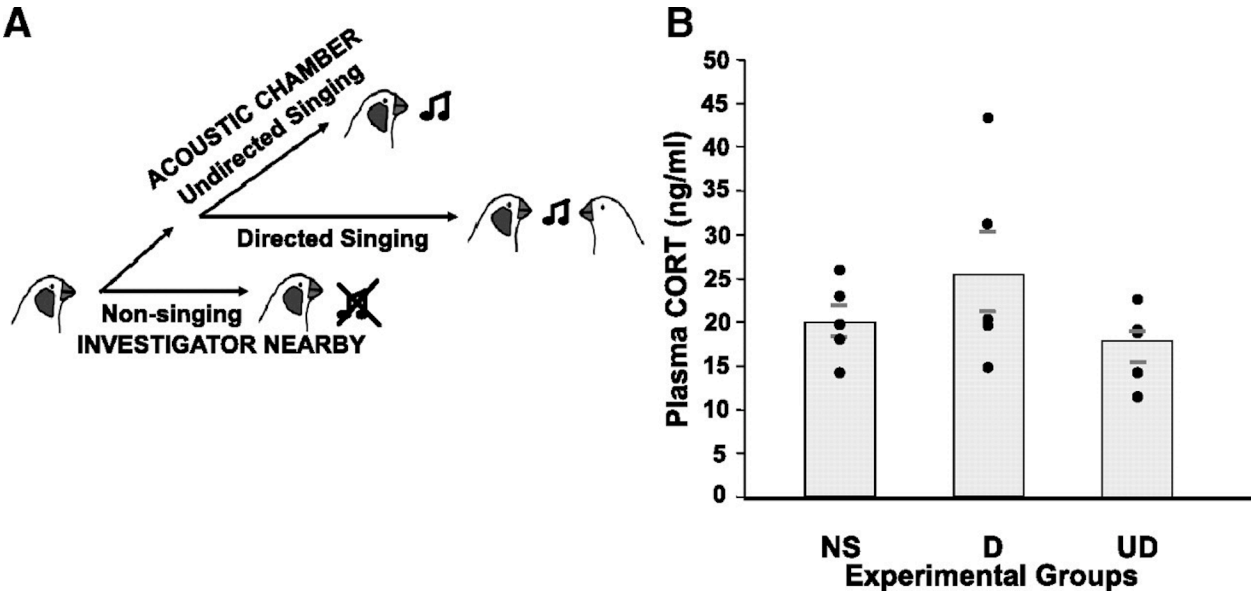

A) Schematic of experimental groups. **B)** Graph of raw CORT levels in ng/ml with group means represented by grey bars and points for individual birds (n=5 per group). Grey lines show the SEM.

Appendix 3: The Potential Role of Postsynaptic Phospholipase C Activity in Synaptic Facilitation and Behavioral Sensitization in Aplysia

Daniel Fulton, Michael C. Condro, Kaycey Pearce, and David Glanzman

Statement of Contribution

I assisted with the behavioral experiments described below that led to the results depicted in Figure A3-3. Specifically I implemented the sensitization protocols schematized in Figure A3-3A so that the first author, Daniel Fulton, would remain blind to the behavioral state when assaying the siphon withdrawal reflex. For each iteration of this experiment, four animals were isolated in chambers with electrodes implanted in their tails, injected with either U73122 or vehicle alone. Using an unbiased method, I randomly selected two of the four animals to sensitize with electrical stimulation through the tail. Stimulation usually resulted in secretion of ink and/or slime, which, if left in the chamber, could be used to identify the sensitized animals. I therefore designed a system to rapidly remove any secretions from the chamber in order to keep the other experimenter blind. This behavioral paradigm was subsequently been used in Cai et al. (2011).

Abstract

Previous findings indicate that synaptic facilitation, a cellular mechanism underlying sensitization of the siphon withdrawal response (SWR) in Aplysia, depends on a cascade of postsynaptic events, including activation of inositol triphosphate (IP_3) receptors and release of Ca^{2+} from postsynaptic intracellular stores. These findings suggest that phospholipase C (PLC), the enzyme that catalyzes IP_3 formation, may play an important role in postsynaptic signaling during facilitation and learning in Aplysia. Using the PLC inhibitor U73122, we found that PLC activity is required for synaptic facilitation following a 10-min treatment with 5-HT, as measured at 20 min after 5-HT washout. Prior work has indicated that facilitation at this time is supported primarily by postsynaptic processes. To determine whether postsynaptic PLC activity is involved in 5-HT–mediated facilitatory actions, we examined the effect of U73122 on enhancement of the response of motor neurons isolated in cell culture to glutamate, the sensory neuron transmitter. A 10-min application of 5-HT induced persistent (>40 min) enhancement of glutamate-evoked potentials (Glu-EPs) recorded from isolated motor neurons, and this enhancement was blocked by U73122. Finally, we showed that injecting U73122 into intact animals before behavioral training impaired intermediate-term sensitization, indicating that PLC activity contributes to this form of nonassociative learning.

Introduction

The siphon withdrawal reflex (SWR) of the marine snail Aplysia provides a valuable model system for neurobiological studies of learning and memory (Glanzman, 2007; Kandel, 2001). In particular, considerable progress has been made in understanding the cellular basis of sensitization, the nonassociative enhancement of the SWR that results from noxious stimulation of the animal's tail (for review, see Glanzman, 2006; Hawkins et al., 2006). It is now firmly established that sensitization training induces facilitation of monosynaptic sensorimotor connections within the circuits mediating the SWR reflex (Antonov et al., 1999; Cleary et al., 1998). Facilitation of these synapses occurs through the action of 5-HT, which is the modulatory neurotransmitter released from interneurons activated by sensitizing stimuli (Glanzman et al., 1989; Mackey et al., 1989; Marinesco and Carew, 2002; Marinesco et al., 2004). Serotonin liberated in this way produces well-defined presynaptic changes, including increased excitability of sensory neurons and enhanced release of transmitter at sensorimotor synapses (for review, see Byrne and Kandel, 1996). However, it is now clear that 5-HT also recruits distinct signaling events in the postsynaptic motor neuron. These learning-related processes have been shown to require an elevation of postsynaptic intracellular Ca^{2+} and culminate in the functional up-regulation of α-amino-3-hydroxy-5-methylisoxazole-4-propoinoic acid receptor (AMPA)-type glutamate receptors, possibly via the synthesis and subsequent insertion of new receptor subunits into the postsynaptic membrane (for review, see Glanzman, 2007). The requirement for postsynaptic modifications during actual learning has also been studied; dishabituation, a form of nonassociative learning related to sensitization (Thompson and Spencer, 1966), depends critically on postsynaptic vesicle exocytosis, as shown by the sensitivity of this form of learning to the injection of botulinum toxin into siphon motor neurons (Li et al., 2005). The Ca^{2+}-

dependent signaling pathways recruited during the induction of facilitation have been examined in experiments on neurons in dissociated cell culture. Serotonin-dependent enhancement of the response of siphon motor neurons to glutamate, the sensorimotor transmitter (Dale and Kandel, 1993; Levenson et al., 2000b; but see Trudeau and Castellucci, 1993), depends on G protein activation (Chitwood et al., 2001), whereas facilitation of the sensorimotor synapse requires postsynaptic activation of inositol triphosphate (IP_3) receptors (Li et al., 2005). Taken together, the data from both isolated motor neurons in culture and sensorimotor cocultures suggests a scenario in which G protein–coupled 5-HT receptor activation stimulates the generation of the second messenger IP_3 and subsequent Ca^{2+} release from IP_3 receptor–mediated stores via the activation of phospholipase C (PLC).

Several reports have established a role for G protein–activated PLC in the cellular processes regulating learning and memory (Buckley and Caldwell, 2004; Nicolle et al., 1999; Sallés et al., 2001). Moreover, activation of the G protein–activated beta subtype of PLC (PLCβ) is necessary for several types of learning-related synaptic plasticity. For example, inhibitory long-term potentiation (LTP) in the visual cortex involves the recruitment of PLCβ via the coordinated activation of $GABA_B$ and $5\text{-}HT_2$ receptors (Komatsu, 1996), and long-term depression (LTD) in the visual cortex is impaired in transgenic mice lacking the PLCβ gene (Choi et al., 2005). In Aplysia, the long-term (24-h) enhancement of sensorimotor synapses and accompanying increase in sensory neuron varicosities require the activation of PLC in the sensory neuron (Udo et al., 2005). In this situation, PLC is believed to be upstream of the Rho GTPase cdc42, a signaling molecular that plays a key role in regulation of the cytoskeleton. Despite these findings, a number of questions regarding the role of PLC during the induction of synaptic plasticity in Aplysia remain unexplored. What role does PLC play in organizing the

signaling required for the induction of earlier forms of facilitation (<1 h)? Is—as suggested by the data from Li et al. (2005)—postsynaptic PLC activation necessary for the induction of facilitation? If so, to what extent does postsynaptic PLC activity contribute to sensitization memory?

Here we describe experiments studying the function of PLC activation during the induction of synaptic facilitation and sensitization in Aplysia. We find that inhibition of PLC activity impairs the induction of facilitation in sensorimotor synapses at a time where facilitation is significantly supported by postsynaptic processes (Liu et al., 2005). To determine whether facilitation depends critically on PLC activation in the motor neuron, we examined the effect of PLC inhibition on 5-HT–dependent enhancement of the glutamate response in isolated motor neurons. These experiments showed that the sustained increase in the glutamatergic response following a 10-min application of 5-HT was completely abolished by blockade of PLC activity. Finally, we showed that pharmacological inhibition of PLC before training reduces intermediate-term sensitization of the SWR; this result supports the notion that PLC-dependent signaling, occurring in postsynaptic motor neurons, contributes to persistent behavioral modification of the SWR.

Methods

Animals

Adult Aplysia californica were obtained from a local supplier (Alacrity Marine Biological, Redondo Beach, CA). Animals were housed in a 50-gal aquarium filled with cooled (12–14°C), aerated seawater (Catalina Water Company, Long Beach, CA).

Cell cultures

Sensorimotor cocultures were fabricated as described by Lin and Glanzman (1994). Briefly, single small siphon (LFS) motor neurons and single presynaptic pleural sensory neurons were individually dissociated from the CNS of Aplysia (60–100 g) before being arranged in pairs in poly-L-lysine coated culture dishes. Cultures were maintained at 18°C for 3–4 days before the start of the experiments. The culture medium contained 50% Aplysia hemolyph and 50% Leibowitz-15 (L-15; Sigma, St. Louis, MO). The cell cultures used in the glutamate puff experiments consisted solely of isolated small siphon (LFS) motor neurons (Chitwood et al., 2001).

Electrophysiology

The electrophysiological methods used in the experiments on sensorimotor cocultures were as described previously (Liu et al., 2005). All electrophysiological tests were performed

using custom protocols programmed into Axograph version 9 (Molecular Devices, Union City, CA). Because a computer executed these protocols automatically, the experiments were not performed blind. During electrophysiological recording, cultures were perfused with perfusion medium consisting of 50% sterile artificial seawater (ASW) and 50% L-15. All experiments were performed at room temperature. The presynaptic sensory neuron and postsynaptic motor neuron in each coculture were impaled with sharp microelectrodes (20–30 MΩ). To prevent spontaneous firing of the motor neurons during testing and to minimize stimulus-evoked firing, the motor neuron was held at –80 mV throughout the experiment by passing negative current (typical range, 0.3–0.8 nA) into the cell via the bridge circuit of the microelectrode amplifier. The threshold for eliciting an action potential in the presynaptic sensory neuron was determined 5 min after impaling the neuron by injection of brief (20 ms) depolarizing current pulses, starting at 0.1 nA, and increasing sequentially in steps of 0.1 nA, until a spike was generated in the presynaptic cell. The amount of current required to activate an action potential in the sensory neuron ranged from 0.4 to 1.2 nA. This value was kept constant in the majority of experiments; however, in 33% of experiments, it was necessary to adjust this value between 0.1 and 0.2 nA. The size of the evoked excitatory postsynaptic potential (EPSP) recorded from the postsynaptic motor neuron was also noted. Synaptic responses were determined again 30 min after the initial test, with the resulting EPSP data serving as the pretest values for the ongoing experiment. Cocultures that exhibited >50% depression between the first and second EPSP tests were excluded from the experiment. The input resistances of the sensory and motor neurons were monitored throughout the experiment by injecting 300-ms pulses of negative current (0.1 nA) before each test. Cocultures that exhibited a drop in input resistance by >50% in either cell were excluded from further analysis. Only one coclulture was thereby excluded. A 10-min pulse of 5-

HT (20 μM) was applied immediately after the pretest. The synaptic response was retested 20 min after the end of the 5-HT application. The PLC inhibitor U73122 (500 nM in 0.025% DMSO; Sigma and Tocris Bioscience) was applied continuously in the perfusion medium starting 20 min before the pretest and continuing until the end of the 5-HT pulse (30-min total application). To control for the effect of 5-HT and to assess baseline synaptic responses, we performed "test alone" experiments in which synapses were stimulated using the same time intervals described above but in the absence of 5-HT. The effect of U73122 on basal synaptic responses was evaluated in test alone experiments. Application of the drug in these experiments was timed as in the experiments with 5-HT. Input resistance in both sensory and motor neurons tended to increase slightly (<30%) through the course of the experiment. Statistical analysis showed that there were no significant differences among input resistance values in the sensory and motor neurons in the four experimental groups (5-HT vehicle, 5-HT U73122, test alone vehicle, and test alone U73122; data not shown).

For experiments on isolated motor neurons, the soma was impaled with a sharp microelectrode (20–30 MΩ) and held at –80 to –85 mV via negative current injection (–0.2 to –0.6 nA) for the duration of the experiment. Motor neurons were stimulated by brief pulses (puffs) of glutamate (final concentration of 2 mM) pressure ejected (10–20 ms, 1–5 psi) using a Picospritzer (General Valve, Fairfield, NJ); the glutamate puffs were directed toward either the soma or initial segment of the major neurite. Glutamate in the ejected puff was rapidly removed from the motor neuron via a perfusion pipette placed in close proximity to the neuron. This arrangement produced a glutamate-evoked potential (Glu-EP) with rapid kinetics resembling those of synaptically evoked EPSPs. Glutamate was dissolved in perfusion medium containing Fast Green (0.02%), which permitted the puffs to be visualized. Puff duration and location were

initially adjusted to produce Glu-EPs of 10–15 mV. Thereafter, these parameters were kept constant for the duration of the experiment. Motor neurons received glutamate puffs once every 10 s throughout the duration of the experiment. The input resistance of the motor neuron was monitored throughout the experiment by injecting 300-ms pulses of negative current (0.1 nA) before each glutamate puff. Motor neurons that exhibited a drop in input resistance by >50% were excluded from further analysis. Three motor neurons treated with 5-HT U73122 and two motor neurons treated with 5-HT plus the vehicle were thereby excluded. No neurons were excluded in either of the test alone groups. Experiments began with a 20-min baseline period during which time the amplitude of the Glu-EP was monitored to confirm that the response was stable. Following 20 min of stable recording, 5-HT (20 μM) was applied to the culture dish via the perfusion medium for 10 min, after which the 5-HT pulse was terminated by perfusion with regular recording medium. The Glu-EP response was recorded for a further 40 min. Application of U73122 (400 nM in 0.02% DMSO) started 10 min before the start of the 5-HT pulse and continued until the washout period began. Input resistance increased slightly in motor neurons treated with U73122 (12.87 ± 5.68% for 5-HT U73122 cells and 3.79 ± 3.62% for test alone-U73122 cells vs. −3.74 ± 3.44% for 5-HT-vehicle cells and −11.57 ± 10.5% for test alone-vehicle cells). However, a statistical comparison of these data did not show significant between-group differences (data not shown). In experiments using the putative PLC activator m-3m3FBS (Calbiochem, EMD Biosciences, San Diego, CA), the Glu-EP was recorded for 20 min after the end of the 5-HT application. In these experiments, a 10-min application of m-3m3FBS (1 μM in 0.01% DMSO) was followed by a 5-min application of 5-HT (20 μM). Thus, m-3m3FBS was applied 10 min into the baseline recording session and was applied for a total of 15 min.

Behavioral experiments

Sensitization experiments were performed on adult Aplysia housed individually in custom-built Plexiglass chambers continuously perfused with cooled (14°C) seawater. One day before training, each animal was weighed and implanted bilaterally with Teflon-coated platinum wires (0.008-in coated diameter, A-M Systems, Carlsborg, WA). For this procedure, the animal was anesthetized by cooling in cold water (4°C) for 13 min. Wires, prepared by removing the Teflon from the ends with forceps, were threaded through a 20-gauge needle, which was used to insert the wire into the animal's tail. Following this procedure, the animal was placed into the training chamber, where it was given ≥24 h to recover and acclimate to the chamber. The SWR was tested as follows: The siphon was lightly stimulated with a soft, flexible probe (broom bristle), and the duration of the ensuing SWR was timed. Timing of the SWR began once the siphon had retracted completely within the parapodia and ended the moment the siphon became visible again. Responses were given a score of 1.0 s if the siphon did not withdraw completely inside the parapodia. Three pretests were delivered once every 10 min beginning 50 min before the start of training. The experimenter conducting these tests was unaware of the experimental treatments each animal had undergone. Pilot experiments indicated that injection of DMSO at levels >1% produced nonspecific effects on sensitization learning (data not shown). For this reason, and because of the relatively poor solubility of U73122, we were limited to a maximum injected concentration of 20 μM U73122. In our experience (see also Levenson et al., 2000a), the effective concentrations for drugs injected into whole Aplysia are typically within the high micromolar to low millimolar range. Thus, to maximize administration of the drug at low micromolar concentrations, animals were given two injections of drug (final U73122 concentration 20 μM in 1% DMSO in ASW) or vehicle (1% DMSO in ASW). Injections were

made at 25 and 5 min before the first training trial. Intrahemocoel injections (1 ml/100 g) were made into the animal's neck. (This site was chosen because it was found to cause the least disturbance to the animal.) Sensitization training consisted of three bouts of electrical shocks at 20-min intervals. During each bout of training, the animal received three trains of shocks spaced once every 2 s. Each train was 1 s in duration and consisted of shocks (10-ms pulse duration, 40 Hz, 120 V) delivered to the animal's tail via a Grass stimulator (S88, Astro-Med, West Warwick, RI) connected to the platinum wires. The SWR was tested 30, 60, 90, and 120 min after the end of the last trial. Repeated testing of the SWR under these conditions did not result in any appreciable habituation of the response.

Statistical analyses

All statistical tests were computed using Prism 4.0 for Macintosh (Graphpad Software, El Camino Real, CA). For electrophysiological experiments on sensorimotor cocultures, the peak amplitude of the evoked EPSP recorded at the posttest was normalized to the amplitude of the pretest EPSP and expressed as the percent mean ± SE. For experiments on isolated motor neurons, the peak amplitude of each Glu-EP was measured and normalized to the mean amplitude of the 60 Glu-EPs observed during the first 10 min of baseline recording. Normalized Glu-EPs were expressed as the percent means ± SE. Frequency histograms of data sets were prepared to determine whether the data exhibited a normal distribution. Because all of the electrophysiological data sets were found to exhibit a normal distribution, the between-group comparisons for these data were analyzed using parametric t-tests. The behavioral data did not exhibit a normal distribution; we therefore used nonparametric statistics to analyze these data.

Behavioral change was assessed as follows: First, mean pretest responses were determined for each animal. Next the posttest data obtained for each time point—30, 60, 90, and 120 min—were corrected by subtracting the appropriate mean pretest value. The corrected posttest scores were averaged for each animal, producing a single mean posttest score. Finally, the mean posttest scores were compared using a Mann-Whitney U test. Data from experiments in which the animals received only the test stimuli (test alone experiments) were analyzed the same way as those in which the animals received training with electrical shocks.

Results

Disruption of PLC activity impairs 5-HT–dependent facilitation of sensorimotor synapses in culture

To examine the role of PLC activation in synaptic facilitation, we studied the effect of U73122, a specific inhibitor of G protein–mediated PLC activity (Yule and Williams, 1992) on facilitation induced by a brief (10-min) application of 5-HT. The experiments were performed using sensorimotor cocultures (Lin and Glanzman, 1994). The cocultures comprised a single sensory neuron monosynaptically connected to a single small siphon (LFS-type) motor neuron (Frost et al., 1988). All cultures were 3–5 days old at the time of experiments.

Previous work by Li et al. (2005) has shown that, following a 10-min application of 5-HT, the balance between pre- and postsynaptic processes changes over time, with postsynaptic processes becoming increasingly prominent in facilitation after washout of the drug. We wished to examine the potential connection between PLC activation and IP_3 receptor-dependent facilitation in the motor neuron. Accordingly, we examined facilitation 20 min after termination of the 5-HT pulse, a time at which postsynaptic mechanisms seem to predominate in facilitation (Li et al., 2005). An initial experiment was performed to examine the affect of U73122 on basal synaptic responses (Figure A3-1Ai). In this experiment, we compared one group of cocultures (test alone-vehicle) treated with the vehicle solution (0.025% DMSO) for 30 min with a second group of cocultures (test alone-U73122) treated with U73122 (500 nM in vehicle) for 30 min. A t-test conducted on the mean normalized EPSP values recorded 20 min after washout of either the U73122 or vehicle did not show a significant difference ($t = 0.95$, $df = 6$, $P = 0.38$; Figure A3-1Aii); therefore application of the PLC inhibitor U73122 for 30 min did not produce a

deleterious effect on basal synaptic transmission. We next examined the effect of U73122 on 5-HT–induced facilitation. In this experiment, synaptic responses in one group of cocultures (5-HT-vehicle) treated with the vehicle solution (0.025% DMSO) for 20 min followed by 5-HT (20 μM) in the vehicle for 10 min were compared with responses recorded from a second group (5-HT-U73122) treated with U73122 (500 nM) for 20 min followed by 5-HT plus U73122 for 10 min (Figure A3-1Bi). Comparison of the mean normalized EPSP values determined 20 min after 5-HT washout in these groups showed a significant difference ($t = 3.22$, $df = 12$, $P < 0.01$; Figure A3-1Bii). Taken together, these data show that synaptic responses in the 5-HT-vehicle group were significantly stronger than those in the 5-HT-U73122 group, indicating that synaptic facilitation was prevented by blockade of PLC activity.

5-HT–dependent enhancement of the glutamate response of isolated motor neurons depends on activation of PLC

The above data provide strong evidence that PLC activation is required for the induction of synaptic facilitation in Aplysia. However, the data do not allow us to determine whether the necessary PLC-dependent pathways reside in the sensory neuron or motor neuron because the drug was applied in the perfusion medium and thus could potentially have affected PLC activity in both pre- and postsynaptic cells. Currently, cell membrane impermeant PLC inhibitors are unavailable; therefore it is not possible to examine this idea directly in sensorimotor cocultures. To address the question of whether synaptic facilitation in Aplysia requires the activation of a PLC-dependent pathway within the motor neuron, we turned to experiments on isolated motor neurons. Application of 5-HT for 10 min to isolated siphon motor neurons in dissociated cell

culture produces an enhancement of the response to glutamate that persists for >50 min (Chitwood et al., 2001; Villareal et al., 2007), and, like facilitation of the sensorimotor synapse (Li et al., 2005), requires an increase in intracellular Ca^{2+} within the motor neuron (Chitwood et al., 2001). The single motor neuron cell culture system therefore provides a valuable tool for isolating the postsynaptic mechanisms that regulate plasticity of the Aplysia sensorimotor synapse. Accordingly, we examined the effect of U73122 on 5-HT–induced enhancement of the Glu-EP in isolated motor neurons. An initial experiment was conducted to determine if U73122 produced a deleterious effect on the basal Glu-EP response of the isolated motor neuron. Two groups of motor neurons were examined in this experiment (Figure A3-2Ai). The first group (test alone-vehicle) received the vehicle solution (0.02% DMSO) for 20 min, whereas the second group (test alone-U73122) received U73122 (400 nM) in the vehicle for 20 min. Glu-EP responses in the test alone-U73122 group remained stable throughout the duration of the experiment (Figure A3-2Aii). Comparison of the averaged postbaseline responses in the test alone-vehicle and test alone-U73122 groups did not show a significant difference ($t = 0.14$, $df = 10$, $P = 0.89$), indicating that application of the PLC inhibitor for 20 min did not produce a measurable effect on the Glu-EP response (Figure A3-2Aiii). We next examined the effect of U73122 on 5-HT–induced enhancement of the Glu-EP. This experiment involved two groups of motor neurons (Figure A3-2Bi). The first group (5-HT-vehicle) was subjected to an application of vehicle (0.02% DMSO, 10 min) followed by 5-HT plus vehicle (20 μM 5-HT, 10 min), whereas the second group (5-HT-U73122) received treatment with U73122 (400 nM, 10 min) in the vehicle followed by 5-HT plus U73122 in vehicle (10 min). Application of 5-HT produced a sustained increase in the amplitude of the Glu-EP that was not observed in the U73122-treated group (Figure A3-2Bii). A comparison of the averaged postbaseline responses in the two groups

showed a significant difference ($t = 2.38$, $df = 9$, $P < 0.05$), indicating that the mean Glu-EP response in the 5-HT-vehicle group was significantly stronger than the mean response recorded in the 5-HT-U73122 group (Figure A3-2Biii). Overall, these data show that stimulation with 5-HT for 10 min recruits a PLC-dependent pathway within the motor neuron that contributes to the persistent enhancement of the neuron's response to glutamate.

As a further test for the role of PLC signaling in the postsynaptic motor neuron, we examined the effect of the PLC activator m-3m3FBS (Bae et al., 2003) on the glutamatergic response of isolated motor neurons. Using human lymphoma cells, Bae et al. reported significant PLC activation with m-3m3FBS at 25–50 μM. However, at this concentration, we observed deleterious effects on both the input resistance and the Glu-EP (data not shown). At lower concentrations (1–2 μM) we observed a slight depression in the Glu-EP response that persisted after washout of the drug (data not shown). Although low concentrations of m-3m3FBS alone did not induce prolonged enhancement of the Glu-EP, we found that a 10-min pretreatment with m-3m3FBS (1 μM), when followed by a brief (5 min) application of 5-HT, led to enhancement of the Glu-EP that persisted for significantly longer (>20 min) than in a control group of motor neurons treated with 5 min of 5-HT alone ($t = 3.39$, $df = 8$, $P < 0.01$; data not shown). Interpretation of these data is complicated by the fact that the specificity of m-3m3FBS as a stimulator of PLC has been questioned (Krjukova et al., 2004). In particular, this compound may stimulate the release of Ca^{2+} from intracellular stores in a PLC-independent fashion. Given that facilitation requires the release of Ca^{2+} from postsynaptic stores (Li et al., 2005), the application of m-3m3FBS might, if it acted to increase Ca^{2+} release in the motor neuron, lead to enhanced facilitation following brief applications of 5-HT. Consequently, whether the enhancement in response observed in this experiment is caused by effects on PLC activation is unclear at present.

Behavioral sensitization memory requires the activation of PLC

Sensitization of the SWR is mediated, in part, by facilitation of the monosynaptic connections between central sensory and motor neurons (Antonov et al., 1999; Cleary et al., 1998). Consequently, one would expect intracellular signaling pathways, such as G protein–mediated PLC activation, that play crucial roles in synaptic facilitation to also be important in sensitization. Accordingly, we examined the necessity of PLC activity for behavioral modification of the SWR by injecting U73122 into animals before training. We first sought to explore the effect of U73122 injection on basal SWR responses. In this experiment, the SWR was monitored in two groups of animals: one that received injections of vehicle solution (1% DMSO in ASW) and another that received injections of U73122 (20 μM) in the vehicle. Analysis of the mean corrected posttest values from these two groups indicated that the mean group responses did not differ ($u = 29$, $P > 0.80$; Figure A3-3B). Thus, injection of the PLC inhibitor did not produce a deleterious effect on the SWR. Having confirmed that U73122 did not affect the normal expression of the SWR, we next examined the effect of this drug on sensitization learning. Two groups of animals were examined in this study: the first group received injections of vehicle solution (1% DMSO in ASW) before training, whereas the second received pretraining injections of U73122 (20 μM) in vehicle (Figure A3-3A). Injection of U73122 disrupted sensitization learning (Figure A3-3C). Comparison of the averaged corrected posttest (post-pre) responses for the two groups showed that the SWR in the U73122-injected animals was significantly weaker than in the vehicle-injected controls ($u = 38$, $P < 0.05$).

Discussion

Potential role of postsynaptic PLC activity in learning-related synaptic facilitation in Aplysia

Our data provide evidence that postsynaptic PLC signaling contributes to synaptic facilitation in Aplysia. Although in our experiments on in vitro sensorimotor synapses, the PLC inhibitor U73122 was bath-applied and therefore might have disrupted presynaptic PLC activity, rather than or in addition to, postsynaptic PLC activity, our experiments on isolated motor neurons in dissociated cell culture provide strong support for the notion that at least part of the effect of U73122 in our synaptic experiments was caused by the drug's disruption of postsynaptic PLC activity. Previous evidence from our laboratory (Chitwood et al., 2001; Li et al., 2005; Villareal et al., 2007) indicates that a 10-min application of 5-HT to isolated motor neurons recruits the postsynaptic component of intermediate-term facilitation (ITF) in Aplysia (see Sutton and Carew, 2002). In this study, we observed that a 10-min pulse of 5-HT produced enhancement of the Glu-EP in isolated motor neurons that persisted for >40 min and that depended on PLC activity because it was blocked by U73122. These results, together with the previous work from our laboratory (Chitwood et al., 2001; Li et al., 2005; Villareal et al., 2007), support the notion that postsynaptic PLC activity is critical for ITF. Note that a defining property of ITF is that it persists for 30 min to 3 h (Sutton and Carew, 2002). Admittedly, in our experiments on in vitro sensorimotor synapses, we tested facilitation only at 20 min after the end of a 10-min pulse of 5-HT; however, we have previously shown that such a treatment induces synaptic facilitation that persists for >40 min (Li et al., 2005) and therefore satisfies the temporal criterion for ITF.

Activation of PLC catalyzes the generation of the second messengers IP_3 and diacylglycerol (DAG) through the hydrolysis of membrane-bound inositol precursors (Katan, 2005). Both of these signaling molecules may contribute to postsynaptic induction of facilitation via distinct pathways. First, IP_3, generated through the activation of PLC, could contribute to the induction of facilitation through its action as a stimulator of Ca^{2+} release from IP_3 receptor-operated stores (Berridge, 1993). In fact, IP_3 receptor-dependent Ca^{2+} release in the motor neuron plays an essential role in the induction of ITF of the sensorimotor synapse (Liu et al., 2005). Accordingly, the data presented here are consistent with a scheme in which G protein–activated PLCβ-type enzymes (Katan, 2005), stimulated by the activation of postsynaptic 5-HT receptors, generate an IP_3-dependent Ca^{2+} signal; this signal, in turn, leads to the recruitment of postsynaptic signaling pathways necessary for the expression of facilitation. Additional support for this idea is provided by experiments that show an increase in IP_3 production in the motor neuron during a 10-min application of 5-HT (Jin et al., 2007). Taken together, these data provide strong evidence that 5-HT–induced facilitation requires the postsynaptic activation of a PLC-IP_3 signaling system and that this IP_3-dependent pathway leads to the functional up-regulation of AMPA-type glutamate receptors (Chitwood et al., 2001; Li et al., 2005). Second, PLC-stimulated DAG would be expected to activate the typical isoforms of protein kinase C (PKC), which have been implicated in several forms of synaptic plasticity in Aplysia (for review, see Sossin, 2007). Contrary to this expectation, however, a recent study by Zhao et al. (2006)—which examined the translocation from the cytoplasm to the cell membrane of fluorescently tagged Aplysia PKC in both sensory and motor neurons of sensorimotor cocultures—found that a brief, 5-min application of 5-HT did not activate postsynaptic PKC. However, Zhao et al. did not test whether postsynaptic PKC activation occurs following a longer (10 min) application of 5-HT, such as that

used in our experiments. Our laboratory has found that bath application of either bisindolylmaleimide (Bis I), a specific inhibitor of typical PKCs, or chelerythrine, an inhibitor of both typical and atypical PKCs, disrupts induction of the enhancement of the glutamate response in isolated siphon motor neurons following a 10-min application of 5-HT (Villareal et al., 2006; but see Hawkins et al., 2006).

Furthermore, we have recently identified a role for PKC during the expression of this form of plasticity. Chelerythrine, applied after the establishment of stable 5-HT–induced enhancement of the Glu-EP, rapidly reversed the enhancement; in contrast, application of Bis I did not reverse the effect of 5-HT on the Glu-EP (Villareal et al., 2006). Because chelerythrine is significantly more potent at inhibiting atypical PKCs than is Bis I (Laudanna et al., 1998; Ling et al., 2002; Martiny-Baron et al., 1993), these data point to a specific requirement for atypical PKC during the expression of 5-HT–dependent enhancement of the Glu-EP. PLC activity would therefore seem not to be needed for expression in this form of plasticity, because activation of the atypical PKCs occurs independently of the generation of DAG (Sossin, 2007). Overall, the pharmacological data suggest that the PLC/DAG pathway in the motor neuron is recruited during the induction of 5-HT–dependent facilitation of the sensorimotor synapse but does not participate in the maintenance of facilitation. Interestingly, a study by Ghirardi et al. (1992) found that PKC activity was specifically required for facilitation of depressed synapses but not for facilitation of rested synapses. On first reading this would seem to suggest that the effect of PLC blockade in these experiments, which involved rested synapses, must not be mediated through disruption of the DAG-PKC pathway. However, Ghirardi et al. explicitly examined short-term facilitation (≤5 min) resulting from only a 1-min application of 5-HT. In contrast, these experiments studied ITF (at 20 min), which is produced by a 10-min treatment with 5-HT (Li et al., 2005). As discussed

above, recent results from our laboratory indicate that the induction of ITF depends on postsynaptic PKC (Villareal et al., 2006). Taken together, these findings suggest that the effects of PLC inhibition observed in our synaptic experiments reflect an influence on both the IP_3- and DAG-PKC–dependent component of the PLC signaling pathway.

Whereas these data indicate that postsynaptic PLC is required for ITF in Aplysia, other data support a role for presynaptic PLC in facilitation of the sensorimotor synapse. For example, PKC has been implicated in presynaptic processes, including spike broadening and mobilization of presynaptic vesicles, that contribute to short-term facilitation (STF) in Aplysia (for review, see Byrne and Kandel, 1996). Furthermore, Zhao et al. (2006) have found that a 5-min pulse of 5-HT translocates Apl II, the Ca^{2+}-independent (novel) isoform of PKC from the cytoplasm to the cell membrane of the sensory neuron, and that this effect can be reproduced by application of PDBu alone, a phorbolester known to activate DAG. These results implicate presynaptic PLC activity in STF. Other evidence indicates that presynaptic PLC activity is required for both long-term facilitation (LTF), as well as the increase in presynaptic varicosities that accompanies LTF (Udo et al., 2005; also see Glanzman et al., 1990). Similarly, recent experiments have provided evidence that presynaptic PKC activity, presumably downstream from PLC activation, is important for ITF of the sensorimotor synapse caused by a 10-min application of 5-HT (for review, see Hawkins et al., 2006) such as was used in this study (see also Sutton and Carew, 2000). In summary, there is significant evidence for roles for presynaptic PLC activity in various forms of synaptic facilitation in Aplysia, in addition to the role for postsynaptic PLC activity indicated by these results.

Behavioral sensitization requires PLC activity

Sensitization training involving repeated spaced applications of tail shocks produces several distinct phases of memory that can be distinguished along temporal and pharmacological lines (Sutton et al., 2001). In these experiments, the SWR was sampled between 30 and 120 min after spaced training. During this time, the memory depends on new protein synthesis, but not transcription; it is therefore distinct from long-term memory for sensitization, which requires both protein and mRNA synthesis (Castellucci et al., 1989; Sutton et al., 2001) and from short-term memory, which requires neither (Sutton et al., 2001; also see Montarolo et al., 1986). This form of sensitization memory, referred to as intermediate-term memory (ITM), has been reported to require protein kinase A (PKA) and calcium/calmodulin-dependent protein kinase II (CaMKII), but not PKC (for review, see Hawkins et al., 2006). However, the requirement for PLC activity in ITM, observed in our experiments, suggests that PKC, IP_3, or both, contribute to the induction of ITM, contrary to a previous report (Antonov et al., 2005). It should be pointed out that another form of ITM has been described that does require persistent PKC activity. This form of ITM, "site-specific" ITM, is shown by testing the trained site on the tail following a single tail shock (Sutton et al., 2004). Site-specific ITM differs from repeated trial ITM in its lack of dependence on PKA and protein synthesis (also see Sutton and Carew, 2000). Clearly, however, the type of ITM shown here is not site-specific ITM, because the test stimuli were applied to a site (the siphon) that was not trained. It is possible that methodological differences between our experiments and those of Antonov et al. (2005) can account for the apparent discrepancy regarding the possible involvement of PKC in ITM caused by spaced training. For example, we used fewer training trials (3 vs. 4), and sampled sensitization over a longer time period (30–120 min posttraining vs. 60 min). It is also possible that PKC was not one of the

learning-related signaling pathways recruited downstream of PLC activation by the sensitization training in this study. However, the fact that cellular evidence from our laboratory implicates PKC in activity-independent ITF (Villareal et al., 2006) means that the question of whether or not activity-independent ITM involves (postsynaptic) PKC activity remains open. Finally, our behavioral results are consistent with previous data from cellular studies that implicate postsynaptic IP_3 receptor activity in intermediate-term synaptic facilitation in Aplysia (Li et al., 2005).

In summary, we showed that the induction of synaptic facilitation in Aplysia depends on activation of PLC. We also showed that the sustained, 5-HT–dependent increase in the response of isolated motor neurons to glutamate, the neurotransmitter of Aplysia sensory neurons, similarly depends on PLC activity. Taken together, these data point to a key role for postsynaptic PLC in 5-HT–dependent facilitation of the sensorimotor synapse. Additionally, we found that intermediate-term sensitization of the SWR is reduced in animals following injection of an inhibitor of PLC, consistent with the involvement of PLC-dependent synaptic facilitation in this form of nonassociative learning.

Grants

This work was supported by National Institutes of Health Grants R37 NS-029563 and K02 MH-067062 to D. L. Glanzman.

Acknowledgements

We thank Drs. Greg Villareal and Adam Roberts for helpful comments on the manuscript.

Figures

Figure A3-1: Bath application of U73122, a specific inhibitor of phospholipase C (PLC) activity, disrupts 5-HT–dependent facilitation of the sensorimotor synapse in culture.

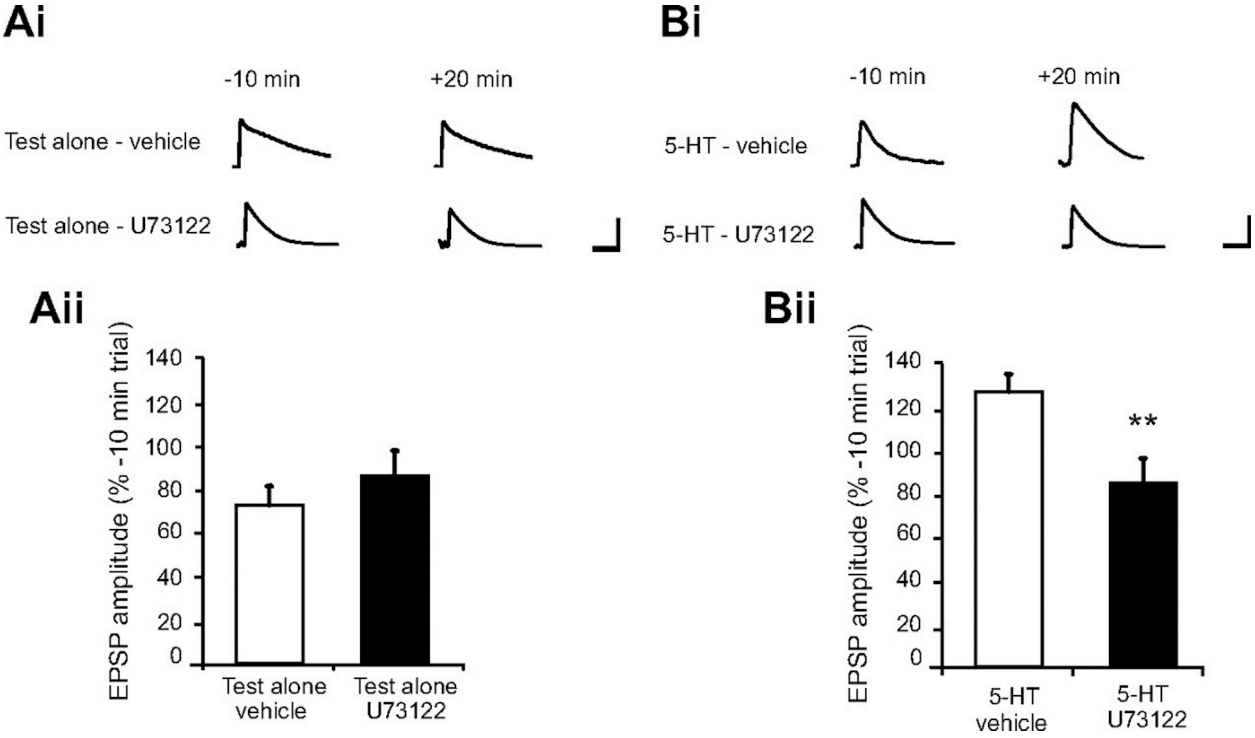

Ai) sample excitatory postsynaptic potentials (EPSPs) recorded from siphon motor neurons for each of the test alone groups. Times shown are relative to the end of the application of either drug or vehicle, i.e., 10 min before and 20 min after washout. Calibration bars represent 10 mV and 50 ms. **Aii**) mean normalized group data for the 2 test alone groups: synapses treated with DMSO solution (test alone-vehicle, n = 4) and synapses treated with U73122 (test alone-U73122, n = 4). The mean EPSP amplitudes in the test alone-vehicle and test alone-U73122 were not significantly different (73.8 ± 8.8 vs. 85.1 ± 11.77%). **Bi**) sample EPSPs recorded from siphon motor neurons in the 2 experimental groups. Times shown are relative to the end of the application of either drug or vehicle, i.e., 10 min before and 20 min after washout. Calibration

bars represent 10 mV and 50 ms. **Bii**) mean normalized group data for the 2 experimental groups of synapses: those treated with 5-HT in the absence of U73122 (5-HT-vehicle, n = 7) and those treated with 5-HT in the presence of U73122 (5-HT-U73122, n = 7). Synaptic responses in the 5-HT–treated synapses were significantly larger than responses in the 5-HT U73122–treated synapses (127.4 ± 5.8 vs. 87.72 ± 11.7%), indicating that inhibition of PLC disrupted synaptic facilitation. **Significance at $P < 0.001$. Data are expressed as means ± SE.

Figure A3-2: 5-HT–induced facilitation in the isolated siphon motor neuron depends on PLC activation.

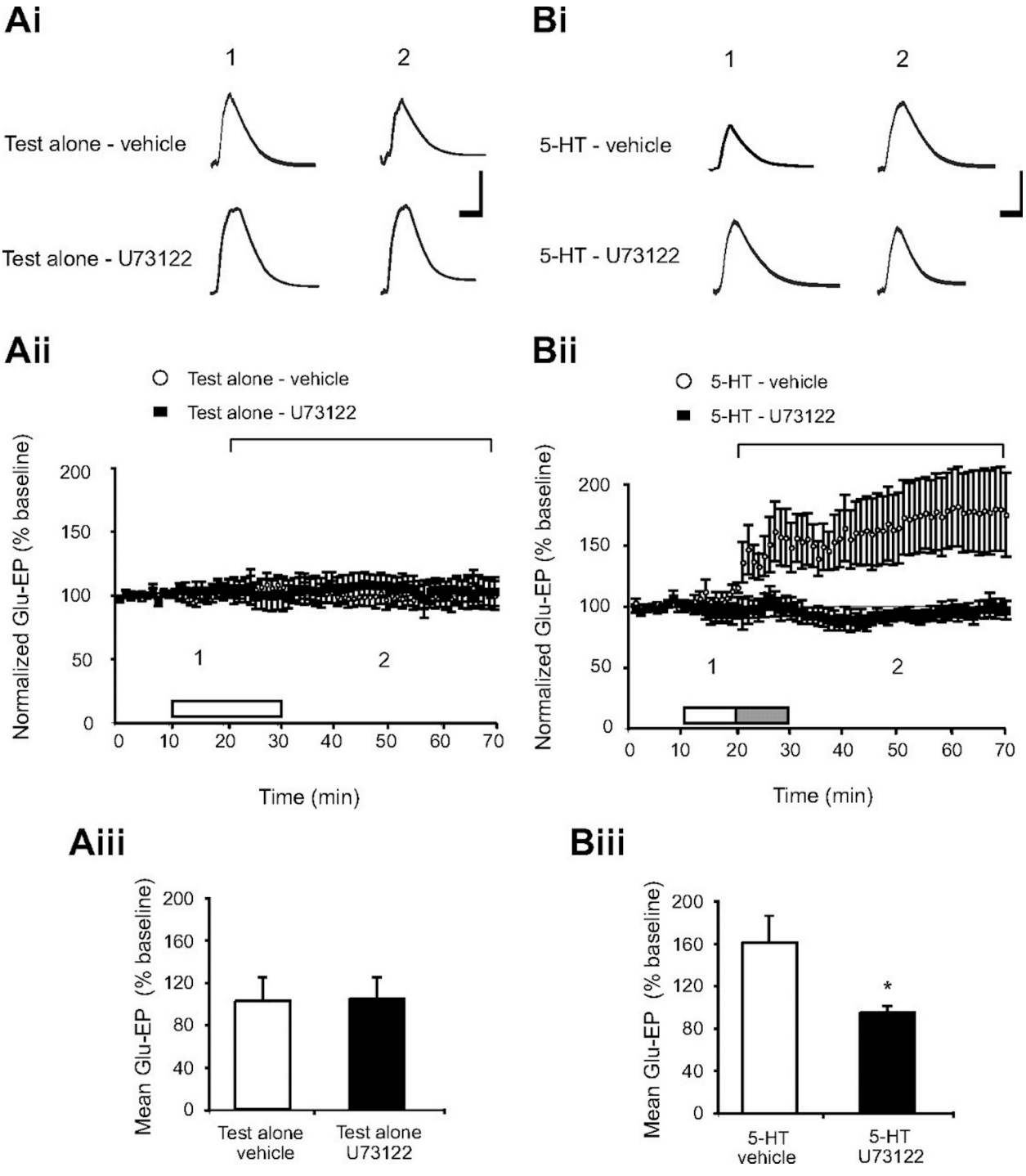

Ai) sample glutamate-evoked potential (Glu-EP) records for 2 time points from each test alone experiment. The numbers above each trace correspond to the time points indicated in the graph

in Aii. Calibration bars represent 10 mV and 50 ms. **Aii**) summary data for the 2 test alone groups: motor neurons treated only with the vehicle (test alone-vehicle, n = 8), and motor neurons exposed to U73122 in the vehicle (test alone-U73122, n = 4). Each data point represents the normalized mean of 6 Glu-EPs. The horizontal bracket identifies the portion of the data summarized in the histogram in Aiii. The white bar indicates an application of either U73122 in the vehicle or the vehicle alone. **Aiii**) histogram showing the mean Glu-EP values recorded in the test alone experiments. There was no significant difference between the mean responses in test alone-vehicle and test alone-U73122 groups recorded during the 50-min period starting 10 min into the application of the drug and ending 40 min after washout (101.9 ± 22.85 vs. 103.7 ± 19.72%). **Bi**) sample Glu-EP records for 2 time points in the 2 5-HT–treated groups. The numbers above each trace correspond to the time points indicated in the graph in Bii. Calibration bars represent 10 mV and 50 ms. **Bii**) summary data for the 2 5-HT–treated groups: motor neurons treated with 5-HT in DMSO (5-HT-vehicle, n = 6) and motor neurons given a 10-min pretreatment with U73122 in the vehicle followed by 5-HT plus U73122 (5-HT-U73122, n = 5). Each data point represents the normalized mean of 6 Glu-EPs. The white bar indicates an application of either U73122 in the vehicle or the vehicle alone. The gray bar indicates an application of 5-HT plus either U73122 or the vehicle. The horizontal bracket identifies the portion of the data displayed in Biii. **Biii**) histogram displaying the mean Glu-EP data recorded during the 50-min period from the start of 5-HT application through the subsequent 40-min washout period. The average Glu-EP values in the 5-HT-vehicle group were significantly larger than those in the 5-HT-U73122 group (161.6 ± 25.18 vs. 94.2 ± 6.22%). *Significance at $P < 0.05$. Data are expressed as means ± SE.

Figure A3-3: Intermediate-term sensitization memory requires PLC activity.

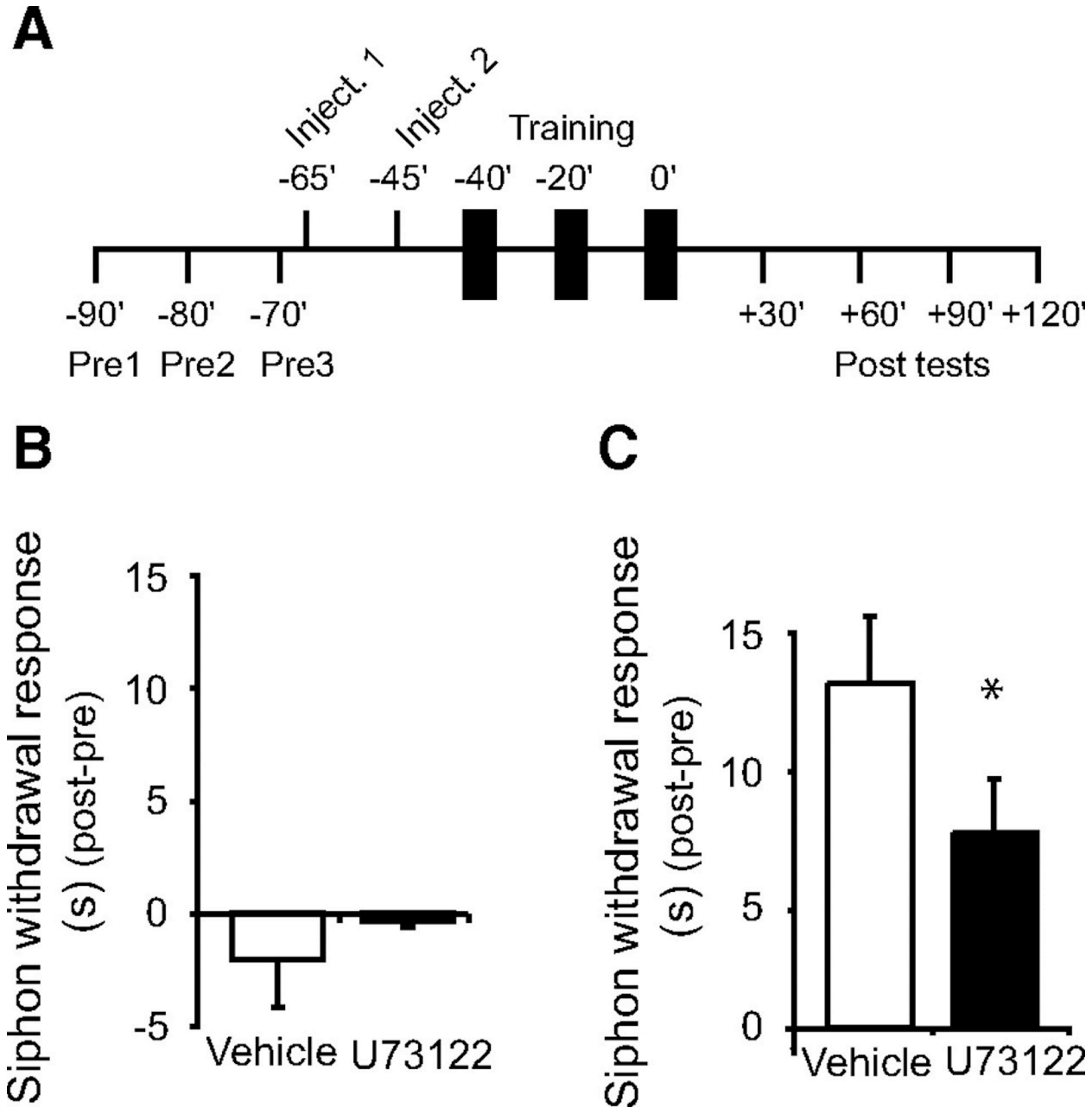

A) schematic showing the procedures used for the behavioral experiments. The timing of the pretests, drug/vehicle injections, training, and posttests are shown relative to the end of the last training session. Vertical black bars represent bouts of sensitization training. An identical protocol was used for the test alone experiments (summarized in B), except that the sensitization

training was omitted. **B**) Data from behavioral experiments in which sensitization training was withheld. Mean corrected siphon withdrawal response (SWR; posttest –pretest) for the 4 tests taken after injection of either vehicle (test alone-vehicle, n = 4) or U73122 (test alone-U73122, n = 4). The withdrawal responses did not differ between vehicle- and U73122-injected groups (–2.06 ± 2.12 vs. –0.35 ± 0.27 s). **C**) graph presenting the mean corrected posttest data for animals that received injections of either the vehicle (n = 12) or U73122 (n = 14) before sensitization training. A statistical comparison of the mean corrected SWR, averaged across the 4 posttests, showed that responses in the vehicle-injected group were of a significantly longer duration than those observed in the U73122-injected group (12.44 ± 2.4 vs. 7.05 ± 1.94 s). *Significance at $P < 0.05$. Data are expressed as the mean corrected siphon withdrawal duration (s) ±SE.

References

Abrahams BS, Geschwind DH. 2008. Advances in autism genetics: on the threshold of a new neurobiology. Nat Rev Genet 9:341–355.

Abrahams BS, Tentler D, Perederiy JV, Oldham MC, Coppola G, Geschwind DH. 2007. Genome-wide analyses of human perisylvian cerebral cortical patterning. Proc Natl Acad Sci USA 104:17849–17854.

Agate RJ, Scott BB, Haripal B, Lois C, Nottebohm F. 2009. Transgenic songbirds offer an opportunity to develop a genetic model for vocal learning. Proc Natl Acad Sci USA 106:17963–17967.

Alarcón M, Abrahams BS, Stone JL, Duvall JA, Perederiy JV, Bomar JM, Sebat J, Wigler M, Martin CL, Ledbetter DH, et al. 2008. Linkage, association, and gene-expression analyses identify CNTNAP2 as an autism-susceptibility gene. Am J Hum Genet 82:150–159.

Ambrose NG, Cox NJ, Yairi E. 1997. The genetic basis of persistence and recovery in stuttering. J Speech Lang Hear Res 40:567–580.

Anderson GR, Galfin T, Xu W, Aoto J, Malenka RC, Südhof TC. 2012. Candidate autism gene screen identifies critical role for cell-adhesion molecule CASPR2 in dendritic arborization and spine development. Proceedings of the National Academy of Sciences.

Antonov I, Kandel ER, Hawkins RD. 1999. The contribution of facilitation of monosynaptic PSPs to dishabituation and sensitization of the Aplysia siphon withdrawal reflex. J Neurosci 19:10438–10450.

Antonov I, Kandel ER, Hawkins RD. 2005. Roles of PKA, PKC, and CamKII in dishabituation and sensitization of the Aplysia siphon-withdrawal reflex. Society for Neuroscience 540.

Arking DE, Cutler DJ, Brune CW, Teslovich TM, West K, Ikeda M, Rea A, Guy M, Lin S, Cook EH, et al. 2008. A common genetic variant in the neurexin superfamily member CNTNAP2 increases familial risk of autism. Am J Hum Genet 82:160–164.

Arnold AP, Chen X, Link JC, Itoh Y, Reue K. 2013. Cell-autonomous sex determination outside of the gonad. Dev Dyn 242:371–379.

Arriaga G, Zhou EP, Jarvis ED. 2012. Of mice, birds, and men: the mouse ultrasonic song system has some features similar to humans and song-learning birds. PLoS ONE 7:e46610.

Bacon C, Rappold GA. 2012. The distinct and overlapping phenotypic spectra of FOXP1 and FOXP2 in cognitive disorders. Human Genetics 131:1687–1698.

Bae Y-S, Lee TG, Park JC, Hur JH, Kim Y, Heo K, Kwak J-Y, Suh P-G, Ryu SH. 2003.

Identification of a compound that directly stimulates phospholipase C activity. Mol Pharmacol 63:1043–1050.

Bakkaloglu B, O'Roak BJ, Louvi A, Gupta AR, Abelson JF, Morgan TM, Chawarska K, Klin A, Ercan-Sencicek AG, Stillman AA, et al. 2008. Molecular cytogenetic analysis and resequencing of contactin associated protein-like 2 in autism spectrum disorders. Am J Hum Genet 82:165–173.

Balmer TS, Carels VM, Frisch JL, Nick TA. 2009. Modulation of perineuronal nets and parvalbumin with developmental song learning. J Neurosci 29:12878–12885.

Baum C, Fehse B. 2003. Mutagenesis by retroviral transgene insertion: risk assessment and potential alternatives. Curr Opin Mol Ther 5:458–462.

Baum C, Kustikova O, Modlich U, Li Z, Fehse B. 2006. Mutagenesis and oncogenesis by chromosomal insertion of gene transfer vectors. Hum Gene Ther 17:253–263.

Bekker JM, Colantonio JR, Stephens AD, Clarke WT, King SJ, Hill KL, Crosbie RH. 2007. Direct interaction of Gas11 with microtubules: implications for the dynein regulatory complex. Cell Motil Cytoskeleton 64:461–473.

Belton E, Salmond CH, Watkins KE, Vargha-Khadem F, Gadian DG. 2003. Bilateral brain abnormalities associated with dominantly inherited verbal and orofacial dyspraxia. Hum Brain Mapp 18:194–200.

Benayoun BA, Caburet S, Veitia RA. 2011. Forkhead transcription factors: key players in health and disease. Trends Genet 27:224–232.

Benítez-Burraco A, Longa VM. 2012. Right-handedness, lateralization and language in Neanderthals: a comment on Frayer et al. (2010). J Anthropol Sci 90:187–92– discussion 193–7.

Berridge MJ. 1993. Inositol trisphosphate and calcium signalling. Nature 361:315–325.

Berwick RC, Friederici AD, Chomsky N, Bolhuis JJ. 2013. Evolution, brain, and the nature of language. Trends in Cognitive Sciences 17:89–98.

Blasi F, Carmeliet P. 2002. uPAR: a versatile signalling orchestrator. Nat Rev Mol Cell Biol 3:932–943.

Borst A, Bahde S. 1987. Comparison between the movement detection systems underlying the optomotor and the landing response in the housefly. Biol Cybern 56:217–224.

Borst A, Egelhaaf M. 1993. Visual Motion and its Role in the Stabilization of Gaze. In: Miles FA, Wallman J, editors. New York: Detecting visual motion: Theory and models, Eds. FA Miles and J. Wallman, Elsevier Science. p 3–27.

Borst A. 1990. How Do Flies Land? From behavior to neuronal circuits. Bioscience 40:292-299.

Bottaro DP, Rubin JS, Faletto DL, Chan AM, Kmiecik TE, Vande Woude GF, Aaronson SA. 1991. Identification of the hepatocyte growth factor receptor as the c-met proto-oncogene product. Science 251:802–804.

Bottjer SW, Johnson F. 1997. Circuits, hormones, and learning: vocal behavior in songbirds. J Neurobiol 33:602–618.

Bottjer SW, Miesner EA, Arnold AP. 1984. Forebrain lesions disrupt development but not maintenance of song in passerine birds. Science 224:901-903.

Bourtchuladze R, Frenguelli B, Blendy J, Cioffi D, Schutz G, Silva AJ. 1994. Deficient long-term memory in mice with a targeted mutation of the cAMP-responsive element-binding protein. Cell 79:59–68.

Bowers JM, Perez-Pouchoulen M, Edwards NS, McCarthy MM. 2013. Foxp2 mediates sex differences in ultrasonic vocalization by rat pups and directs order of maternal retrieval. J Neurosci 33:3276–3283.

Brainard MS, Doupe AJ. 2000a. Auditory feedback in learning and maintenance of vocal behaviour. Nat Rev Neurosci 1:31–40.

Brainard MS, Doupe AJ. 2000b. Interruption of a basal ganglia-forebrain circuit prevents plasticity of learned vocalizations. Nature 404:762–766.

Bredy TW, Lin Q, Wei W, Baker-Andresen D, Mattick JS. 2011. MicroRNA regulation of neural plasticity and memory. Neurobiol Learn Mem 96:89–94.

Brenowitz EA. 2013. Testosterone and brain-derived neurotrophic factor interactions in the avian song control system. Neuroscience 239:115–123.

Bruce HA, Margolis RL. 2002. FOXP2: novel exons, splice variants, and CAG repeat length stability. Human Genetics 111:136–144.

Buchner E. 1984. Behavioural Analysis of Spatial Vision in Insects. In: Ali MA, editor. NATO ASI Series. Vol. 74. Photoreception and Vision in Invertebrates. Boston, MA: Springer US. p 561–621–621..

Byrne JH, Kandel ER. 1996. Presynaptic facilitation revisited: state and time dependence. J Neurosci 16:425–435.

Cai D, Pearce K, Chen S, Glanzman DL. 2011. Protein kinase M maintains long-term sensitization and long-term facilitation in aplysia. J Neurosci 31:6421–6431.

Campbell DB, D'Oronzio R, Garbett K, Ebert PJ, Mirnics K, Levitt P, Persico AM. 2007. Disruption of cerebral cortex MET signaling in autism spectrum disorder. Ann Neurol 62:243–250.

Campbell DB, Li C, Sutcliffe JS, Persico AM, Levitt P. 2008. Genetic evidence implicating

multiple genes in the MET receptor tyrosine kinase pathway in autism spectrum disorder. Autism Res 1:159–168.

Campbell DB, Sutcliffe JS, Ebert PJ, Militerni R, Bravaccio C, Trillo S, Elia M, Schneider C, Melmed R, Sacco R, et al. 2006. A genetic variant that disrupts MET transcription is associated with autism. Proc Natl Acad Sci USA 103:16834–16839.

Campbell DB, Warren D, Sutcliffe JS, Lee EB, Levitt P. 2010. Association of MET with social and communication phenotypes in individuals with autism spectrum disorder. Am J Med Genet B Neuropsychiatr Genet 153B:438–446.

Carlsson P, Mahlapuu M. 2002. Forkhead transcription factors: key players in development and metabolism. Dev Biol 250:1–23.

Carr CW, Moreno-De-Luca D, Parker C, Zimmerman HH, Ledbetter N, Martin CL, Dobyns WB, Abdul-Rahman OA. 2010. Chiari I malformation, delayed gross motor skills, severe speech delay, and epileptiform discharges in a child with FOXP1 haploinsufficiency. Eur J Hum Genet 18:1216–1220.

Castellucci VF, Blumenfeld H, Goelet P, Kandel ER. 1989. Inhibitor of protein synthesis blocks long-term behavioral sensitization in the isolated gill-withdrawal reflex of Aplysia. J Neurobiol 20:1–9.

Celio MR, Baier W, Schärer L, de Viragh PA, Gerday C. 1988. Monoclonal antibodies directed against the calcium binding protein parvalbumin. Cell Calcium 9:81–86.

Centanni TM, Booker AB, Sloan AM, Chen F, Maher BJ, Carraway RS, Khodaparast N, Rennaker R, Loturco JJ, Kilgard MP. 2013. Knockdown of the Dyslexia-Associated Gene Kiaa0319 Impairs Temporal Responses to Speech Stimuli in Rat Primary Auditory Cortex. Cereb Cortex.

Cheng L-C, Pastrana E, Tavazoie M, Doetsch F. 2009. miR-124 regulates adult neurogenesis in the subventricular zone stem cell niche. Nat Neurosci 12:399–408.

Chitwood RA, Li Q, Glanzman DL. 2001. Serotonin facilitates AMPA-type responses in isolated siphon motor neurons of Aplysia in culture. J Physiol (Lond) 534:501–510.

Choi S-Y, Chang J, Jiang B, Seol G-H, Min S-S, Han J-S, Shin H-S, Gallagher M, Kirkwood A. 2005. Multiple receptors coupled to phospholipase C gate long-term depression in visual cortex. J Neurosci 25:11433–11443.

Cleary LJ, Lee WL, Byrne JH. 1998. Cellular correlates of long-term sensitization in Aplysia. J Neurosci 18:5988–5998.

Cline H. 2005. Synaptogenesis: a balancing act between excitation and inhibition. Curr Biol 15:R203–5.

Clovis YM, Enard W, Marinaro F, Huttner WB, De Pietri Tonelli D. 2012. Convergent repression of Foxp2 3'UTR by miR-9 and miR-132 in embryonic mouse neocortex: implications for radial migration of neurons. Development 139:3332–3342.

Collett TS. 1980. Some operating rules for the optomotor system of a hoverfly during voluntary flight. J Comp Physiol A 138:271–282–282.

Colomb J, Mendoza E, Pflueger H-J, Zars T, Scharff C, Brembs B. 2012. PKC and dFoxP are necessary for operant self-learning. Forum of Neuroscience [Internet].

Condro MC, White SA. in press. Distribution of language-related Cntnap2 protein in neural circuitry dedicated to vocal learning.. J Comp Neurol.

Coolen M, Thieffry D, Drivenes Ø, Becker TS, Bally-Cuif L. 2012. miR-9 controls the timing of neurogenesis through the direct inhibition of antagonistic factors. Dev Cell 22:1052–1064.

Cynx J, Rad von U. 2001. Immediate and transitory effects of delayed auditory feedback on bird song production. Anim Behav 62:305–312..

Czamara D, Bruder J, Becker J, Bartling J, Hoffmann P, Ludwig KU, Müller-Myhsok B, Schulte-Körne G. 2011. Association of a rare variant with mismatch negativity in a region between KIAA0319 and DCDC2 in dyslexia. Behav Genet 41:110–119.

Dajas-Bailador F, Bonev B, Garcez P, Stanley P, Guillemot F, Papalopulu N. 2012. microRNA-9 regulates axon extension and branching by targeting Map1b in mouse cortical neurons. Nat Neurosci.

Dale N, Kandel ER. 1993. L-glutamate may be the fast excitatory transmitter of Aplysia sensory neurons. Proc Natl Acad Sci USA 90:7163–7167.

Devaux J, Gola M, Jacquet G, Crest M. 2002. Effects of K+ channel blockers on developing rat myelinated CNS axons: identification of four types of K+ channels. J Neurophysiol 87:1376–1385.

Doherty FC, Schaack JB, Sladek CD. 2011. Comparison of the efficacy of four viral vectors for transducing hypothalamic magnocellular neurosecretory neurons in the rat supraoptic nucleus. J Neurosci Methods 197:238–248.

Doupe AJ, Kuhl PK. 1999. Birdsong and human speech: common themes and mechanisms. Annu Rev Neurosci 22:567–631.

Dow LE, Premsrirut PK, Zuber J, Fellmann C, McJunkin K, Miething C, Park Y, Dickins RA, Hannon GJ, Lowe SW. 2012. A pipeline for the generation of shRNA transgenic mice. Nat Protoc 7:374–393.

Duistermars BJ, Reiser MB, Zhu Y, Frye MA. 2007. Dynamic properties of large-field and small-field optomotor flight responses in Drosophila. J Comp Physiol A 193:787–799.

Dunn AM, Zann RA. 1996. Undirected song in wild zebra finch flocks: contexts and effects of mate removal. Ethology.

Dvorak D, Srinivasan MV, French AS. 1980. The contrast sensitivity of fly movement-detecting neurons. Vision Res 20:397–407.

Eagleson KL, Bonnin A, Levitt P. 2005. Region- and age-specific deficits in γ-aminobutyric acidergic neuron development in the telencephalon of theuPAR-/- mouse. J Comp Neurol 489:449–466.

Eagleson KL, Campbell DB, Thompson BL, Bergman MY, Levitt P. 2011. The autism risk genes MET and PLAUR differentially impact cortical development. Autism Res 4:68–83.

Eales LA. 1985. Song learning in zebra finches: some effects of song model availability on what is learnt and when. Anim Behav 33:1293–1300.

Egelhaaf M, Borst A. 1993. Movement detection in arthropods. Rev Oculomot Res 5:53–77.

Egelhaaf M, Hausen K, Reichardt W, Wehrhahn C. 1988. Visual course control in flies relies on neuronal computation of object and background motion. Trends Neurosci 11:351–358.

Egelhaaf M. 1987. Dynamic properties of two control systems underlying visually guided turning in house-flies. Journal of Comparative Physiology A.

Egelhaaf M. 1989. Visual afferences to flight steering muscles controlling optomotor responses of the fly. J Comp Physiol A 165:719–730.

Enard W, Gehre S, Hammerschmidt K, Holter SM, Blass T, Somel M, Bruckner MK, Schreiweis C, Winter C, Sohr R, et al. 2009. A humanized version of Foxp2 affects cortico-basal ganglia circuits in mice. Cell 137:961–971.

Enard W, Przeworski M, Fisher SE, Lai CSL, Wiebe V, Kitano T, Monaco AP, Pääbo S. 2002. Molecular evolution of FOXP2, a gene involved in speech and language. Nature 418:869–872.

Evans MR, Roberts ML, Buchanan KL, Goldsmith AR. 2006. Heritability of corticosterone response and changes in life history traits during selection in the zebra finch. J Evol Biol 19:343–352.

Faddy HM, Smart CE, Xu R, Lee GY, Kenny PA, Feng M, Rao R, Brown MA, Bissell MJ, Roberts-Thomson SJ, et al. 2008. Localization of plasma membrane and secretory calcium pumps in the mammary gland. Biochemical and Biophysical Research Communications 369:977–981.

Falivelli G, De Jaco A, Favaloro FL, Kim H, Wilson J, Dubi N, Ellisman MH, Abrahams BS, Taylor P, Comoletti D. 2012. Inherited genetic variants in autism-related CNTNAP2 show perturbed trafficking and ATF6 activation. Hum Mol Genet.

Farries MA, Perkel DJ. 2002. A telencephalic nucleus essential for song learning contains neurons with physiological characteristics of both striatum and globus pallidus. J Neurosci 22:3776–3787.

Farries MA. 2001. The oscine song system considered in the context of the avian brain: lessons learned from comparative neurobiology. Brain Behav Evol 58:80–100.

Fehér O, Wang H, Saar S, Mitra PP, Tchernichovski O. 2009. De novo establishment of wild-type song culture in the zebra finch. Nature 459:564–568.

Ferland RD, Cherry T, Preware P, Morrisey EE, et al. 2003. Characterization of Foxp 2 and Foxp 1 mRNA and protein in the developing and mature brain. J Comp Neurol.

Feuk L, Kalervo A, Lipsanen-Nyman M, Skaug J, et al. 2006. Absence of a paternally inherited FOXP2 gene in developmental verbal dyspraxia. Am J Hum Genet.

Finestack LH, Richmond EK, Abbeduto L. 2009. Language Development in Individuals with Fragile X Syndrome. Top Lang Disord 29:133–148.

Fiore R, Khudayberdiev S, Saba R, Schratt G. 2011. MicroRNA function in the nervous system. Prog Mol Biol Transl Sci 102:47–100.

Fisher SE, Vargha-Khadem F, Watkins KE, Monaco AP, Pembrey ME. 1998. Localisation of a gene implicated in a severe speech and language disorder. Nat Genet 18:168–170.

Fisher SE. 2005. On genes, speech, and language. N Engl J Med 353:1655–1657.

Fitch W. 2000. The evolution of speech: a comparative review. Trends in Cognitive Sciences 4:258–267.

Fitch WT. 2012. Evolutionary developmental biology and human language evolution: constraints on adaptation. Evol Biol 39:613–637.

French CA, Jin X, Campbell TG, Gerfen E, Groszer M, Fisher SE, Costa RM. 2012. An aetiological Foxp2 mutation causes aberrant striatal activity and alters plasticity during skill learning. Mol Psychiatry 17:1077–1085.

Friedman JI, Vrijenhoek T, Markx S, Janssen IM, der Vliet van WA, Faas BHW, Knoers NV, Cahn W, Kahn RS, Edelmann L, et al. 2008. CNTNAP2 gene dosage variation is associated with schizophrenia and epilepsy. Mol Psychiatry 13:261–266.

Frost WN, Clark GA, Kandel ER. 1988. Parallel processing of short-term memory for sensitization in Aplysia. J Neurobiol 19:297–334.

Fujita E, Tanabe Y, Shiota A, Ueda M, Suwa K, Momoi MY, Momoi T. 2008. Ultrasonic vocalization impairment of Foxp2 (R552H) knockin mice related to speech-language disorder and abnormality of Purkinje cells. Proc Natl Acad Sci USA 105:3117–3122.

Gabbiani F, Krapp HG, Laurent G. 1999. Computation of object approach by a wide-field, motion-sensitive neuron. J Neurosci 19:1122–1141.

Gaub S, Groszer M, Fisher SE, Ehret G. 2010. The structure of innate vocalizations in Foxp2-deficient mouse pups. Genes, brain, and behavior 9:390–401.

Gentner TQ, Hulse SH, Bentley GE, Ball GF. 2000. Individual vocal recognition and the effect of partial lesions to HVc on discrimination, learning, and categorization of conspecific song in adult songbirds. J Neurobiol 42:117–133.

Ghirardi M, Braha O, Hochner B, Montarolo PG, Kandel ER, Dale N. 1992. Roles of PKA and PKC in facilitation of evoked and spontaneous transmitter release at depressed and nondepressed synapses in Aplysia sensory neurons. Neuron 9:479–489.

Glanzman DL, Kandel ER, Schacher S. 1990. Target-dependent structural changes accompanying long-term synaptic facilitation in Aplysia neurons. Science 249:799–802.

Glanzman DL, Mackey SL, Hawkins RD, Dyke AM, Lloyd PE, Kandel ER. 1989. Depletion of serotonin in the nervous system of Aplysia reduces the behavioral enhancement of gill withdrawal as well as the heterosynaptic facilitation produced by tail shock. J Neurosci 9:4200–4213.

Glanzman DL. 2006. The cellular mechanisms of learning in Aplysia: of blind men and elephants. Biol Bull 210:271–279.

Glanzman DL. 2007. Simple Minds: The Neurobiology of Invertebrate Learning and Memory. In: North G, Greenspan RJ, editors. Invertebrate Neurobiology. New York: Cold Spring Harbor Laboratory Press. p 347–380.

Goldberg JH, Adler A, Bergman H, Fee MS. 2010. Singing-Related Neural Activity Distinguishes Two Putative Pallidal Cell Types in the Songbird Basal Ganglia: Comparison to the Primate Internal and External Pallidal Segments. J Neurosci 30:7088–7098.

Goldberg JH, Fee MS. 2012. A cortical motor nucleus drives the basal ganglia-recipient thalamus in singing birds. Nat Neurosci 15:620–627.

Götz K, Wandel U. 1984. Optomotor control of the force of flight in Drosophila and Musca. Biol Cybern 51:135–139.

Götz KG. 1964. Optomotor studies of the visual system of several eye mutants of the fruit fly Drosophila. Kybernetik 2:77–92.

Götz K. 1975. The optomotor equilibrium of theDrosophila navigation system. J Comp Physiol A 99:187–210–210.

Götz KG. 1987. Course-control, metabolism and wing interference during ultralong tethered flight in Drosophila melanogaster. J Exp Biol 128:35-46.

Graham SA, Fisher SE. 2013. Decoding the genetics of speech and language. Curr Opin Neurobiol 23:43–51.

Green RE, Krause J, Briggs AW, Maricic T, Stenzel U, Kircher M, Patterson N, Li H, Zhai W, Fritz MH-Y, et al. 2010. A draft sequence of the Neandertal genome. Science 328:710–722.

Griggs EM, Young EJ, Rumbaugh G, Miller CA. 2013. MicroRNA-182 regulates amygdala-dependent memory formation. J Neurosci 33:1734–1740.

Grimbert P, Valanciute A, Audard V, Pawlak A, Le gouvelo S, Lang P, Niaudet P, Bensman A, Guellaën G, Sahali D. 2003. Truncation of C-mip (Tc-mip), a new proximal signaling protein, induces c-maf Th2 transcription factor and cytoskeleton reorganization. J Exp Med 198:797–807.

Gronenberg W, Strausfeld NJ. 1992. Premotor descending neurons responding selectively to local visual stimuli in flies. J Comp Neurol 316:87–103.

Groszer M, Keays DA, Deacon RMJ, de Bono JP, Prasad-Mulcare S, Gaub S, Baum MG, French CA, Nicod J, Coventry JA, et al. 2008. Impaired synaptic plasticity and motor learning in mice with a point mutation implicated in human speech deficits. Curr Biol 18:354–362.

Gunaratne PH, Lin Y-C, Benham AL, Drnevich J, Coarfa C, Tennakoon JB, Creighton CJ, Kim JH, Milosavljevic A, Watson M, et al. 2011. Song exposure regulates known and novel microRNAs in the zebra finch auditory forebrain. BMC Genomics 12:277.

Haag J, Borst A. 2002. Dendro-dendritic interactions between motion-sensitive large-field neurons in the fly. J Neurosci 22:3227–3233.

Haesler S, Rochefort C, Georgi B, Licznerski P, Osten P, Scharff C. 2007. Incomplete and inaccurate vocal imitation after knockdown of FoxP2 in songbird basal ganglia nucleus area X. PLoS Biol 5:e321.

Haesler S, Wada K, Nshdejan A, Morrisey EE, Lints T, Jarvis ED, Scharff C. 2004. FoxP2 expression in avian vocal learners and non-learners. J Neurosci 24:3164–3175.

Hall M. 1962. Evolutionary aspects of estralid song. Symp Zool Soc Lond 8:37–55.

Hamdan FF, Daoud H, Rochefort D, Piton A, Gauthier J, Langlois M, Foomani G, Dobrzeniecka S, Krebs M-O, Joober R, et al. 2010. De novo mutations in FOXP1 in cases with intellectual disability, autism, and language impairment. Am J Hum Genet 87:671–678.

Harris RA, O'Carroll DC, Laughlin SB. 2000. Contrast gain reduction in fly motion adaptation. Neuron 28:595–606.

Hassenstain B, Reichardt W. 1956. Systemtheoretische analyse der zeit-, Reihenfolgen- und vorzeichenauswertung bei der bewegungsperzeption des russelkafers Cholorophanus. Zeitschrift fur Naturforschung B 11:513–524.

Hausen K. 1982. Motion sensitive interneurons in the optomotor system of the fly. Biol Cybern.

Hawkins RD, Kandel ER, Bailey CH. 2006. Molecular mechanisms of memory storage in Aplysia. Biol Bull 210:174–191.

He L, Hannon GJ. 2004. MicroRNAs: small RNAs with a big role in gene regulation. Nat Rev Genet 5:522–531.

Heisenberg M, Wolf R. 1984. Vision in Drosophila. Berlin: Springer-Verlag.

Hessler NA, Doupe AJ. 1999a. Social context modulates singing-related neural activity in the songbird forebrain. Nat Neurosci 2:209–211.

Hessler NA, Doupe AJ. 1999b. Singing-related neural activity in a dorsal forebrain-basal ganglia circuit of adult zebra finches. J Neurosci 19:10461–10481.

Higgins CM, Douglass JK, Strausfeld NJ. 2004. The computational basis of an identified neuronal circuit for elementary motion detection in dipterous insects. Vis Neurosci 21:567–586.

Hilliard AT, Miller JE, Fraley ER, Horvath S, White SA. 2012a. Molecular microcircuitry underlies functional specification in a Basal Ganglia circuit dedicated to vocal learning. Neuron 73:537–552.

Hilliard AT, Miller JE, Horvath S, White SA. 2012b. Distinct neurogenomic states in basal ganglia subregions relate differently to singing behavior in songbirds. PLoS Comp Biol 8:e1002773.

Hockemeyer D, Sfeir AJ, Shay JW, Wright WE, de Lange T. 2005. POT1 protects telomeres from a transient DNA damage response and determines how human chromosomes end. EMBO J 24:2667–2678.

Hodgson ZG, Meddle SL, Roberts ML, Buchanan KL, et al. 2007. Spatial ability is impaired and hippocampal mineralocorticoid receptor mRNA expression reduced in zebra finches (Taeniopygia guttata) selected for acute high corticosterone response to stress. Proc Roy Soc B: Biological Sciences.

Hopman AHN, Ramaekers FCS, Speel EJM. 1998. Rapid Synthesis of Biotin-, Digoxigenin-, Trinitrophenyl-, and Fluorochrome-labeled Tyramides and Their Application for In Situ Hybridization Using CARD Amplification. J Hist & Cytochem 46:771–777.

Horn D, Kapeller J, Rivera-Brugués N, Moog U, Lorenz-Depiereux B, Eck S, Hempel M, Wagenstaller J, Gawthrope A, Monaco AP, et al. 2010. Identification of FOXP1 deletions in three unrelated patients with mental retardation and significant speech and language deficits. Hum Mutat 31:E1851–60.

Horn D. 2012. Mild to moderate intellectual disability and significant speech and language

deficits in patients with FOXP1 deletions and mutations. Mol Syndromol 2:213–216.

Horresh I, Poliak S, Grant S, Bredt D, Rasband MN, Peles E. 2008. Multiple molecular interactions determine the clustering of Caspr2 and Kv1 channels in myelinated axons. J Neurosci 28:14213–14222.

Hutson TH, Verhaagen J, Yáñez-Muñoz RJ, Moon LDF. 2012. Corticospinal tract transduction: a comparison of seven adeno-associated viral vector serotypes and a non-integrating lentiviral vector. Gene Ther 19:49–60.

Immelmann K. 1969. Song development in the zebra finch and other estrildid finches. In: Hinde RA, editor. Bird Vocalizations. New York: Cambridge Univ Pr. p 61–74.

Itoh Y, Arnold AP. 2011. Zebra finch cell lines from naturally occurring tumors. In Vitro Cell Dev Biol Anim 47(4): 280–282.

Ivliev AE, 't Hoen PAC, van Roon-Mom WMC, Peters DJM, Sergeeva MG. 2012. Exploring the transcriptome of ciliated cells using in silico dissection of human tissues. PLoS ONE 7:e35618.

Jarvis ED, Güntürkün O, Bruce L, Csillag A, Karten H, Kuenzel W, Medina L, Paxinos G, Perkel DJ, Shimizu T, et al. 2005. Avian brains and a new understanding of vertebrate brain evolution. Nat Rev Neurosci 6:151–159.

Jarvis ED, Nottebohm F. 1997. Motor-driven gene expression. Proc Natl Acad Sci USA 94:4097–4102.

Jarvis ED, Scharff C, Grossman MR, Ramos JA, Nottebohm F. 1998. For whom the bird sings: context-dependent gene expression. Neuron 21:775–788.

Jarvis ED. 2004. Learned birdsong and the neurobiology of human language. Ann N Y Acad Sci 1016:749–777.

Jin I, Rayman JB, Puthanveettil S, Vishwasrao H, Kandel ER, Hawkins RD. 2007. Spontaneous transmitter release from the presynaptic sensory neuron recruits IP3 production in the postsynaptic motor neuron during the induction of intermediate-term facilitation in Aplysia. Society for Neuroscience 429.

Judge S, Rind F. 1997. The locust DCMD, a movement-detecting neurone tightly tuned to collision trajectories. J Exp Biol 200:2209–2216.

Judson MC, Bergman MY, Campbell DB, Eagleson KL, Levitt P. 2009. Dynamic gene and protein expression patterns of the autism-associated Met receptor tyrosine kinase in the developing mouse forebrain. J Comp Neurol 513:511–531.

Jürgens U. 2009. The neural control of vocalization in mammals: a review. J Voice 23:1–10.

Kandel ER. 2001. The molecular biology of memory storage: a dialogue between genes and

synapses. Science 294:1030–1038.

Kang C, Domingues BS, Sainz E, Domingues CEF, Drayna D, Moretti-Ferreira D. 2011. Evaluation of the association between polymorphisms at the DRD2 locus and stuttering. J Hum Genet 56:472–473.

Kang C, Drayna D. 2011. Genetics of speech and language disorders. Annu Rev Genomics Hum Genet.

Kang C, Drayna D. 2012. A role for inherited metabolic deficits in persistent developmental stuttering. Mol Genet Metab 107:276–280.

Kang C, Riazuddin S, Mundorff J, Krasnewich D, Friedman P, Mullikin JC, Drayna D. 2010. Mutations in the lysosomal enzyme-targeting pathway and persistent stuttering. N Engl J Med 362:677–685.

Kao MH, Brainard MS. 2006. Lesions of an avian basal ganglia circuit prevent context-dependent changes to song variability. J Neurophysiol 96:1441–1455.

Kao MH, Doupe AJ, Brainard MS. 2005. Contributions of an avian basal ganglia-forebrain circuit to real-time modulation of song. Nature 433:638–643.

Katan M. 2005. New insights into the families of PLC enzymes: looking back and going forward. Biochem J 391:e7–9.

Kegl J. 2002. Language emergence in a language-ready brain. In: Morgan G, Woll B, editors. Directions in sign language acquisition. Philadelphia, PA: John Benjamins Publishing. p 207–254.

Kern R, Petereit C, Egelhaaf M. 2001. Neural processing of naturalistic optic flow. J Neurosci 21:RC139.

Kern R, van Hateren JH, Michaelis C, Lindemann JP, Egelhaaf M. 2005. Function of a fly motion-sensitive neuron matches eye movements during free flight. PLoS Biol 3:e171.

Kittelberger JM, Mooney R. 2005. Acute injections of brain-derived neurotrophic factor in a vocal premotor nucleus reversibly disrupt adult birdsong stability and trigger syllable deletion. J Neurobiol 62:406–424.

Kiya T, Itoh Y, Kubo T. 2008. Expression analysis of the FoxP homologue in the brain of the honeybee, Apis mellifera. Insect Mol Biol 17:53–60.

Kleiderlein JJ, Nisson PE, Jessee J, Li WB, Becker KG, Derby ML, Ross CA, Margolis RL. 1998. CCG repeats in cDNAs from human brain. Human Genetics 103:666–673.

Knornschild M, Nagy M, Metz M, Mayer F, Helversen von O. 2010. Complex vocal imitation during ontogeny in a bat. Biology Letters 6:156–159.

Kojima S, Kao MH, Doupe AJ. 2013. Task-related "cortical" bursting depends critically on basal ganglia input and is linked to vocal plasticity. Proc Nat Acad Sci 110:4756–4761.

Kole MHP, Letzkus JJ, Stuart GJ. 2007. Axon initial segment Kv1 channels control axonal action potential waveform and synaptic efficacy. Neuron 55:633–647.

Komatsu Y. 1996. GABAB receptors, monoamine receptors, and postsynaptic inositol trisphosphate-induced Ca2+ release are involved in the induction of long-term potentiation at visual cortical inhibitory synapses. J Neurosci 16:6342–6352.

Konishi M, Akutagawa E. 1985. Neuronal growth, atrophy and death in a sexually dimorphic song nucleus in the zebra finch brain. Nature 315:145–147.

Konishi M, Akutagawa E. 1990. Growth and atrophy of neurons labeled at their birth in a song nucleus of the zebra finch. Proc Natl Acad Sci USA 87:3538–3541.

Konopka G, Wexler E, Rosen E, Mukamel Z, Osborn GE, Chen L, Lu D, Gao F, Gao K, Lowe JK, et al. 2012. Modeling the functional genomics of autism using human neurons. Mol Psychiatry 17:202–214.

Konopka W, Kiryk A, Novak M, Herwerth M, Parkitna JR, Wawrzyniak M, Kowarsch A, Michaluk P, Dzwonek J, Arnsperger T, et al. 2010. MicroRNA loss enhances learning and memory in mice. J Neurosci 30:14835–14842.

Kos M, van den Brink D, Snijders TM, Rijpkema M, Franke B, Fernandez G, Hagoort P. 2012. CNTNAP2 and language processing in healthy individuals as measured with ERPs. PLoS ONE 7:e46995.

Kraft SJ, Yairi E. 2012. Genetic bases of stuttering: the state of the art, 2011. Folia Phoniatr Logop 64:34–47.

Kral K, Prete F. 2004. In the mind of a hunter: the visual world of the praying mantis. In: Prete F, ed. Complex worlds from simpler nervous systems. Cambridge: The MIT Press. 77-115.

Krapp HG, Hengstenberg B, Hengstenberg R. 1998. Dendritic structure and receptive-field organization of optic flow processing interneurons in the fly. J Neurophysiol 79:1902–1917.

Krapp HG, Hengstenberg R. 1996. Estimation of self-motion by optic flow processing in single visual interneurons. Nature 384:463–466.

Krapp HG. 2000. Neuronal matched filters for optic flow processing in flying insects. Int Rev Neurobiol 44:93–120.

Krause J, Lalueza-Fox C, Orlando L, Enard W, Green RE, Burbano HA, Hublin J-J, Hänni C, Fortea J, la Rasilla de M, et al. 2007. The derived FOXP2 variant of modern humans was shared with Neandertals. Curr Biol 17:1908–1912.

Krjukova J, Holmqvist T, Danis AS, Akerman KEO, Kukkonen JP. 2004. Phospholipase C

activator m-3M3FBS affects $Ca2^{+}$ homeostasis independently of phospholipase C activation. Br J Pharmacol 143:3–7.

Kuramochi-Miyagawa S, Watanabe T, Gotoh K, Totoki Y, Toyoda A, Ikawa M, Asada N, Kojima K, Yamaguchi Y, Ijiri TW, et al. 2008. DNA methylation of retrotransposon genes is regulated by Piwi family members MILI and MIWI2 in murine fetal testes. Genes Dev 22:908–917.

Lai CS, Fisher SE, Hurst JA, Vargha-Khadem F, Monaco AP. 2001. A forkhead-domain gene is mutated in a severe speech and language disorder. Nature 413:519–523.

Lan J, Song M, Pan C, Zhuang G, Wang Y, Ma W, Chu Q, Lai Q, Xu F, Li Y, et al. 2009. Association between dopaminergic genes (SLC6A3 and DRD2) and stuttering among Han Chinese. J Hum Genet 54:457–460.

Land MF. 1992. Visual tracking and pursuit: humans and arthropods compared. Journal of insect physiology.

Laudanna C, Mochly-Rosen D, Liron T, Constantin G, Butcher EC. 1998. Evidence of zeta protein kinase C involvement in polymorphonuclear neutrophil integrin-dependent adhesion and chemotaxis. J Bio Chem 273:30306–30315.

Lazaro MT, Penagarikano O, Dong H, Geschwind DH, Golshani P. 2012. Excitatory/inhibitory imbalance in the mPFC of the Cntnap2 mouse model of autism. Society for Neuroscience.

Leonardo A, Konishi M. 1999. Decrystallization of adult birdsong by perturbation of auditory feedback. Nature 399:466–470.

Levecque C, Velayos-Baeza A, Holloway ZG, Monaco AP. 2009. The dyslexia-associated protein KIAA0319 interacts with adaptor protein 2 and follows the classical clathrin-mediated endocytosis pathway. Am J Physiol, Cell Physiol 297:C160–8.

Levenson J, Endo S, Kategaya LS, Fernandez RI, Brabham DG, Chin J, Byrne JH, Eskin A. 2000a. Long-term regulation of neuronal high-affinity glutamate and glutamine uptake in Aplysia. Proc Natl Acad Sci USA 97:12858–12863.

Levenson J, Sherry DM, Dryer L, Chin J, Byrne JH, Eskin A. 2000b. Localization of glutamate and glutamate transporters in the sensory neurons of Aplysia. J Comp Neurol 423:121–131.

Li G, Wang J, Rossiter SJ, Jones G, Zhang S. 2007. Accelerated FoxP2 evolution in echolocating bats. PLoS ONE 2:e900.

Li Q, Roberts AC, Glanzman DL. 2005. Synaptic facilitation and behavioral dishabituation in Aplysia: dependence on release of Ca2+ from postsynaptic intracellular stores, postsynaptic exocytosis, and modulation of postsynaptic AMPA receptor efficacy. J Neurosci 25:5623–5637.

Li S, Weidenfeld J, Morrisey EE. 2004. Transcriptional and DNA binding activity of the Foxp1/2/4 family is modulated by heterotypic and homotypic protein interactions. Mol Cell Biol 24:809–822.

Li X, Hu Z, He Y, Xiong Z, Long Z, Peng Y, Bu F, Ling J, Xun G, Mo X, et al. 2010. Association analysis of CNTNAP2 polymorphisms with autism in the Chinese Han population. Psychiatr Genet 20:113–117.

Li Z, Düllmann J, Schiedlmeier B, Schmidt M, Kalle von C, Meyer J, Forster M, Stocking C, Wahlers A, Frank O, et al. 2002. Murine leukemia induced by retroviral gene marking. Science 296:497.

Lieberman P. 2007. The Evolution of Human Speech. Current Anthropology 48:39–66.

Liégeois F, Baldeweg T, Connelly A, Gadian DG, Mishkin M, Vargha-Khadem F. 2003. Language fMRI abnormalities associated with FOXP2 gene mutation. Nat Neurosci 6:1230–1237.

Lim LP, Lau NC, Garrett-Engele P, Grimson A, Schelter JM, Castle J, Bartel DP, Linsley PS, Johnson JM. 2005. Microarray analysis shows that some microRNAs downregulate large numbers of target mRNAs. Nature 433:769–773.

Lin XY, Glanzman DL. 1994. Long-term potentiation of Aplysia sensorimotor synapses in cell culture: regulation by postsynaptic voltage. Proc Biol Sci 255:113–118.

Ling DSF, Benardo LS, Serrano PA, Blace N, Kelly MT, Crary JF, Sacktor TC. 2002. Protein kinase Mzeta is necessary and sufficient for LTP maintenance. Nat Neurosci 5:295–296.

Lippi G, Steinert JR, Marczylo EL, D'Oro S, Fiore R, Forsythe ID, Schratt G, Zoli M, Nicotera P, Young KW. 2011. Targeting of the Arpc3 actin nucleation factor by miR-29a/b regulates dendritic spine morphology. J Cell Biol 194:889–904.

Liu C, Zhao X. 2009. MicroRNAs in adult and embryonic neurogenesis. Neuromol Med 11:141–152.

Liu Q-S, Pu L, Poo M-M. 2005. Repeated cocaine exposure in vivo facilitates LTP induction in midbrain dopamine neurons. Nature 437:1027–1031.

Livingston FS, White SA, Mooney R. 2000. Slow NMDA-EPSCs at synapses critical for song development are not required for song learning in zebra finches. Nat Neurosci 3:482–488.

Lu MM, Li S, Yang H, Morrisey EE. 2002. Foxp4: a novel member of the Foxp subfamily of winged-helix genes co-expressed with Foxp1 and Foxp2 in pulmonary and gut tissues. Mech Dev 119 Suppl 1:S197–202.

Luo G-Z, Hafner M, Shi Z, Brown M, Feng G-H, Tuschl T, Wang X-J, Li X. 2012. Genome-wide annotation and analysis of zebra finch microRNA repertoire reveal sex-biased

expression. BMC Genomics 13:727.

Lyon GR, Shaywitz SE, Shaywitz BA. 2003. A definition of dyslexia. Annals of dyslexia 53:1–14.

MacDermot KD, Bonora E, Sykes N, Coupe A-M, Lai CSL, Vernes SC, Vargha-Khadem F, McKenzie F, Smith RL, Monaco AP, et al. 2005. Identification of FOXP2 truncation as a novel cause of developmental speech and language deficits. Am J Hum Genet 76:1074–1080.

Mackey SL, Kandel ER, Hawkins RD. 1989. Identified serotonergic neurons LCB1 and RCB1 in the cerebral ganglia of Aplysia produce presynaptic facilitation of siphon sensory neurons. J Neurosci 9:4227–4235.

Mahrt EJ, Perkel DJ, Tong L, Rubel EW, Portfors CV. 2013. Engineered deafness reveals that mouse courtship vocalizations do not require auditory experience. J Neurosci 33:5573–5583.

Makeyev EV, Zhang J, Carrasco MA, Maniatis T. 2007. The MicroRNA miR-124 promotes neuronal differentiation by triggering brain-specific alternative pre-mRNA splicing. Mol Cell 27:435–448.

Marinesco S, Carew TJ. 2002. Serotonin release evoked by tail nerve stimulation in the CNS of aplysia: characterization and relationship to heterosynaptic plasticity. J Neurosci 22:2299–2312.

Marinesco S, Kolkman KE, Carew TJ. 2004. Serotonergic modulation in aplysia. I. Distributed serotonergic network persistently activated by sensitizing stimuli. J Neurophysiol 92:2468–2486.

Mars WM, Zarnegar R, Michalopoulos GK. 1993. Activation of hepatocyte growth factor by the plasminogen activators uPA and tPA. Am J Pathol 143:949–958.

Martiny-Baron G, Kazanietz MG, Mischak H, Blumberg PM, Kochs G, Hug H, Marmé D, Schächtele C. 1993. Selective inhibition of protein kinase C isozymes by the indolocarbazole Gö 6976. J Biol Chem 268:9194–9197.

Marui T, Koishi S, Funatogawa I, Yamamoto K, Matsumoto H, Hashimoto O, Nanba E, Kato C, Ishijima M, Watanabe K, et al. 2005. No association of FOXP2 and PTPRZ1 on 7q31 with autism from the Japanese population. Neurosci Res 53:91–94.

Mason MRJ, Ehlert EME, Eggers R, Pool CW, Hermening S, Huseinovic A, Timmermans E, Blits B, Verhaagen J. 2010. Comparison of AAV serotypes for gene delivery to dorsal root ganglion neurons. Mol Ther 18:715–724.

Massinen S, Hokkanen M-E, Matsson H, Tammimies K, Tapia-Páez I, Dahlström-Heuser V, Kuja-Panula J, Burghoorn J, Jeppsson KE, Swoboda P, et al. 2011. Increased expression of

the dyslexia candidate gene DCDC2 affects length and signaling of primary cilia in neurons. PLoS ONE 6:e20580.

Masson MEJ. 2003. Using confidence intervals for graphically based data interpretation. Can J Exp Psychol 57:203–220.

McRae PA, Rocco MM, Kelly G, Brumberg JC, Matthews RT. 2007. Sensory deprivation alters aggrecan and perineuronal net expression in the mouse barrel cortex. J Neurosci 27:5405–5413.

Megason SG, McMahon AP. 2002. A mitogen gradient of dorsal midline Wnts organizes growth in the CNS. Development 129:2087–2098.

Miller JE, Spiteri E, Condro MC, Dosumu-Johnson RT, Geschwind DH, White SA. 2008. Birdsong decreases protein levels of FoxP2, a molecule required for human speech. J Neurophysiol 100:2015–2025.

Missiaen L, Dode L, Vanoevelen J, Raeymaekers L, Wuytack F. 2007. Calcium in the Golgi apparatus. Cell Calcium 41:405–416.

Mizutani A, Matsuzaki A, Momoi MY, Fujita E, Tanabe Y, Momoi T. 2007. Intracellular distribution of a speech/language disorder associated FOXP2 mutant. Biochemical and Biophysical Research Communications 353:869–874.

Montagnese CM, Krebs JR, Meyer G. 1996. The dorsomedial and dorsolateral forebrain of the zebra finch, Taeniopygia guttata: a Golgi study. Cell Tissue Res 283:263–282.

Montarolo PG, Goelet P, Castellucci VF, Morgan J, Kandel ER, Schacher S. 1986. A critical period for macromolecular synthesis in long-term heterosynaptic facilitation in Aplysia. Science 234:1249–1254.

Mooney R. 1992. Synaptic basis for developmental plasticity in a birdsong nucleus. J Neurosci 12:2464–2477.

Morris D. 1954. The reproductive behaviour of the Zebra Finch (Poephila guttata), with special reference to pseudofemale behaviour and displacement activities. Behaviour 271-322.

Muhle R, Trentacoste SV, Rapin I. 2004. The genetics of autism. Pediatrics 113:e472–86.

Mukamel Z, Konopka G, Wexler E, Osborn GE, Dong H, Bergman MY, Levitt P, Geschwind DH. 2011. Regulation of MET by FOXP2, genes implicated in higher cognitive dysfunction and autism risk. J Neurosci 31:11437–11442.

Nelson DA, Marler P. 1994. Selection-based learning in bird song development. Proc Natl Acad Sci USA 91:10498–10501.

Newbury DF, Bonora E, Lamb JA, Fisher SE, Lai CSL, Baird G, Jannoun L, Slonims V, Stott CM, Merricks MJ, et al. 2002. FOXP2 is not a major susceptibility gene for autism or

specific language impairment. Am J HumGenet 70:1318–1327.

Newbury DF, Paracchini S, Scerri TS, Winchester L, Addis L, Richardson AJ, Walter J, Stein JF, Talcott JB, Monaco AP. 2011. Investigation of dyslexia and SLI risk variants in reading- and language-impaired subjects. Behav Genet 41:90–104.

Newbury DF, Winchester L, Addis L, Paracchini S, Buckingham L-L, Clark A, Cohen W, Cowie H, Dworzynski K, Everitt A, et al. 2009. CMIP and ATP2C2 modulate phonological short-term memory in language impairment. Am J Hum Genet 85:264–272.

Nicolle MM, Colombo PJ, Gallagher M, McKinney M. 1999. Metabotropic glutamate receptor-mediated hippocampal phosphoinositide turnover is blunted in spatial learning-impaired aged rats. J Neurosci 19:9604–9610.

Nixdorf-Bergweiler BE. 1996. Divergent and parallel development in volume sizes of telencephalic song nuclei in male and female zebra finches. J Comp Neurol 375:445–456.

Nordeen KW, Nordeen EJ. 1992. Auditory feedback is necessary for the maintenance of stereotyped song in adult zebra finches. Behav Neural Biol 57:58–66.

Nottebohm F, Kelley DB, Paton JA. 1982. Connections of vocal control nuclei in the canary telencephalon. J Comp Neurol 207:344–357.

Nottebohm F, Stokes TM, Leonard CM. 1976. Central control of song in the canary, Serinus canarius. J Comp Neurol 165:457–486.

O'Carroll DC, Bidwell NJ, Laughlin SB, Warrant EJ. 1996. Insect motion detectors matched to visual ecology. Nature 382:63–66.

O'Roak BJ, Deriziotis P, Lee C, Vives L, Schwartz JJ, Girirajan S, Karakoc E, Mackenzie AP, Ng SB, Baker C, et al. 2011. Exome sequencing in sporadic autism spectrum disorders identifies severe de novo mutations. Nat Genet 43:585–589.

Olde Loohuis NFM, Kos A, Martens GJM, Bokhoven H, Nadif Kasri N, Aschrafi A. 2011. MicroRNA networks direct neuronal development and plasticity. Cell Mol Life Sci 69:89–102.

Olveczky BP, Andalman AS, Fee MS. 2005. Vocal experimentation in the juvenile songbird requires a basal ganglia circuit. PLoS Biol 3:e153.

Otaegi G, Pollock A, Hong J, Sun T. 2011. MicroRNA miR-9 modifies motor neuron columns by a tuning regulation of FoxP1 levels in developing spinal cords. J Neurosci 31:809–818.

Owen KA, Qiu D, Alves J, Schumacher AM, Kilpatrick LM, Li J, Harris JL, Ellis V. 2010. Pericellular activation of hepatocyte growth factor by the transmembrane serine proteases matriptase and hepsin, but not by the membrane-associated protease uPA. Biochem J 426:219–228.

Palka C, Alfonsi M, Mohn A, Cerbo R, Guanciali Franchi P, Fantasia D, Morizio E, Stuppia L, Calabrese G, Zori R, et al. 2012. Mosaic 7q31 deletion involving FOXP2 gene associated with language impairment. Pediatrics 129:e183–8.

Palumbo O, D'Agruma L, Minenna AF, Palumbo P, Stallone R, Palladino T, Zelante L, Carella M. 2013. 3p14.1 de novo microdeletion involving the FOXP1 gene in an adult patient with autism, severe speech delay and deficit of motor coordination. Gene 516:107–113.

Panaitof SC, Abrahams BS, Dong H, Geschwind DH, White SA. 2010. Language-related Cntnap2 gene is differentially expressed in sexually dimorphic song nuclei essential for vocal learning in songbirds. J Comp Neurol 518:1995–2018.

Panaitof SC. 2012. A songbird animal model for dissecting the genetic bases of autism spectrum disorder. Dis Markers 33:241–249.

Papale A, Cerovic M, Brambilla R. 2009. Viral vector approaches to modify gene expression in the brain. J Neurosci Methods 185:1–14.

Pariani MJ, Spencer A, Graham JM, Rimoin DL. 2009. A 785kb deletion of 3p14.1p13, including the FOXP1 gene, associated with speech delay, contractures, hypertonia and blepharophimosis. Eur J Med Genet 52:123–127.

Pasquinelli AE. 2012. MicroRNAs and their targets: recognition, regulation and an emerging reciprocal relationship. Nat Rev Genet 13:271–282.

Penagarikano O, Abrahams BS, Herman EI, Winden KD, Gdalyahu A, Dong H, Sonnenblick LI, Gruver R, Almajano J, Bragin A, et al. 2011. Absence of CNTNAP2 leads to epilepsy, neuronal migration abnormalities, and core autism-related deficits. Cell 147:235–246.

Peter B, Raskind WH, Matsushita M, Lisowski M, Vu T, Berninger VW, Wijsman EM, Brkanac Z. 2011. Replication of CNTNAP2 association with nonword repetition and support for FOXP2 association with timed reading and motor activities in a dyslexia family sample. J Neurodev Disord 3:39–49.

Petrin AL, Giacheti CM, Maximino LP, Abramides DVM, Zanchetta S, Rossi NF, Richieri-Costa A, Murray JC. 2010. Identification of a microdeletion at the 7q33-q35 disrupting the CNTNAP2 gene in a Brazilian stuttering case. Am J Med Genet A 152A:3164–3172.

Poliak S, Gollan L, Martinez R, Custer A, Einheber S, Salzer JL, Trimmer JS, Shrager P, Peles E. 1999. Caspr2, a new member of the neurexin superfamily, is localized at the juxtaparanodes of myelinated axons and associates with K+ channels. Neuron 24:1037–1047.

Poliak S, Gollan L, Salomon D, Berglund EO, Ohara R, Ranscht B, Peles E. 2001. Localization of Caspr2 in myelinated nerves depends on axon-glia interactions and the generation of barriers along the axon. J Neurosci 21:7568–7575.

Poliak S, Salomon D, Elhanany H, Sabanay H, Kiernan B, Pevny L, Stewart CL, Xu X, Chiu S-Y, Shrager P, et al. 2003. Juxtaparanodal clustering of Shaker-like K+ channels in myelinated axons depends on Caspr2 and TAG-1. J Cell Biol 162:1149–1160.

Poopatanapong A, Teramitsu I, Byun JS, Vician LJ, Herschman HR, White SA. 2006. Singing, but not seizure, induces synaptotagmin IV in zebra finch song circuit nuclei. J Neurobiol 66:1613–1629.

Poot M, van der Smagt JJ, Brilstra EH, Bourgeron T. 2011. Disentangling the Myriad Genomics of Complex Disorders, Specifically Focusing on Autism, Epilepsy, and Schizophrenia. Cytogenet Genome Res 135:228–240.

Powell EM, Campbell DB, Stanwood GD, Davis C, Noebels JL, Levitt P. 2003. Genetic disruption of cortical interneuron development causes region- and GABA cell type-specific deficits, epilepsy, and behavioral dysfunction. J Neurosci 23:622–631.

Price PH. 1979. Developmental determinants of structure in zebra finch song. J Comp Physiol Psych 93:260–277.

Raca G, Baas BS, Kirmani S, Laffin JJ, Jackson CA, Strand EA, Jakielski KJ, Shriberg LD. 2013. Childhood Apraxia of Speech (CAS) in two patients with 16p11.2 microdeletion syndrome. Eur J Hum Genet 21:455–459.

Rajasethupathy P, Antonov I, Sheridan R, Frey S, Sander C, Tuschl T, Kandel ER. 2012. A role for neuronal piRNAs in the epigenetic control of memory-related synaptic plasticity. Cell 149:693–707.

Rajasethupathy P, Fiumara F, Sheridan R, Betel D, Puthanveettil SV, Russo JJ, Sander C, Tuschl T, Kandel E. 2009. Characterization of small RNAs in Aplysia reveals a role for miR-124 in constraining synaptic plasticity through CREB. Neuron 63:803–817.

Ramon y Cajal S. 1911. Le lobe optique des vertébrés inférieurs, toit optique des oiseaux. In: Ramon y Cajal S, editor. Histologie du systéme nerveux de l′homme e des vertébrés. Maloine.

RASBAND WS. 2008. ImageJ. http://rsbwebnihgov/ij/.

Raza MH, Amjad R, Riazuddin S, Drayna D. 2012. Studies in a consanguineous family reveal a novel locus for stuttering on chromosome 16q. Human Genetics 131:311–313.

Reich D, Green RE, Kircher M, Krause J, Patterson N, Durand EY, Viola B, Briggs AW, Stenzel U, Johnson PLF, et al. 2010. Genetic history of an archaic hominin group from Denisova Cave in Siberia. Nature 468:1053–1060.

Reichardt W, Reichardt WE. 1966. Detection of single quanta by the compound eye of the fly Musca. The Functional Organization of the Compound Eye} 66:291–307.

Reimers-Kipping S, Hevers W, Pääbo S, Enard W. 2011. Humanized Foxp2 specifically affects cortico-basal ganglia circuits. Neuroscience 175:75–84.

Reiner A, Laverghetta AV, Meade CA, Cuthbertson SL, Bottjer SW. 2004a. An immunohistochemical and pathway tracing study of the striatopallidal organization of area X in the male zebra finch. J Comp Neurol 469:239–261.

Reiner A, Perkel DJ, Bruce LL, Butler AB, Csillag A, Kuenzel W, Medina L, Paxinos G, Shimizu T, Striedter G, et al. 2004b. Revised nomenclature for avian telencephalon and some related brainstem nuclei. J Comp Neurol 473:377–414.

Reiser MB, Dickinson MH. 2008. A modular display system for insect behavioral neuroscience. J Neurosci Methods 167:127–139.

Reiser MB, Humbert JS, Dunlop MJ, Del Vecchio D, Murray RM, Dickinson MH. 2004. Vision as a compensatory mechanism for disturbance rejection in upwind flight. In: Vol. 1. IEEE. p 311–316 vol.1.

Riaz N, Steinberg S, Ahmad J, Pluzhnikov A, Riazuddin S, Cox NJ, Drayna D. 2005. Genomewide significant linkage to stuttering on chromosome 12. Am J Hum Genet 76:647–651.

Rice GM, Raca G, Jakielski KJ, Laffin JJ, Iyama-Kurtycz CM, Hartley SL, Sprague RE, Heintzelman AT, Shriberg LD. 2012. Phenotype of FOXP2 haploinsufficiency in a mother and son. Am J Med Genet A 158A:174–181.

Rice ML, Smith SD, Gayán J. 2009. Convergent genetic linkage and associations to language, speech and reading measures in families of probands with Specific Language Impairment. J Neurodev Disord 1:264–282.

Roberts TF, Tschida KA, Klein ME, Mooney R. 2010. Rapid spine stabilization and synaptic enhancement at the onset of behavioural learning. Nature 463:948–952.

Roberts TF, Wild JM, Kubke MF, Mooney R. 2007. Homogeneity of intrinsic properties of sexually dimorphic vocal motoneurons in male and female zebra finches. J Comp Neurol 502:157–169.

Rochefort C, He X, Scotto-Lomassese S, Scharff C. 2007. Recruitment of FoxP2-expressing neurons to area X varies during song development. Dev Neurobiol 67:809–817.

Roll P, Rudolf G, Pereira S, Royer B, Scheffer IE, Massacrier A, Valenti M-P, Roeckel-Trevisiol N, Jamali S, Beclin C, et al. 2006. SRPX2 mutations in disorders of language cortex and cognition. Hum Mol Genet 15:1195–1207.

Roll P, Vernes SC, Bruneau N, Cillario J, Ponsole-Lenfant M, Massacrier A, Rudolf G, Khalife M, Hirsch E, Fisher SE, et al. 2010. Molecular networks implicated in speech-related disorders: FOXP2 regulates the SRPX2/uPAR complex. Hum Mol Genet 19:4848–4860.

Romero LM, Reed JM. 2005. Collecting baseline corticosterone samples in the field: is under 3 min good enough? Comp Biochem & Physiol Part A: Mol & Int Physio140:73–79.

Rousso DL, Pearson CA, Gaber ZB, Miquelajauregui A, Li S, Portera-Cailliau C, Morrisey EE, Novitch BG. 2012. Foxp-mediated suppression of N-cadherin regulates neuroepithelial character and progenitor maintenance in the CNS. Neuron 74:314–330.

Royer B, Soares DC, Barlow PN, Bontrop RE, Roll P, Robaglia-Schlupp A, Blancher A, Levasseur A, Cau P, Pontarotti P, et al. 2007. Molecular evolution of the human SRPX2 gene that causes brain disorders of the Rolandic and Sylvian speech areas. BMC Genet 8:72.

Royer-Zemmour B, Ponsole-Lenfant M, Gara H, Roll P, Lévêque C, Massacrier A, Ferracci G, Cillario J, Robaglia-Schlupp A, Vincentelli R, et al. 2008. Epileptic and developmental disorders of the speech cortex: ligand/receptor interaction of wild-type and mutant SRPX2 with the plasminogen activator receptor uPAR. Hum Mol Genet 17:3617–3630.

Sakata JT, Hampton CM, Brainard MS. 2008. Social modulation of sequence and syllable variability in adult birdsong. J Neurophysiol 99:1700–1711.

Sallés J, López de Jesús M, Goñi O, Fernández-Teruel A, Driscoll P, Tobeña A, Escorihuela RM. 2001. Transmembrane signaling through phospholipase C in cortical and hippocampal membranes of psychogenetically selected rat lines. Psychopharmacology (Berl) 154:115–125.

Sanuki R, Onishi A, Koike C, Muramatsu R, Watanabe S, Muranishi Y, Irie S, Uneo S, Koyasu T, Matsui R, et al. 2011. miR-124a is required for hippocampal axogenesis and retinal cone survival through Lhx2 suppression. Nat Neurosci 14:1125–1134.

Saunders LR, Sharma AD, Tawney J, Nakagawa M, Okita K, Yamanaka S, Willenbring H, Verdin E. 2010. miRNAs regulate SIRT1 expression during mouse embryonic stem cell differentiation and in adult mouse tissues. Aging (Albany NY) 2:415–431.

Scerri TS, Morris AP, Buckingham L-L, Newbury DF, Miller LL, Monaco AP, Bishop DVM, Paracchini S. 2011. DCDC2, KIAA0319 and CMIP are associated with reading-related traits. Biol Psychiatry 70:237–245.

Scharff C, Nottebohm F. 1991. A comparative study of the behavioral deficits following lesions of various parts of the zebra finch song system: implications for vocal learning. J Neurosci 11:2896–2913.

Scharff C, Petri J. 2011. Evo-devo, deep homology and FoxP2: implications for the evolution of speech and language. Philos Trans R Soc Lond, B, Biol Sci 366:2124–2140.

Schilstra C, van Hateren JH. 1998. Stabilizing gaze in flying blowflies. Nature 395:654.

Schneider CA, Rasband WS, Eliceiri KW. 2012. NIH Image to ImageJ: 25 years of image

analysis. Nat Meth 9:671–675.

Schulz SB, Haesler S, Scharff C, Rochefort C. 2010. Knockdown of FoxP2 alters spine density in Area X of the zebra finch. Genes, brain, and behavior 9:732–740.

Scott BB, Lois C. 2007. Developmental origin and identity of song system neurons born during vocal learning in songbirds. J Comp Neurol 502:202–214.

Scott EK, Raabe T, Luo L. 2002. Structure of the vertical and horizontal system neurons of the lobula plate in Drosophila. J Comp Neurol 454:470–481.

Scott-Van Zeeland AA, Abrahams BS, Alvarez-Retuerto AI, Sonnenblick LI, Rudie JD, Ghahremani D, Mumford JA, Poldrack RA, Dapretto M, Geschwind DH, et al. 2010. Altered functional connectivity in frontal lobe circuits is associated with variation in the autism risk gene CNTNAP2. Sci Transl Med 2:56ra80.

Shi Z, Fu L, Luo G, WANG X, Li X. 2013. miR-9 and miR-140-5p are regulated by song behavior and target to the zebra finch FoxP2 gene. :1–2.

Shibata M, Nakao H, Kiyonari H, Abe T, Aizawa S. 2011. MicroRNA-9 regulates neurogenesis in mouse telencephalon by targeting multiple transcription factors. J Neurosci 31:3407–3422.

Shriberg LD, Ballard KJ, Tomblin JB, Duffy JR, Odell KH, Williams CA. 2006. Speech, prosody, and voice characteristics of a mother and daughter with a 7;13 translocation affecting FOXP2. J Speech Lang Hear Res 49:500–525.

Shu W, Cho JY, Jiang Y, Zhang M, Weisz D, Elder GA, Schmeidler J, De Gasperi R, Sosa MAG, Rabidou D, et al. 2005. Altered ultrasonic vocalization in mice with a disruption in the Foxp2 gene. Proc Natl Acad Sci USA 102:9643–9648.

Shu W, Yang H, Zhang L, Lu MM, Morrisey EE. 2001. Characterization of a new subfamily of winged-helix/forkhead (Fox) genes that are expressed in the lung and act as transcriptional repressors. J Biol Chem 276:27488–27497.

Simonyan K, Horwitz B, Jarvis ED. 2012. Dopamine regulation of human speech and bird song: a critical review. Brain Lang 122:142–150.

Simpson HB, Vicario DS. 1990. Brain pathways for learned and unlearned vocalizations differ in zebra finches. J Neurosci 10:1541–1556.

Single S, Borst A. 1998. Dendritic integration and its role in computing image velocity. Science 281:1848–1850.

Skaggs K, Martin DM, Novitch BG. 2011. Regulation of spinal interneuron development by the Olig-related protein Bhlhb5 and Notch signaling. Development 138:3199–3211.

Smith SD. 2007. Genes, language development, and language disorders. Ment Retard Dev

Disabil Res Rev 13:96–105.

Smrt RD, Szulwach KE, Pfeiffer RL, Li X, Guo W, Pathania M, Teng Z-Q, Luo Y, Peng J, Bordey A, et al. 2010. MicroRNA miR-137 regulates neuronal maturation by targeting ubiquitin ligase mind bomb-1. Stem Cells 28:1060–1070.

Sohrabji F, Nordeen EJ, Nordeen KW. 1990. Selective impairment of song learning following lesions of a forebrain nucleus in the juvenile zebra finch. Behav Neural Biol 53:51–63.

Sossin WS. 2007. Isoform specificity of protein kinase Cs in synaptic plasticity. Learn Mem 14:236–246.

Spiro JE, Dalva MB, Mooney R. 1999. Long-range inhibition within the zebra finch song nucleus RA can coordinate the firing of multiple projection neurons. J Neurophysiol 81:3007–3020.

Spiteri E, Konopka G, Coppola G, Bomar J, Oldham M, Ou J, Vernes SC, Fisher SE, Ren B, Geschwind DH. 2007. Identification of the transcriptional targets of FOXP2, a gene linked to speech and language, in developing human brain. Am J Hum Genet 81:1144–1157.

Srinivasan MV, Poteser M, Kral K. 1999. Motion detection in insect orientation and navigation. Vision Res 39:2749–2766.

Stoeger AS, Mietchen D, Oh S, de Silva S, Herbst CT, Kwon S, Fitch WT. 2012. An asian elephant imitates human speech. Curr Biol 22:2144–2148.

Strapps WR, Pickering V, Muiru GT, Rice J, Orsborn S, Polisky BA, Sachs A, Bartz SR. 2010. The siRNA sequence and guide strand overhangs are determinants of in vivo duration of silencing. Nucleic Acids Research 38:4788–4797.

Strauss KA, Puffenberger EG, Huentelman MJ, Gottlieb S, Dobrin SE, Parod JM, Stephan DA, Morton DH. 2006. Recessive symptomatic focal epilepsy and mutant contactin-associated protein-like 2. N Engl J Med 354:1370–1377.

Stroud JC, Wu Y, Bates DL, Han A, Nowick K, Pääbo S, Tong H, Chen L. 2006. Structure of the forkhead domain of FOXP2 bound to DNA. Structure 14:159–166.

Sturdy CB, Wild JM, Mooney R. 2003. Respiratory and telencephalic modulation of vocal motor neurons in the zebra finch. J Neurosci 23:1072–1086.

Sun AX, Crabtree GR, Yoo AS. 2013. MicroRNAs: regulators of neuronal fate. Curr Opin Cell Biol 25:215–221.

Sutton MA, Bagnall MW, Sharma SK, Shobe J, Carew TJ. 2004. Intermediate-term memory for site-specific sensitization in aplysia is maintained by persistent activation of protein kinase C. J Neurosci 24:3600–3609.

Sutton MA, Carew TJ. 2000. Parallel molecular pathways mediate expression of distinct forms

of intermediate-term facilitation at tail sensory-motor synapses in Aplysia. Neuron 26:219–231.

Sutton MA, Carew TJ. 2002. Behavioral, cellular, and molecular analysis of memory in Aplysia I: intermediate-term memory. Integrative and comparative biology.

Sutton MA, Masters SE, Bagnall MW, Carew TJ. 2001. Molecular mechanisms underlying a unique intermediate phase of memory in aplysia. Neuron 31:143–154.

Südhof TC. 2008. Neuroligins and neurexins link synaptic function to cognitive disease. Nature 455:903–911.

Talkowski ME, Rosenfeld JA, Blumenthal I, Pillalamarri V, Chiang C, Heilbut A, Ernst C, Hanscom C, Rossin E, Lindgren AM, et al. 2012. Sequencing chromosomal abnormalities reveals neurodevelopmental loci that confer risk across diagnostic boundaries. Cell 149:525–537.

Tammero LF, Dickinson MH. 2002a. The influence of visual landscape on the free flight behavior of the fruit fly Drosophila melanogaster. J Exp Biol 205:327–343.

Tammero LF, Dickinson MH. 2002b. Collision-avoidance and landing responses are mediated by separate pathways in the fruit fly, Drosophila melanogaster. J Exp Biol 205:2785–2798.

Tammero LF, Frye MA, Dickinson MH. 2004. Spatial organization of visuomotor reflexes in Drosophila. J Exp Biol 207:113–122.

Tan S-L, Ohtsuka T, González A, Kageyama R. 2012. MicroRNA9 regulates neural stem cell differentiation by controlling Hes1 expression dynamics in the developing brain. Genes Cells 17:952–961.

Tanabe Y, Fujita E, Momoi T. 2011. FOXP2 promotes the nuclear translocation of POT1, but FOXP2(R553H), mutation related to speech-language disorder, partially prevents it. Biochemical and Biophysical Research Communications 410:593–596.

Tanaka K, Arao T, Tamura D, Aomatsu K, Furuta K, Matsumoto K, Kaneda H, Kudo K, Fujita Y, Kimura H, et al. 2012. SRPX2 Is a Novel Chondroitin Sulfate Proteoglycan That Is Overexpressed in Gastrointestinal Cancer. PLoS ONE 7:e27922.

Tchernichovski O, Nottebohm F, Ho C, Pesaran B, Mitra P. 2000. A procedure for an automated measurement of song similarity. Anim Behav 59:1167–1176.

Teramitsu I, Kudo LC, London SE, Geschwind DH, White SA. 2004. Parallel FoxP1 and FoxP2 expression in songbird and human brain predicts functional interaction. J Neurosci 24:3152–3163.

Teramitsu I, Poopatanapong A, Torrisi S, White SA. 2010. Striatal FoxP2 is actively regulated during songbird sensorimotor learning. PLoS ONE 5:e8548.

Teramitsu I, White SA. 2006. FoxP2 regulation during undirected singing in adult songbirds. J Neurosci 26:7390–7394.

Teramitsu I. 2007. Brain-Behavior Relationships in Songbird Common Molecular Mechanisms for Birdsong and Human Speech. Retrieved from ProQuest Dissertations and Theses (Accession Order Number 3257164).

Thompson CK, Schwabe F, Schoof A, Mendoza E, Gampe J, Rochefort C, Scharff C. 2013. Young and intense: FoxP2 immunoreactivity in Area X varies with age, song stereotypy, and singing in male zebra finches. Front Neural Circuits 7(24):1-17.

Thompson RF, Spencer WA. 1966. Habituation: a model phenomenon for the study of neuronal substrates of behavior. Psychol Rev 73:16–43.

Toma C, Hervás A, Torrico B, Balmaña N, Salgado M, Maristany M, Vilella E, Martínez-Leal R, Planelles MI, Cuscó I, et al. 2013. Analysis of two language-related genes in autism: a case-control association study of FOXP2 and CNTNAP2. Psychiatr Genet 23:82–85.

Troyer TW, Doupe AJ. 2000a. An associational model of birdsong sensorimotor learning I. Efference copy and the learning of song syllables. J Neurophysiol 84:1204–1223.

Troyer TW, Doupe AJ. 2000b. An associational model of birdsong sensorimotor learning II. Temporal hierarchies and the learning of song sequence. J Neurophysiol 84:1224–1239.

Trudeau LE, Castellucci VF. 1993. Excitatory amino acid neurotransmission at sensory-motor and interneuronal synapses of Aplysia californica. J Neurophysiol 70:1221–1230.

Tsui D, Vessey JP, Tomita H, Kaplan DR, Miller FD. 2013. FoxP2 Regulates Neurogenesis during Embryonic Cortical Development. J Neurosci 33:244–258.

Tumer EC, Brainard MS. 2007. Performance variability enables adaptive plasticity of "crystallized" adult birdsong. Nature 450:1240–1244.

Udo H, Jin I, Kim J-H, Li H-L, Youn T, Hawkins RD, Kandel ER, Bailey CH. 2005. Serotonin-induced regulation of the actin network for learning-related synaptic growth requires Cdc42, N-WASP, and PAK in Aplysia sensory neurons. Neuron 45:887–901.

Ui-Tei K, Naito Y, Takahashi F, Haraguchi T, Ohki-Hamazaki H, Juni A, Ueda R, Saigo K. 2004. Guidelines for the selection of highly effective siRNA sequences for mammalian and chick RNA interference. Nucleic Acids Research 32:936–948.

Ushkaryov YA, Hata Y, Ichtchenko K, Moomaw C, Afendis S, Slaughter CA, Südhof TC. 1994. Conserved domain structure of beta-neurexins. Unusual cleaved signal sequences in receptor-like neuronal cell-surface proteins. J Biol Chem 269:11987–11992.

Van Hateren NJ, Jones RS, Wilson SA. 2009. RNA Interference in Chicken Embryos. In: Electroporation and Sonoporation in Developmental Biology. Springer. p 295–314.

Vargha-Khadem F, Watkins K, Alcock K, Fletcher P, Passingham R. 1995. Praxic and nonverbal cognitive deficits in a large family with a genetically transmitted speech and language disorder. Proc Natl Acad Sci USA 92:930–933.

Vargha-Khadem F, Watkins KE, Price CJ, Ashburner J, Alcock KJ, Connelly A, Frackowiak RS, Friston KJ, Pembrey ME, Mishkin M, et al. 1998. Neural basis of an inherited speech and language disorder. Proc Natl Acad Sci USA 95:12695–12700.

Verkerk AJMH, Mathews CA, Joosse M, Eussen BHJ, Heutink P, Oostra BA, Tourette Syndrome Association International Consortium for Genetics. 2003. CNTNAP2 is disrupted in a family with Gilles de la Tourette syndrome and obsessive compulsive disorder. Genomics 82:1–9.

Vernes SC, MacDermot KD, Monaco AP, Fisher SE. 2009. Assessing the impact of FOXP1 mutations on developmental verbal dyspraxia. Eur J Hum Genet 17:1354–1358.

Vernes SC, Newbury DF, Abrahams BS, Winchester L, Nicod J, Groszer M, Alarcón M, Oliver PL, Davies KE, Geschwind DH, et al. 2008. A functional genetic link between distinct developmental language disorders. N Engl J Med 359:2337–2345.

Vernes SC, Nicod J, Elahi FM, Coventry JA, Kenny N, Coupe A-M, Bird LE, Davies KE, Fisher SE. 2006. Functional genetic analysis of mutations implicated in a human speech and language disorder. Hum Mol Genet 15:3154–3167.

Vernes SC, Oliver PL, Spiteri E, Lockstone HE, Puliyadi R, Taylor JM, Ho J, Mombereau C, Brewer A, Lowy E, et al. 2011. Foxp2 regulates gene networks implicated in neurite outgrowth in the developing brain. PLoS Genet 7:e1002145.

Vernes SC, Spiteri E, Nicod J, Groszer M, Taylor JM, Davies KE, Geschwind DH, Fisher SE. 2007. High-throughput analysis of promoter occupancy reveals direct neural targets of FOXP2, a gene mutated in speech and language disorders. Am J Hum Genet 81:1232–1250.

Vicario DS. 1991. Organization of the zebra finch song control system: II. Functional organization of outputs from nucleus Robustus archistriatalis. J Comp Neurol 309:486–494.

Villareal G, Li Q, Cai D, Glanzman DL. 2007. The role of rapid, local, postsynaptic protein synthesis in learning-related synaptic facilitation in aplysia. Curr Biol 17:2073–2080.

Villareal GJ, Cai D, Fink A, Glanzman D. 2006. Serotonin-dependent enhancement of the glutamate-evoked response in isolated siphon motor neurons requires temporal and isoform specific activation of protein kinase C in aplysia. FENS Abstr.

Visvanathan J, Lee S, Lee B, Lee JW, Lee SK. 2007. The microRNA miR-124 antagonizes the anti-neural REST/SCP1 pathway during embryonic CNS development. Genes Dev 21:744–749.

Wada H, Hahn TP, Breuner CW. 2007. Development of stress reactivity in white-crowned

sparrow nestlings: total corticosterone response increases with age, while free corticosterone response remains low. Gen Comp Endocrinol 150:405–413.

Wada K, Howard JT, McConnell P, Whitney O, Lints T, Rivas MV, Horita H, Patterson MA, White SA, Scharff C, et al. 2006. A molecular neuroethological approach for identifying and characterizing a cascade of behaviorally regulated genes. Proceedings of the National Academy of Sciences 103:15212–15217.

Wang B, Lin D, Li C, Tucker P. 2003. Multiple domains define the expression and regulatory properties of Foxp1 forkhead transcriptional repressors. J Biol Chem 278:24259–24268.

Wang W, Kwon EJ, Tsai L-H. 2012. MicroRNAs in learning, memory, and neurological diseases. Learn Mem 19:359–368.

Watkins KE, Dronkers NF, Vargha-Khadem F. 2002. Behavioural analysis of an inherited speech and language disorder: comparison with acquired aphasia. Brain 125:452–464.

Wehrhahn C. 1985. Visual guidance of flies during flight. In Comprehensive Insect Physiology, Biochemistry, and Pharmacology (ed. G. A. Kerkut andL. I. Gilbert), pp. 673-684. Oxford: Pergamon Press.

Whalley HC, O'Connell G, Sussmann JE, Peel A, Stanfield AC, Hayiou-Thomas ME, Johnstone EC, Lawrie SM, McIntosh AM, Hall J. 2011. Genetic variation in CNTNAP2 alters brain function during linguistic processing in healthy individuals. Am J Med Genet B Neuropsychiatr Genet 156:941–948.

White SA, Fisher SE, Geschwind DH, Scharff C, Holy TE. 2006. Singing mice, songbirds, and more: models for FOXP2 function and dysfunction in human speech and language. J Neurosci 26:10376–10379.

White SA. 2010. Genes and vocal learning. Brain Lang 115:21–28.

Whitehouse AJO, Bishop DVM, Ang QW, Pennell CE, Fisher SE. 2011. CNTNAP2 variants affect early language development in the general population. Genes, brain, and behavior 10:451–456.

Whitney O, Johnson F. 2005. Motor-induced transcription but sensory-regulated translation of ZENK in socially interactive songbirds. J Neurobiol 65:251–259.

Wicklein M, Strausfeld NJ. 2000. Organization and significance of neurons that detect change of visual depth in the hawk moth Manduca sexta. J Comp Neurol 424:356–376.

Wild JM, Kubke MF, Mooney R. 2009. Avian nucleus retroambigualis: cell types and projections to other respiratory-vocal nuclei in the brain of the zebra finch (Taeniopygia guttata). J Comp Neurol 512:768–783.

Wild JM, Williams MN, Howie GJ, Mooney R. 2005. Calcium-binding proteins define

interneurons in HVC of the zebra finch (Taeniopygia guttata). J Comp Neurol 483:76–90.

Wild JM, Williams MN, Suthers RA. 2001. Parvalbumin-positive projection neurons characterise the vocal premotor pathway in male, but not female, zebra finches. Brain Res 917:235–252.

Wild JM. 1993. Descending projections of the songbird nucleus robustus archistriatalis. J Comp Neurol 338:225–241.

Williams H, Mehta N. 1999. Changes in adult zebra finch song require a forebrain nucleus that is not necessary for song production. J Neurobiol 39:14–28.

Wingfield JC, Smith JP, Farner DS. 1982. Endocrine responses of white-crowned sparrows to environmental stress. The Condor 84:399–409.

Winograd C, Clayton D, Ceman S. 2008. Expression of fragile X mental retardation protein within the vocal control system of developing and adult male zebra finches. Neuroscience 157:132–142.

Xu X, Coats JK, Yang CF, Wang A, Ahmed OM, Alvarado M, Izumi T, Shah NM. 2012. Modular Genetic Control of Sexually Dimorphic Behaviors. Cell 148:596–607.

Yu J-Y, Chung K-H, Deo M, Thompson RC, Turner DL. 2008. MicroRNA miR-124 regulates neurite outgrowth during neuronal differentiation. Exp Cell Res 314:2618–2633.

Yule DI, Williams JA. 1992. U73122 inhibits Ca2+ oscillations in response to cholecystokinin and carbachol but not to JMV-180 in rat pancreatic acinar cells. J Biol Chem 267:13830–13835.

Zeesman S, Nowaczyk MJM, Teshima I, Roberts W, Cardy JO, Brian J, Senman L, Feuk L, Osborne LR, Scherer SW. 2006. Speech and language impairment and oromotor dyspraxia due to deletion of 7q31 that involves FOXP2. Am J Med Genet A 140:509–514.

Zhao C, Sun G, Li S, Shi Y. 2009. A feedback regulatory loop involving microRNA-9 and nuclear receptor TLX in neural stem cell fate determination. Nat Struct Mol Biol 16:365–371.

Zhao Y, Leal K, Abi-Farah C, Martin KC, Sossin WS, Klein M. 2006. Isoform specificity of PKC translocation in living Aplysia sensory neurons and a role for Ca2+-dependent PKC APL I in the induction of intermediate-term facilitation. J Neurosci 26:8847–8856.